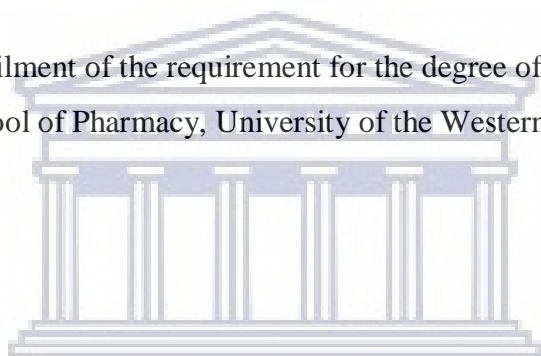


NOVEL NORBORNANE DERIVATIVES AS POTENTIAL NEUROPROTECTIVE AGENTS

Ayodeji Olatunde Egunlusi

A thesis submitted in fulfilment of the requirement for the degree of Philosophiae Doctor in
the School of Pharmacy, University of the Western Cape



**UNIVERSITY of the
WESTERN CAPE**

Supervisor: Prof Jacques Joubert

Co-Supervisor: Prof Sarel F. Malan

May 2020

<http://etd.uwc.ac.za/>

Dedicated

To God almighty, the author and finisher of my faith,

To the late Modupe Kofoworola Abaniwonda, a friend dear to my heart who was called to
glory during the course of this study,

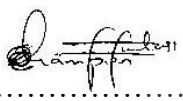
To my late grandmother madam Julianah Eguntola Egunlusi



Declaration

I declare that the thesis titled '*Novel norbornane derivatives as potential neuroprotective agents*' is my own work, that it has never been submitted for any degree or examination in any other University, and that all the sources I have used or quoted have been indicated and acknowledged by complete references.

Ayodeji Olatunde Egunlusi

Signature:.....

Date:..28/04/2020..



UNIVERSITY *of the*
WESTERN CAPE

Contents

Acknowledgement	xi
Keywords	xii
Abstract	xiii
Chapter 1 Introduction	1
1.1 Neurodegeneration.....	1
1.1.1 Neurodegenerative disorders.....	1
1.1.2 Mechanism of neurodegeneration.....	2
1.1.3 Excitotoxicity in neurodegenerative disorders.....	3
1.1.4 MPP ⁺ -induced toxicity in neurodegenerative disorders.....	4
1.2 Rationale.....	4
1.3 Objectives.....	6
1.4 Conclusion.....	7
Chapter 2 Literature review	9
2.1 Neurodegenerative disorders.....	9
2.1.1 Introduction.....	9
2.1.2 Incidence, prevalence and cost implication of neurodegenerative disorders.....	10
2.1.3 Gender role in neurodegenerative disorders.....	11
2.2 Pathology of neurodegenerative disorders and established therapeutic approach...13	
2.2.1 Introduction.....	13
2.2.2 Parkinson's disease.....	14
2.2.3 Alzheimer's disease.....	19
2.2.4 Amyotrophic lateral sclerosis.....	22

2.2.5	Huntington's disease.....	24
2.3	Oxidative stress and excitotoxicity in neurodegenerative disorders.....	28
2.3.1	The role of oxidative stress in neurodegenerative disorders.....	28
2.3.2	The role of excitotoxicity in neurodegenerative disorders.....	30
2.4	NMDA receptors and voltage gated calcium channels.....	34
2.4.1	Structure and functions of NMDA receptors.....	34
2.4.2	Structure and functions of voltage gated calcium channels.....	37
2.4.3	The role of NMDA receptor and voltage-gated channel blockers in attenuating glutamate-induced excitotoxicity.....	40
2.5	Polycyclic cage amine as neuroprotective agents.....	45
2.5.1	Neuroprotective functions of polycyclic cages and it derivatives <i>vial</i> dual attenuation of calcium entry pathways.....	45
2.5.2	Polycyclic cages and attenuation of MPP ⁺ -induced neurotoxicity.....	47
2.6	Norbornane derivatives in medicinal chemistry.....	48
2.7	Summary.....	51
Chapter 3	Synthetic procedures	53
3.1	Introduction.....	53
3.2	Instrumentation used for synthesis.....	53
3.2.1	Apparatus for reaction conditions.....	53
3.2.1.1	Weighing apparatus and stirrers.....	53
3.2.1.2	Heating apparatus for reactions.....	54
3.2.1.3	Cooling baths.....	54
3.2.1.4	Microwave reactor.....	54
3.2.1.5	High pressure metal reactor.....	54

3.2.2 Separation techniques.....	54
3.2.2.1 Thin layer chromatography.....	54
3.2.2.2 Column chromatography.....	54
3.2.2.3 Mobile phases.....	55
3.2.2.4 Crystallisation.....	55
3.2.3 Spectroscopic and physical characterisation.....	55
3.2.3.1 NMR.....	55
3.2.3.2 MS.....	56
3.2.3.3 IR.....	56
3.2.3.4 Melting point apparatus.....	56
3.2.3.5 Elemental analysis.....	56
3.3 Synthesis of designed compounds.....	56
3.3.1 Reagents.....	56
3.3.2 General synthetic approach.....	57
3.3.2.1 Synthetic procedures and characterisation data of compound 1-6	57
3.3.2.1.1 Tricyclo[6.2.1.0 ^{2,7}]undeca-4,9-diene-3,6-dione.....	57
3.3.2.1.2 Pentacyclo[10.2.1.1 ^{5,8} .0 ^{2,11} .0 ^{4,9}]hexadeca-6,13-diene-3,10-dione.....	57
3.3.2.1.3 Tricyclo[6.2.1.0 ^{2,7}]undec-9-ene-3,6-dione.....	59
3.3.2.1.4 6-Hydroxytricyclo[6.2.1.0 ^{2,7}]undec-9-en-3-one.....	60
3.3.2.1.5 6-(Benzylamino)tricyclo[6.2.1.0 ^{2,7}]undec-9-en-3-one.....	61

3.3.2.1.6 6-(1-Piperidylamino)tricyclo[6.2.1.0 ^{2,6}]undec-9-en-3-one.....	62
3.3.2.2 Synthetic procedures and characterisation data of compound 7-18	63
3.3.2.2.1 4-Oxatricyclo[5.2.1.0 ^{2,6}]dec-8-ene-3,5-dione.....	63
3.3.2.2.2 Synthetic procedures and characterisation data of compounds 8 and 9	64
3.3.2.2.2.1 4-Benzyl-4-azatricyclo[5.2.1.0 ^{2,6}]dec-8-ene-3,5-dione.....	64
3.3.2.2.2.2 <i>N</i> 2, <i>N</i> 3-Dibenzylbicyclo[2.2.1]hept-5-ene-2,3-dicarboxamide.....	65
3.3.2.2.3 4-(1-Piperidyl)-4-azatricyclo[5.2.1.0 ^{2,6}]dec-8-ene-3,5-dione.....	65
3.3.2.2.4 4-Prop-2-ynyl-4-azatricyclo[5.2.1.0 ^{2,6}]dec-8-ene-3,5-dione.....	66
3.3.2.2.5 4-Propyl-4-azatricyclo[5.2.1.0 ^{2,6}]dec-8-ene-3,5-dione.....	67
3.3.2.2.6 4-Anilino-4-azatricyclo[5.2.1.0 ^{2,6}]dec-8-ene-3,5-dione.....	68
3.3.2.2.7 4-(2-Aminoethyl)-4-azatricyclo[5.2.1.0 ^{2,6}]dec-8-ene-3,5-dione.....	69
3.3.2.2.8 4-[2-(3,5-Dioxo-4-azatricyclo[5.2.1.0 ^{2,6}]dec-8-en-4-yl)ethyl]-4-azatricyclo[5.2.1.0 ^{2,6}]dec-8-ene-3,5-dione.....	70

3.3.2.2.9 4-(3-Aminopropyl)-4-azatricyclo[5.2.1.0 ^{2,6}]dec-8-ene-3,5-dione.....	71
3.3.2.2.10 4-(4-Aminobutyl)-4-azatricyclo[5.2.1.0 ^{2,6}]dec-8-ene-3,5-dione.....	72
3.3.2.2.11 4-[2-(Dimethylamino)ethyl]-4-azatricyclo[5.2.1.0 ^{2,6}]dec-8-ene-3,5-dione.....	73
3.3.2.3 Synthetic procedures and characterisation data of compound 19-23	74
3.3.2.3.1 4,10-Dioxapentacyclo[6.3.1.0 ^{2,7} .0 ^{3,5} .0 ^{9,11}]dodecane.	74
3.3.2.3.2 Synthetic procedures and characterisation data of compounds 20 and 21	75
3.3.2.3.2.1 7-Benzyl-7-azatetracyclo[6.2.1.0 ^{2,6} .0 ^{4,10}]undecane-5,11-diol.....	75
3.3.2.3.2.2 7-Benzyl-7-azatetracyclo[6.2.1.0 ^{2,6} .0 ^{4,10}]undecane-5,9-diol.....	76
3.3.2.3.3 Synthetic procedures and characterisation data of compounds 22 and 23	76
3.3.2.3.3.1 7-Phenyl-7-azatetracyclo[6.2.1.0 ^{2,6} .0 ^{4,10}]undecane-5,11-diol.....	77
3.3.2.3.3.2 7-Phenyl-7-azatetracyclo[6.2.1.0 ^{2,6} .0 ^{4,10}]undecane-5,9-diol.....	77
3.3.2.4 Characterisation data of compound 24-27	77
3.3.2.4.1 2-Azabicyclo[2.2.2]octan-6-ol.....	78
3.3.2.4.2 4-Azatricyclo[5.2.2.0 ^{2,6}]undec-8-ene.....	78

3.3.2.4.3 7-Azatetracyclo[6.3.0.0 ^{2,6} .0 ^{3,10}]undecane-5,9-diol...	79
3.3.2.4.4 Bicyclo[3.3.1]nonane-2,6-dione.....	79
3.4 Discussion.....	79
3.5 Conclusion.....	91
Chapter 4 Biological studies.....	93
4.1 Introduction.....	93
4.2 Instrumentation.....	94
4.3 Cytotoxicity studies.....	94
4.3.1 Background.....	94
4.3.2 Material and methods.....	95
4.3.2.1 Cell line and culture.....	95
4.3.2.2 Screening protocol.....	96
4.3.2.3 MTT assay.....	96
4.3.2.4 Data analysis.....	96
4.3.2.5 Result and discussion.....	97
4.4 Neuroprotection studies.....	99
4.4.1 Background.....	99
4.4.2 Material and methods.....	100
4.4.2.1 Cell line and culture.....	100
4.4.2.2 Neuroprotection protocol.....	100
4.4.2.3 MTT assay and data analysis.....	100
4.4.2.4 Result and discussion.....	100
4.5 Calcium influx studies.....	104
4.5.1 Introduction.....	104

4.5.2 NMDA mediated Ca ²⁺ influx studies.....	106
4.5.2.1 Background.....	106
4.5.2.2 Experiment design.....	107
4.5.2.3 Material and methods.....	108
4.5.2.3.1 Calcium and magnesium free buffer.....	108
4.5.2.3.2 Calcium containing buffer.....	108
4.5.2.3.3 Stimulation or activation buffer.....	108
4.5.2.3.4 Cell line and culture conditions.....	108
4.5.2.3.5 Cell treatment.....	109
4.5.2.3.6 Measurement of intracellular calcium.....	109
4.5.2.3.7 Data and statistical analysis.....	110
4.5.2.4 Result and discussion.....	110
4.5.3 Voltage gated Ca ²⁺ influx studies.....	115
4.5.3.1 Background.....	115
4.5.3.2 Experiment design.....	117
4.5.3.3 Material and methods.....	117
4.5.3.3.1 Calcium free buffer.....	117
4.5.3.3.2 Calcium containing buffer.....	118
4.5.3.3.3 Depolarisation buffer.....	118
4.5.3.3.4 Cell line and culture conditions.....	118
4.5.3.3.5 Cell treatment.....	118
4.5.3.3.6 Measurement of intracellular calcium.....	119
4.5.3.3.7 Data and statistical analysis.....	119
4.5.3.4 Result and discussion.....	119

4.6 Conclusion.....	123
Chapter 5 Conclusion.....	127
5.1 Introduction.....	127
5.2 Synthesis.....	128
5.3 Biological studies.....	132
5.4 Conclusion and recommendations.....	135
References.....	138
List of figures.....	173
List of tables	176
Spectra	177



UNIVERSITY *of the*
WESTERN CAPE

Acknowledgements

Firstly, I will like to appreciate God almighty for his unmerited grace and favour throughout the course of my study. He was my pillar during the difficult times. May his name be Glorified (Amen).

An immense gratitude to Prof Jacques Joubert (supervisor) and Prof Sarel Malan (co-supervisor) for their overwhelming support, time and generous contributions toward the completion of this project.

I will like to thank NRF (South Africa), the School of Pharmacy, and the University of the Western Cape for providing financial support and creating a suitable platform for my project.

Special thanks to Audrey Ramplin and Yunus Kippie for their administrative and technical support. I acknowledge the input of Prof Edith Beukes, Department of Chemistry, UWC for always willing to assist in running a handful of samples for NMR. I sincerely appreciate the effort and work of Dr Sylvester Omoruyi and Prof Okobi Ekpo, Department of Medical Bioscience, University of the Western Cape for assisting with my biological studies. I also appreciate the work done by the people of Central Analytical Facilities at Stellenbosch University in providing MS data of my samples. To my wonderful colleagues in the laboratory, I am forever grateful for your unquantifiable support throughout the course of my study.

To my family and friends that include my dad (Dr Mathew Adelusi Egunlusi), my mom (Mrs Veronica Olufunmilayo Egunlusi), my sisters (Oluwatosin A. Egunlusi; Abimbola O. Egunlusi; & Oluwafunmilayo G. Egunlusi), Dr Oluwaseun A. Fadipe and family, Dr Segun A. Akinyemi and family, my wonderful in-laws (Mr & Mrs Solomon Adeleye, Tobi Adeleye & Samuel Adeleye), Mrs Ayodele D. Adeniyi and family, Adeyemi Adegoke, Omolola Afolayan, Reverend Paul Aghedo, Mrs Oluwakemi Adewumi and family, Dr Oluwatoyin Ayodele, Mr Tosin Aina and family, Onyinye Akunne, Dr Olushola R. Adeniyi and family, Dr Ifeoluwa Omodanisi, RCCG household of God parish, staff of Clicks, Mediclinic Cape gate, VPH pinelands and others, I am grateful for your prayers, emotional support and words of encouragement, particularly during difficult times throughout my project.

To my dear wife Adeola (Onitemi), your prayers, love, patience, support and sacrifices are invaluable. You are indeed a blessing, and I love you now and always. Thank you very much. Lastly, to my son (Israel O. Egunlusi) and my princess (Elizabeth E. Egunlusi), the smiles on your faces each time I get home after a hectic day uplifts my spirit. You are deeply loved.

Key words

Neurodegenerative disorders

Excitotoxicity

Norbornane

Cytotoxicity

NMDA receptors

Voltage gated calcium channels

Oxidative stress

Neuroblastomas SH-SY5Y cells

Polycyclic cage

Apoptosis

Calcium influx

Neuroprotection



Abstract

Neurodegenerative disorders are characterised by progressive loss of the brain's physiological functions as a result of gradual degeneration of neurons in the central nervous system. Even though they are classified as diseases of the elderly, occurrence earlier in life is possible, but that would suggest the influence of genetic and/or environmental factors. Due to the continuous rise in modernisation and industrialisation over the years, there has been an increase in incidence and prevalence of neurodegenerative disorders. With the advances in technology and life expectancy, the rates of the common forms (Alzheimer's disease and Parkinson's disease), are expected to increase exponentially by 2050. Unfortunately, there is still no clinically approved treatment or therapy to slow down or halt the degenerative process as most registered drugs only offer symptomatic relief. Confounding this issue is the lack of definite mechanism of neurodegeneration, which is still poorly defined and not completely understood. Nonetheless, the pathology of most neurodegenerative disorders is believed to be a combination of interrelated processes that eventually leads to neuronal cell death. Among the postulated processes, the impact of excitotoxicity mediated by NMDA receptor over-activation is prominent and it is implicated in virtually all neurodegenerative disorders. With this basic insight, it is believed that molecules capable of inhibiting NMDA receptors and associated calcium channels, without affecting the normal physiological functions of the brain, could potentially serve as good neuroprotective drugs. Competitive and uncompetitive blockers (MK-801 and ketamine) have been explored, but none were clinically accepted due to undesirable side effects such as hallucinations, sedation and depression. However, NGP1-01, a polycyclic cage molecule, has been shown to be neuroprotective through modulation of NMDA receptors and voltage gated calcium channels and attenuation of MPP⁺-induced toxicity. A similar approach could be useful in the design and development of new neuroprotective drugs.

The aim of this study was to synthesise a series of open and rearranged cage-like molecules and explore their neuroprotective potential in neuroblastoma SH-SY5Y cells. The proposed structures, with norbornane scaffolds that contained different moieties, were designed to structurally resemble NGP1-01 and MK-801. Once synthesised, the compounds were purified and characterised, and were evaluated for their biological activities. Compounds were first screened for cytotoxicity at different concentrations. Thereafter, they were evaluated for

neuroprotective effects against MPP⁺-induced excitotoxicity and for calcium flux modulatory effects on NMDA receptor and voltage gated calcium channels.

The norbornane derivatives were synthesised and characterised, and all final products were afforded in sufficient yields. All compounds with the exception of two compounds displayed good cytotoxic profiles towards the SH-SY5Y neuroblastoma cells at 10 µM, 50 µM and 100 µM concentrations as they demonstrated percentage cell viabilities close to 100% (control treated cells). Only two compounds showed percentage cell viability of 51% and 59% at 100 µM. Utilising the same cell line, all compounds, tested at 10 µM, attenuated MPP⁺-induced toxicity after 24 hours of exposure to a neurotoxin. This was evident in the 23% to 53% enhancement (significant with $p < 0.05$) in cell viability when compared to the MPP⁺ only treated cells. In comparison to known NMDA receptor and/or voltage gated calcium channel blockers (MK-801, NGP1-01 or nimodipine), the synthesised compounds demonstrated mono or dual inhibition of calcium channels as they effectively attenuated calcium influx by blocking NMDA receptors and/or voltage gated calcium channels expressed in neuroblastoma SH-SY5Y cells. This group of compounds were found to be more potent NMDA receptor inhibitors, probably due to similarities with MK-801 and memantine, than voltage gated calcium channel inhibitors. All compounds demonstrated moderate to good calcium inhibitory effects at NMDA receptors in the range of 23% to 70% while a selected few displayed very little or no activity at the voltage gated calcium channels.

In conclusion, 27 compounds with norbornane scaffolds were successfully synthesised and evaluated for cytotoxicity and neuroprotection. The abilities of the synthesised compounds to protect neurons from the neurotoxin MPP⁺ and reduce calcium flux into neuronal cells were successfully demonstrated. These characteristics are essential in neuroprotection as they may prove significant in halting or slowing down the disease progression. The compounds showing a good cytotoxicity profile, neuroprotective effects and ability to reduce calcium overload, could potentially act as neuroprotective agents with good safety profiles or contribute as lead structures to the development and design of structurally related molecules that could clinically benefit people with neurodegenerative disorders.

CHAPTER 1

Introduction

1.1 Neurodegeneration

1.1.1 Neurodegenerative disorders

In neurodegenerative disorders, neuronal cells are subjected to death either by necrosis or apoptosis in response to cellular stimuli or injury. Neuronal damages are usually slow and progressive leading to loss of cell physiological functions (Ghavami *et al.*, 2014). These disorders, which share similar histopathological features; include Parkinson's disease (PD), multiple sclerosis (MS), human prion disease, Alzheimer's disease (AD), frontotemporal dementia, Huntington's disease (HD) and amyotrophic lateral sclerosis (ALS). They have been shown to exhibit common cellular and molecular mechanism (Gibbs and Braun, 2008; Eftekharzadeh *et al.*, 2016; Hasegawa *et al.*, 2017; Croese and Furlan, 2018). Generally, neurodegenerative disorders are characterised by distinctive features like selective loss of neurons, change in synapses and neuro-inflammation. However, clinical features presented by respective diseases differ and depend on the area of the brain or central nervous system affected (Kumar *et al.*, 2016; Dwivedi *et al.*, 2019). In AD, degeneration of neurons is detected mainly in the hypothalamus, amygdala and cortex regions of brain. These regions are essential part of the brain necessary for memory and cognitive functions. Neuronal loss and functions in the substantia nigra and striatum are characteristic features of PD, which are clinically presented as tremor, rigidity, bradykinesia and postural instability. The loss of several neurons in the basal ganglia, striatum and cerebral cortex is associated with the clinical presentations like involuntary movements, cognitive impairment, dementia and psychiatric disturbances, observed in HD. ALS is characterised by progressive loss of lower motor neurons in the spinal cord and brainstem and atrophy of upper motor neurons in the motor cortex, resulting in muscle weakness and paralysis (Fratiglioni and Qiu, 2009; Kumar *et al.*, 2016).

The pathogenesis of most neurodegenerative disorders are linked to a quite number of factors that are summarised into three namely: age, environmental and genetic factors. It has been shown that as one ages, the brain begins to lose its functional and structural plasticity through processes such as altered brain proteostasis, oxidative stress creation, alteration in gene expression, dysfunction of neuroendocrine due to corticosteroid exposure, alteration of calcium metabolism, mitochondrial dysfunction, impaired energy metabolism, and dysregulation of

neuro-transmission homeostasis, at both cellular and molecular levels. Exposure to environment variables such as metals, pesticides, pollutants, toxic food, microorganisms, virus infections, smoking and drug abused have been identified as factors that contribute to the pathogenesis of neurodegenerative disorders either by influencing expression of genes *via* DNA methylation, histone modification and micro-RNA-postranscriptional gene silencing or by direct injury. Moreover, some disorders such as ALS and HD are linked to mutations in specific genes that completely alter the functions of expressed proteins leading to neuronal cell death (Prolla and Mattson, 2001; Musgrove *et al.*, 2015; Kavitha *et al.*, 2020).

Most commonly neurodegenerative disorders such as PD and AD occur predominantly in the elderly. However, it can also emerge at early stage of aging, but that would suggest genetic influence or exposure to toxic chemicals as observed in HD and ALS (Bondy, 2016). Nonetheless, ageing is still considered to be one of the major risk factors of neurodegenerative disorders as it is associated with significant loss of synapses, neurons and brain functionality in specific region of the brain (Daniele *et al.*, 2018). AD is the most common neurodegenerative disorder, followed by PD. These disorders affect nearly 1% of the world's older population with this numbers expected to escalate exponentially in the next 20 years owing to increase in life expectancy of the population (Malhotra, 2018). Due to increasing prevalence, the financial costs for the management of AD and PD are expected to rise to \$ 1.2 trillion and \$ 18.5 billion, respectively by 2050. In addition to the treatment costs, patients' quality of life is also drastically reduced, causing significant economic and social burdens to both the patient and their families (Yacoubian, 2017; Pena-Bautista *et al.*, 2019).

Drug discovery for major neurodegenerative disorders has been a challenge for years as they are associated with extremely high failure rate and an ever increasing clinical trial cost. Moreover, the mechanism of neurodegeneration is still poorly defined despite several human and animal studies. As such, the treatments approved only offer symptomatic relief with no prospect of halting or slowing down disease progression (van Eijk *et al.*, 2018; Swalley, 2020).

1.1.2 Mechanism of neurodegeneration

Using various models and approaches, countless studies have proposed several pathways or mechanisms leading to neuronal cell death. Despite the vast knowledge, the mechanisms of neurodegeneration are still poorly defined. However, it is believed that the pathology of neurodegenerative disorders is caused by interrelated processes that include dysregulation of protein homeostasis or proteostasis, oxidative stress, excitotoxicity, mitochondrial dysfunction

(Elfawy and Das, 2019), protein aggregation (Garcia-moreno *et al.*, 2019), lipid peroxidation, neuroinflammation (Ellwardt and Zipp, 2014), dysregulation of microglia, and defects in axonal transport and nucleocytoplasmic transport (Gan *et al.*, 2018). Protein homeostasis can be dysregulated through the inhibition of ubiquitin-proteasome and autophagy-lysosome systems to promote accumulation of protein aggregates that in turn inhibit proteasome activities, thus promoting the neurodegenerative process (Daniele *et al.*, 2018). Although the exact reason for mitochondrial dysfunction is not clear, abnormal change in mitochondrial morphology mediated by mtDNA mutation, oxidative damage and/or mitochondrial protein aggregation is believed to be the main reason for the dysfunction. Of the mediated factors, the effect of oxidative stress is prominent as it generates reacting oxygen species (ROS) that is capable of damaging mitochondrial proteins, nucleic acids, and lipids, and in turn generate more intracellular ROS leading to more mtDNA mutations (Elfawy and Das, 2019). In addition to these detrimental effects, mitochondrial dysfunction also results in ATP depletion, electron transport chain enzyme inhibition, Ca^{2+} imbalance and caspase-3 activation, which all contribute to the degenerative process (Wu *et al.*, 2019). In excitotoxicity, prolonged activation of glutamate receptors leads to downstream effects such as calcium influx, oxidative stress and mitochondrial dysfunction (Shinoda *et al.*, 2016). Oxidation of lipids, mediated by oxidative stress, results in lipid peroxidation, which produces cellular damage and generate new free radicals that alters membrane- and circulating lipids and cellular functions, as observed in various neurodegenerative disorders. Increase in lipid peroxidation has also been linked to high enzymatic activities of acetylcholinesterase and butyrylcholinesterase and toxin (arbin and methylmercury) exposure. Despite the documented effects of lipid peroxidation, it is still not clear if lipid peroxidation is the cause or the consequence of neurodegenerative processes (Pena-Bautista *et al.*, 2019). Altogether, this and other mechanisms of neurodegeneration lead to neuronal cell death either by apoptosis or necrosis.

1.1.3 Excitotoxicity in neurodegenerative disorders

Among the major pathways leading to neurodegenerative disorder, the effect of excitotoxicity is profound, and it is implicated in virtually all forms of neurological disorders. In excitotoxicity, excessive extracellular glutamate prolongs the activation of NMDA receptor channels and associated channels (voltage gated calcium channels), and subsequently elevate intracellular Ca^{2+} to such an extent that it disrupts the calcium homeostasis process (Shinoda *et al.*, 2016; Boussicault *et al.*, 2018). Ultimately, the consistent elevation of intracellular calcium ion induces a cascade of events *via* enzymatic pathways (Liu *et al.*, 2020), which

inevitably compromise cell survival (Bano and Ankarcona, 2018) leading to detrimental effects such as mitochondrial dysfunction, calpain activation, lipid peroxidation, endoplasmic reticulum, oxidative stress and protein aggregation (Zadori *et al.*, 2012). These detrimental effects consequently damage cellular components or organelles thus promoting neuronal cell death.

1.1.4 MPP⁺-induced toxicity in neurodegenerative disorders

Several *in vivo* and *in vitro* studies, mainly in Parkinsonian model, have demonstrated the toxic and destructive effects of 1-methyl-4-phenylpyridinium (MPP⁺) on dopaminergic neurons (Cai *et al.*, 2017). MPP⁺ is an active metabolite of 1-methyl-4-phenyl-1,2,3,6-tetrahydropyridine (MPTP) formed *via* enzymatic action of monoamine oxidase type B (MAO-B) in the brain. MPTP can penetrate the blood brain barrier easily to be oxidised into MPP⁺. This active metabolite, a toxic cation, is known to have high affinity for the dopamine active transporter, and is able to gain entry into the dopaminergic neurons *via* this medium (Jouha *et al.*, 2017; Amo *et al.*, 2019). Upon entry, MPP⁺ accumulates in the dopaminergic neuron and elicits a number of effects that include neuroinflammation (Peng *et al.*, 2019), generation of ROS and mitochondrial dysfunction, which trigger apoptotic death of dopaminergic neurons (Bondy, 2016; Elfawy and Das, 2019; Obata, 2019). MPP⁺ induce mitochondrial dysfunction in neurons by interfering with the mitochondrial complex 1 of the electron transport chain. Such interference compromises mitochondrial integrity by opening mitochondrial transition pore, thus resulting in the production of reactive oxygen species (Jovanovic-Tucovic *et al.*, 2019; Shishido *et al.*, 2019). Due to dopaminergic neuronal loss, the cortical control of movement is destroyed leading to the symptoms of Parkinsonism (Jouha *et al.*, 2017).

1.2 Rationale

As discussed earlier, the role of calcium overload through glutamate induced excitotoxicity is crucial in the pathology of several neurodegenerative disorders. As such, regulating calcium influx by inhibiting NMDA receptors and voltage gated calcium channels (VGCC) is expected to produce significant neuroprotection. However, achieving a clinically acceptable molecule to block glutamate-induced neurotoxicity has been a major challenge in the sense that the same process needed for normal glutamatergic physiological function is also responsible, in excess, for excitotoxicity. Competitive (midafotel and selfotel) and uncompetitive (MK-801) NMDA receptor blockers have been shown to potently counteract glutamate-induced excitotoxicity, but are marked by undesirable psychotomimetic side effects. On the other hand, the polycyclic

cage amines, amantadine and memantine, are approved by the FDA and are clinically tolerated for the treatment of Parkinson's disease and Alzheimer's disease, respectively. Their tolerability and safe side effect profiles are linked to moderate affinity at the PCP binding site of NMDA receptors. Despite the activities of these polyamine amines, they only offer symptomatic relief without the prospect of halting or slowing down disease progression. Interestingly, a series of pentacycloundecylamines with the norbornane scaffold have been shown to exhibit neuroprotection properties. One very good example is NGP1-01, a polycyclic closed cage amine with a mode of NMDA receptor antagonism similar to memantine that may suggest similar safe side effect profile (Duque *et al.*, 2010; Geldenhuys *et al.*, 2007; Van der Schyf and Geldenhuys, 2009). This cage molecule and its derivatives possess multifunctional neuroprotection through dual attenuation of calcium influx (NMDA receptor and voltage-gated channels) and inhibition of MPP⁺-induced toxicity (Geldenhuys *et al.*, 2003; Youdim *et al.*, 2007).

The synthesis of opened cages with norbornane scaffold has been explored, but the medicinal chemistry profiles are pretty much limited to antiviral, antibacterial, and antitumor activities. The neuroprotective effects, *via* NMDA receptors, voltage gated calcium channels and MPP⁺ induced neurotoxicity of these norbornane derivatives, are yet to be properly explored. The need to develop neuroprotective molecules, with safe side-effect profiles, against glutamate- and MPP⁺-induced neurotoxicity justify the investigation of opened- and rearranged- cage norbornane derivatives, structurally similar to NGP1-01 and MK-801 (figure 1.1), as potential multifunctional neuroprotective agents.

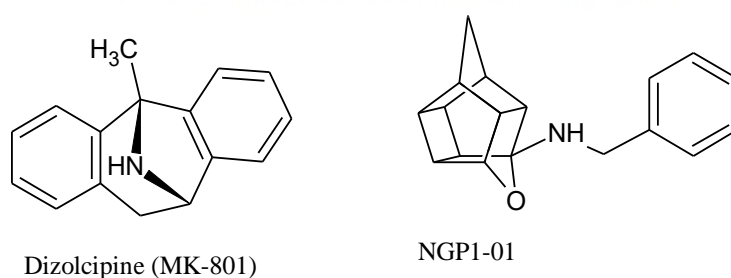


Figure 1.1: Polycyclic NMDA receptor antagonists.

SH-SY5Y cells are the most commonly used cell line in neurological research. Their activities and functions are believed to mimic that of the human brain and justify their usage in neurochemical studies. Whenever this cell line is used, particularly in a MPP⁺-induced

excitotoxicity study, MPP⁺ as opposed to MPTP is generally required to induce cellular model of PD due to inability of the SH-SY5Y cells to convert MPTP to MPP⁺ (Amo *et al.*, 2019).

1.3 Objectives

The crucial role of the glutamate- and MPP⁺-induced excitotoxicity in neurodegenerative disorders have been highlighted, and the neuroprotective effects of certain polycyclic closed cage amines, NGP1-01 in particular, have been illustrated. However, little is known about the neuroprotective effects of polycyclic open cage molecules with the norbornane scaffold. The proposed novel opened- or rearranged cages were designed to structurally resemble NGP1-01, memantine or MK-801 and to exhibit functional moieties necessary for neuroprotection. As such, we postulated that these polycyclic cage molecules would mimic the NMDA receptor and voltage gated calcium channel antagonism and the MPP⁺ neurodegeneration inhibition of NGP1-01. Modification of the functional moieties is expected to allow better understanding of the structure-activity relationship of these groups of compounds. On the basis of this information, the following objectives were set:

1. The synthesis, purification, and structural characterisation of novel opened cage norbornane scaffolds containing moieties such as furandione, pyrrolidinedione and benzoquinone, and these moieties will be conjugated with various aliphatic and heterocyclic amines (figure 1.2). These moieties are cyclic molecules that differ in ring size and electron withdrawing group type. The influence of these functional moieties will be explored;

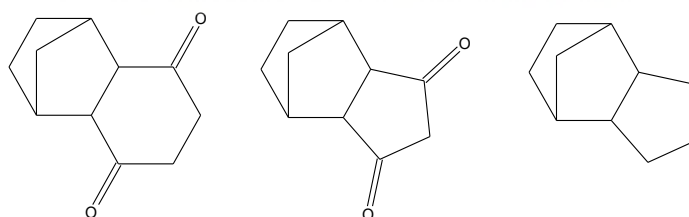


Figure 1.2: Analogues of opened cage norbornane scaffolds.

2. The synthesis, purification, and structural characterisation of novel rearrange closed cage norbornane scaffolds fused with piperidine moieties (figure 1.3);

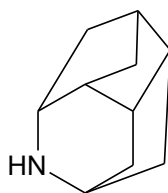


Figure 1.3: Rearranged closed cage analogue.

3. The cytotoxic screening of synthesised compounds against the neuroblastoma SH-SY5Y cell line for the purpose of identifying a suitable concentration for further biological testing;
4. The evaluation of potential neuroprotective effects and structure activity relationship of synthesised compounds against MPP⁺-induced excitotoxicity in a neuroblastoma SH-SY5Y cells;
5. And the evaluation of calcium inhibitory effects and structure activity relationship of synthesised compounds, compared to known blockers, on NMDA receptor and voltage gated calcium channels after NMDA/glycine stimulation and/or KCl depolarisation, respectively.

With these objectives, the aim was to develop multifunctional neuroprotective agents with safe side effect and/or toxicity profiles, which will potentially not only manage the symptoms but also halt or slow down the neurodegenerative process.

1.4 Conclusion

This chapter highlights the persistent and detrimental effects of neurodegenerative disorders in modern days. If these problems are not addressed, particularly with increasing life expectancy, they will escalate in the near future. Not only will the impact be felt by the affected individual as quality of life is reduced, it also becomes a burden to the society as a whole. Understanding the mechanism of neurodegeneration is crucial in devising strategies to effectively treat these disorders. However, no study has established a definite mechanism and current clinically approved treatments are only able to provide symptomatic relief. Therapeutic agents or molecules with safe side effect and/or toxicity profiles are required to either halt or slow down disease progression. NGP1-01 has shown to be neuroprotective, and as such is regarded as a promising therapeutic lead. Structurally related analogues, as clearly defined in the objectives, are hypothesised to exhibit neuroprotective properties. If the set objectives are met, it will add to the series of existing molecules with promising therapeutic effects as well as assist our

understanding of the structure activity relationships of these set of compounds. The remaining chapters in this study contain, the review of relevant literature (**chapter 2**), the synthesis of desired compounds (**chapter 3**), the biological evaluation of the synthesised compounds (**chapter 4**), and finally the concluding remarks of the study (**chapter 5**).



CHAPTER 2

Literature review

2.1 Neurodegenerative disorders

2.1.1 Introduction

Neurodegenerative disorders (NDs) are disorders characterised by persistent and progressive loss of neuronal function that eventually lead to neuronal death and reduction of sensory, motor, cognition and memory function (Luo *et al.*, 2016; Procaccini *et al.*, 2016). This neuronal cell death is the reason for the profound decrease in size and volume of brain tissue observed in the human brain (Ahmad *et al.*, 2016). These diseases, with diverse pathologies, share similarities in clinical manifestation and connections (Ghani *et al.*, 2015; Vranova *et al.*, 2016). Most of these disorders are associated with gradual loss of bodily or physiological functions, which eventually leads to neuronal cell death (Mazibuko *et al.*, 2015).

These disorders, the main cause of disability among the elderly, occur in over 30 million persons worldwide and is expected to increase sequentially over the years because of increased lifespan and age of individuals. The occurrence of these diseases at an early age depends solely on exposure to xenobiotics, defective lysosomal function and other environment factors. Studies have demonstrated that prenatal and/or postnatal exposure to xenobiotics such as metals, ambient particulate matter, organochlorine pesticides or organophosphate pesticides, are associated with neurodegenerative disorders and impairment of neuropsychological development (Hernandez *et al.*, 2016; Heusinkveld *et al.*, 2016; Saravi and Dehpour, 2016). The exposure to xenobiotics and aging remains important aetiological factors of many neurodegenerative disorders (Vadakkan, 2016; Vincenzetti *et al.*, 2016). Evidence in at least 40 neurodevelopmental and neurodegenerative diseases of childhood described the impact of defective lysosomal function as a major factor in the pathogenesis of adult and late-age onset disorders. In fact, an alteration in just a single lysosomal gene can induce a congenital disorder or late-onset neurodegenerative disease. However, this depends on the type of mutant gene and the level of severity of associated lysosomal disruption. Also, evidence from associated genetic studies strengthen the argument that exposure to additional pathogenic factors, during adulthood and aging, may hasten subclinical lysosomal impaired functions towards a catastrophic or severe lysosomal dysfunction, which ultimately promote neuronal cell death associated with neurodegenerative disease. Genetic disorders linked to a mutant lysosomal

gene exert their destructive effects by disrupting lysosome functions throughout organs or cells in the body. Of the organs affected, the lysosomal disruption in the brain is prominent. This explains why the central nervous system is highly prone to autophagic-lysosomal destruction (Colacurcio & Nixon, 2016).

These disorders include Parkinson's disease (PD), Parkinson's disease dementia (PDD), Alzheimer's disease (AD), progressive supranuclear palsy (PSP), amyotrophic lateral sclerosis (ALS), Huntington disease (HD), dementia with Lewy bodies (DLB), multiple system atrophy (MSA), Prion disease, corticobasal degeneration (CD) and frontotemporal dementia (FTD) (Mazibuko *et al.*, 2015). AD is characterised by the accumulation of extracellular deposits of amyloid- β peptides (A β) and hyperphosphorylated tau protein that forms senile plaques and neurofibrillary tangles, respectively. These plaques and tangles mediate a cascade of events that result in progressive cognitive decline. As such, it is the most prominent neurodegenerative disease in which cytoskeleton damage is commonly discussed. PD is generally associated with the formation of Lewy bodies, cytoplasmic inclusion of α -synuclein, and the progressive loss of dopaminergic neurons that are linked to its clinical characteristic features like motor impairment. In HD, mutation of the huntingtin genes is the major pathological hallmark of this disorder. The altered genes are known to form neuronal intranuclear inclusion, which ultimately affect various muscle coordination-, cognitive- and behavioural functions. ALS is characterised by a progressive loss of motor neurons, mainly in the upper and lower parts and it is associated with limited voluntary movement of muscles (Eira *et al.*, 2016).

2.1.2 Incidence, prevalence and cost implication of neurodegenerative disorders

The incidence of neurodegenerative disorders that reportedly cause irrevocable harm to the human brain is increasing at an exponential rate worldwide (Yang *et al.*, 2015). According to the World Health Organisation (WHO), neurological disorders have affected nearly 1 billion people worldwide with 450 million suffering from mental or associated behavioural disorders. Approximately 6.8 million deaths linked to brain-related disorders are recorded worldwide each year (Hanamsagar and Bilbo, 2016). The prevalence of these disorders, particularly PD and AD, is about 3% at the age of 65 and rises to 55% by the age of 95 (Procaccini *et al.*, 2016). AD is the most common form of neurodegenerative disorder in the elderly, and it is reported to be the sixth-leading cause of death in the United States. In 2010, roughly 5 million of the American population (above 65 years old) were diagnosed with AD, which correspond to approximately 11% of the total population. The prevalence for PD, the second most common

neurodegenerative disorder (Di Domenico *et al.*, 2017), in the United States of America was estimated at 630,000 cases as at 2010. By 2040, it is predicted that neurodegenerative disorders will surpass cancer as the most prevalent cause of death in industrialised countries. Numerous strategies and devises that involve the design and development of drugs and diagnostic tools have already been employed and extensively researched. Moreover, there is a need for effective diagnostic tools for early detection of these disorders as well as effective drugs with good safety profiles to slow down or halt the degenerative process. This approach is crucial for the successful treatment of these disorders. Current treatments primarily offer palliative care and very modest advancement has been achieved (Mazibuko *et al.*, 2015; Luo *et al.*, 2016; Yacoubian, 2017). With increasing healthcare cost as a result of the proportional increase of elderly individuals in the population, NDs are often considered a major health problem with a significant economic burden. The socioeconomic effects of these disorders are felt in different parts of the world. The worldwide prevalence of dementia has doubled in the last 20 years and the cost on health care, in dementia and related cases, is increasing at an alarming rate (Ghani *et al.*, 2015). The rise in numbers of AD and PD cases is expected to continue in the next several decades. As such, the societal burden and financial costs on these common disorders are predicted to be massive and unaffordable, particular for developing countries. In the case of AD and related dementias, the total health care costs were estimated at \$214 billion in 2014, and with the anticipated rise in AD prevalence, health care costs for AD is tipped to escalate and reach the \$1.2 trillion mark by 2050. By comparison, health care costs for PD are far much less due to lower prevalence but are still considered a high cost. In the United States alone, all medical costs associated with treatment of PD were estimated at \$8 billion in 2010, and the cost related to retrenchments and other indirect costs were estimated at \$6.3 billion. By 2050, these medical costs and associated costs is predicted to reach a staggering \$18.5 billion. Even though other neurodegenerative disorders such as ALS and HD are less common, there impact in terms of disability and loss of life is still substantial (Yacoubian, 2017). In addition to the high treatment cost, patients with neurodegenerative diseases and other mental illnesses are subjected to stigma and social exclusion as well as reduced or loss of quality of life.

2.1.3 Gender role in neurodegenerative disorders

A number of neurodegenerative disorders and associated disorders differ in the prevalence and/or therapeutic outcomes based on gender differences. This justifies the need for the consideration of gender when considering treatment, although the links between gender differences and neurodegenerative disease progression still remain unclear to many

researchers. Nonetheless, in numerous neurodegenerative disorders, there are noticeable gender differences in the incidence, severity, and/or the progression of diseases. For example, autism is more often diagnosed in male children than female children, while the number of females who suffers from depression and anxiety is significantly higher than their male counterparts. Also, the incidence of stroke is lower in females than males. However, they tend to demonstrate poorer outcomes and suffer a horrific and catastrophic decline in brain functions after a stroke incident when compared to males (table 1). Gender differences linked to occurrence and outcome of neurodegenerative disorders still pose problems in the diagnosis and treatment of patients. This strengthen the need for more investigation or studies to properly understand the molecular mechanisms or pathways that determine these differences in both the male and female (Hanamsagar and Bilbo, 2016).

Table 1: Sex differences in incidence and outcomes of neurological conditions commonly see in humans (Hanamsagar and Bilbo, 2016).

Neurological condition	Sex difference in incidence and prevalence	Sex difference in severity or outcome
Attention deficit hyperactivity disorder	Occur more in boys (70%) than Girls (30%)	Deterioration of motor skill function is more severe in boys. Also, distractibility is higher in boys than girls.
Alzheimer's disease	Higher prevalence in women above age 65 years	Higher decline in cognitive functions observed in women
Amyotrophic lateral sclerosis	Higher occurrence and earlier onset in men. Increased risk with post-menopausal women	Poorer survival rate in women
Autism spectrum disorders	Incidence and prevalence are higher in boys than girls	Vague and heterogeneous findings. Meta-analysis shows that females have less severe stereotyped and repetitive behaviours
Depression and anxiety disorder	Higher prevalence are common among females than males	Severity of clinical associated symptoms or features are prominent in women than

		men. Women more prone to subclinical depression
Juvenile Batten's disease	Available data on incidence are inconclusive. However, late onset are observed in females	Females known to experience more severe symptoms. The morbidity rate is higher in females than males.
Multiple sclerosis	Mostly affect women	The progression of disease is faster in men.
Parkinson's disease	Higher incidence in men	Neuronal degeneration occurs at a slower rate in women than men
Schizophrenia	Early onset and higher incidence in men	Poorer prognosis in men owing to severe symptoms and weaker response to antipsychotic drugs
Stroke	Later onset in women and higher incidence in men	Women tend to not fully recover after a stroke as they suffer from more physical disability, thus less favourable outcome displayed when compared to men.

2.2 Pathology of neurodegenerative disorders and established therapeutic approaches

2.2.1 Introduction

Neurodegenerative disorders are multifactorial diseases that share many common features such as a late appearance in life, neuronal loss and synaptic abnormalities. They also share common molecular mechanisms that include excitotoxicity, mitochondrial dysfunction, apoptosis, oxidative stress and impaired protein homeostasis (Ahmad *et al.*, 2016). These disorders exhibit various overlapping symptoms that include, amongst others, cognitive impairment, dysarthria, or motor dysfunction. The fundamental pathological trademark commonly observed in most neurodegenerative disorders is the continuous degeneration of a group of neurons in the brain and/or the spinal cord. Specific parts of the brain and/or spinal cord where neurons are

degenerated often dictates the clinical manifestation or symptoms of each neurodegenerative disorder (Yacoubian, 2017). The condition of neurons is exacerbated by continuous decrease in cerebral blood flow or cerebral hypoperfusion leading to further degeneration of neurons. This decreased blood supply to the brain have been observed in several dementia patients and in various patients with age-related neurological disorders, particularly those suffering from AD and PD. Interestingly, evidence from a neurological study has provided a link between low cerebral blood flow and worsened neurodegenerative disease. The same study also suggested that reduced blood flow could accelerate disease progression from a mild cognitive impairment to full-blown Alzheimer's disease (Tomycz, 2016). Countless studies have proposed overlapping factors such as age, genetic and environmental, and molecular mechanisms that are often crucial in the development or pathogenesis of most neurodegenerative disorders. However, each detailed mechanism is inconclusive as none could establish a structurally clear mechanism. Nonetheless, the general consensus is that, in each distinct neurodegenerative disorder, a group of vulnerable neurons is subjected to cell death that is necrotic or apoptotic in nature. This neuronal cell death is usually a result of several interrelated processes including, amongst others: oxidative stress, excitotoxicity (Leist & Nicotera, 1998), RNA metabolism, mitochondria dysfunction (Moreira *et al.*, 2012), protein aggregation and propagation (Celsi *et al.*, 2009; Mehta *et al.*, 2013), proteasomal dysfunction, autophagic/lysosomal dysfunction, prion-like spread, loss of growth factors and neuroinflammation (Yacoubian, 2017). Despite immense research and knowledge, and the continuous refinement and improvement in these basic insights, the mechanisms of development of most neurodegenerative disorders are still structurally disjointed and poorly defined (Qureshi & Mehler, 2013). More experimental models are thus needed to understand the underlying molecular mechanisms or pathways and to develop pharmacological and therapeutic interventions that will successfully treat these neurodegenerative disorders (Dey and Nath De, 2015).

2.2.2 Parkinson's disease

PD is a progressive age-related and incurable neurodegenerative disorder. It is sporadic in nature, and defined as a multi-factorial disorder, where a genetic basis interacts with environmental factors in a complexly linked manner (Landolfi *et al.*, 2017; Pezzi *et al.*, 2017). PD is the second most frequent neurodegenerative disorder, characterized by a progressive loss of dopaminergic neurons projecting from the substantia nigra to the basal ganglia. Patients with PD often experience cardinal motor symptoms such as gait disorder (Eisinger *et al.*, 2017; Miller *et al.*, 2018), rest tremor, bradykinesia, dysarthria, hypomimia, hypophonia,

micrographia, dysphagia, rigidity and postural instability (Landolfi *et al.*, 2017; Dickson, 2018; Mao *et al.*, 2018), and a range of frequent non-motor symptoms such as mood disorder, cognitive impairment, psychiatric disorders (Deng *et al.*, 2018), chronic fatigue, impulsivity (Du Plessis *et al.*, 2018), anxiety, depression, loss of smell, bladder dysfunction, diaphoresis, apathy, sialorrhea, sexual dysfunction, sleep disorders and gastrointestinal symptoms, particularly constipation (Chen & Dashipour, 2017; Cury *et al.*, 2018; Liddle, 2018; Wilson *et al.*, 2018; Tuovinen *et al.*, 2018; Aminoff, 2019).

The key pathological postulated features of PD are: (1) The loss of dopaminergic neurons concentrated in the substantia nigra pars compacta of the brain. Neuronal degeneration in this part of the brain is responsible for the distinctive movement disorder and vagal nerve dysfunction associated with PD; (2) Distinctive α -synuclein-containing cytoplasmic inclusion known as Lewy bodies generated from misfolded α -synuclein accumulation that forms oligomers, fibrils, and ultimately Lewy bodies. It seems that high mitochondrial stress and elevated cytosolic calcium levels are characteristic features of the dopaminergic neurons found in the substantia nigra. These features have been implicated in the promotion of α -synuclein aggregation (figure 2.1). It is believed that the pathogenic α -synuclein together with endogenous factors that make neurons more prone to destruction is likely the reason for toxicity of dopaminergic neurons observed in Parkinson's disease (Liddle, 2018). The Braak staging is well documented in many studies and the phenomenon highlight the progression of synuclein pathology from the periphery (enteric nervous system) to the caudal brainstem and then spread anterogradely or retrogradely to specific brain region, including the cortical region. As soon as Lewy bodies appear in the midbrain, particularly the substantia nigra pars compacta (SNc), motor features begin to emerge, and in advanced stages, they spread to the cortex. This may be the reason for the cognitive impairment and associated behavioural change in PD. Lewy bodies have also been shown to spread into adjacent healthy neurons in a prion-like manner. However, only a small number of patients follow this progression hence the questioning and debates around the Braak hypothesis (Chen & Dashipour, 2017; Deng *et al.*, 2018). In addition to this pathogenesis, the role of somatic mitochondrial DNA (mtDNA) mutation and accumulation in postmitotic cell population has been reported. The MtDNA accumulations are linked to increased age, and if high enough would cause a dysfunction in the respiratory chain in dopaminergic neurons of the substantia nigra (Nido *et al.*, 2018).

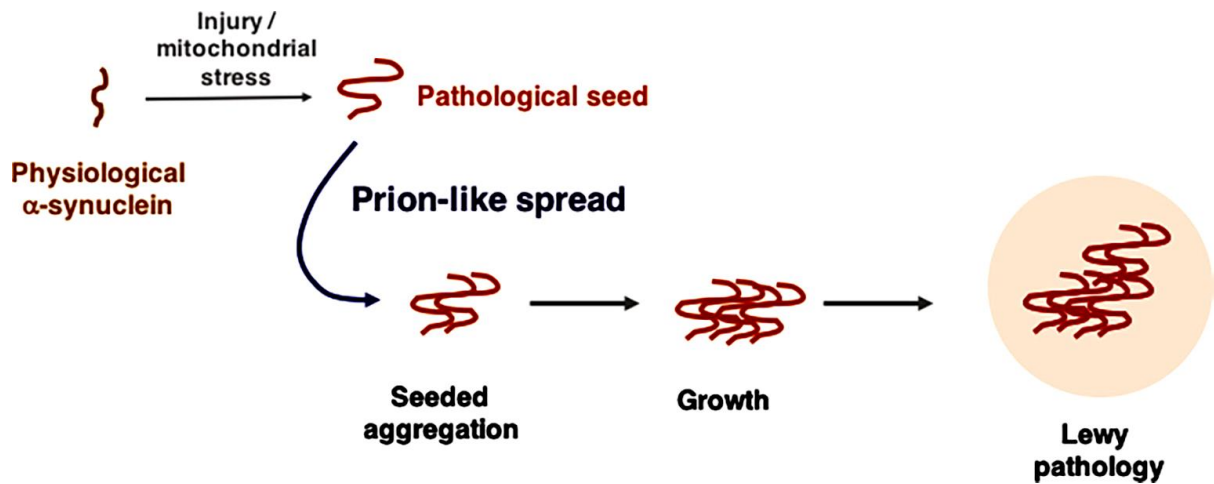


Figure 2.1: Pathological formation of Lewy bodies from seeded protein aggregation derived from distorted α -synuclein (Liddle, 2018).

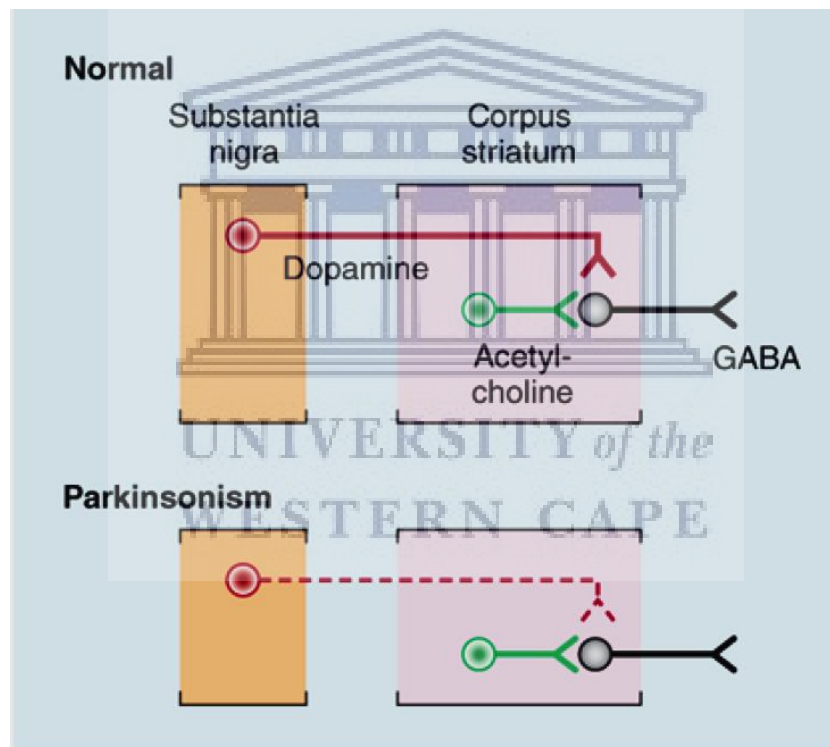


Figure 2.2: Illustration of the sequence of neurons observed in parkinsonism. Top: Dopaminergic neurons (red) originate from substantia nigra to inhibit GABAergic mediated effects from the striatum, thus allowing cholinergic neurons (green) to exert its excitatory effect. Bottom: In parkinsonism, there is a selective degeneration of dopaminergic neurons (dashed, red) (Aminoff, 2019).

Despite the continuous rise in the incidence and prevalence of PD and extensive research for several decades, the origin of the pathogenesis and the molecular determinants associated with this disorder is not completely understood and still remains vague. Moreover, there is the issue

of lack of experimental models or resources that could perfectly summarize the disease state. Unfortunately, since this disease was first described with much learnt about the pathology and pathogenesis, a large void in understanding this disease still remain. It is only by complete understanding of the pathogenic mechanisms that define this disease that one can devise or design therapeutic strategies that would halt or slow disease progression, rather than merely treat the symptoms (Ludtmann & Abramov, 2018).

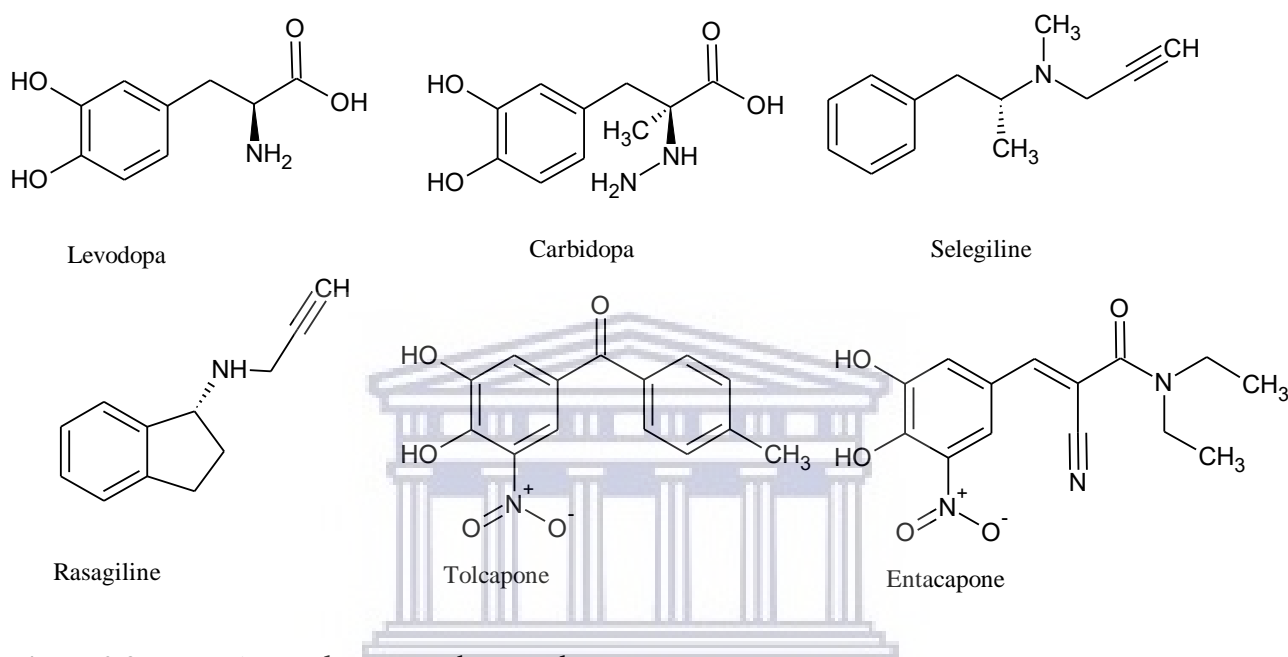


Figure 2.3: Dopamine replacement therapy drugs.

In PD, the loss in dopaminergic neurons is not only confined to the substantia nigra, but also project to the caudate putamen, a part of the basal ganglia, where dopamine indirectly inhibits the function of cholinergic neurons. In this view, it would make sense to consider both cholinergic and dopaminergic neuron imbalances in the therapeutic approaches for PD treatment (figure 2.2).

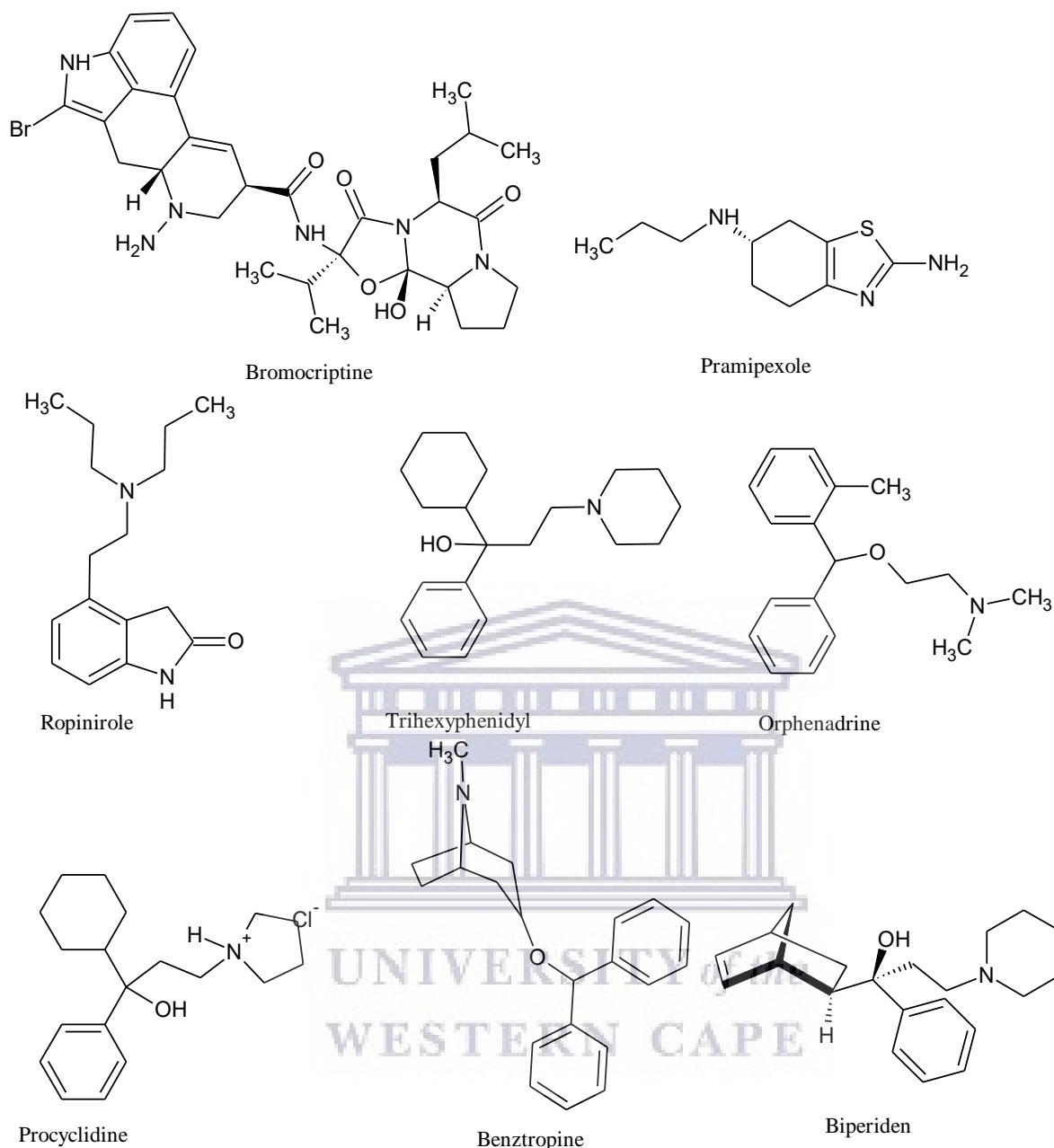


Figure 2.4: Dopamine agonists and anticholinergic drugs.

Currently, therapeutic approaches such as dopamine replacement therapy, dopamine agonist therapy, and anticholinergic therapy are employed. Dopamine replacement therapies include: levodopa and carbidopa combination; monoamine-oxidase inhibitors (MAO) such as selegiline and rasagiline; catechol-O-methyl-transferase (COMT) inhibitors such as tolcapone and entacapone; (figure 2.3) and amantadine. The dopamine agonists used in the treatment of PD include bromocriptine, pramipexole and ropinirole. Although they are less common, anticholinergic agents such as trihexyphenidyl, orphenadrine, procyclidine, benztropine, and biperiden (figure 2.4) reduce the activity of the uninhibited cholinergic neurons in the basal

ganglia (Landolfi *et al.*, 2017; Aminoff, 2019; Stringer, 2019). Unfortunately, these drugs only help to relieve symptoms without halting or slowing down the disease progression (figure 2.5).

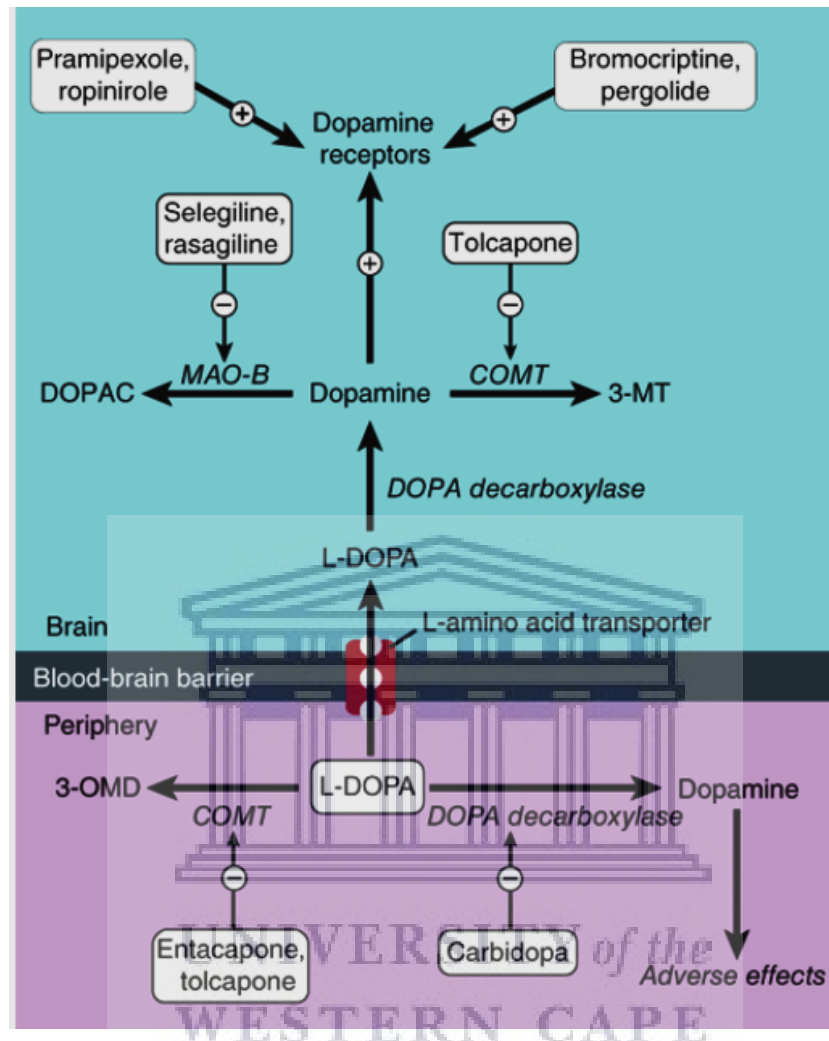


Figure 2.5: Different therapeutic strategies that enhance dopamine activities in Parkinson's disease. Clinically approved drugs and their pharmacological effects are indicated. COMT, catechol-O-methyltransferase; DOPAC, Dihydroxyphenyl acetic acid; L-DOPA, levodopa; MAO, monoamine oxidase; 3-MT, 3-methoxytyramine; 3-OMD, 3-O-methyldopa (Aminoff, 2019).

2.2.3 Alzheimer's disease

AD, first described as neuropsychiatric disorder by Alois Alzheimer (Maccioni *et al.*, 2001), affects the elderly and it is the most common among known age-linked neurodegenerative disorders. It is characterised by the irreversible degeneration and progressive damage to neurons and synapses throughout the brain, particularly the brain cortex, leading to profound inability to memorise, learn or participate in other cognitive functions (Di Domenico *et al.*, 2017; Matej *et al.*, 2019; Derakhshankhah *et al.*, 2020; Nirale *et al.*, 2020)). AD is the most

common form of dementia (60-70%) in all dementia related cases. In 2016, the number of people suffering from AD was estimated at 47.5 million with an estimated annual increase of 7.7 million per year. Worse than this, the figure is likely to reach 150 million by 2050 (Commins & Kirby, 2019; Havekes *et al.*, 2019; Singh *et al.*, 2020).

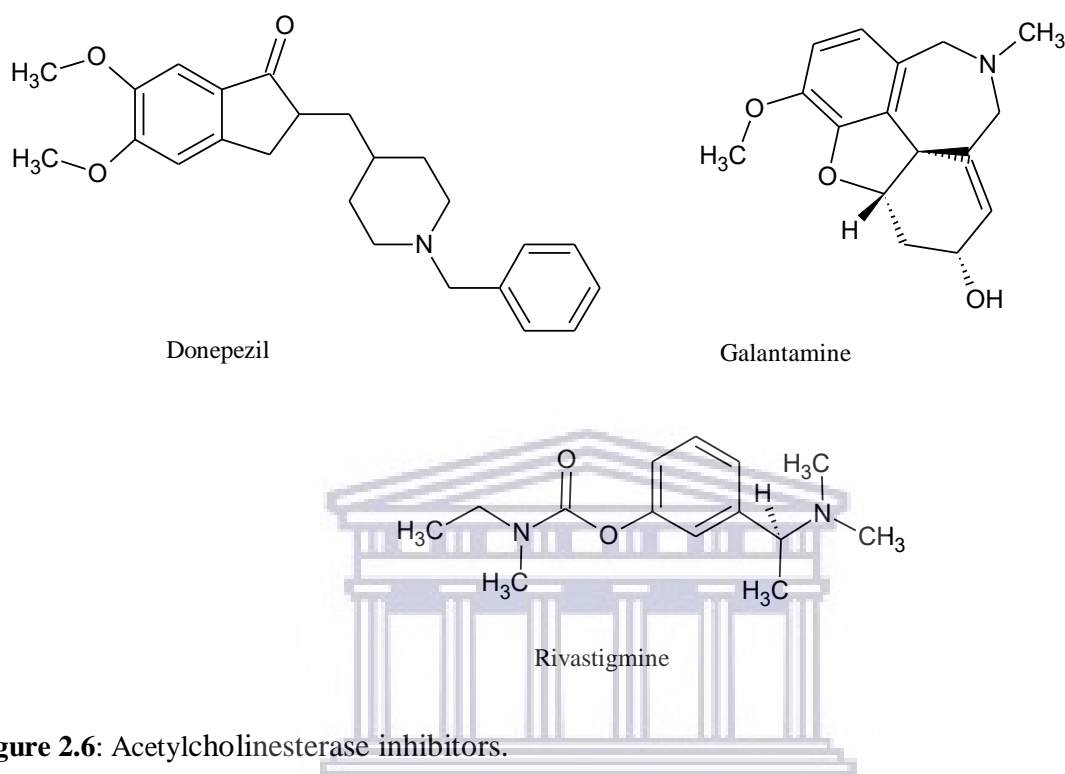


Figure 2.6: Acetylcholinesterase inhibitors.

The pathology of AD can be categorised into three hypotheses that include amyloid hypothesis, tau hypothesis and cholinergic hypothesis (Singh *et al.*, 2020). In the amyloid hypothesis, amyloid- β precursor proteins are cleaved by β - and γ -secretases in succession to produce A β peptides. These aberrant proteins (A β peptides) eventually form the core of parenchymal A β plaques that accumulate outside the cell. The distribution of these plaques, around the brain, changes with time and reflect the extent of spread of A β deposit in the diseased brain. They first appear as diffused and fleecy plaques in the neocortex of the brain and later spread to the other parts of the brain (allocortical areas, basal ganglia, thalamus, hypothalamus, midbrain, medulla, pons and cerebellum) to form neuritic and dense cored A β plaques. In the tau hypothesis, aggregation of a hyperphosphorylated form of tau proteins that would normally help in organelle transportation and microtubular assembling, results in the formation of intracellular neurofibrillary tangles (NFTs), mainly in the soma and neurites of neurons. NFTs are highly associated with a decline in cognitive function, and they are known to spread in a particular pattern. They are first detected around the entorhinal cortex and hippocampal regions. These regions are essential for cognitive functions. The next stage is to spread across

the amygdala and the anterodorsal thalamus. Thereafter, they increase their network to other cortical areas to inflict gross neuronal cell death and associated neuronal dysfunction and cognitive deterioration (Mufson *et al.*, 2016; Drygalski *et al.*, 2018; Commins and Kirby, 2019; Ozben and Ozben, 2019; Havekes *et al.*, 2019). In the cholinergic hypothesis, increased activity of acetylcholinesterase, an enzyme that hydrolyse acetylcholine, is believed to reduce the level of acetylcholine (neurotransmitter) leading to inhibition of neural transmission. This reduction negatively impact the various physiological responses or functions mediated by acetylcholine in the brain (Singh *et al.*, 2020).

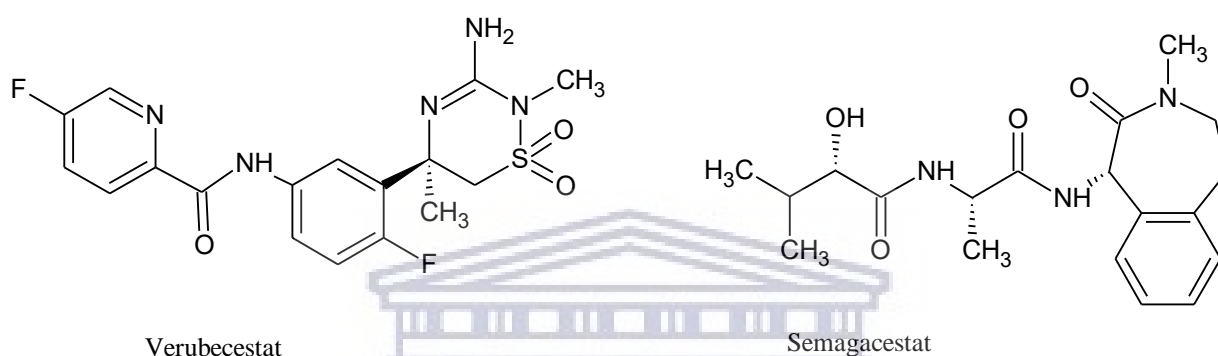


Figure 2.7: Secretase inhibitors.

Currently, there are no effective treatment that act on the pathogenic mechanisms to slow down or halt the progression of AD. However, there are a few treatment options to alleviate some of the symptoms. The pharmacological treatment of AD is based on two classes of drugs registered and approved by the FDA. They are the cholinesterase inhibitors and the NMDA receptor antagonists. Anti-cholinesterase drugs such as donepezil, galantamine and rivastigmine (figure 2.6) are known to increase cholinergic transmission while NMDA receptor antagonists, such as memantine, have been shown to inhibit excessive glutamate induced excitotoxicity mediated by NMDA receptors or other ionotropic receptors. Despite the therapeutic benefits (improved cognitive function) associated with these classes of drugs, they are only able to ameliorate a fraction of the symptoms as the neuronal cells are still being progressively degenerated (Arbo *et al.*, 2019; Fish *et al.*, 2019; Ozben and Ozben, 2019). In the past decade, verubecestat and semagacestat (figure 2.7) that inhibit β -secretase and γ -secretase and anti-A β antibodies (bapineuzumab and solanezumab) were identified as promising drugs with therapeutic effects in preclinical studies, but all have failed when tested in phase 3 clinical trials (Arbo *et al.*, 2019).

2.2.4 Amyotrophic lateral sclerosis

Amyotrophic lateral sclerosis (ALS), a rare but fatal disease (Vinceti *et al.*, 2019), is a progressive and debilitating neurologic disorder characterised by selective degeneration or loss of motor neurons (upper and lower) located in the cerebral motor cortex, brainstem and spinal cord (figure 2.8; Zhang *et al.*, 2013; Gamez *et al.*, 2016; Lee *et al.*, 2016; Bennett *et al.*, 2019; Cai and Yang, 2019; Nomura *et al.*, 2019; Juntas-Morales *et al.*, 2020).

Generally, symptoms begin with focal weakness and later rapidly spread to most muscles including the diaphragm, leading to the loss of muscle functions. Due to damage incurred by upper and lower motor neurons, patients often experience dysfunctional deep tendon reflex (increase activity). Patients also display pathological reflexes and weakness in the limb, body trunk, and bulbar muscles. In fact, patients succumb to death within 2-5 years of onset of symptoms due to oesophageal, oropharyngeal and respiratory complications or failure (Blatzhelm, 2009; Katz *et al.*, 2017; Fang *et al.*, 2018; Steventon and Mitchell, 2018; Akaishi *et al.*, 2019; Steinbach *et al.*, 2020; Yang *et al.*, 2020). Despite numerous proposed mechanisms and clinical trials, a definite mechanism of ALS is still unknown, and there is still no cure (Lee *et al.*, 2016). This is partly due to unavailable biomarkers, which potentially could assist in early diagnosis, understanding how disease progress, and identifying therapeutic targets (Steinbach *et al.*, 2020; Yang *et al.*, 2020).

ALS can be classified into 2 categories: familial and sporadic, and they both share similar pathology (Bennett *et al.*, 2019). They are both caused by extensive variety of different mutations from a wide number of genes, the prominent being copper/zinc superoxide dismutase 1. The mutations in genes are more prominent in familial cases than in sporadic cases. Sporadic ALS, with no previous family history, occurs in 90% of all ALS cases while the remaining 10% are linked to the familial type. The sporadic type has been linked to a series of environmental and genetic factors that lack clarity in mechanisms while the familial type has been heavily linked with genetic factors. However, interrelated mechanisms such as calcium-induced excitotoxicity, endoplasmic reticulum (ER) stress, mitochondrial dysfunction, axon transport impairment, protein quality control disturbance, microglia hyperactivation, neuroinflammation, prion-like propagation, a deficit of neurotrophic factors, a diminished energy supply associated with reduced monocarboxylate transporter 1 (MCT), cytoskeletal defects, RNA metabolism (splicing, miRNA biogenesis, mRNA stability, translation) disturbance, apoptosis, proteasomal, protein aggregation and oxidative stress have been

proposed as the molecular pathways through which neuronal death occurs in ALS (Boll *et al.*, 2014; Yamashita and Kwak, 2014; Browne *et al.*, 2016; Browne and Abbott, 2016; Cai and Yang, 2019; Mathis *et al.*, 2019; Brown *et al.*, 2020). One of the pathologic hallmarks of both sporadic and familial ALS is the aggregation or misfolding of mutant superoxide dismutase 1 (SOD1), a protein encoded by SOD1 genes. It is proposed that mutation in SOD1 alleles results in expressions of mutant toxic proteins. The mutant proteins are believed to adopt atypical orientation or conformation that promotes its aggregation, particularly in the neurons. These aggregates in turns induce co-aggregation of the other normal protein leading to dysfunctional neurons and subsequent death of motor neurons (Browne *et al.*, 2016; Lee *et al.*, 2016; Katz *et al.*, 2017).

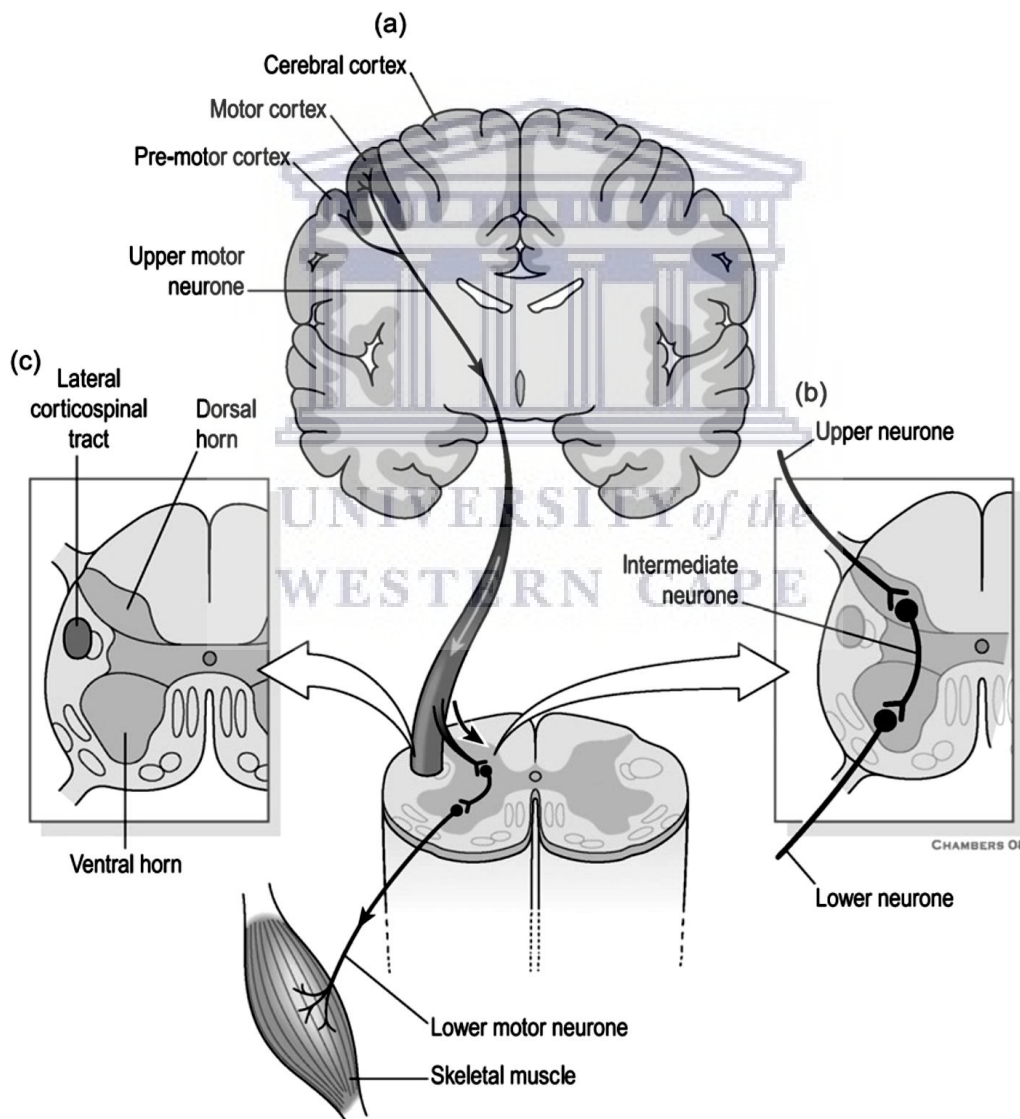


Figure 2.8: (a) The connectivity of the brain to the muscles *via* lateral cortical spinal pathway in the spinal cord (b) displays the interlocking location of upper and lower motor neurons. It is the sole

responsibility of lower motor neurons to transmit signals to the muscles for various muscular related activities. (c) Indicates the location of the lateral cortical spinal track in the spinal cord (Blatzheim, 2009).

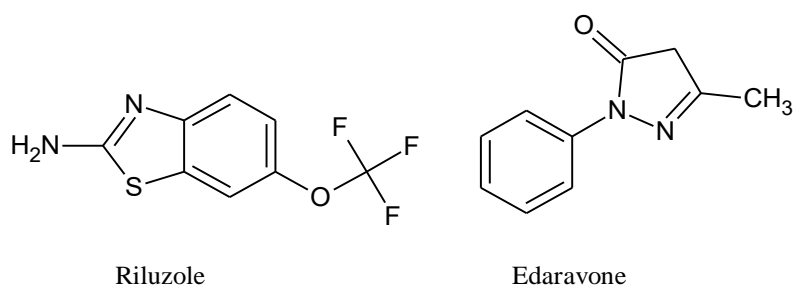


Figure 2.9: Drugs used in the management of ALS.

Admittedly, therapeutic options in the treatment of ALS are very limited. Even though riluzole (glutamate release inhibitor) and edaravone (antioxidant drugs) have been approved by the FDA in 1995 and 2017 (figure 2.9) to address these pathological mechanisms (Brown *et al.*, 2020), they are still only able to extend the patient's life by 2-3 months. Moreover, they are marked by a number of unbearable side effects like neuropsychiatric symptoms, muscle stiffness or gait disturbance. Riluzole, through its inhibitory effects on glutamate release and neuroprotective effects against neurotoxin induced cell damage, has proven to prolong the lives of patients in the early stages of ALS or to prolong the time for tracheostomy in patients. Despite the effects of these drugs, there is still no effective treatment to slow down or stop disease progression (Blatzheim, 2009; Boll *et al.*, 2014; Cai and Yang, 2019).

2.2.5 Huntington's disease

Huntington's disease (HD), a genetically inherited autosomal-dominant disease of the neurons that affects muscle coordination, is characterised by progressive and irreversible damage to neurons in the striatum, basal ganglia and cerebral cortex. These crucial areas of the brain are necessary for motor and cognitive functions. The loss of neurons in these prominent parts ultimately leads to patients' premature death. HD is also associated with psychiatric disorders. The age of onset for most people is in the mid-adult life (35-45 years), but the onset may occur earlier. In terms of clinical manifestation of HD, symptoms can be categorised into three clusters namely motor, neuropsychiatric and/or cognitive. Dysfunctional motor neurons produce symptoms such as chorea, dystonia, tics and parkinsonism while the neuropsychiatric symptoms include vast and comprehensive apathy, irritability, depression, anxiety, psychosis, obsessive-compulsive disorder and addictive behaviour. In the cognitive symptoms, the

patient's ability to pay attention and exercise executive function deteriorate significantly. However, these symptoms are typical of advanced stages of Huntington's disease (Van Der Burg *et al.*, 2009; Bayram-Weston *et al.*, 2012; Mestre and Ferreira, 2012; Dey and Nath De, 2015; Di Domenico *et al.*, 2017).

HD is linked to unstable expanded cytosine-adenine-guanine (CAG) or cytosine-adenine-adenine (CAA) trinucleotide repeats that exist within the first exon of the IT15 (Htt) gene, an important causative gene in HD. This gene encodes the protein huntingtin (Htt) that translates into an elongated mutant polyglutamine (polyQ) stretched within the N-terminus of mutant huntingtin (mHtt) protein resulting in the loss of functional proteins or allele, as well as protein misfolding and aggregation in nucleus and neuronal processes (Kennedy *et al.*, 2005; Carroll *et al.*, 2011; Deschepper *et al.*, 2012; Valor, 2015; Walter *et al.*, 2016; Fukuoka *et al.*, 2018; Oosterloo *et al.*, 2019). In a normal healthy individual, the number of CAG repeats ranges between 11 to 35 repeats. However, a repeat number that exceed 35 increases the risk, with high probability, of an individual with such gene to develop HD. Expanded polyglutamine repeats induce change in conformation of Htt and subsequently mediate the Htt protein aggregation associated with HD. Although the functions of normal Htt protein have not been clearly defined as yet, their association with synaptic vesicles and microtubules are well established and they are vital, as a functional essential scaffolding protein, in the regulation of axonal transport of vesicles including the brain-derived neurotrophic factor. In pathological state, the mHtt protein mediated aggregation is neurotoxic, and induces progressive neuronal loss, mostly in the striatum and other basal ganglia structures, but also all over the cerebral cortex, thus contributing to the expression of clinical symptoms observed in HD (Di Domenico *et al.*, 2017; Dey and Nath De, 2015; Ciosi *et al.*, 2019; Gusella, 2019). The precise mechanism for mutant Htt protein-induced neuronal cell death is still not understood. However, studies on both animal and cellular models have demonstrated the prominent role of excitotoxicity, oxidative stress and mitochondrial dysfunction, axon transport disruption, autophagic abnormalities, deficient energy metabolism, proteolytic processes, transcription dysregulation and loss of striatal growth factors in dysfunctional neurons implicated in HD (Brooks *et al.*, 2012; Deschepper *et al.*, 2012). Based on the knowledge of neuropathology of HD, a few therapeutic approaches have been proposed and advanced (figure 2.10; Godinho *et al.*, 2015).

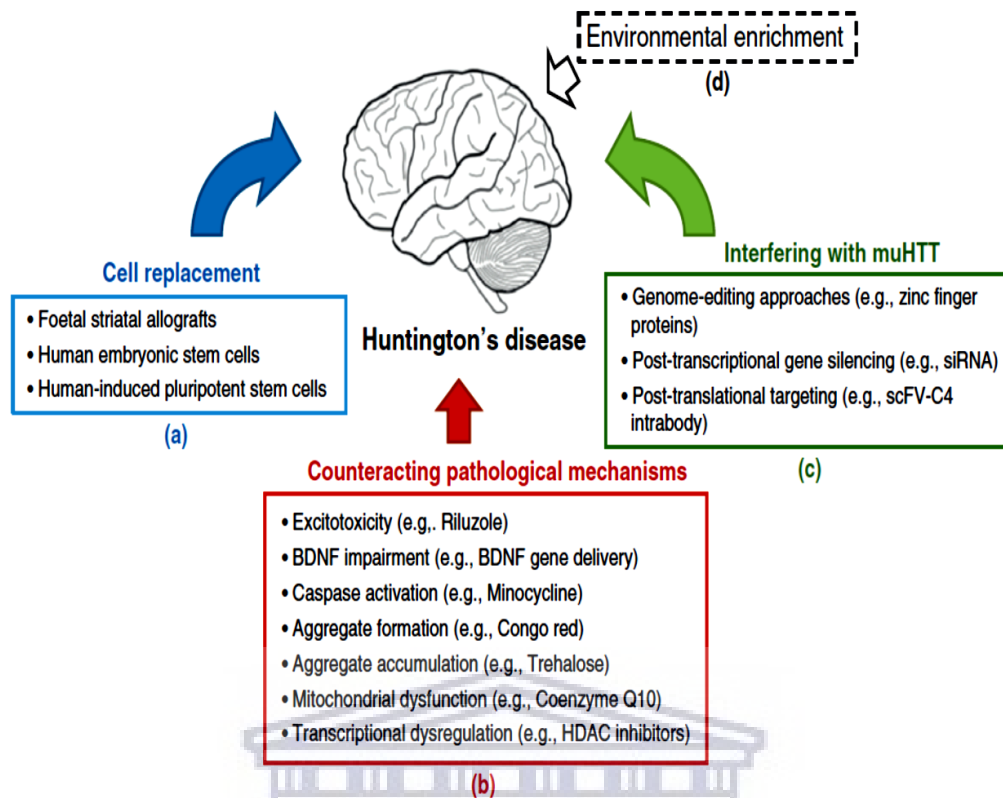


Figure 2.10: Potential therapeutic targets or approaches in the management of Huntington's disease (HD). Numerous alternative therapeutic approaches that could potentially elevate Huntington's disease symptoms include: (a) cell replacement approaches that could replace neurons in the striatum; (b) strategies that slow down or halt the neurodegenerative processes; and (c) factors that prevent mutation of Huntingtin (muHTT) at molecular level such as the genomic, post-transcriptionally or at post-translational level. Additionally, (d) environmental enrichment has been shown to effectively delay disease progression in animal models of HD. As such, this could be useful as non-pharmacological treatments. Abbreviations: BDNF, brain-derived neurotrophic factor; HDAC, histone deacetylase; muHTT, mutant HTT; siRNA, short interfering RNA (Godinho *et al.*, 2015).

In search for drugs to effectively treat HD disease, a significant number of projects that include both pre-clinical and clinical studies have been conducted over the years. However, therapeutic options with efficacy appear to be limited. Despite the substantial effort, the only drug that has been formally approved to date for HD is tetrabenazine. This drug, however, only offers symptomatic relief as it is approved for and treat the chorea features associated with HD. Some other drugs have also been explored, but none was able to attain the same robust efficacy displayed by tetrabenazine. In some European countries, the use of drugs such as haliperidol, pimozide and tiapride are allowed for the treatment of chorea features in HD patients. Tetrabenazine, although effective, is marked by serious adverse events like bradykinesia, hypertonia, akathisia, muscle rigidity, dysphagia or depression. Perospirone has also been shown to be clinically effective and tolerated when used to treat symptoms such as

choreoathetoid movement disorders and psychosis (fear and anxiety) associated with advanced Huntington's disease. Unfortunately, treatments for other symptoms observed in HD are still poorly addressed (Roppongi *et al.*, 2007; Adam & Jankovic, 2008; Garcia de Yebenes *et al.*, 2011; Ross and Tabrizi, 2011; Mestre and Ferreira, 2012). Despite the effectiveness of some of these drugs (figure 2.11), they are only able to provide temporal symptomatic relief as they fail to slow down or halt the disease progression. Currently, no clinically approved drug to effectively treat or stop disease from progressing is available, despite extraordinary growth in knowledge about cellular mechanism and numerous efforts made to develop better treatment (Fukuoka *et al.*, 2018; Valionyte *et al.*, 2020).

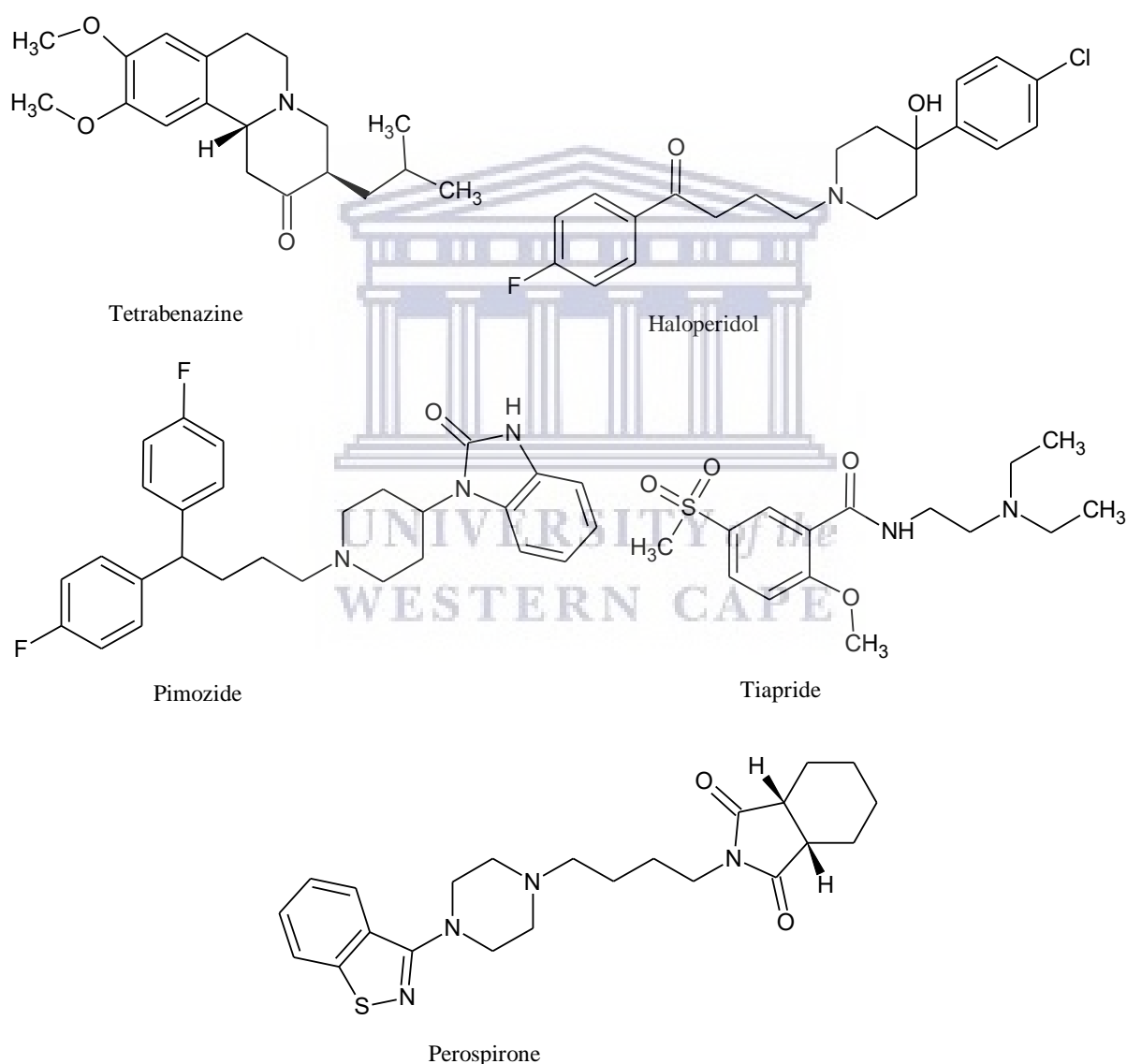


Figure 2.11: Drugs used in the management of HD.

2.3 Oxidative stress and excitotoxicity in neurodegenerative disorders

2.3.1 The role of oxidative stress in neurodegenerative disorders

Reactive oxygen species (ROS) or free radicals are toxic ionised molecules exhibiting one or two unpaired electrons that are generated during metabolism in a biological system, and they are an integral part of normal brain functions involved in calcium signalling, synaptic plasticity, memory and neurotransmission. The most common ROS include hydroxyl ions, hydrogen peroxide, superoxide anions, nitric oxide and peroxy nitrite anions (Sas *et al.*, 2007; Migliore and Coppede, 2009; Sivandzade *et al.*, 2019). Under physiological condition, production of these free radicals are regulated by enzymatic and non-enzymatic scavengers in the brain. However, excessive free radicals can overcome neuronal antioxidant response systems and other coping mechanism leading to oxidative stress, a disruptive cellular process that negatively impacts on the normal function of the brain (Di Domenico *et al.*, 2017; Neal and Richardson, 2018).

The loss of neuronal cells mediated by oxidative stress processes in the central nervous system, *via* a cascade of events linked to imbalance between oxidative events and antioxidant defence mechanism, is well studied and documented. This phenomenon is common in the mechanism underlying the pathogenesis of most neurodegenerative disorders like AD, PD, ALS and HD. The role played by oxidative stress in most neurodegenerative disorders has been suggested to be mainly causative rather than an epiphenomenon of pathological processes. The detrimental effect of oxidative stress on AD progression has also been demonstrated by a number of studies. In the pathogenesis of AD, various animal and cell culture studies have proven beyond reasonable doubt the early detection and occurrence of oxidative stress that precede the formation of amyloid plaques in the disease model of neurological disorders. Currently, it is believed that the amyloid peptide first act as a scavenger to reduce oxidative stress in neuronal cells and only later evolves into a pro-oxidant after accumulating and forming plaques in neuronal cells. In addition to the plaque-mediated oxidative stress, macromolecule peroxidation, abnormal levels of oxidized proteins, advanced glycation end products and mitochondrial dysfunction are also involved in the generation of ROS and reactive nitrogen species (RNS) (Garcia-Blanco *et al.*, 2017; Aghajanov *et al.*, 2019; Cassidy *et al.*, 2020). In PD, protein deglycase DJ-1 is known to protect dopaminergic neurons from oxidative stress and the toxic consequence of mutant human α -synuclein through upregulation of glutathione synthesis and increased expression of heat shock protein, respectively. However, mutation of

DJ-1, as seen in inherited early-onset PD forms, would result in loss of function of the oxidative defence mechanism leading to increased oxidative damage to lipids, proteins and nucleic acid in dopaminergic neurons. An additional source of oxidative stress is the generation of free radicals arising from the metabolism of dopamine and the over-expression of monoamine oxidase-B (Bains and Shaw, 1997; Migliore and Coppede, 2009; Jiang *et al.*, 2016). In ALS, increase in oxidative stress is attributed to mutation of SOD1 genes through production of dysfunctional superoxide dismutase protein. Normally, this protein is a precursor to superoxide dismutase enzyme, and it assists in the attenuation of oxidative stress through the scavenging of free radicals produced by mitochondrial respiration. However, this loss of protection allows the neurons to be susceptible to oxidative damage. Indeed, the elevation of ROS and resultant damage to mitochondrial DNA, proteins and lipids have been demonstrated in both mutant SOD1 mouse models of ALS and human patients. Such damage is generally a precursor to apoptotic cell death of motor neurons, which is likely to occur in ALS (Carri *et al.*, 2003; Zhang *et al.*, 2019). Knowledge about the crucial role of oxidative stress in the pathogenesis of HD has been growing in recent years as several studies have demonstrated the detrimental effect of oxidative damage on HD. Particularly, the high level of oxidative stress in HD is associated with proteasome malfunction, which exacerbates aggregate formation, somatic CAG expansion in neurons, cell death, and the deficiency of the mitochondrial complex IV (Ju *et al.*, 2014). Moreover, during CAG trinucleotide expansion in somatic cells, a process for repairing damaged DNA using 7,8-dihydro-8-oxoguanine-DNA glycosylase enzymes is postulated to be responsible for oxidative damage in HD patients (Sorolla *et al.*, 2008; Migliore and Coppede, 2009; Jonson *et al.*, 2013). The Oxidative damage further increases the DNA triplet expansion leading to more aggregation and neuronal cell death (Jonson *et al.*, 2013).

The mitochondria are extremely important in the physiological functions of many cellular processes like the generation of ATP energy, the maintenance of calcium homeostasis, the synthesis of steroidal hormones, and the activation of programmed cell death (apoptosis). It is fundamentally the main site for oxidative stress as it allows leakage of electrons during cellular oxidation, leading to constant production of superoxide anion that is responsible for 90% of endogenous reactive oxygen and nitrogen species. The metabolism of neurons requires high energy that demands a high oxygen consumption rate. Due to this increase in demands and consumptions, the generation of ROS by products such as hydrogen peroxide, superoxide radical anions, and hydroxyl radicals is high. The brain is also rich in peroxidizable polyunsaturated fatty acids and contains a high level of potent catalyst iron. Unfortunately, the

ability or capacity of neurons to regenerate or scavenge is limited, therefore allowing it to be susceptible to oxidative damage (Wang *et al.*, 2014; Yang *et al.*, 2020). Mitochondrial dysfunction is instrumental in the progression of neurodegenerative disorder such as AD, HD, ALS and PD. Notably, numerous studies with substantial evidence have suggested that mitochondrial dysfunction triggered by events such as bioenergetics effects, mitochondrial dynamics (mitochondrial fusion and fission process) imbalance, mitochondrial permeability transition pore (mPTP) opening, mitochondrial DNA (mtDNA) mutations and gene mutation, is identified at the early pathological stage of most neurodegenerative disorders (Wang *et al.*, 2019). Physiologically, mitochondria are regarded as the engine where most of the cell's energy, in the form of ATP and essential for metabolism, are generated. In addition to this basic but crucial function, they also respond to oxidative stress by generating endogenous reactive oxygen species, which are physiologically eliminated by various enzymatic actions, particularly the mitochondrial manganese-dependent enzymes such as dismutase and catalase (Rodriguez-Martinez *et al.*, 2013; Jha *et al.*, 2017; Kumar *et al.*, 2019; Lin *et al.*, 2020). However, in pathological state, as observed in many neurodegenerative disorders, mitochondrial respiration is compromised and the ATP production needed for energy is depleted resulting in a cascade of events that include the blocking of the activities of electron transport chain, the generation of more reactive oxygen species in a vicious self-destructive cycle, the reduction of mitochondrial DNA and caspase-3 release (Bhat *et al.*, 2014; Jha *et al.*, 2017; Wu *et al.*, 2019). The excess production of ROS attacks the mitochondria and aggravates oxidative damage to mitochondrial proteins and structures and other cellular components, leading to compromised cell functions that ultimately advances neuronal cell death through apoptosis (Chen *et al.*, 2019).

2.3.2 The role of excitotoxicity in neurodegenerative disorders

Glutamate is a primary excitatory neurotransmitter whose activity is crucial for neuronal physiological functions and a wide range of receptor mediated downstream signalling cascades in the central nervous system (Park *et al.*, 2010; Bano and Ankarcona, 2018). Glutamate is known to control activity-dependent neuronal depolarization for the purpose of differentiation and survival of neurons, and play a prominent role in various physiological functions such as synaptic plasticity, learning, memory and other cognitive processes. In order to fulfil this physiological role, low micromolar concentrations of extracellular glutamate are constantly maintained by both neuronal or astroglial cells (Haerberlein and Lipton, 2009; Mehta *et al.*, 2013; Bano and Ankarcona, 2018; Park *et al.*, 2020). However, under certain pathological

conditions such as AD, PD, ALS, and HD, there is an increase in the level of extracellular glutamate caused by a decreased expression of glutamate transporter, reduced glutamine synthase (in astrocytes) capacity, or/and reduced function of potassium channels and aquaporins. These increased levels are usually mediated by multiple factors such as age, genes or a suboptimal generation of energy in neurons and glial cells (Figure 2.12). The elevated extracellular glutamate becomes toxic to the neuronal cells leading to excitotoxicity (Bano and Ankarcona, 2018; Zhao *et al.*, 2019).

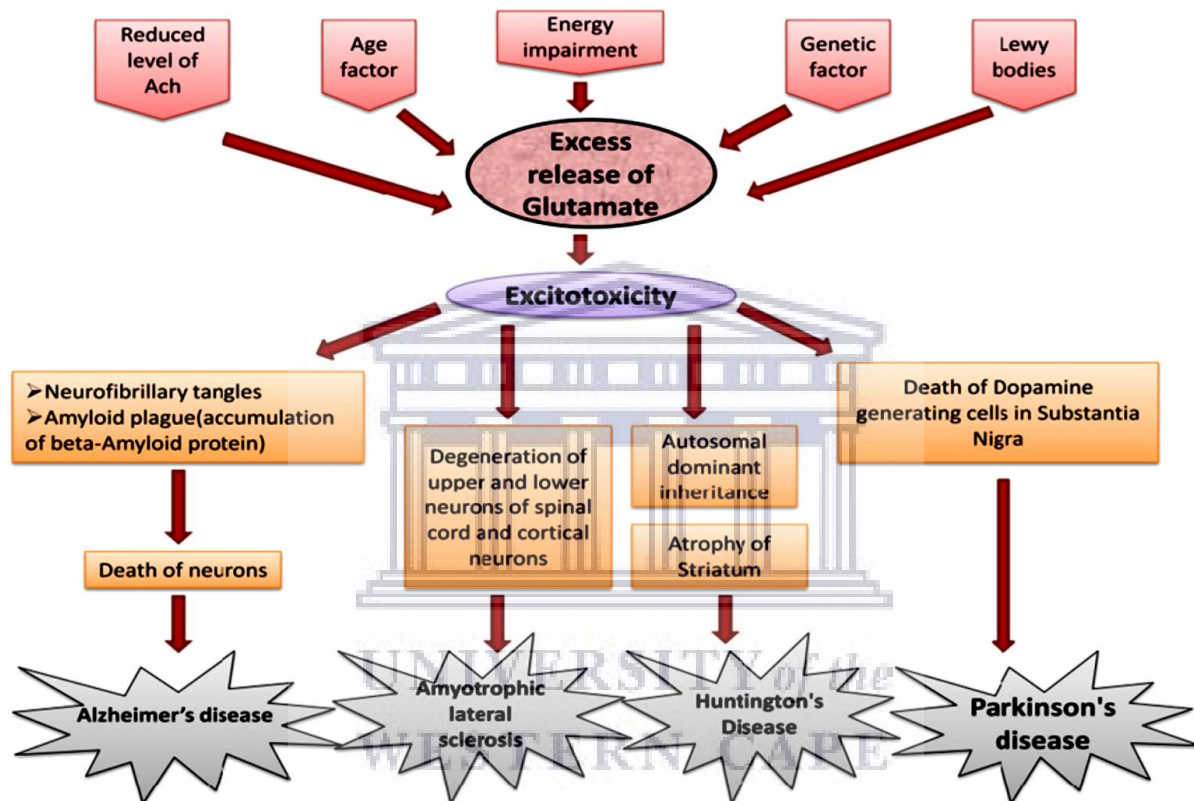


Figure 2.12: Factors that mediate glutamate induced excitotoxicity leading to the loss of neurons in specific part of the and their corresponding neurodegenerative disorders (Mehta *et al.*, 2013).

In excitotoxicity, excessive extracellular glutamate over-activates ionotropic receptors in the neurons. While almost all ionotropic receptors are activated, the effects on NMDA receptors are prominent (Jing *et al.*, 2004). Over-activation of these receptors, along with voltage-gated calcium channels, results in the increase of intracellular calcium ions, thus disrupting the calcium homeostasis process (Breyer, *et al*, 2007). Under normal resting conditions, neuronal cells are able to efficiently prevent rise in intracellular Ca^{2+} concentration above critical threshold and maintain calcium homeostasis. This is achieved through the sequestration of calcium ions by intracellular organelles such as mitochondria or endoplasmic reticulum (calcium depot compartment) or the binding of calcium ions to buffering proteins in the cytosol

or the extrusion of calcium ions outside the cells through $\text{Na}^+/\text{Ca}^{2+}$ exchanger (figure 2.13). However, these recovery processes are hindered in the excitotoxic cells as the activities of glutamate at receptors and channels are prolonged, leading to elevation of calcium load to a level that exceeds the capacity of the Ca^{2+} regulatory mechanisms (Arundine and Tymianski, 2003; Lai *et al.*, 2014; Bano and Ankarcona, 2018). Due to the sensitivity of neurons towards intracellular calcium ion concentration, disruption of calcium homeostasis can lead to destructive consequences such as damage to cell dendrites or neuronal cell death, in part, by activating calpain, a cysteine protease, that degrades a variety of substrates such as cytoskeletal proteins, membrane receptors, and metabolic enzymes. Interestingly, calpain is known to have many substrates and some of these substrates are involved in the re-organisation of post-synaptic density long-term potentiation. However, excessive calpain activation, a prominent event in pathological conditions, destabilised the microtubules in the neuronal cell leading to axonal structure impairment, substrate transport alteration and eventually cell death. Additionally, activation of cyclooxygenases and lipoxygenase, up-regulation of neuronal nitric oxide synthase (nNOS), endoplasmic reticulum (ER) stress, induction of lipid peroxidation, and dysfunction of mitochondria also respond to glutamate-induced excitotoxicity or calcium influx leading to the generation of reactive oxygen species, an important contributor to neurodegeneration (Yang *et al.*, 2013; Gold *et al.*, 2015; Xu *et al.*, 2016; Jeong *et al.*, 2017; Mattson, 2019; Rivero-Segura *et al.*, 2019).

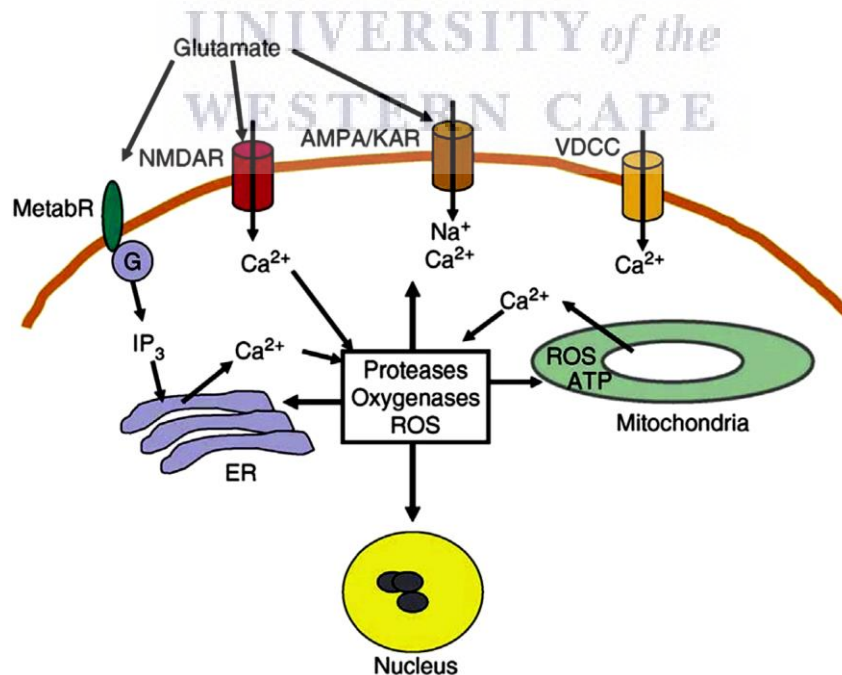


Figure 2.13: The role of calcium in excitotoxicity.

Excessive glutamate on NMDA receptors are known to induce both neuronal necrosis and apoptosis, with the latter form of cell death well established in the development of several neurodegenerative disorders, including HD, ALS, multiple sclerosis, AD, PD, and metabolic deficiencies of brain related to ischemic or epileptic injury (Jing *et al.*, 2004; Kostic *et al.*, 2017). The link between NMDA receptors and A β effects in AD has been extensively studied. In these studies, it has been suggested that A β oligomers, applied on cultured cortical neurons, are capable of activating GluN2B-containing NMDA receptors to subsequently induce immediate intracellular calcium influx, dysregulation of NMDA receptor expression to impair synaptic plasticity, and enhancing endocytosis. Some studies have also indicated the direct link between mutated presenilins and Ca²⁺ dysregulation in AD. It is believed that neurons expressing mutated presenilins genes (PSEN1 and PSEN2), as observed in AD, promote ER Ca²⁺ overfilling and excessive Ca²⁺ release *via* inositol-1,4,5-trisphosphate receptor (InsP₃R) or ryanodine receptors (RyR) in the ER (Abeti & Abramov, 2015; Pchitskaya *et al.*, 2018). In the pathological studies of HD, evidence of calcium dysregulation through disruption of the mitochondrial Ca²⁺ uptake system is well documented. It is proposed that the mutant form of Huntingtin protein is capable of sensitising mPTP opening in neuronal cells to disrupt mitochondrial calcium ion homeostasis or sequestration, and to increase neuronal susceptibility to NMDA-induced excitotoxicity (Zadori *et al.*, 2012; Abeti & Abramov, 2015; Boussicault *et al.*, 2018). Calcium dysregulation in HD has also been linked to increased surface expression and currents of NR2B-bearing NMDA receptors as a result of mutant Huntingtin protein. This leads to excessive function of extrasynaptic NMDA receptors resulting in synaptic loss, as observed in the early stage of HD. Similar to AD, mHtt appears to bind to InsP₃R and RyR to enhance Ca²⁺ release from the ER, thus contributing to the calcium overload (Abeti & Abramov, 2015; Pchitskaya *et al.*, 2018; Moraes *et al.*, 2020). PD pathology is strongly linked with mitochondrial dysfunction and Ca²⁺ signalling dysregulation. In the absence of synaptic input, SNc dopaminergic neurons are known to display pace-making activity leading to increased calcium influx through the L-type VGCC, which if it persists, disrupt the intracellular calcium homeostasis process and increase the vulnerability of SNc neurons to calcium overload leading to basal mitochondrial oxidative stress (Pchitskaya *et al.*, 2018). α -Synuclein is a gene implicated in the pathogenesis of PD and its oligomeric form has been shown to induce mitochondrial calcium overload, mitochondrial dysfunction and mPTP opening. In ALS, a mutation of the SOD1 gene is mainly associated with abnormal change in ER-mitochondrial intercommunication and reduction in the Ca²⁺-binding protein cytosol leading to mitochondrial

calcium overload and dysfunction and mPTP opening, which subsequently promotes neuronal cell death *via* apoptosis (Abeti & Abramov, 2015).

2.4 NMDA receptors and Voltage gated calcium channels

2.4.1 Structure and functions of NMDA receptors

Of all the ionotropic glutamate receptors, the activity or role of NMDA receptor activity are distinct as they are able to act as coincidence detectors for pre- and post-synaptic activity, converting specific patterns of neuronal activity into long term changes in synaptic strength. In addition to these characteristics, they are activated simultaneously by glycine and glutamate, highly permeable to calcium, and are prone to voltage-dependent magnesium blockage. They are also of significant interest in the search for therapeutic targets in neurodegenerative disorders since their dysfunction are associated with several neuropathological conditions such as AD, ALS, HD, PD, ischemia, epilepsy, mental retardation, depression and schizophrenia (Dong *et al.*, 2018; Stroebel *et al.*, 2018; Zhang *et al.*, 2018).

NMDA receptors are heterotetrameric membrane proteins consisting of two GluN1 subunit and two GluN2 or GluN3 subunits. The GluN2 and GluN3 subunits are encoded by four (2A-2D) and two (A-B) genes, respectively (Tovar and Westbrook, 2017; Regan *et al.*, 2018). Even though the subunit composition of presynaptic, postsynaptic, perisynaptic and extrasynaptic NMDA receptor is dissimilar, the molecular structure of each subunit is very much alike and it is grouped into four different functional domains that include: An ion channel formed by 4 hydrophobic segments (M1-M4), the transmembrane region, and the M2 segment that partially enter the membrane; a carboxyl tail domain located in the intracellular region; an amino terminal domain situated in the extracellular region; and a ligand binding domain (figure 2.14).

A functional NMDA receptor comprises of two obligatory GluN1 subunits and two GluN2 and/or GluN3 subunits. The activation of NMDA receptors requires it binding to glutamate and glycine (co-agonist) concurrently, with selectivity towards GluN2 subunit for glutamate while GluN1 and GluN3 subunits provide binding sites for glycine (figure 2.15). While the functional role of GluN1 and GluN2 subunits have been explored in depth, very little information on the functional role of GluN3 subunits are available. At resting potential state of neuronal membranes, the channels are constantly blocked by extracellular Mg^{2+} . However, due to the voltage sensitivity of these receptors and excitation by synaptic inputs, postsynaptic depolarisation is capable of relieving Mg^{2+} block as the affinity of Mg^{2+} to the binding sites is

drastically reduced leading to NMDA receptor mediated calcium influx. The Ca^{2+} influx, mediated by NMDA receptors, is crucial for long-term potentiation (LTP) and other cellular processes, and for both neuroprotection and apoptotic cell death (Chaffey and Chazot, 2008; Zito and Scheuss, 2009; Flores-Soto *et al.*, 2012; Mellone and Gardoni, 2013; Yu and Lau, 2018; Ingram *et al.*, 2018; Amidfar *et al.*, 2019). Calcium influx at synaptic sites is believed to activate signalling pathways that lead to LTP or long-term depression (LTD), depending on the temporal pattern and amplitude of the calcium transient. On one hand, synaptic calcium influx activates cyclic adenosine monophosphate response element binding protein (CREB) to upregulate the brain-derived neurotrophic factor (BDNF) gene that acts to promote pro-survival program. On the other hand, extrasynaptic NMDA receptor mediated calcium influx is thought to deactivate CREB leading to downregulation of BDNF, which are detrimental to neuronal cells. Despite the functional role of NMDA receptors, the opening of the NMDA receptors linked to cation channels are regulated through allosteric modulation or various ligand binding sites that are involved in the binding of endogenous extracellular substances like zinc ions, Mg^{2+} , glutamate, glycine, protons, polyamines, and reducing and oxidizing agents to the respective binding sites at the receptor or the binding of exogenous substance like phencyclidine to its binding site (Aepkers and Wunsch, 2005; Zito and Scheuss, 2009).

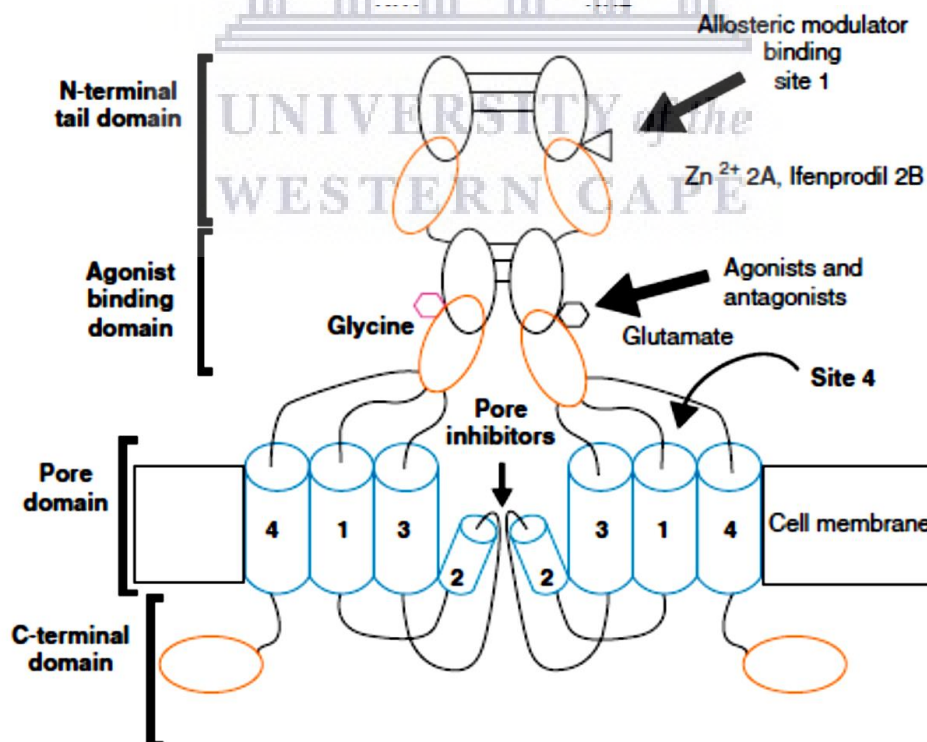


Figure 2.14: Schematic representation of the structure of a NMDA-type glutamate receptor and its pharmacological regulation sites (Flores-Soto *et al.*, 2012).

Functionally, NMDA receptors are crucial as mediators of fast synaptic transmission and are necessary for the LTP and LTD functions at glutamatergic synapses in the central nervous system. This plasticity processes, mediated by NMDA receptors, are believed to be important for learning and memory that is attributed to the NMDA receptor's ability to regulate excitatory synaptic transmission (Nagasawa *et al.*, 1996; Zito and Scheuss, 2009; Moreau and Kullman, 2013; Ingram *et al.*, 2018). In addition to these functional roles, NMDA receptors also play an important role in the synaptogenesis, strengthening and maturation of synapses and the growth and retraction of dendritic spine (Zito and Scheuss, 2009; Mellone and Gardoni, 2013; Moraes *et al.*, 2020).

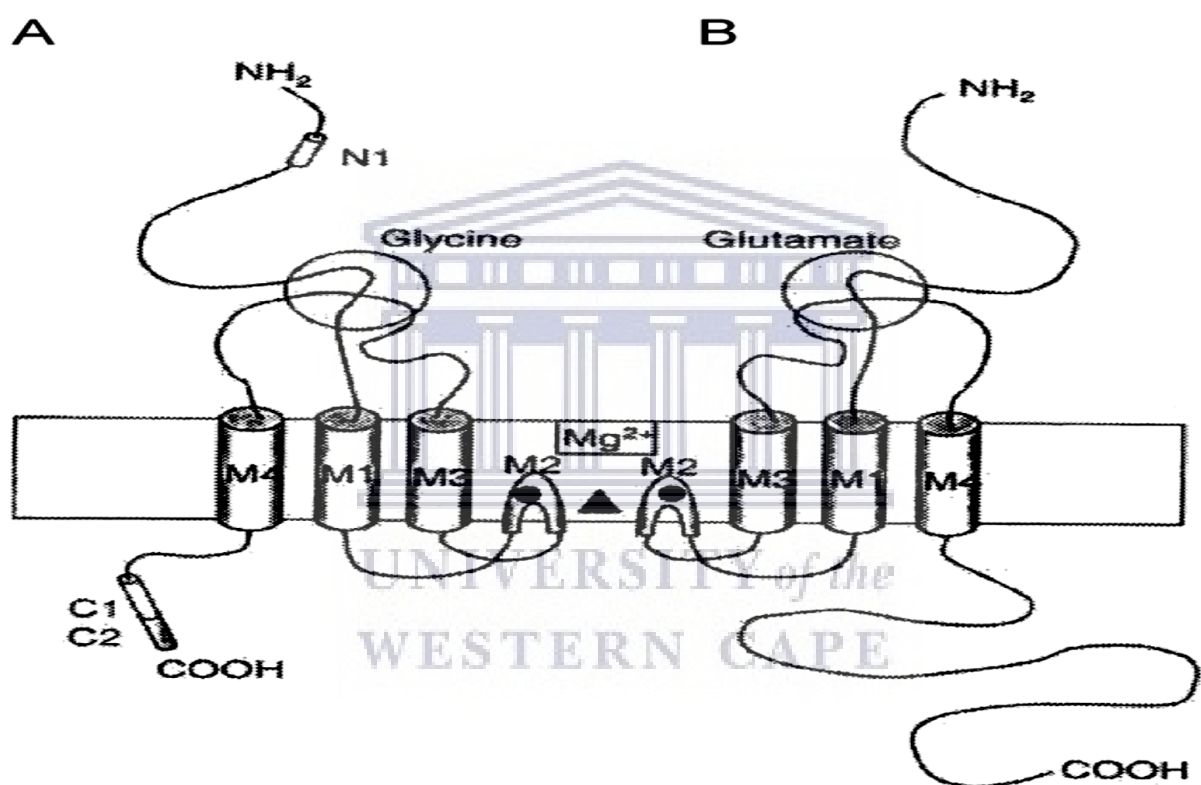


Figure 2.15: Schematic representation of the transmembrane topology of a Glu1 (A) and a Glu2 (B) subunits displaying the extracellular amino terminals, the intracellular carboxyl terminals, the membrane domains (M1-M4) and the agonist binding sites (Chaffey and Chazot, 2008).

In spite of the crucial physiological roles of glutamate in the central nervous system, its effect, in response to hyperexcitability can be detrimental to the neuronal cells due to overactivation of NMDA receptors that mediate dysfunctional calcium homeostasis leading to damage of neuronal cells and apoptosis. This phenomenon is common among several chronic neurodegenerative disorders (Moraes *et al.*, 2020).

2.4.2 Structure and functions of voltage gated calcium channels

The voltage-gated calcium channels can be categorised into two major channels namely the high voltage-activated channels that respond to large membrane depolarisation and the low voltage-activated channels that are unlocked when subjected to smaller voltage changes near typical neuronal resting membrane potential (Chen *et al.*, 2008; Simms and Zamponi, 2014). Voltage-gated Ca^{2+} channels, associated with high voltage-activated channels (HVA), are macromolecular protein complexes consisting of a core α_1 pore-forming subunit and a number of auxiliary subunits that include β , $\alpha_{2\delta}$, and γ , encoded by multiple genes. Whereas, those associated with low voltage-activated channels (LVA) appear to lack the auxiliary subunits. While the α_1 -subunits provide binding sites for drugs and regulators, the β -, $\alpha_{2\delta}$ -, and γ -subunits assist in trafficking, anchorage, and modulating the biophysical function of the α_1 complex (figure 2.16). The α_1 -subunits are made up of approximately 2000 amino acid residues that are organised into four repeated domains (I to IV), and each domain contains six transmembrane segments (S1 to S6) with a pore situated in between S5 and S6 and a voltage sensor site formed by the S1-S4 segments (figure 2.17). These characteristics make up the conduction pore, voltage sensor and gating apparatus, and allosteric modulation binding sites needed for the physiological functions of the channels. (Arikkath *et al.*, 2002; Wang *et al.*, 2004; Hurley and Dexter, 2012; Dolphin, 2013; Simms and Zamponi, 2014; Tuluc *et al.*, 2016; Lazniewska and Weiss, 2017; Kushnir and Marx, 2018; Abderemane-Ali *et al.*, 2019).

These channels comprise four types that include L-type Ca^{2+} channels ($\text{Ca}_v1.1$, $\text{Ca}_v1.2$, $\text{Ca}_v1.3$ and $\text{Ca}_v1.4$), T-type Ca^{2+} channels ($\text{Ca}_v3.1$, $\text{Ca}_v3.2$ and $\text{Ca}_v3.3$), P/Q-type Ca^{2+} channels ($\text{Ca}_v2.1$), N-type Ca^{2+} channels ($\text{Ca}_v2.2$), and R-type Ca^{2+} channels ($\text{Ca}_v2.3$). The L-type is known to exhibit long lasting currents while the T-type exhibit relatively transient Ca^{2+} current (McDonough *et al.*, 2007; Piedras-Renteria *et al.*, 2007; Neumaier *et al.*, 2015; Kushnir and Marx, 2018). The low threshold and slow deactivation (due to hyperpolarised voltage range of activation) of T-type channels are the main characteristic features that distinguish them from L-, P/Q-, N-, and R-type channels (Barbado *et al.*, 2009; Lipscombe *et al.*, 2013; Bourinet and Zamponi, 2017). The $\text{Ca}_v1.2$, $\text{Ca}_v1.3$ and $\text{Ca}_v1.4$ -subtypes of the L-type channels are predominantly expressed on the neuronal membrane while the $\text{Ca}_v1.1$ isoform is specific to the skeletal muscle. These channels are known to display slow voltage-dependent gating characteristic and are sensitive to dihydropyridine agonists and antagonists. The P/Q, N, R-type are expressed mainly in the nerve terminals, dendrites, and neuronal cell bodies (Piedras-

Renteria *et al.*, 2007; Nieto-Rostro *et al.*, 2014; Simms and Zamponi, 2014; Heyes *et al.*, 2015; Neumaier *et al.*, 2015; Kushnir and Marx, 2018).

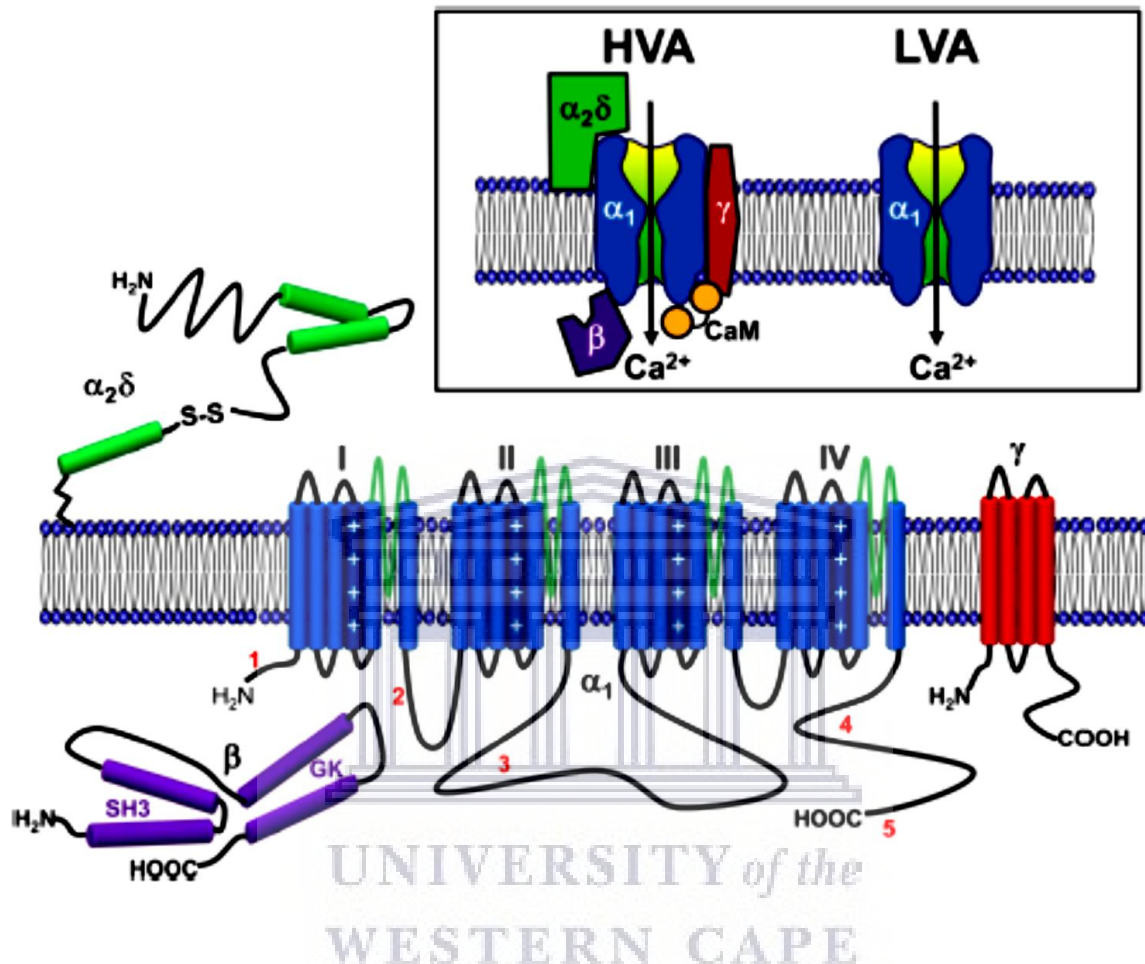


Figure 2.16: Subunit composition and transmembrane topology of voltage-gated calcium channel subunits (Simms and Zamponi, 2014).

Voltage-gated calcium channels are the major medium through which Ca^{2+} enters the neuronal cells. They are activated by a voltage sensor that detects change in membrane depolarisation following an exposure to stimulus. They are expressed throughout the excitable neuronal cells and play an important role in maintaining calcium homeostasis and regulating excitability (Hristov *et al.*, 2018). Under normal resting conditions, the concentration of intracellular calcium ions is constantly kept below 100 nM by buffers, efflux and cytosol sequestration. However, if stimulated, functional voltage gated calcium channels respond to neuronal membrane depolarisation by allowing Ca^{2+} influx, along the electrochemical gradient, across the membrane into neuronal cells to shift the intracellular calcium concentration into the high micromolar range. This in turn mediate processes such as the regulation of neuronal electrical

activity, modulation of other ion channel gating, the control of cellular processes such as synaptic neurotransmitter release, neuronal survival through the regulation of membrane excitability, activation of calcium-dependent enzymes (Calmodulin-dependent kinase and protein kinase C), neurite outgrowth, intracellular signal transduction and gene transcription (Chen *et al.*, 2008; Hurley and Dexter, 2012; Simms and Zamponi, 2014; Nanou and Catterall). On the other hand, persistent depolarisation that results in calcium overload is detrimental to the neuronal cells. Thus, there is need to constantly regulate the activities of voltage-gated channels and other type of calcium-permeable channels either by intrinsic gating processes or by cell signalling pathways. The cell signalling pathways involve presynaptic calcium channel proteins through forming large signalling complexes at active zones, G protein of $\beta\gamma$ subunits through activation of G-protein-coupled autoreceptors, and/or multiple protein kinases through protein phosphorylation, which control channel activity and trafficking to and from the plasma membrane. Interestingly, calcium influx through voltage-gated channels are capable of controlling and regulating intracellular calcium ions through positive (Ca^{2+} -dependent inactivation) and negative (Ca^{2+} -dependent facilitation) feedback regulatory mechanisms. However, this fundamental function depends solely on calmodulin binding to the pore-forming α_1 subunit. Dysfunction of these calcium regulatory mechanisms and associated disruption of calcium homeostasis have been implicated in several neurodegenerative disorders (Christel and Lee, 2012; Simms and Zamponi, 2014; Nanou and Catterall, 2018).

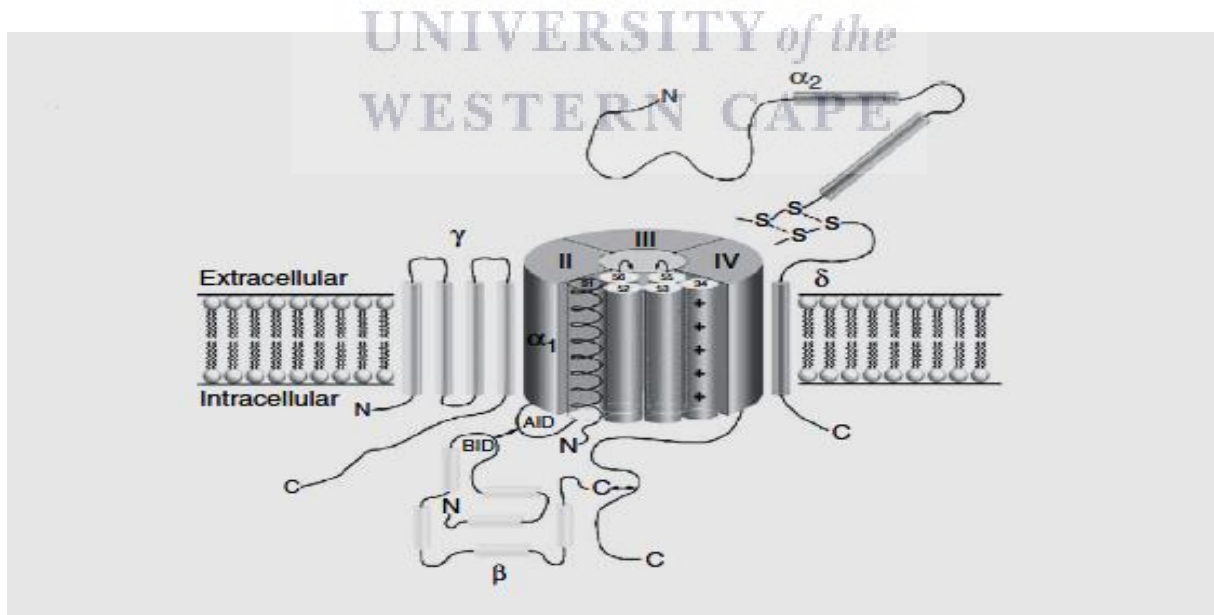


Figure 2.17: Diagram showing the multi-heteromeric nature of voltage-gated Ca^{2+} channels. Disulfide bonds between the α_2 and the δ subunits are indicated. AID, α_1 -interacting domain, which interacts with the auxiliary subunit; BID, β -interacting domain (Piedras-Renteria *et al.*, 2007).

2.4.3 The roles of NMDA receptor and voltage-gated channel blockers in attenuating glutamate-induced excitotoxicity

Despite the vast knowledge acquired in the years of investigating the pathology of neurodegenerative disorders, the mechanism of degeneration is still poorly defined. However, several mechanisms have been proposed as described earlier. Of the proposed mechanisms, the effects of excitotoxicity via glutamate activation are prominent. In excitotoxicity, excessive glutamate overactivates NMDA receptors and VGCC leading to increased intracellular Ca^{2+} in the neurons that subsequently destroy cellular components of neurons. Under physiological conditions, neuronal cells inherently possess the abilities to regulate the intracellular Ca^{2+} rise. However, in pathological state, organelles in the cytoplasm become dysfunctional and are susceptible to oxidative stress leading to various overlapping events that ultimately leads to cell death. Compounds blocking or regulating the excessive calcium influx is thus of major interest as neuroprotective agents. Moreover, the crucial role of excitotoxicity has been discussed in the pathology of most neurodegenerative disorders such as PD, AD, ALS and HD. Altogether, the use of NMDA receptor and/or voltage gated calcium blockers may be therapeutically relevant and represent promising targets in regulating or controlling intracellular calcium ions so as to minimise or halt degeneration of neurons (Aepkers and Wunsch, 2005).

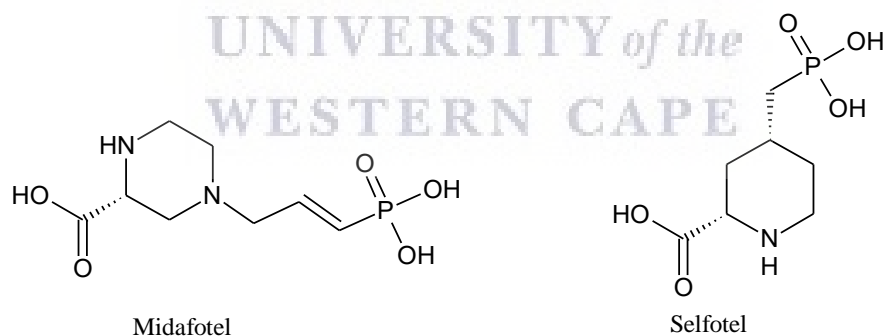


Figure 2.18: Competitive NMDA receptor antagonists.

Developing strategies to combat glutamate induced excitotoxicity have been a major challenge because the same processes (e.g. prolong glutamate activity) that mediates excitotoxic cell death are, at physiological concentration, extremely important for normal physiological functions of the neurons and the brain (Lipton, 2004). At first, competitive NMDA receptor antagonists such as midafotel and selfotel (figure 2.18), which binds to the same binding site as glutamate in the NMDA receptor, were developed, but were quickly discontinued due to the

undesirable dose-related psychotomimetic side effects observed with this set of antagonists (Sonkusare and Ramarao, 2005). For years, focus has been on the phenylcyclidine (PCP) binding site of the NMDA receptor ion channels. It is generally believed that ligands or molecules that interact with the PCP binding site would inhibit calcium influx to function as NMDA receptor antagonist (Krull and Wunsch, 2004). As such, a number of compounds or molecules with structural diversity, including those similar to PCP, MK-801, ketamine and dextromethorphan (figure 2.19) have been shown to interact with the PCP binding site to effectively antagonise NMDA receptors in an uncompetitive manner. In the past decades, open channel blockers (uncompetitive NMDA receptor antagonists) such as MK-801 and phencyclidine (PCP) activities have been extensively studied. Although these blockers strongly block NMDA receptor associated ion channels, they are regrettably marked by undesirable psychotomimetic side effect such as hallucination, psychosis, dysphoria and amnesia and are thus unsuitable for practical purposes. These side effects are attributed to the high affinity of the antagonists towards the PCP binding site of receptors. On the other hand, amantadine and memantine (figure 2.19) are open channel blockers (uncompetitive NMDA receptor antagonist) with moderate affinity towards the PCP binding site and are clinically well tolerated for the treatment of Parkinson's disease and Alzheimer's disease, respectively due to their atypical mechanism of action on the NMDA receptors (Barygin *et al.*, 2009; Zambrano *et al.*, 2018; Smidkova *et al.*, 2019; Temme *et al.*, 2020). The moderate affinity is due to the steric bulk not sufficiently tolerated in the region that binds the cyclohexyl ring of PCP or one of the aromatic rings of MK-801. These compounds have been shown to block NMDA receptor effectively with safe side effect profiles (Jirgensons *et al.*, 2000; Temme *et al.*, 2020). Memantine, in comparison to MK-801, has been showed to have favourable kinetics (substantial shorter dwelling time (faster off-rate)) in the NMDA receptor channels to exert its neuroprotective effects while also demonstrating minimal adverse effects in the form of occasional restlessness and rare cases of light dizziness even at higher dosages (Lipton, 2004; Jiang *et al.*, 2010).

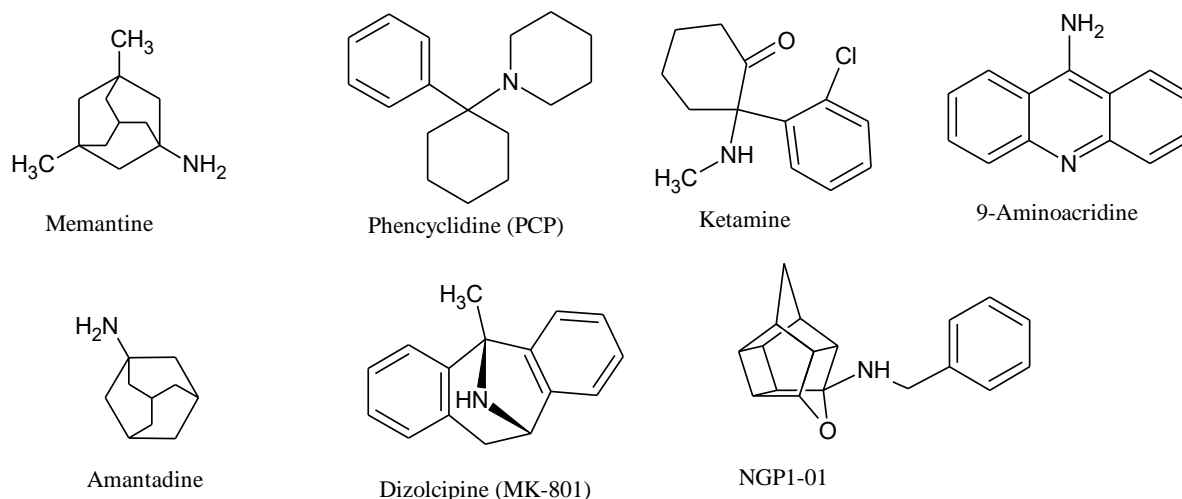


Figure 2.19: Uncompetitive NMDA receptor antagonists.

Based on the mechanism of interaction between the NMDA receptor channel and its blockers or antagonists, they are grouped into two categories; namely trapping and foot-in-the-door blockers. It has been shown that antagonists or blockers can either bind to the deep or shallow site of the NMDA receptor to exert their inhibitory effects. Binding of trapping blockers such as MK-801 and phencyclidine (Figure 2.19) to the deep site of the receptor allow channel closure and agonist dissociation. As a result, molecules that are trapped in the closed state are unable to leave the channels until it is open again. This corresponds to the trapping mechanism. In contrast, foot-in-the-door channel blockers such as memantine, adamantane, ketamine and 9-aminoacridine (Figure 2.19) bind to the shallow site of the receptor to prevent channel closure. As a result, molecules that act in this manner are not trapped in the receptor channels while in the closed states. An important feature of the foot-in-the-door mechanism is the shift of the equilibrium of channel activation towards an open state in the blocker's presence (Bolshakov *et al.*, 2005; Barygin *et al.*, 2009). This form of block is common among selective NMDA receptor blockers. It is believed that most selective NMDA receptor blockers are monocations displaying a V-like molecular shape together with hydrophobic wings and a ionisable amino group at the vertex, and the proton donating moiety of these blockers interact with the filter that incur selectivity to the channels (Barygin *et al.*, 2009).

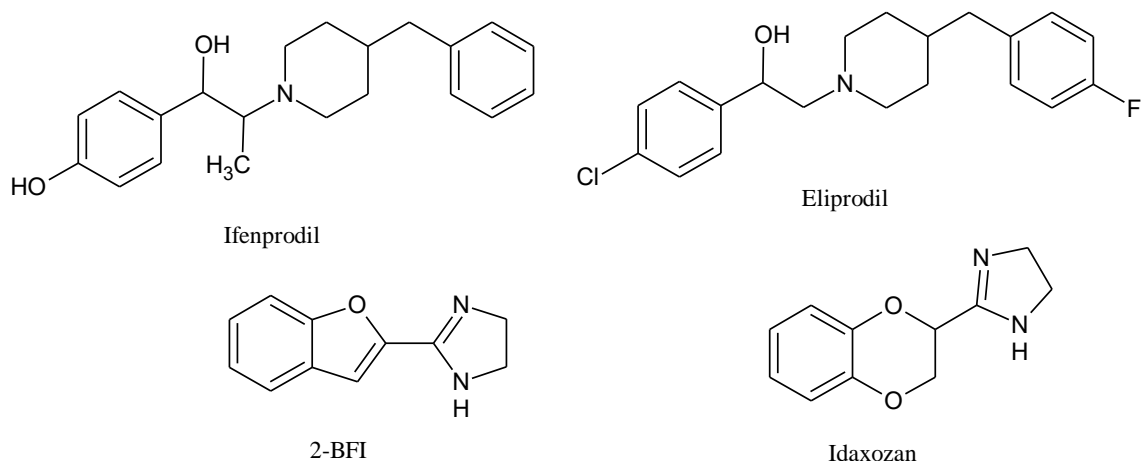


Figure 2.20: Allosteric modulators of NMDA receptors.

An alternative approach to block NMDA receptor-induced calcium influx is the design and development of allosteric modulators with improved pharmacological properties (Costa *et al.*, 2012). An allosteric binding site that modulates the NMDA receptor has emerged as a potential target for blocking calcium influx in neuronal cells. This binding site, referred to as the ifenprodil binding site, is confined to the region of the forebrain and is located at the interface between the GluN1 and GluN2B subunits of NMDA receptors. The inhibitory activity of compounds at the allosteric binding site depends on the ability of the compounds to form H-bonds and lipophilic interactions with the functional groups of the GluN2B subunits (Temme *et al.*, 2020). Non-selective GluN2B antagonists such as ifenprodil, eliprodil and haloperidol (figure 2.20) have been shown to modulate NMDA receptors, but exhibit limited therapeutic application due to their off target pharmacological and pharmacokinetic properties. Of these modulators, ifenprodil was the first to be developed and it exhibits high affinity for the GluN2B subunit of NMDA receptors. Despite its high affinity, ifenprodil is marked by undesirable side effects such as impairment of reaction and low blood pressure. These effects are attributed to its activity at α_1 , 5-HT, σ_1 and σ_2 receptors. Also, ifenprodil exhibit low bioavailability due to fast metabolism in the form of phenol glucuronidation. These unfavourable characteristics limits its clinical use as potential neuroprotective agent. However, several selective GluN2B antagonists, derived from ifenprodil, that demonstrate full therapeutic effects of non-selective NMDA receptors with a reduced side effect profile are being developed (Bienat *et al.*, 2014; Lutnant *et al.*, 2016).

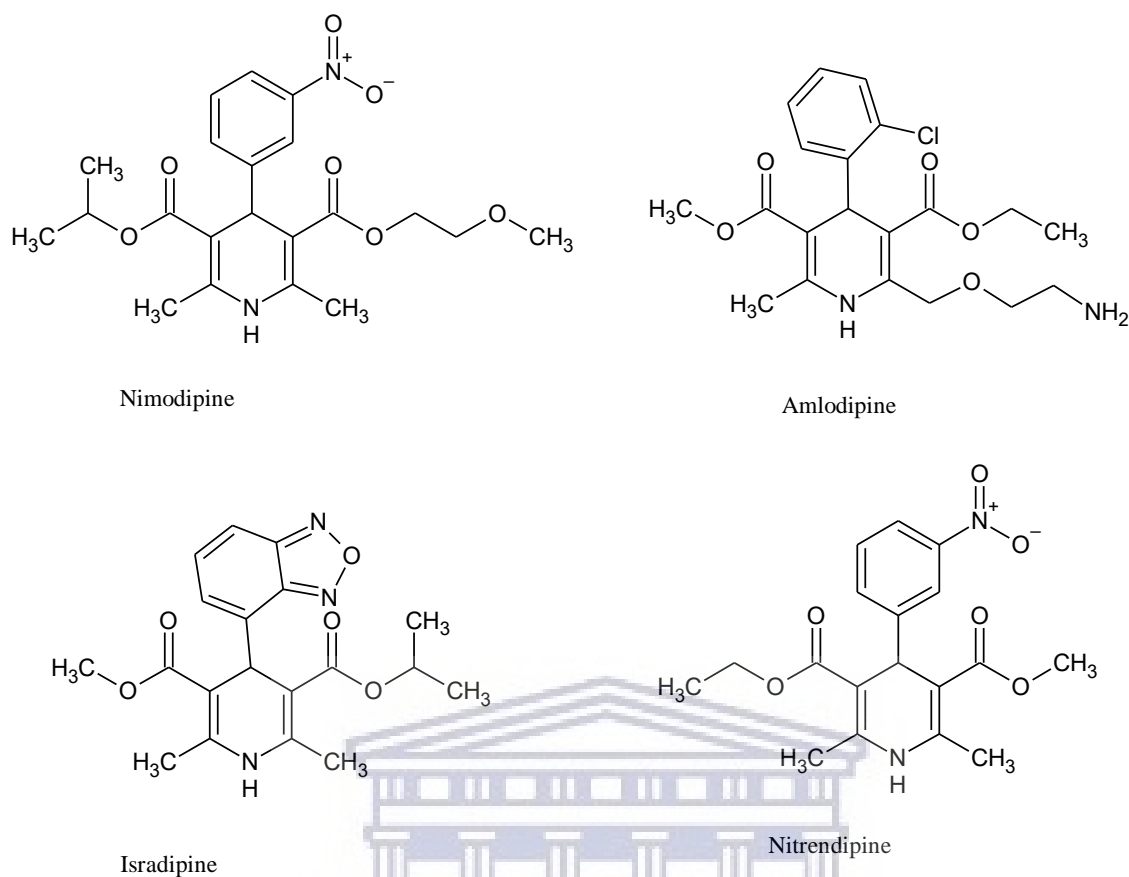


Figure 2.21: L-type calcium channel antagonists.

Ligands that bind to imidazoline I_2 receptors are another class of modulators with good regulatory activities at NMDA receptor channels. Idazoxan and 2-BFI (figure 2.20) are good examples of such modulators. These compounds have been shown to effectively attenuate calcium influx (through NMDA receptor-gated calcium channels) in a voltage-dependent manner in neuronal cells, particularly those in the cerebellar granule and the striatum. In fact, a NMDA receptor-mediated Ca^{2+} influx study has demonstrated the calcium inhibitory effects of these antagonists utilising cortical neurons. With compelling evidence, they were able to show that idazoxan and 2-BFI reversibly block Ca^{2+} in cortical neurons in a way similar to memantine, and to exhibit potent neuroprotection against glutamate-induced excitotoxicity (Jiang *et al.*, 2010).

During glutamate induced excitotoxicity, voltage gated calcium channels are also depolarised, thus contributing to the rise in intracellular calcium ions. It is proposed that compounds or molecules that block or modulate voltage gated calcium channels would be therapeutically useful in lowering intracellular calcium ions to prevent catastrophic consequence of calcium overload. Several studies have indicated that amlodipine, a dihydropyrimidine calcium

antagonist, and other structural related calcium channel antagonists predominantly block L-type voltage calcium channels with additional blocking effects on N- and P/Q-type calcium channels (figure 2.21). These distinctive characteristics enable these compounds to act as neuroprotective agents against neuronal apoptosis mediated by excessive intracellular calcium. Studies have also demonstrated the calcium concentration lowering and neuroprotection effects of voltage gated calcium channel blockers such nimodipine, amlodipine, isradipine and nitrendipine in rat brain, following exposure to 6-hydroxydopamine (6-OHDA) or MPTP. Additionally, amlodipine has been shown to exhibit neuroprotective activity against oxidative stress as it minimises the detrimental effects of oxidative stress in numerous tissue models of neurotoxicity. The neuroprotective benefits of these voltage gated calcium channel blockers are supported by epidemiological studies (retrospective analysis) that show a reduced risk for neurodegenerative disorders in patients treated for hypertension with the dihydropyridine blockers (Anekonda *et al.*, 2011; Hurley and Dexter, 2012; Warnock *et al.*, 2013; Singh *et al.*, 2016). However, more studies are required to understand the neuroprotective effect of this group of blockers.

2.5 Polycyclic cage amine as neuroprotective agents

2.5.1 Neuroprotective functions of polycyclic cages and it derivatives *via* dual attenuation of calcium entry pathways

Since the serendipitous discovery of amantadine and memantine as a neuroprotective agent, a number of structural related analogues or moieties have been developed. Classical analogues are the pentacycloundecylamines, which are polycyclic amines derived from reductive amination of Cookson's 'bird cage' diketone. Other polycyclic cages include the adamantanes, cubanes, homocubanes, bishomocubanes, and trishomocubanes (figure 2.22). These analogues are expected to serve as prototypes for the development of more potentially active compounds. The analogues, when incorporated in drug molecules, have been shown to improve the pharmacological and pharmacokinetics (cell membrane permeability and half-life) properties of drugs. Moreover, most of these analogues are stable and lipophilic in nature, thus enhancing the blood brain barrier permeability of incorporated drugs in the central nervous system. Pentacycloundecylamines have been described as versatile scaffolds with derivatives that target ion channels, second messenger receptors, enzymes and viruses. One good example of a functional pentacycloundecylamines is NGP1-01, a polycyclic cage amine shown to be a multifunctional ion-channel blocker (Grobler *et al.*, 2006; Van der Schyf and Geldenhuys,

2009; Kelani *et al.*, 2020). The structural similarities that exist between memantine and NGP1-01 prompted the investigation into possible neuroprotective activities of NGP1-01 (Geldenhuys *et al.*, 2003). Like memantine, NGP1-01 has been shown to uncompetitively block NMDA receptor channels with a good safety profile and inhibition slightly less potent than memantine. Unlike memantine, it also effectively blocks *L*-type voltage gated calcium channels with blocking activity related to nimodipine, thus a good candidate for dual attenuation of calcium entry pathways in neuronal cells. As such, it exhibits neuroprotective properties as evidently demonstrated by several studies (Duque *et al.*, 2009; Geldenhuys *et al.*, 2004; Mdzinarishvili *et al.*, 2005; Hao *et al.*, 2008; Lockman *et al.*, 2012).

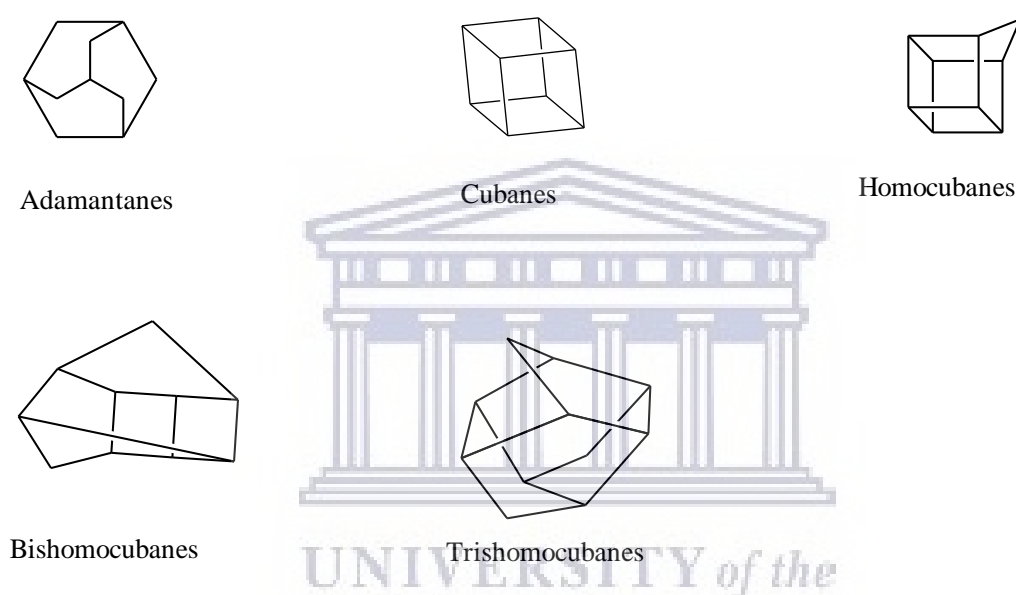


Figure 2.22: Polycyclic cages.

Structure-activity relationship studies of NGP1-01 derivatives suggested that the activities on NMDA receptors and VGCC seems to be more of geometry interaction or steric constraints rather than an electronic consideration as enlarged polycyclic cages tend to exhibit improved calcium inhibitions. However, there are limitations to the size of the polycyclic cages required to enhance inhibitory effects at the ion channel pores of these receptors or channels (Geldenhuys *et al.*, 2003). In the series (NGP1-01 and structurally related derivatives), it was suggested that the polycyclic cage amine may be the most important pharmacophoric element necessary for interaction with the NMDA receptor. However, the addition of the phenyl ring, as observed in NG1-01, increase the inhibitory activity of the pentacycloundecylamine molecule. The enhanced activity has been attributed to the ability of the phenyl ring to form a π - π type aromatic interaction with aromatic amino acids located at the entrance of NMDA receptors. Similar to memantine and amantadine, NGP1-01 is known to exhibit uncompetitive

antagonism in the functional calcium influx assay. At first, it was predicted to bind to the MK-801 binding site. However, binding studies demonstrated otherwise as NGP1-01 seems to interact with a unique binding site that is different from the PCP binding site in the NMDA receptors/ion channel complex (Geldenhuys *et al.*, 2007).

(2-Oxaadamant-1-yl)amines (figure 2.23) are also polycyclic cage amines, which are structurally similar to memantine or amantadine. The NMDA receptor antagonisms of various derivatives, modified with different moieties, were investigated. Of all the moieties, only the ethyl and hexyl moieties showed activities similar to amantadine. However, the alkylation of the amines to form a tertiary or secondary amines resulted in increased NMDA inhibition with potency that is seven times greater than amantadine, but still ten-fold weaker than memantine. Surprisingly, all the benzyl moieties were found to be inactive. This contradicts the structure activity relationship of NGP1-01 that demonstrates such feature is necessary or essential for NMDA receptor antagonism (Dugue *et al.*, 2009; 2010). No study has reported the activity of these polycyclic cages as a voltage gated calcium blocker.

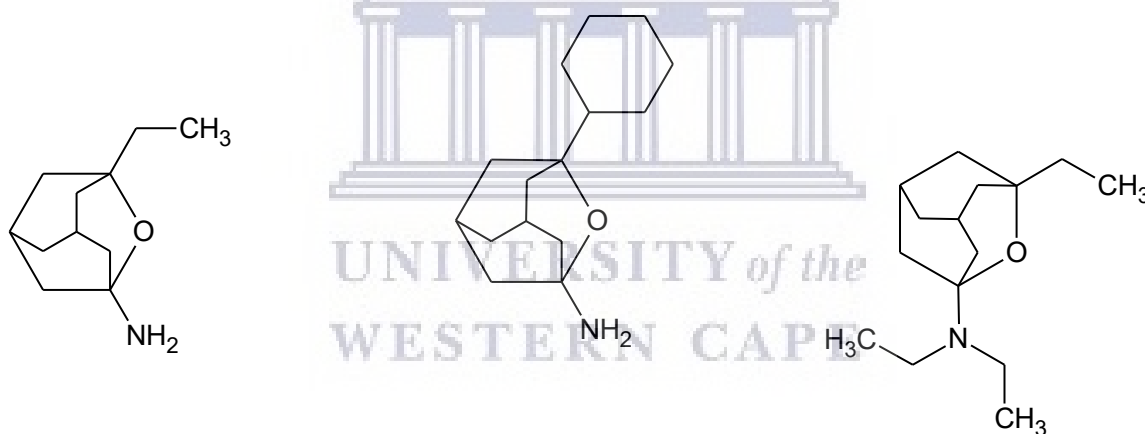


Figure 2.23: (2-Oxaadamant-1-yl)amine derivatives.

2.5.2 Polycyclic cages and attenuation of MPP⁺-induce neurotoxicity

1-Methyl-4-phenylpyridinium (MPP⁺) is a neurotoxin derived from 1-methyl-4-phenyl-1,2,3,6-tetrahydropyridine (MPTP) through oxidative metabolism by astroglial cells. It is actively transported, *via* the dopamine active transporter, into the dopaminergic neurons, where it accumulates and interferes with mitochondrial functions to induce harmful effects to cell's organelles and promote neuronal cell death. MPP⁺ induces neuronal cell death by targeting and inhibiting electron transport at mitochondrial complex 1, organelle crucial for respiration in cells, so as to interfere and destroy ATP synthesis that subsequently promote MPP⁺ toxic

effects. These toxic effects are mainly attributed to excessive production and accumulation of ROS that activate oxidative stress and consequential promote peroxidative damage to proteins, lipids and nucleic acids. As such, compounds that prevent MPP⁺ from entering the neurons may protect the neuronal cells from degeneration (Geldenhuis *et al.*, 2003; Prins *et al.*, 2009; Wang *et al.*, 2018; Bhurtel *et al.*, 2019). NGP1-01, if co-treated with MPTP, has proven to significantly improve the dopamine content and activities in the brain of mice-model parkinsonian studies, potently inhibiting dopamine re-uptake into the pre-synaptic terminal of murine synaptosomes through the blockage of the dopamine transporter (DAT). In fact, the phenylethylamine derivative of NGP1-01 had demonstrated a more potent neuroprotection than NGP1-01 in a MPTP-parkinsonian mouse model (Youdim *et al.*, 2007; Geldenhuis *et al.*, 2009). In a neuron-glia cultured cell line exposed to MPP⁺ in a PD model, amantadine was shown to significantly protect dopaminergic neurons from MPP⁺ induced neurotoxicity by preventing MPP⁺ entry *via* the same transporter (DAT). This characteristic may make these compounds neuroprotective against MPP⁺ induced cell (Ossola *et al.*, 2011).

The protection against MPP⁺-induced toxicity, *via* DAT inhibition, of polycyclic cage amines is well known. Other protective pathways could potentially include: restoration of antioxidant enzymes such as SOD and GSH; downregulation of the Bax/Bcl-2 ratio and Apaf-1; inhibition of cytochrome *c* release; and inactivation of caspase-9 and caspase-3. However, no study has reported or investigated the protective effects of polycyclic cage amines against MPP⁺ induced neurotoxicity *via* these pathways (Wang *et al.*, 2018).

2.6 Norbornane derivatives in medicinal chemistry

Norbornane scaffolds are moieties common in a number of pharmacologically active compounds. Synthesised derivatives of norbornane scaffolds include, amidst others, the dicyclic, tricyclic (oxatricyclo[5.2.1.0^{2,6}]dec-8-ene-3,5-dione and tricyclo[6.2.1.0^{2,7}]undeca-4,9-diene-3,6-dione) and tetracyclic derivatives (figure 2.24), and the pentacycloundecane derivatives (pentacycloundecylamines). While pentacycloundecylamines are closed cages, di- and tricyclic derivatives are open cage molecules derived from the Diels-Adduct reaction of benzoquinone and cyclopentadiene (Diels and Alder, 1928). The dicyclic and tricyclic derivatives (open cages) have been demonstrated to be active against feline herpes virus (FHV-1; Dejmek *et al.*, 2014), coxsackievirus (Sala *et al.*, 2009; 2011; 2012; Hrebabecky *et al.*, 2012) and Gram-positive and Gram-negative bacteria strains (Hickey *et al.*, 2018).

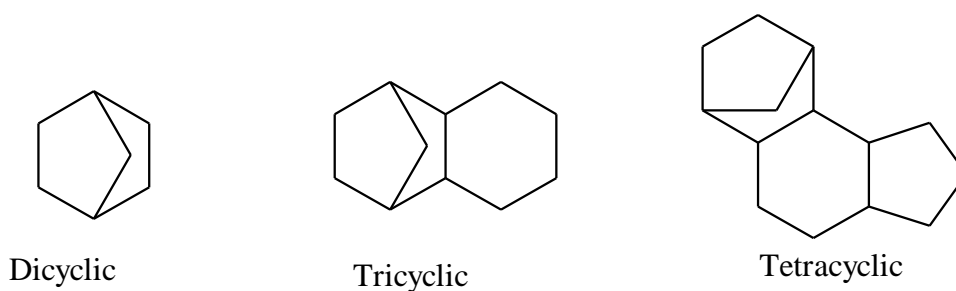


Figure 2.24: Opened polycyclic cages with norbornane scaffolds.

Interestingly, lurasidone (figure 2.25) is an antipsychotic agent approved by the FDA for treatment of the acute phase of schizophrenia. This tricyclic derivative with a norbornane scaffold has been shown to be well tolerated when compared to the second-generation antipsychotic drugs such as ziprasidone or olanzepine (figure 2.25). The tolerability of lurasidone is attributed to negligible interaction or affinity with histamine H₁ and muscarinic M₁ Receptors. The reduced interactions or affinities with these receptors are believed to be the reason for the absence of side effects such as increased appetite, drowsiness and aggravated cognitive functions that are prominent in the second-generation antipsychotic agents. In binding studies, the structure activity relationship of lurasidone demonstrated that the bulkiness of the norbornane-2,3-dicarboximide is, in part, responsible for the high selectivity against H₁ and M₁ receptors (Ichikawa *et al.*, 2012). The antipsychotic property of lurasidone is due to its ability to fully block, with high affinity, dopamine (D₂ and D₃), α_{2C}-adrenergic and 5-hydroxytryptamine (5-HT_{2A}, 5-HT₇ and 5-HT_{1A}) receptors. Additional effects observed during preclinical trials of lurasidone include antidepressant effects, improvement of cognition associated with executive functions and anxiolytic efficacy (Findling *et al.*, 2015; Jaeschke *et al.*, 2016).

Like the pentacycloundecylamines, these open cages have also been used to alter the bioavailability features of certain drugs due to their bulkiness and lipophilicity. In a recent study, a series of thiopyrano[2,3-d][1,3]thiazol-2-one (figure 2.26) derivatives conjugated with tricyclic norbornane derivatives displayed anti-tumor activities that target cancer of the lungs, breast, blood, kidneys, and skin (Lesyk *et al.*, 2006).

The neuroprotective effects of the closed cages have been extensively studied and are well known, and numerous studies have already reported the multifunctional targets modulated by these cages. Despite the vast knowledge and extensive studies on the synthesis of open cage

molecules with a norbornane scaffold, the evaluations as potential therapeutic agents in medicinal chemistry are still only limited to antiviral, anti-bacterial and antipsychotic effects.

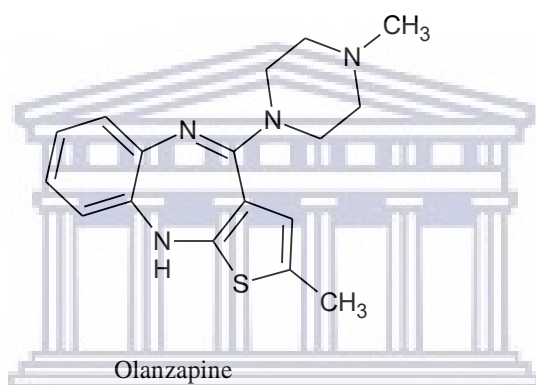
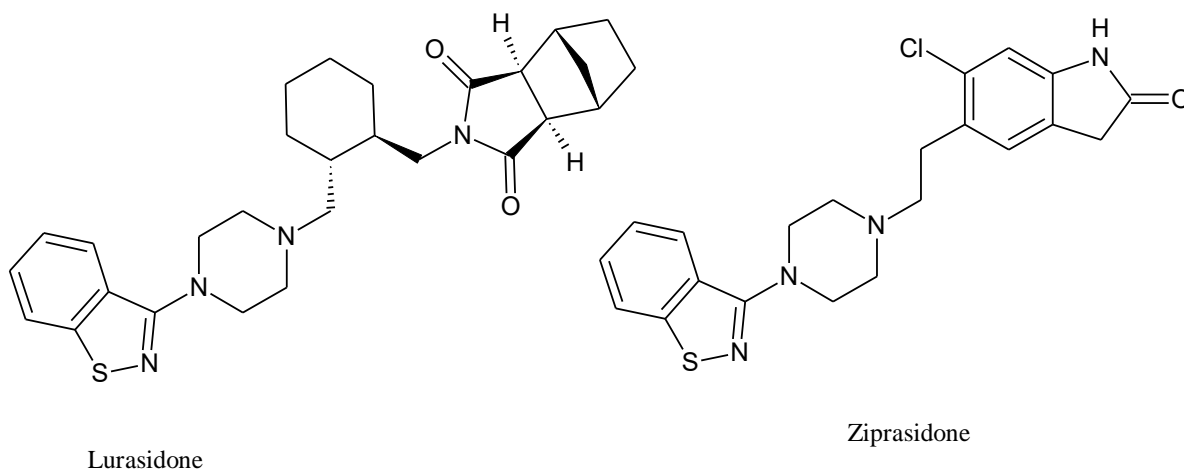
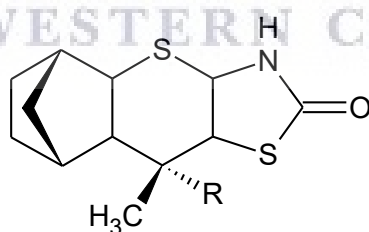


Figure 2.25: Antipsychotic agents.



Thiopyrano[2,3-d][1,3]thiazol-2-one

Figure 2.26: An anticancer agent.

A previous study reported the neurobiological effects of a small series of open cage molecules (tricycloundecane derivatives). The inhibitory effects of these molecules through attenuation of NMDA receptor- and voltage gated calcium channel-mediated calcium influx were evaluated, at 100 μ M, in murine synaptoneurosomes (Egunlusi *et al.*, 2015). To the best of our knowledge, no study has reported the neuroprotective effects of these open cages.

2.7 Summary

Neurodegenerative disorders are diseases characterised by a progressive loss of neuronal functions, because of cell death either by necrosis or apoptosis. These disorders, associated with the elderly, occur in over 30 million persons worldwide with the environment, gender and genetic factors playing a crucial role in its pathology. These disorders can also occur earlier in life, but such occurrences are usually associated with genetic factors and, in some cases, exposure to environmental contaminants. The disorders, amidst others, include Alzheimer's disease, Parkinson's disease, amyotrophic lateral sclerosis, and Huntington disease. Symptoms or clinical features associated with each disorder are dictated by the part of the brain or central nervous system affected in the degenerative process. Of all the neurodegenerative disease cases, AD and PD are the most common and an anticipated rise in numbers and cost are expected in the next several decades. Current treatments for each disorder only offer symptomatic relief without halting the degenerative process.

Despite countless studies proposing various mechanism of neurodegeneration, the pathogenesis and mechanisms of neurodegeneration are still poorly defined. However, the general consensus is that neuronal cells undergo cell death either by necrosis or apoptosis *via* interrelated processes that include oxidative stress, excitotoxicity, RNA metabolism, mitochondria dysfunction, protein aggregation and propagation, proteasomal dysfunction, autophagic/lysosomal dysfunction, prion-like spread, loss of growth factors and neuroinflammation. In the processes, the role of excitotoxicity *via* glutamate-induced activation of receptors and channels is prominent. Moreover, excitotoxicity is implicated in the pathology of several neurodegenerative disorders. In excitotoxicity, it is believed that excessive extracellular glutamate overactivates NMDA receptor and voltage gated calcium channels leading to intracellular calcium overload that through a cascade of events result in neuronal cell death.

Therefore, it is therapeutically logical to use compounds with inhibitory activities at NMDA receptor and voltage-gated calcium channels. These inhibitors could provide protection through regulation of excessive calcium influx mediated by prolonged glutamate activity. However, combatting glutamate-induced excitotoxicity has been a major challenge as the same process that leads to excitotoxic cell death is required for the normal physiological function of the brain. Competitive NMDA receptor blockers (midafotel and selfotel) were first introduced but were quickly withdrawn due their dose-relative psychotomimetic side effects.

Uncompetitive NMDA receptor blockers (MK-801 and phenylcyclidine) with high binding affinities were later considered, but were also marked by undesirable psychotomimetic side effects. However, uncompetitive NMDA receptor blockers (memantine and amantadine) have been shown to be clinically well tolerated for the treatment of Alzheimer's disease and Parkinson's disease, respectively. The tolerability is attributed to the moderate affinity of these blockers to the PCP binding site. Nonetheless, they exhibit significant NMDA receptor inhibitory effect and safe side effect profiles. During glutamate induced excitotoxicity, voltage-gated channels are also depolarised, contributing to the intracellular calcium rise. Nimodipine and other dihydropyridines calcium blockers have displayed intracellular calcium lower and neuroprotective effects in rat brain neurotoxicity studies.

Polycyclic cage derivatives, open and closed, are interesting compounds with several established pharmacological activities. Moreover, they have been shown to enhance the pharmacological and pharmacokinetic properties of other drug molecules after conjugation. NGP1-01 is a closed polycyclic cage amine that has been shown to effectively block NMDA receptors and *L*-type voltage gated calcium channels in a manner similar to memantine and nimodipine, respectively, with good safety profiles. This multifunctional ion channel block exhibited by NGP1-01 ensures that neurons are protected from the destructive consequence of calcium overload. Additionally, NGP1-01, a pentacycloundecylamine, has been shown to demonstrate significant neuroprotection against MPP⁺-induced cell death.

The synthesis of open cage analogues with norbornane scaffold has been extensively explored. However, their uses in medicinal chemistry as a pharmacological active molecules are limited. These analogues have been shown to be active against certain virus and bacterial strains. Some analogues such as lurasidone have demonstrated significant antipsychotic effects with few side effects when compared to the second generation antipsychotic drugs.

The neuroprotective effects of closed cages such as NGP1-01, *via* dual calcium inhibition and MPP⁺ mediated neurotoxicity attenuation, are well documented in several studies. The neuroprotective effects of the open- and rearranged-cage molecules (developed analogues), in the present study, are yet to be explored or investigated. Analogues that exhibit structural similarities with NGP1-01 or other polycyclic closed cage amines are postulated to be neuroprotective, as observed in a previous study (Egunlusi *et al.*, 2015), and may present with therapeutic properties able to halt the progression of neurodegenerative disorders.

CHAPTER 3

Synthetic procedure

3.1 Introduction

Compounds containing the norbornane structure are versatile building blocks that not only exist as agonists or antagonists of biologically active substances, but are also used in the synthesis of polycyclic analogues or derivatives. Some of these analogues exhibit a wide variety of pharmacological activities. These characteristics make them fundamentally important in medicinal chemistry as potentially useful scaffolds to be used in drug design. This study involves the synthesis of norbornane derivatives fused with moieties such as furandione, pyrrolidinedione, piperidine and benzoquinone, which were conjugated with various aliphatic and heterocyclic amines to obtain the desired compounds.

3.2 Instrumentation used for synthesis

The following instrumentation were used in the synthesis of the intermediates and desired compounds, the measurement and weighing of reactants and solvents, the identification and isolation of compounds, the monitoring of reaction progression, the selection of mobile phase, the separation and/or purification of reaction products, and the structural and physical characterisation of the final compounds.

3.2.1 Apparatus for reaction conditions

The reactions were performed at the different conditions necessary to provide sufficient activation energy for each product formation.

3.2.1.1 Weighing apparatus and stirrers

A Sartorius analytic balance, up to four decimal places, was used to weigh reactants and products during synthesis. The weighing of samples for the analytical work or biological assays was done on the Shimadzu (AUD 220D) analytical balance. This analytical balance is a dual-range semi micro balance up to five decimal places.

For continuous stirring during the reactions, IKA and RCT basic magnetic stirrers were used.

3.2.1.2 Heating apparatus for reactions

Heating mantles (Electromantle MV) and hotplates (IKA and RCT basic) were used to supply thermal energy to certain reactions.

3.2.1.3 Cooling baths

In synthetic steps where temperature below the room temperature were required, an ice bath was set up and used.

3.2.1.4 Microwave reactor

A CEM Discovery SMP microwave reactor that is fitted with an intellivent™ Pressure Control System and CEM's synergy™ software was used to supply microwave energy where this type of energy was required in the reaction condition.

3.2.1.5 High pressure metal reactor

A sealed tube made of stainless steel was used to carry out reactions under high pressure. The high pressure metal reactor was used to contain the pressure generated by solvent-reactant mixtures. The metal reactor is designed to withstand high pressure up to 700 kPa.

3.2.2 Separation techniques

The different techniques that were used in the separation and the purification of intermediates and products are as follows:

3.2.2.1 Thin layer Chromatography

The progress of reactions and column chromatographic elution were monitored using thin layer chromatography on aluminium silica gel sheets (TLC silica gel 60 F₂₅₄, product catalogue no. 105555, Merck Millipore), which also aided the isolation processes. Visualisation of thin layer chromatography was achieved using ultra violet (UV) light at 254 nm and 366 nm in a Chromato-vue® cabinet (Ultra-violet product, USA). For the development of TLC, saturated iodine vapours in a transparent glass chamber was used.

3.2.2.2 Column chromatography

The separation of reaction mixtures and the purification of desired products were performed by column chromatography using silica gel 60 (particle size 63-200 μm) in standard glass

columns. The lengths and diameters of the glass column chosen for column chromatography depended on the amount of the reaction mixtures.

3.2.2.3 Mobile phases

Different ratios of mobile phases were prepared for TLC plate development and chromatographic elution or separations. Solvents such as hexane, ethyl acetate, chloroform, dichloromethane, methanol, and ammonia solution (25%) were used for preparing the different mobile phases.

3.2.2.4 Crystallisation

Re-crystallisation of some products was required for purification and isolation. The suitable solvents for this process were hexane, ethyl acetate, methanol and dichloromethane. The choice of solvents was dependent on the polarity of the reaction mixtures and/or products.

3.2.3 Spectroscopic and physical characterisation

The structures of the desired compounds were characterised and confirmed by means of nuclear magnetic resonance (NMR), Fourier transform infrared (FT-IR) and mass spectrometry (MS) techniques. In the NMR spectroscopy, ^1H , ^{13}C and distortionless enhancement of polarisation transfer (DEPT) analysis were performed for structural elucidation. The spectra obtained from the DEPT-135 analysis enable CH_3 , CH or CH_2 differentiation. The carbon peaks of CH_3 and CH gave positive signals and CH_2 gave negative signal.

The physical characteristics of the compounds are reported as physical state, colour and melting point.

3.2.3.1 NMR

NMR's were obtained using the Bruker 400 MHz instrument. The ^1H spectra were obtained at 400 MHz while the ^{13}C spectra were obtained at 100 MHz on the NMR spectrometer. Tetramethylsilane (TMS) and deuterated residue solvent peaks were used as internal standards. The chemical shifts are reported as δ in parts per million (ppm) using TMS (δH : 0 ppm; δC : 0 ppm) and CDCl_3 (δH : 7.26 ppm; δC : 77.16 ppm) or CD_3OD (δH : 3.35, 4.78 ppm; δC : 49.3 ppm) or DMSO-d_6 (δH : 2.49 ppm; δC : 39.7 ppm) peaks as reference. The multiplicities of NMR signals are expressed as: s, singlet; bs, broad singlet; d, doublet; dd, doublet of doublets; dt, doublet of triplets; t, triplet; td, triplet of doublets; q, quartet; Q, quintet; St, septet; m,

multiplet, and the coupling constants (J) are given in hertz (Hz). The ^1H data is presented as follows: chemical shift in ppm (multiplicity, coupling constant, integration as number of protons).

3.2.3.2 MS

High-resolution mass spectra (HRMS) were recorded on a Water API Q-TOF Ultima spectrometer (Stellenbosch University, Stellenbosch, South Africa) using electrospray ionization technique.

3.2.3.3 IR

Infrared spectra were obtained on a Perkin Elmer Spectrum 400 FT-IR/FT-NIR spectrometer, fitted with a diamond attenuated total reflectance (ATR) attachment.

3.2.3.4 Melting point apparatus

Melting points were measured using glass capillary method. The melting points were determined using a Stuart SMP-300 melting point apparatus and capillary tubes. The melting points are uncorrected.

3.2.3.5 Elemental analysis

A Vario EL Cube Elemental Analyzer (Elementar[®]) was used to determine the C, H, N, & S in products that required additional structural analysis. A sample size of at least 1 mg was used to calculate the percentage of each atom in some of the synthesised compounds.

3.3 Synthesis of designed compounds

3.3.1 Reagents

Unless otherwise specified, all reagents were obtained from Merck (St Louis, MO, USA) and Sigma-Aldrich[®] (UK). The reagents were of analytical grade and used without further purification unless specified. Solvents used for reactions and chromatography were purchased from various commercial sources and dried using standard methods. To get dry DCM, commercially available DCM was initially dried over anhydrous calcium chloride and then distilled. The distillate was collected and stored in an amber glass bottle away from light over 3\AA molecular sieves. Solvents such as ethyl acetate, hexane, acetone and benzene were also distilled, and the distillates were stored in amber glass bottles.

3.3.2 General synthetic approach

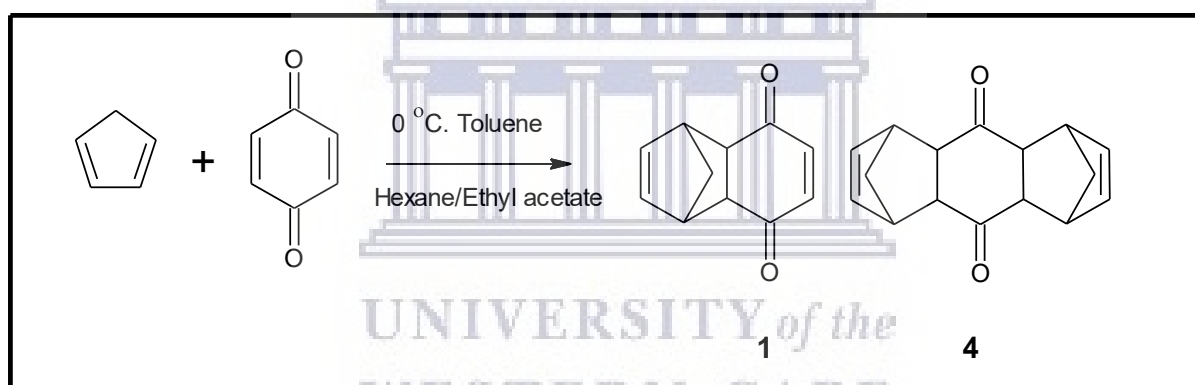
The synthesis of the proposed series of compounds involved several experimental procedures and methods. In this part, general synthetic approaches for the different series of compounds and challenges faced during synthesis are discussed. In each series, the primary structure was synthesised and used as the scaffold for further synthesis within each series.

3.3.2.1 Synthetic procedures and characterisation data of compound 1-7

The cycloaddition reaction between *p*-benzoquinone and monomerised dicyclopentadiene yielded tricycloundeca-4,9-diene-3,6-dione (**1**) which was used as the scaffold for all further synthesis within this series.

3.3.2.1.1: Tricyclo[6.2.1.0^{2,7}]undeca-4,9-diene-3,6-dione (**1**)

3.3.2.1.2: Pentacyclo[10.2.1.1^{5,8}.0^{2,11}.0^{4,9}]hexadeca-6,13-diene-3,10-dione (**4**)



A solution of *p*-benzoquinone (6 g, 55.50 mmol) in benzene (50 ml) and 25 ml of hexane:ethylacetate (4:1) were mixed in a 250 ml round-bottom flask. The resulting solution was stirred and cooled to 0 °C using an ice bath. A stoichiometric volume of monomerised cyclopentadiene (7 ml, 83.24 mmol) was slowly added, with an increment of 3.5 ml, to the mixture and stirred for 3.5 hours. The reaction mixture was concentrated *in vacuo* to form a crude yellow product. The product was purified by re-crystallisation in hexane to form a pure yellow crystal (yield: 9.7 g, 100%). The NMR data and melting points of compound **1** correspond to those reported in the literature (Ito *et al.*, 2007; Egunlusi *et al.*, 2015).

The isolation of one of the fractions obtained from a reaction involving tricyclo[6.2.1.0^{2,7}]undec-9-ene-3,6-dione (**2**) and propylamine afforded a di-substituted Diels Alder conjugate, compound **4** in 12.5% yield. The formation of this compound was possible due to impurities

from intermediate reactions. It was proposed that reaction between cyclopentadiene and tricyclo[6.2.1.0^{2,7}]undeca-4,9-diene-3,6-dione (**1**), both impurities, gave the tetracyclic conjugate, as seen in compound **4**. Ideally, it would have been discarded but the structural similarities existing between the conjugate and MK-801 allows us to include it in the list of compounds for biological evaluation.

The procedure and work up leading to the isolation of impurities, **4**, was as follows:

Tricyclo[6.2.1.0^{2,7}]undec-9-ene-3,6-dione (**2**, 1 g, 5.68 mmol) was dissolved in THF (25ml). Sodium hydride (0.1 g, 4.17 mmol) and acetic acid (2 g, 33.30 mmol) was added to the solution. Propylamine was added in excess, and the solution was continuously stirred at room temperature. After 24 hours, the reaction mixture was washed with saturated brine (50 ml), saturated sodium bicarbonate solution (50 ml) and water (50 ml). The organic fraction was dried over anhydrous magnesium sulphate and filtered. The filtrate was concentrated in *vacuo* to give a crude yellow mixture. The crude mixture was purified by silica gel column chromatography using a mobile phase of hexane and ethyl acetate in ratio of 1:1 (yield: 0.17 g, 12.4%). The NMR data and melting points of compound **4** correspond to those reported in the literature (Gielsing *et al.*, 2004).

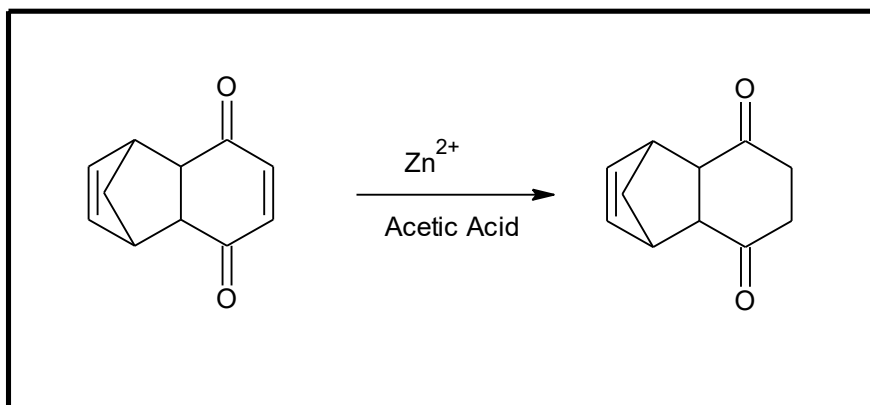
Tricyclo[6.2.1.0^{2,7}]undeca-4,9-diene-3,6-dione (1**)**

Physical characteristics: A yellow crystal, Mp: 70-71 °C. FT-IR (ATR): V_{\max} (cm⁻¹) = 3034, 2987, 2955, 1660, 1334, 1298, 1065, 726. ¹H NMR (400 MHz, CDCl₃): δ 6.54 (s, 2H), 6.04 (t, J = 1.7 Hz, 2H), 3.52 (t, J = 1.6 Hz, 2H) 3.20-3.19 (m, 2H), 1.53-1.50 (dt, J = 8.8, 1.8 Hz, 1H), 1.41 (d, J = 8.7 Hz, 1H). ¹³C NMR (100 MHz, CDCl₃) and DEPT-135: δ 199.43 (C=O), 142.04 (C=C), 135.29 (C=C), 48.76 (CH), 48.70 (CH₂), 48.34 (CH).

Pentacyclo[10.2.1.1^{5,8}.0^{2,11}.0^{4,9}]hexadeca-6,13-diene-3,10-dione (4**)**

Physical characteristics: A white crystal, Mp: 154-158 °C. FT-IR (ATR): V_{\max} (cm⁻¹) = 3008, 2982, 1682, 1330, 1243, 1031, 706. ¹H NMR (400 MHz, CDCl₃): δ 6.17 (t, J = 1.7 Hz, 4H), 3.34 (s, 4H), 2.86 (s, 4H), 1.46-1.43 (dt, J = 8.6, 1.7 Hz, 2H), 1.28-1.26 (d, J = 8.6 Hz, 2H). ¹³C NMR (100 MHz, CDCl₃) and DEPT-135: δ 212.66 (C=O), 136.36 (C=C), 53.21 (CH), 49.58 (CH₂), 48.26 (CH). MS (HR-ESI) m/z : calc. 241.1223 (M+H⁺), found 241.1195 (M+H⁺), 263.1039 (M+Na). Anal. Calcd for C₁₆H₁₆O₂: C, 79.97; H, 6.71. Found: C, 81.53; H, 4.44.

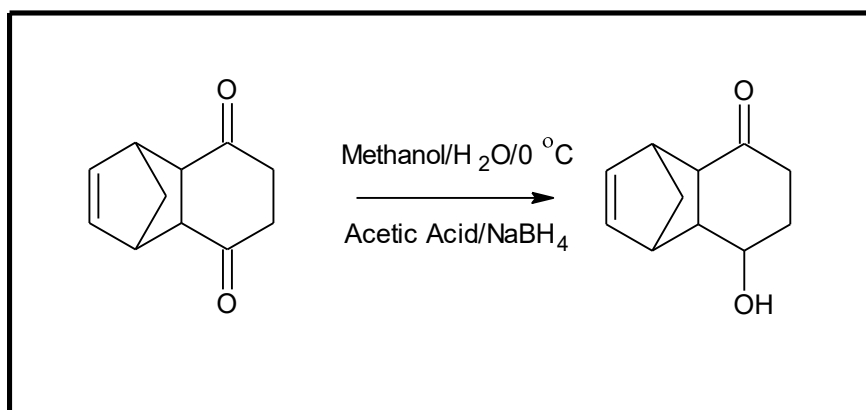
3.3.2.1.3: Tricyclo[6.2.1.0^{2,7}]undec-9-ene-3,6-dione (2)



To a solution of tricyclo[6.2.1.0^{2,7}]undeca-4,9-diene-3,6-dione (**1**, 9.7 g, 55.75 mmol) in 100 ml of glacial acetic acid, powdered zinc (12 g, 183.54 mmol) was added. The mixture was sonicated, in a Soniprep 150, for 30 minutes. After 30 minutes, the mixture was filtered and the residue washed with dichloromethane (20 ml). Brine (50 ml) was added to the combined filtrates and shook vigorously. Further extraction of the aqueous phase was done using dichloromethane (4 x 50 ml). The organic fractions were combined and washed with water (100 ml), a saturated aqueous NaHCO₃ solution (100 ml), and again with water (100 ml). Anhydrous magnesium sulphate was added to the organic fraction to remove any trace of water after extraction. The mixture was filtered and the solvent was evaporated under reduced pressure to give a crude yellow oil. The final product was further purified from the crude reaction mixture by silica gel column chromatography using a mobile phase of hexane/ethyl acetate/dichloromethane (10/5/2) to render the pure product as a yellow oil (yield: 6.98 g, 71.2%). The NMR data and melting points of compound **2** correspond to those reported in the literature (Ito *et al.*, 2007; Egunlusi *et al.*, 2015).

Physical characteristics: A yellow oil. FT-IR (ATR): ν_{\max} (cm⁻¹) = 2921, 1701, 1301, 1256, 1156, 726. ¹H NMR (400 MHz, CDCl₃): δ 6.18 (t, J = 1.6 Hz, 2H), 3.45 (t, J = 1.6 Hz, 2H), 3.21 (m, 2H), 2.68-2.58 (m, 2H), 2.36-2.26 (m, 2H), 1.50-1.47 (dt, J = 8.7, 1.6 Hz, 1H), 1.35 (d, J = 8.7 Hz, 1H). ¹³C NMR (100 MHz, CDCl₃) and DEPT-135: δ 209.57 (C=O), 136.65 (C=C), 51.85 (CH), 48.76 (CH₂), 47.46 (CH), 37.95 (CH₂).

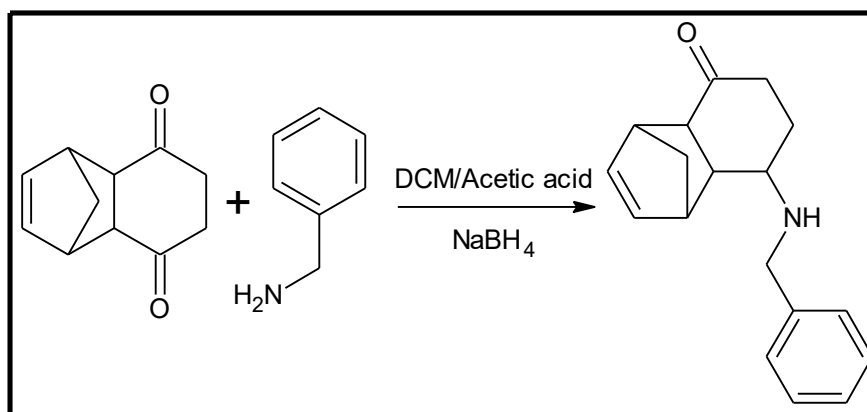
3.3.2.1.4: 6-Hydroxytricyclo[6.2.1.0^{2,7}]undec-9-en-3-one (3)



Tricyclo[6.2.1.0^{2,7}]undec-9-ene-3,6-dione (**2**, 3.3 g, 18.75 mmol) was dissolved in a mixture of methanol (60 ml) and water (10 ml) contained in 250 ml round bottom flask. The solution in the flask was cooled to 0 °C on an external ice bath. Sodium borohydride (0.25 g, 6.61 mmol) was added to the cooled mixture and it was stirred to room temperature, and then continuously for an additional 4 hours. After approximately 5 hours, glacial acetic acid (0.85 ml) was added, followed by the addition of ice (14 g). The resulting mixture was extracted with dichloromethane (3 x 50 ml). The combined organic fractions were washed with water (100 ml), dried over anhydrous magnesium sulphate and filtered. The solvent was evaporated *in vacuo* to afford the crude mixture as light yellow oil. The crude mixture was purified by column chromatography using the mobile phase of hexane, ethyl acetate and dichloromethane in the ratio of 10:5:2 (yield: 2.85 g, 86.4%). The NMR data and melting points of compound **3** correspond to those reported in the literature (Ito *et al.*, 2007; Egunlusi *et al.*, 2015).

Physical characteristics: A light-yellow oil. FT-IR (ATR): ν_{\max} (cm⁻¹) = 3398, 2940, 1687, 1331, 1217, 1049, 722. ¹H NMR (400 MHz, CDCl₃): δ 6.19 (m, 2H), 4.33-4.28 (m, 1H), 3.27 (bs, OH), 3.07 (m, 1H), 2.90-2.87 (dd, J = 10.4, 3.8 Hz, 1H), 2.85-2.81 (m, J = 8.4, 5.3, 2.9 Hz, 1H), 2.23-2.15 (dt, J = 14.0, 6.9 Hz, 2H), 1.93-1.84 (m, 2H), 1.83-1.75 (m, 1H), 1.45-1.42 (dt, J = 8.4, 1.8 Hz, 1H), 1.30 (d, J = 8.4 Hz, 1H). ¹³C NMR (100 MHz, CDCl₃) and DEPT-135: δ 212.96 (C=O), 137.30 (C=C), 134.81 (C=C), 67.74 (C-OH), 51.59 (CH), 50.15 (CH₂), 46.21 (CH), 45.59 (CH), 45.23 (CH), 35.71 (CH₂), 28.05 (CH₂). MS (HR-ESI) m/z : calc. 179.1067 (M+H⁺), found 179.1068 (M+H⁺), 201.0889 (M+Na).

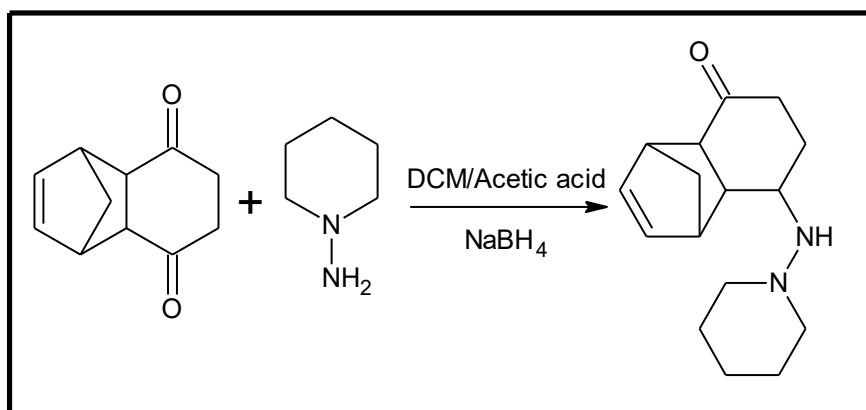
3.3.2.1.5: 6-(Benzylamino)tricyclo[6.2.1.0^{2,7}]undec-9-en-3-one (5)



Tricyclo[6.2.1.0^{2,7}]undec-9-ene-3,6-dione (**2**, 0.9 g, 5.11 mmol) was dissolved in 30 ml dichloromethane in a round-bottom flask. To the mixture, a solution of sodium borohydride (0.1 g, 2.64 mmol) in acetic acid (2 g, 33.30 mmol) was added. Benzylamine (1.47 g, 13.73 mmol) was added to the combined mixture, and was continuously stirred at room temperature for 60 hours. The reaction mixture was washed with saturated brine (50 ml), saturated sodium bicarbonate (50 ml) and water (50 ml). Anhydrous magnesium sulphate was used to dry the organic fraction, and upon filtration and evaporation it gave a brownish reaction mixture. The crude mixture was purified using silica gel column chromatography with 50% ethyl acetate in chloroform as mobile phase. The final product gave a light brown oil that solidified at room temperature (yield: 0.22 g, 16.2%).

Physical characteristics: A light brown oil. FT-IR (ATR): ν_{\max} (cm⁻¹) = 3289, 2984, 2940, 1685, 1450, 1352, 1128, 903, 735. ¹H NMR (400 MHz, CDCl₃): δ 7.38-7.25 (m, 5H), 6.24-6.22 (dd, J = 5.4, 2.9 Hz, 1H), 6.12-6.09 (dd, J = 5.6, 2.9 Hz, 1H), 3.89 (s, 2H), 3.33 (m, 1H), 3.17-3.13 (m, 2H), 2.93-2.83 (m, 2H), 2.28-2.21 (m, 1H), 2.15-2.05 (m, 1H), 1.75-1.68 (m, 1H), 1.66-1.58 (m, 1H), 1.45-1.42 (dt, J = 8.6, 1.9 Hz, 1H), 1.33 (d, J = 8.3 Hz, 1H). ¹³C NMR (100 MHz, CDCl₃) and DEPT-135: δ 213.40 (C=O), 140.54 (Ar-C), 136.65 (C=C), 136.02 (C=C), 128.50 (Ar-C), 127.98 (Ar-C), 127.06 (Ar-C), 54.57 (CH), 51.53 (CH₂), 51.32 (CH), 50.26 (CH₂), 47.26 (CH), 45.26 (CH), 43.17 (CH), 38.90 (CH₂), 25.14 (CH₂). MS (HR-ESI) m/z : calc. 268.1696 (M+H⁺), found 268.1700 (M+H⁺), 269.1734, 270.1760.

3.3.2.1.6: 6-(1-Piperidylamino)tricyclo[6.2.1.0^{2,7}]undec-9-en-3-one (6)



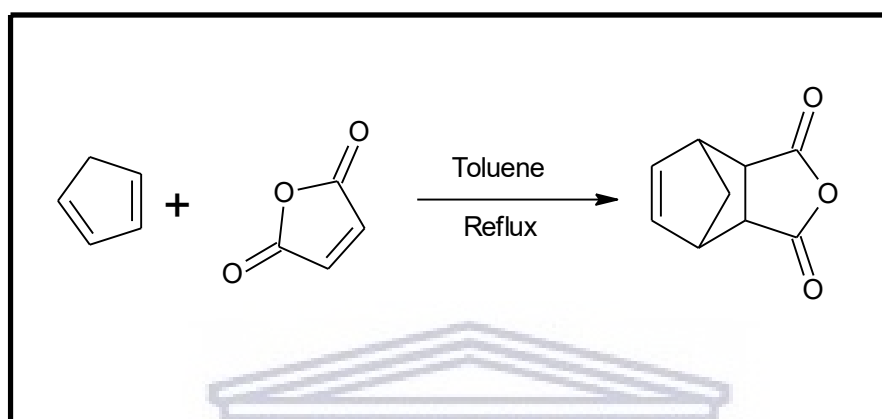
To a solution of tricyclo[6.2.1.0^{2,7}]undec-9-ene-3,6-dione (**2**, 0.8 g, 4.55 mmol) in dichloromethane (30 ml), a mixture of sodium borohydride (0.1 g, 4.17 mmol) and acetic acid (2 g, 33.30 mmol) was added. To the combined solution, 1-aminopiperidine (0.45 g, 4.49 mmol) was added and stirred for 18 hours. After completion, the reaction mixture was washed with saturated brine (50 ml), saturated sodium bicarbonate (50 ml) and water (50 ml). Anhydrous magnesium sulphate was added to eliminate traces of water and filtered. The solvent of the dried organic fraction was evaporated under reduced pressure to give a dark crude mixture. The final product was obtained by silica gel column chromatography with 70% ethyl acetate in chloroform used as mobile phase to afford a dark brown oil that solidified at room temperature (yield: 0.43 g, 36.44%).

Physical characteristics: A dark brown oil. FT-IR (ATR): ν_{\max} (cm⁻¹) = 3288, 2984, 2939, 1686, 1450, 1352, 1251, 1167, 904, 724. ¹H NMR (400 MHz, CDCl₃): δ 6.19-6.17 (dd, J = 5.6, 3.0 Hz, 1H), 6.02-6.00 (dd, J = 5.6, 2.9 Hz, 1H), 3.39-3.34 (dd, J = 15.1, 6.6 Hz, 1H), 3.27 (m, 1H), 3.11 (m, 1H), 2.85-2.78 (m, 2H), 2.71-2.43 (m, 4H), 2.21-2.19 (t, J = 4.1 Hz, 1H), 2.15-2.08 (q, J = 18.2, 9.5 Hz, 1H), 1.62-1.56 (m, J = 11.4, 5.8 Hz, 4H), 1.55-1.52 (td, J = 7.9, 4.2 Hz, 2H), 1.42-1.36 (m, 2H), 1.35 (d, J = 1.7 Hz, 1H), 1.27 (d, J = 8.2 Hz, 1H). ¹³C NMR (100 MHz, CDCl₃) and DEPT-135: δ 214.12 (C=O), 136.84 (C=C), 136.73 (C=C), 57.79 (CH₂), 53.61 (CH), 51.26 (CH), 50.17 (CH₂), 47.29 (CH), 45.58 (CH), 42.48 (CH), 38.83 (CH₂), 26.17 (CH₂), 24.37 (CH₂), 24.06 (CH₂). MS (HR-ESI) m/z : calc. 261.1961 (M+H⁺), found 261.1965 (M+H⁺), 262.1996.

3.3.2.2 Synthetic procedures and characterisation data of compound 7-18

Cycloaddition reaction between maleic anhydride and monomerised dicyclopentadiene yielded 4-oxatricyclo[5.2.1.0^{2,6}]dec-8-ene-3,5-dione (**7**) which was used as the scaffold for all further synthesis within this series.

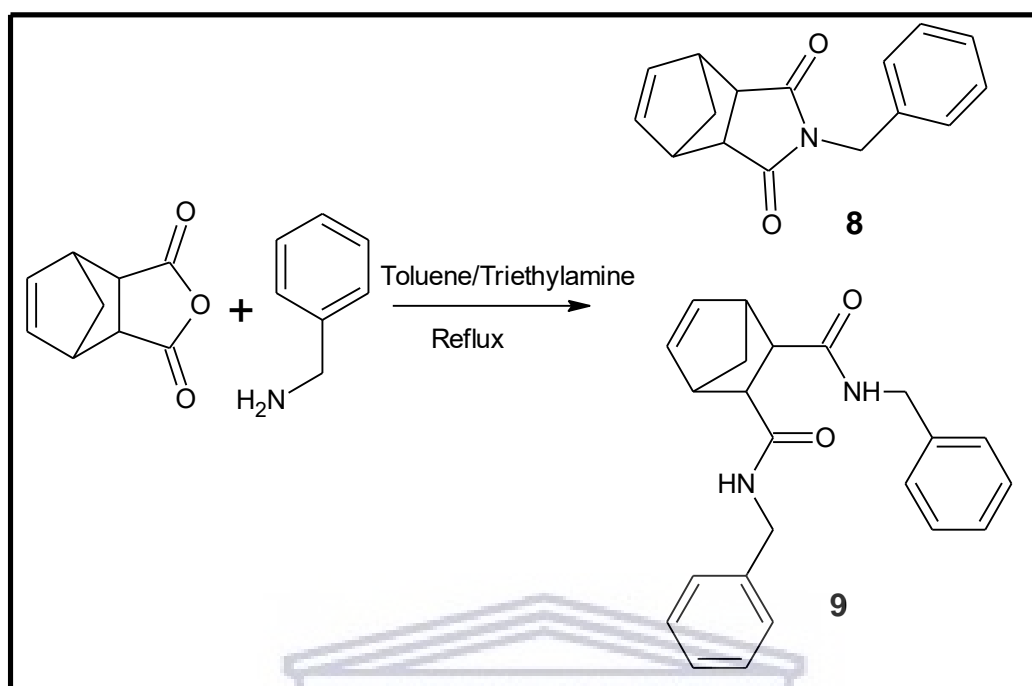
3.3.2.2.1: 4-Oxatricyclo[5.2.1.0^{2,6}]dec-8-ene-3,5-dione (**7**)



To a solution of maleic anhydride (10 g, 100 mmol) in toluene (100 ml) in a 250 ml round-bottom flask, monomerised cyclopentadiene (7 g, 105.90 mmol) was added in stoichiometric ratio. The resulting solution was stirred and refluxed for 1.5 hours and cooled to room temperature. The solvent was evaporated under reduced pressure to give a crude white mixture. The final product was purified by re-crystallising the crude mixture in methanol to give a white crystal (yield: 8.03 g, 48.94%). The NMR data and melting point of compound **7** correspond to those reported in the literature (Reid and Bellinger, 1984; Brown and Sheares, 2007; Mulpuri *et al.*, 2011).

A white crystal, Mp: 163-165 °C. FT-IR (ATR): ν_{\max} (cm⁻¹) = 1840, 1766, 1229, 1088, 901, 733. ¹H NMR (400 MHz, CDCl₃): δ 6.31 (t, J = 1.6 Hz, 2H), 3.58-3.57 (dd, J = 3, 1.7 Hz, 2H), 3.51-3.50 (dd, J = 2.9, 1.6 Hz, 2H), 1.80-1.77 (dt, J = 9, 1.5 Hz, 1H), 1.58-1.56 (d, J = 9 Hz, 1H). ¹³C NMR (100 MHz, CDCl₃) and DEPT-135: δ 171.29 (C=O), 135.55 (C=C), 52.76 (CH₂), 47.08 (CH), 46.13 (CH).

3.3.2.2.2: Synthetic procedures and characterisation data of compounds 8 and 9



4-Oxatricyclo[5.2.1.0^{2,6}]dec-8-ene-3,5-dione (**7**, 0.62 g, 3.78 mmol) was dissolved in 100 ml of toluene. To this solution, benzylamine (3.92 g, 36.62 mmol) was added. The reaction mixture was stirred and refluxed for 24 hours, cooled to room temperature and concentrated *in vacuo* to give a crude light yellow oil. Purification by column chromatography (25% hexane in ethyl acetate) on silica gel gave compounds **8** and **9** as white powders (yield: **8**, 0.79 g, 82.62%; **9**, 0.06 g, 6.27%).

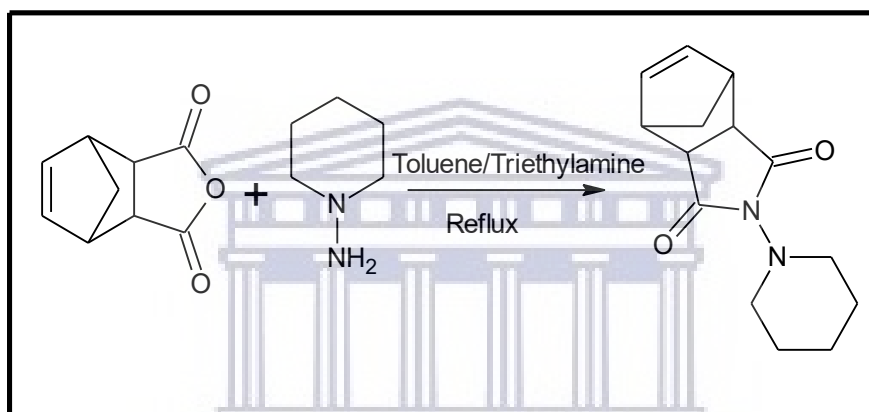
3.3.2.2.2.1: 4-Benzyl-4-azatricyclo[5.2.1.0^{2,6}]dec-8-ene-3,5-dione (**8**)

Physical characteristics: A white powder, Mp: 87-89 °C. FT-IR (ATR): V_{\max} (cm⁻¹) = 2875, 1689, 1391, 1336, 1169, 901, 702. ¹H NMR (400 MHz, CDCl₃): δ 7.31-7.22 (m, 5H), 5.89 (t, J = 1.6 Hz, 2H), 4.48 (s, 2H), 3.37-3.36 (dd, J = 2.7, 1.6 Hz, 2H), 3.25-3.24 (dd, J = 2.8, 1.5 Hz, 2H), 1.70-1.67 (dt, J = 8.8, 1.4 Hz, 1H), 1.50-1.52 (d, J = 8.8 Hz, 1H). ¹³C NMR (100 MHz, CDCl₃) and DEPT-135: δ 177.44 (C=O), 136.03 (Ar-C), 134.34 (C=C), 128.92 (Ar-C), 128.39 (Ar-C), 127.76 (Ar-C), 52.14 (CH₂), 45.76 (CH), 45.02 (CH), 42.03 (CH₂). MS (HR-ESI) m/z : calc. 254.1176 (M+H⁺), found 254.1177 (M+H⁺), 255.1207, 276.0993 (M+Na), 277.1034 (M+Na+H⁺).

3.3.2.2.2: *N2,N3-Dibenzylbicyclo[2.2.1]hept-5-ene-2,3-dicarboxamide (9)*

Physical characteristics: A white powder, Mp: 141-143 °C. FT-IR (ATR): V_{\max} (cm^{-1}) = 3304, 2977, 1654, 1532, 1454, 1227, 1028, 908, 698. ^1H NMR (400 MHz, CDCl_3): δ 7.31-7.18 (m, 10H), 6.33 (m, 2H), 4.25-4.14 (m, 4H), 3.23 (m, 2H), 3.10 (m, 2H), 1.44 (d, $J = 8.5$, 1H), 1.24 (d, $J = 9.2$ Hz, 1H). ^{13}C NMR (100 MHz, CDCl_3) and DEPT-135: δ 172.80 (C=O), 138.21 (Ar-C), 135.76 (C=C), 128.62 (Ar-C), 127.73 (Ar-C), 127.34 (Ar-C), 52.04 (CH), 49.98 (CH_2), 47.35 (CH), 43.52 (CH_2). MS (HR-ESI) m/z : calc. 361.1910 ($\text{M}+\text{H}^+$), found 361.1913 ($\text{M}+\text{H}^+$), 362.1945, 363.1979, 383.1732 ($\text{M}+\text{Na}$), 384.1761, 385.1793.

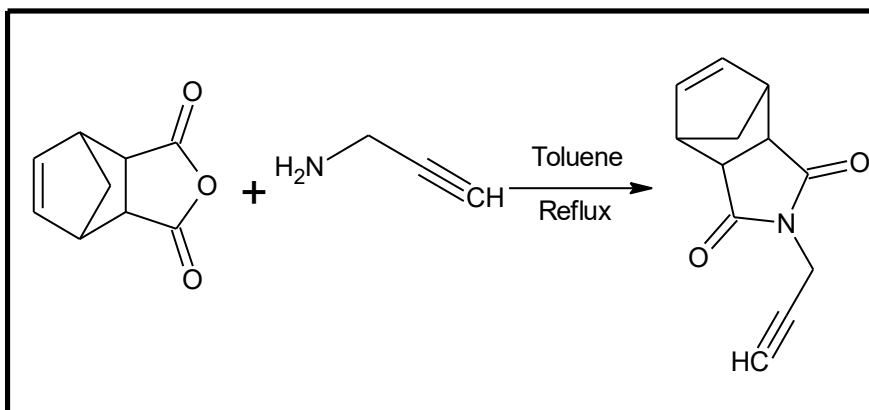
3.3.2.2.3: 4-(1-Piperidyl)-4-azatricyclo[5.2.1.0^{2,6}]dec-8-ene-3,5-dione (10)



To a solution of 4-oxatricyclo[5.2.1.0^{2,6}]dec-8-ene-3,5-dione (7, 0.45 g, 2.74 mmol) in toluene (200 ml), 1-aminopiperidine (1 g, 9.98 mmol) and triethylamine (0.3 g, 2.96 mmol) was added. The mixture was continuously stirred under reflux conditions. After 12 hours, the reaction mixture was cooled to room temperature and the solvent was evaporated under reduced pressure to give a crude light yellow powder. The crude mixture was crystallised from methanol to afford the product as white crystals (yield: 0.32 g, 47.05%).

Physical characteristics: A white crystal, Mp: 163-166 °C. FT-IR (ATR): V_{\max} (cm^{-1}) = 2996, 2938, 1708, 1452, 1339, 1285, 1185, 845, 718. ^1H NMR (400 MHz, CDCl_3): δ 6.12-6.11 (t, $J = 1.6$ Hz, 2H), 3.39 (m, 2H), 3.12-3.11 (dd, $J = 2.8, 1.5$ Hz, 2H), 3.10-3.07 (t, $J = 5.4$ Hz, 4H), 1.70-1.67 (dt, $J = 8.8, 1.6$ Hz, 1H), 1.67-1.61 (m, 4H), 1.48-1.45 (d, $J = 8.8$ Hz, 1H), 1.43-1.37 (m, 2H). ^{13}C NMR (100 MHz, CDCl_3) and DEPT-135: δ 176.48 (C=O), 134.45 (C=C), 52.22 (CH_2), 51.55 (CH_2), 45.17 (CH), 43.46 (CH), 25.89 (CH_2), 23.06 (CH_2). MS (HR-ESI) m/z : calc. 247.1441 ($\text{M}+\text{H}^+$), found 247.1446 ($\text{M}+\text{H}^+$), 248.1470, 249.1492, 269.1260 ($\text{M}+\text{Na}$), 270.1290.

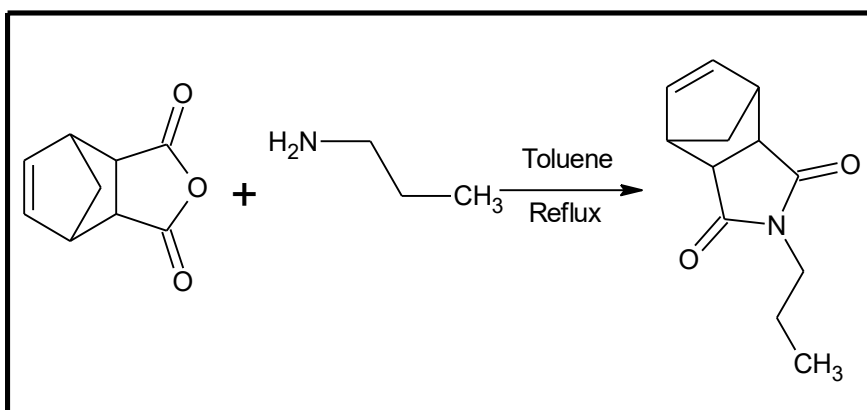
3.3.2.2.4:4-Prop-2-ynyl-4-azatricyclo[5.2.1.0^{2,6}]dec-8-ene-3,5-dione (11)



4-Oxatricyclo[5.2.1.0^{2,6}]dec-8-ene-3,5-dione (**7**, 0.7 g, 4.26 mmol) was dissolved in toluene (200 ml). To this solution, propargylamine (0.6 g, 10.89 mmol) was added. The resulting mixture was continuously stirred and heated to reflux for 15 hours. On completion, the reaction mixture was brought to room temperature and concentrated using a rotary evaporator under reduced pressure to give a crude yellow oil. The final product was obtained by re-crystallising the crude oil in a mixture of hexane and ethyl acetate to afford a yellow crystal (yield: 0.65 g, 75.58%).

Physical characteristics: A yellow crystal, Mp: 99-101 °C. FT-IR (ATR): ν_{\max} (cm⁻¹) = 3265, 1759, 1703, 1530, 1423, 1383, 1323, 1175, 1120, 1090, 951, 906, 845, 715, 668. ¹H NMR (400 MHz, CDCl₃): δ 6.11-6.10 (t, J = 1.6 Hz, 2H), 4.09-4.08 (d, J = 2.5 Hz, 2H), 3.42 (m, 2H), 3.30-3.29 (dd, J = 2.8, 1.5 Hz, 2H), 2.14-2.12 (t, J = 2.5 Hz, 1H), 1.75-1.72 (dt, J = 8.8, 1.5 Hz, 1H), 1.55-1.53 (d, J = 8.8 Hz, 1H). ¹³C NMR (100 MHz, CDCl₃) and DEPT-135: δ 176.38 (C=O), 134.46 (C=C), 70.97 (C), 52.14 (CH₂), 45.86 (CH), 45.17 (CH), 27.21 (CH₂). MS (HR-ESI) m/z : calc. 202.0863 (M+H⁺), found 202.0866 (M+H⁺), 203.0898, 224.0679 (M+Na), 225.0722.

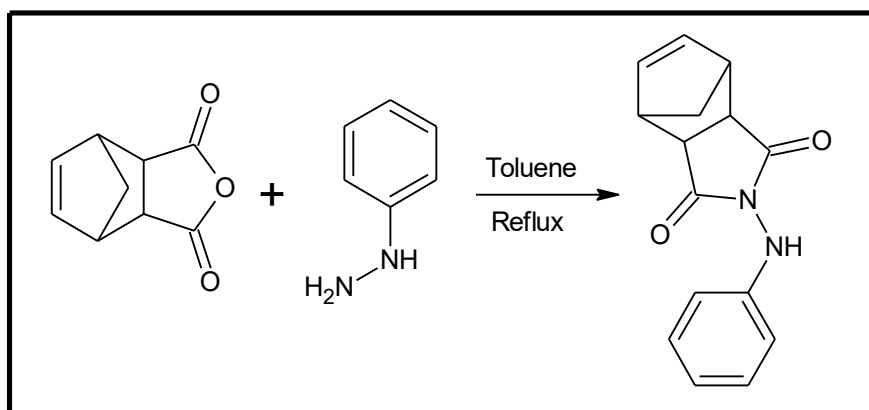
3.3.2.2.5: 4-Propyl-4-azatricyclo[5.2.1.0^{2,6}]dec-8-ene-3,5-dione (12)



A solution of 4-oxatricyclo[5.2.1.0^{2,6}]dec-8-ene-3,5-dione (**7**, 0.5 g, 3.05 mmol) in toluene (150 ml) was prepared in a 250 ml round-bottom flask. To this solution, 0.7 g (11.84 mmol) of propylamine was added, and continuously stirred and refluxed for 15 hours. Upon completion, the reaction mixture was evaporated to dryness *in vacuo* to give a crude residue. The residue was crystallised from hexane to afford the final product as white crystals (yield: 0.59 g, 94.55%).

Physical characteristics: A white crystal, Mp: 70-72 °C. FT-IR (ATR): ν_{\max} (cm⁻¹) = 3267, 2965, 1763, 1683, 1550, 1467, 1337, 1301, 1198, 1138, 1015, 874, 737, 666. ¹H NMR (400 MHz, CDCl₃): δ 6.10 (t, J = 1.5 Hz, 2H), 3.39 (m, 2H), 3.31-3.28 (t, J = 7.4 Hz, 2H), 3.25-3.24 (dd, J = 2.8, 1.5 Hz, 2H), 1.74-1.72 (dt, J = 8.7, 1.5 Hz, 1H), 1.55-1.53 (d, J = 8.8 Hz, 1H), 1.51-1.41 (m, 2H), 0.87-0.84 (t, J = 7.4 Hz, 3H). ¹³C NMR (100 MHz, CDCl₃) and DEPT-135: δ 177.84 (C=O), 134.43 (C=C), 52.23 (CH₂), 45.73 (CH), 44.90 (CH), 40.05 (CH₂), 21.16 (CH₂), 11.38 (CH₃). MS (HR-ESI) m/z : calc. 206.1176 (M+H⁺), found 206.1179 (M+H⁺), 207.1213, 208.1238.

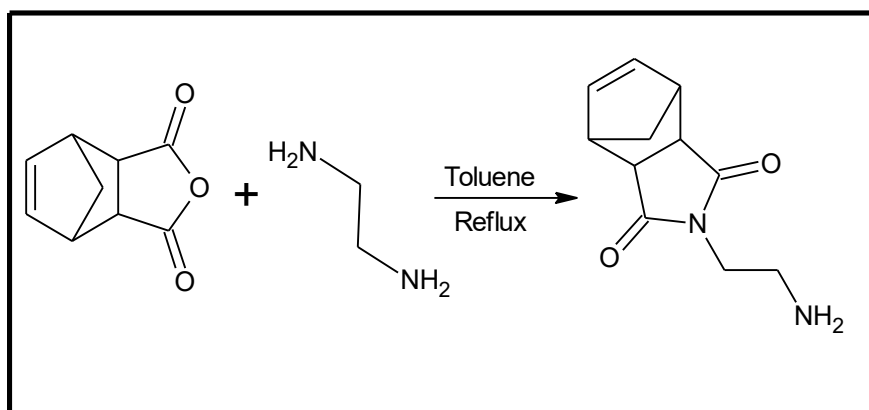
3.3.2.2.6: 4-Anilino-4-azatricyclo[5.2.1.0^{2,6}]dec-8-ene-3,5-dione (13)



4-Oxatricyclo[5.2.1.0^{2,6}]dec-8-ene-3,5-dione (**7**, 0.63 g, 3.84 mmol) was dissolved in toluene (150 ml), and phenylhydrazine (1.65 g, 15.26 mmol) was added to the solution. The solution was stirred and refluxed for 10 hours. After completion, the reaction mixture was concentrated *in vacuo* to give a crude white powder. The crude powder was purified by precipitation from ice-cold methanol to give a white powder (yield: 0.47 g, 48.54%).

Physical characteristics: A white powder, Mp: 191-194°C. FT-IR (ATR): ν_{\max} (cm⁻¹) = 3282, 2955, 1767, 1703, 1601, 1497, 1381, 1295, 1184, 1138, 1056, 980, 845, 727, 696. ¹H NMR (400 MHz, CDCl₃): δ 7.24-7.20 (dd, J = 8.4, 7.6 Hz, 2H), 6.97-6.93 (t, J = 7.4 Hz, 1H), 6.76-6.75 (d, J = 7.7 Hz, 2H), 6.22-6.21 (t, J = 1.6 Hz, 2H), 6.01 (s, NH), 3.49 (m, 2H), 3.36-3.35 (dd, J = 2.7, 1.5 Hz, 2H), 1.81-1.78 (dt, J = 8.9, 1.5 Hz, 1H), 1.59-1.57 (d, J = 8.9 Hz, 1H). ¹³C NMR (100 MHz, CDCl₃) and DEPT-135: δ 175.32 (C=O), 145.13 (Ar-C), 135.03 (C=C), 129.15 (Ar-C), 122.57 (Ar-C), 115.03 (Ar-C), 52.14 (CH₂), 44.99 (CH), 44.12 (CH). MS (HR-ESI) m/z : calc. 255.1128 (M+H⁺), found 255.1133 (M+H⁺), 256.1164, 257.1188, 277.0952 (M+Na), 278.0981.

3.3.2.2.7: 4-(2-Aminoethyl)-4-azatricyclo[5.2.1.0^{2,6}]dec-8-ene-3,5-dione (14)

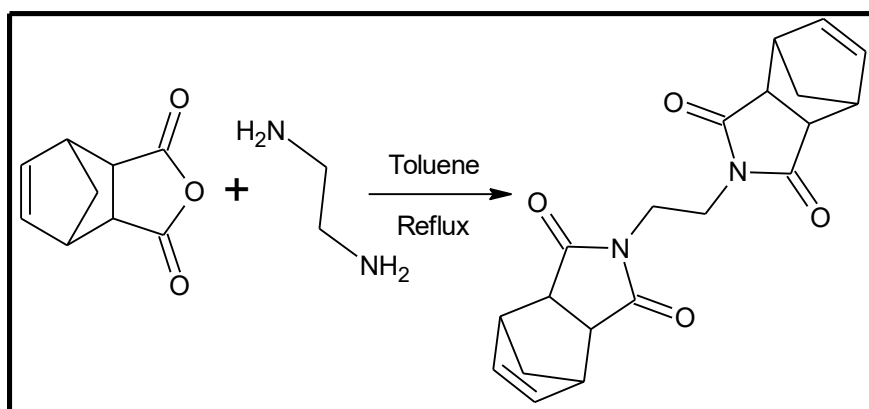


To a solution of 4-oxatricyclo[5.2.1.0^{2,6}]dec-8-ene-3,5-dione (**7**, 1 g, 6.09 mmol) in toluene (150 ml), ethylenediamine (1 g, 16.64 mmol) was added and stirred. The solution was continuously stirred and refluxed for 12 hours. The resulting reaction mixture was allowed to cool to room temperature and concentrated under reduced pressure to give a crude mixture. Ethyl acetate (100 ml) was added to the mixture and stirred at room temperature for 30 minutes. The mixture was filtered and the filtrate was concentrated under reduced pressure to give a light-yellow oil which solidified at room temperature (yield: 1.13 g, 89.94%).

Physical characteristics: A yellow oil. FT-IR (ATR): ν_{\max} (cm⁻¹) = 3379, 2946, 1762, 1687, 1549, 1490, 1440, 1400, 1335, 1156, 1051, 842, 778, 724. ¹H NMR (400 MHz, CDCl₃): δ 6.12-6.11 (t, J = 1.7 Hz, 2H), 3.40 (d, J = 6.4 Hz, 2H), 3.38 (m, 2H), 3.27-3.26 (dd, J = 2.8, 1.5 Hz, 2H), 2.75-2.72 (t, J = 6.4 Hz, 2H), 1.75-1.72 (dt, J = 8.8, 1.5 Hz, 1H), 1.55-1.53 (d, J = 8.8 Hz, 1H). ¹³C NMR (100 MHz, CDCl₃) and DEPT-135: δ 177.98 (C=O), 134.57 (C=C), 52.31 (CH₂), 45.81 (CH), 44.92 (CH), 41.67 (CH₂), 40.11 (CH₂). MS (HR-ESI) m/z : calc. 207.1128 (M+H⁺), found 207.1135 (M+H⁺), 208.1165, 209.1179, 229.0949 (M+Na), 230.0991.

3.3.2.2.8: 4-[2-(3,5-Dioxo-4-azatricyclo[5.2.1.0^{2,6}]dec-8-en-4-yl)ethyl]-4-azatricyclo

[5.2.1.0^{2,6}]dec-8-ene-3,5-dione (15)

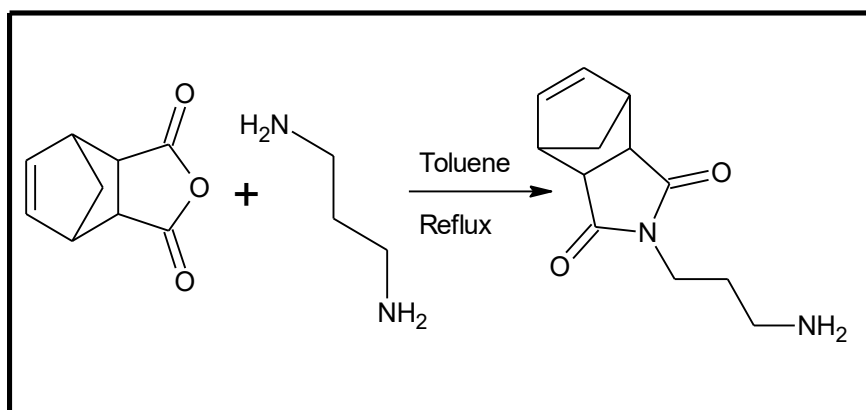


To a solution of 4-oxatricyclo[5.2.1.0^{2,6}]dec-8-ene-3,5-dione (**7**, 0.5 g, 3.05 mmol) in toluene (150 ml), ethylenediamine (0.5 g, 8.32 mmol) was added and stirred. The solution was continuously stirred and refluxed for 12 hours. The resulting reaction mixture was allowed to cool to room temperature and concentrated under reduced pressure to give the crude mixture. The crude mixture was re-crystallised from ice-cold methanol to give white crystals (yield: 0.13 g, 12.32%).

Physical characteristics: A white crystal, Mp: 262-265 °C. FT-IR (ATR): ν_{\max} (cm⁻¹) = 2998, 1759, 1690, 1435, 1379, 1336, 1154, 1029, 975, 842, 780, 716. ¹H NMR (400 MHz, CDCl₃): δ 6.05 (m, 4H), 3.46 (m, 4H), 3.33(m, 4H), 3.23-3.22 (dd, J = 2.8, 1.5 Hz, 4H), 1.72-1.70 (d, J = 8.7 Hz, 2H), 1.52-1.50 (d, J = 8.7 Hz, 1H). ¹³C NMR (100 MHz, CDCl₃) and DEPT-135: δ 177.70 (C=O), 134.45 (C=C), 52.14 (CH₂), 45.96 (CH), 44.67 (CH), 36.37 (CH₂). MS (HR-ESI) m/z : calc. 353.1496 (M+H⁺), found 353.1497 (M+H⁺), 354.1530, 355.1556, 375.1319 (M+Na), 376.1349, 377.1372.

It should be noted that the procedure leading to the formation of compound **15** is similar to that of compound **14** thus it could be described as secondary product. However, they differed in the work-ups and reagents concentrations. This, and the fact that the reactions were performed at different time justified the reason why the reaction procedures were outlined differently.

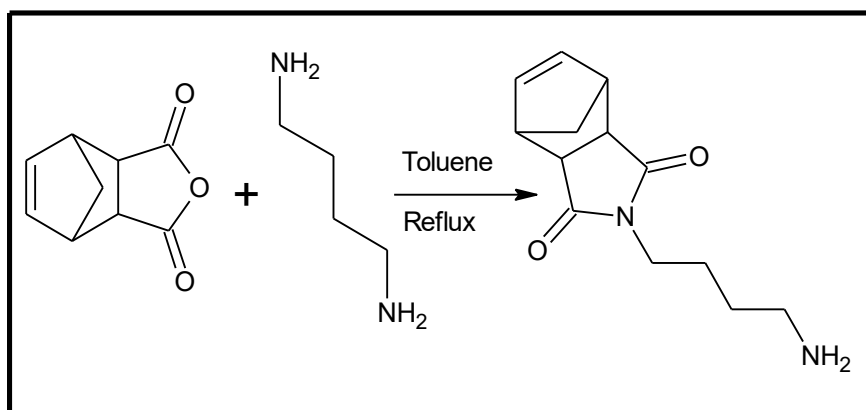
3.3.2.2.9: 4-(3-Aminopropyl)-4-azatricyclo[5.2.1.0^{2,6}]dec-8-ene-3,5-dione (16)



4-Oxatricyclo[5.2.1.0^{2,6}]dec-8-ene-3,5-dione (**7**, 0.8 g, 4.87 mmol) was dissolved in toluene (150 ml). To this solution, 1,3-diaminopropane (0.5 g, 6.75 mmol) was added. After the addition, the reaction mixture was stirred and refluxed for 14 hours. The reaction mixture was allowed to cool to room temperature and the solvent was evaporated under reduce pressure to give a crude yellow mixture. To purify, the crude mixture was column chromatographed on silica gel. Elution with 90% ethyl acetate in methanol afforded the final product as a light-yellow oil (yield: 0.54 g, 50.76%).

Physical characteristics: A light yellow oil. FT-IR (ATR): ν_{\max} (cm⁻¹) = 3372, 2944, 2868, 1729, 1658, 1474, 1406, 1339, 1299, 1251, 1193, 1127, 977, 918, 840, 747, 717. ¹H NMR (400 MHz, CD₃OD): δ 6.03-6.01 (dd, J = 5.6, 2.7 Hz, 1H), 5.99-5.97 (dd, J = 5.6, 2.7 Hz, 1H), 3.33-3.30 (m, 2H), 3.29-3.26 (m, 2H), 3.23-3.22 (dd, J = 3.2, 1.6 Hz, 2H), 3.17-3.16 (m, 1H), 3.15-3.12 (dd, J = 7.8, 4.6 Hz, 1H), 1.71-1.65 (dd, J = 13.7, 5.1 Hz, 1H), 1.64-1.59 (dt, J = 6.7, 4.8 Hz, 1H), 1.58-1.55 (dt, J = 8.6, 1.6 Hz, 1H), 1.49-1.47 (d, J = 8.6 Hz, 1H). ¹³C NMR (100 MHz, CD₃OD) and DEPT-135: δ 176.9 (C=O), 159.23 (C=O), 134.28 (C=C), 134.03 (C=C), 50.83 (CH₂), 45.56 (CH), 45.50 (CH), 44.42 (CH), 43.79 (CH), 43.73 (CH₂), 37.30 (CH₂), 18.72 (CH₂). MS (HR-ESI) m/z : calc. 221.1285 (M+H⁺), found 221.1288 (M+H⁺), 222.1316.

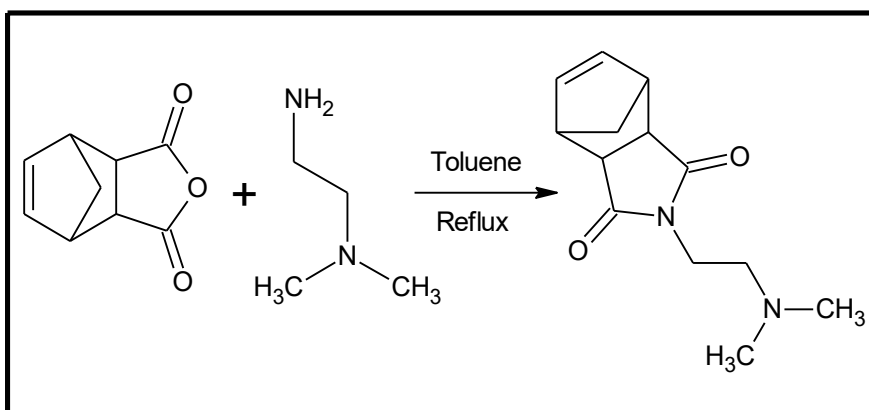
3.3.2.2.10: 4-(4-Aminobutyl)-4-azatricyclo[5.2.1.0^{2,6}]dec-8-ene-3,5-dione (17)



To a 250 ml round-bottom flask, 4-oxatricyclo[5.2.1.0^{2,6}]dec-8-ene-3,5-dione (**7**, 0.5 g, 3.05 mmol) dissolved in toluene (150 ml) and 1,4-diaminobutane (0.8 g, 9.08 mmol) were added. The resulting solution was stirred and refluxed for 15 hours. The reaction mixture was allowed to reach room temperature and concentrated *in vacuo* to give a crude yellow mixture. For the purpose of purification, the crude mixture was subjected to column chromatography on silica gel and elution with ethyl acetate/ammonia/methanol (69:1:30). The elution gave the final product as light-yellow oil (0.4 g, 56.34%).

Physical characteristics: A light yellow oil. FT-IR (ATR): ν_{\max} (cm⁻¹) = 3387, 2941, 2869, 1760, 1684, 1567, 1436, 1337, 1217, 1146, 1024, 896, 843, 723. ¹H NMR (400 MHz, CDCl₃): δ 6.08 (t, *J* = 1.6 Hz, 2H), 3.37 (m, 2H), 3.34-3.30 (t, *J* = 7.1 Hz, 2H), 3.23-3.22 (dd, *J* = 2.7, 1.4 Hz, 2H), 2.68-2.65 (t, *J* = 6.9 Hz, 2H), 1.73-1.70 (dt, *J* = 8.8, 1.4 Hz, 1H), 1.53-1.51 (d, *J* = 8 Hz, 1H), 1.48-1.42 (m, 2H) 1.41-1.34 (m, 2H). ¹³C NMR (100 MHz, CDCl₃) and DEPT-135: δ 177.76 (C=O), 134.23 (C=C), 52.24 (CH₂), 45.74 (CH), 44.90 (CH), 41.61 (CH₂), 38.15 (CH₂), 30.88 (CH₂), 25.14 (CH₂). MS (HR-ESI) *m/z*: calc. 235.1441 (M+H⁺), found 235.1443 (M+H⁺), 236.1475, 237.1502, 257.1261 (M+Na).

3.3.2.2.11: 4-[2-(Dimethylamino)ethyl]-4-azatricyclo[5.2.1.0^{2,6}]dec-8-ene-3,5-dione (18)



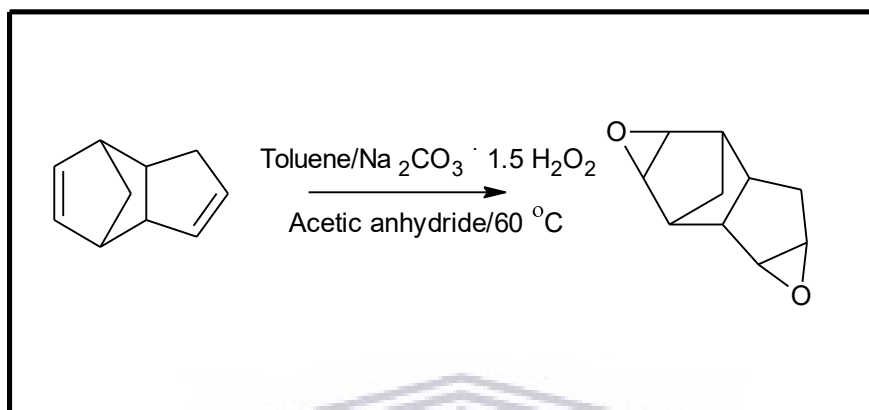
To a solution of 4-oxatricyclo[5.2.1.0^{2,6}]dec-8-ene-3,5-dione (**7**, 0.6 g, 3.65 mmol) in toluene (150 ml), 0.8 g (9.08 mmol) of *N,N*-dimethylethylenediamine was added. The resulting solution was continuously stirred and refluxed for 15 hours. The reaction mixture was allowed to return to room temperature while stirring. The solvent was evaporated under reduced pressure, and the residue was subjected to column chromatography on silica gel. Elution of the residue with 90% ethyl acetate in methanol gave a white oil that solidified at room temperature to give the final product as white powder (0.83 g, 96.5 %).

Physical characteristics: A white powder, Mp: 83-85 °C. FT-IR (ATR): ν_{\max} (cm⁻¹) = 3456, 2971, 2789, 1739, 1687, 1355, 1229, 1152, 1046, 1001, 950, 914, 843, 778, 722. ¹H NMR (400 MHz, CDCl₃): δ 6.06 (t, *J* = 1.6 Hz, 2H), 3.44-3.41 (t, *J* = 6.9 Hz, 2H), 3.35 (m, 2H), 3.24-3.23 (dd, *J* = 2.8, 1.5 Hz, 2H), 2.32-2.29 (t, *J* = 6.9 Hz, 2H), 2.20 (s, 6H), 1.71-1.69 (dt, *J* = 8.7, 1.4 Hz, 1H), 1.52-1.50 (d, *J* = 8.7 Hz, 2H). ¹³C NMR (100 MHz, CDCl₃) and DEPT-135: δ 177.70 (C=O), 134.37 (C=C), 56.26 (CH₂), 52.09 (CH₂), 45.77 (CH), 45.37 (CH₃), 44.85 (CH), 36.19 (CH₂). MS (HR-ESI) *m/z*: calc. 235.1441 (M+H⁺), found 235.1442 (M+H⁺), 236.1475, 237.1505, 257.1267 (M+Na).

3.3.2.3 Synthetic procedures and characterisation data of compound 19-23

Epoxidation of dicyclopentadiene yielded 4,10-dioxapentacyclo[6.3.1.0^{2,7}.0^{3,5}.0^{9,11}]dodecane (**19**) which was used as scaffold for all further synthesis within this series.

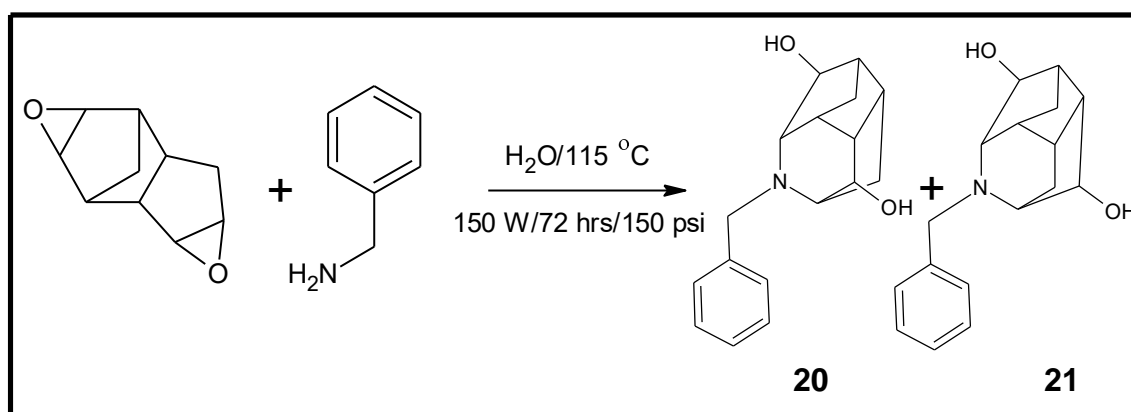
3.3.2.3.1: 4,10-Dioxapentacyclo[6.3.1.0^{2,7}.0^{3,5}.0^{9,11}]dodecane (**19**)



To a mixture of dicyclopentadiene (7.2 ml, 52.95 mmol) and toluene (200 ml) in a high-pressure metal reactor, sodium percarbonate (45 g, 286.61 mmol) and acetic anhydride (50 ml, 528.95 mmol) were added. The reaction mixture in the reactor was heated to 60 °C and was continuously stirred. After 24 hours, the reaction mixture was allowed to cool to room temperature and washed with water (100 ml x 4). The organic fraction was dried over anhydrous magnesium sulphate and the solvent was evaporated under reduced pressure affording a white residue, which was crystallized from hexane to give a white crystal as the final product (yield: 4.72 g, 54.32%). The NMR data and melting points of compound **19** correspond to those reported in the literature (Zhao *et al.*, 2013).

Physical characteristics: A white crystal, Mp: 176-180 °C. FT-IR (ATR): ν_{\max} (cm⁻¹) = 3456, 2971, 1739, 1367, 1217, 997, 827, 691. ¹H NMR (400 MHz, CDCl₃): δ 3.54-3.53 (t, *J* = 2.2 Hz, 1H), 3.40-3.39 (d, *J* = 2.3 Hz, 1H), 3.27-3.26 (d, *J* = 3.3 Hz, 1H), 3.22 (d, *J* = 2.9 Hz, 1H), 2.69-2.67 (dd, *J* = 4.2, 1.4 Hz, 1H), 2.62-2.59 (dd, *J* = 8.2, 4.4 Hz, 1H), 2.51-2.45 (m, 2H), 1.93-1.87 (dd, *J* = 15.4, 8.9 Hz, 1H), 1.83-1.77 (m, *J* = 15.6, 3.5, 2.6 Hz, 1H), 1.44-1.42 (d, *J* = 9.8 Hz, 1H), 0.85-0.83 (d, *J* = 9.8 Hz, 1H). ¹³C NMR (100 MHz, CDCl₃) and DEPT-135: δ 61.76 (CHO), 58.70 (CHO), 49.01 (CHO), 48.77 (CHO), 48.35 (CH), 44.60 (CH), 39.92 (CH), 39.17 (CH), 29.63 (CH₂), 26.98 (CH₂).

3.3.2.3.2: Synthetic procedures and characterisation data of compounds **20** and **21**



A mixture of 4,10-dioxapentacyclo[6.3.1.0^{2,7}.0^{3,5}.0^{9,11}]dodecane (**19**, 0.82 g, 4.99 mmol) and benzylamine (0.4 g, 3.72 mmol) were added to a microwave reaction vessel containing a magnetic stirrer. To this mixture, water (10 ml) was added. The vessel was placed in the microwave reactor and subjected to the following conditions: Power = 150 W; T = 110 °C; P = 250 psi. After 72 hours, the cloudy mixture was cooled to room temperature and extracted with dichloromethane (15 ml x 4). The combined organic layers were dried over anhydrous magnesium sulphate and concentrated *in vacuo* to give a dark brown oil containing a mixture of diastereomers **20** and **21**. The crude material was purified by silica gel column chromatography eluting with 100% ethyl acetate to afford yellow oils which solidified at room temperature to give creamy white powders (yield: **20**; 0.43 g, 31.85%) (yield: **21**; 0.29 g, 21.48%).

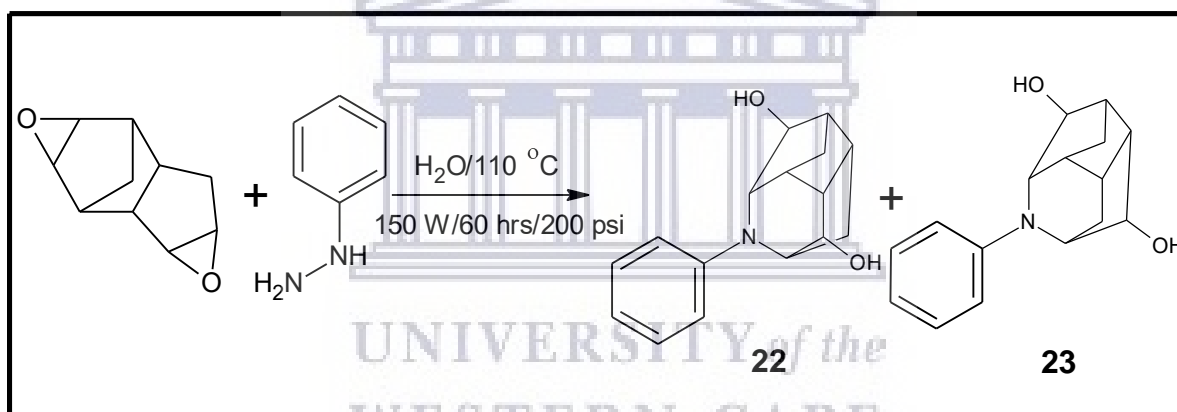
3.3.2.3.2.1: 7-Benzyl-7-azatetracyclo[6.2.1.0^{2,6}.0^{4,10}]undecane-5,11-diol (**20**)

Physical characteristics: A creamy white powder, Mp: 143-145 °C. FT-IR (ATR): ν_{\max} (cm⁻¹) = 3409, 2970, 2950, 1739, 1450, 1366, 1217, 1043, 991, 890, 774, 699. ¹H NMR (400 MHz, CDCl₃): δ 7.35-7.21 (m, 5H), 5.29 (bs, OH), 4.28 (m, 1H), 3.89 (m, 1H), 3.85-3.70 (dd, J = 13.7 Hz, 2H), 2.90-2.89 (d, J = 1.8 Hz, 1H), 2.76-2.75 (d, J = 4.8 Hz, 1H), 2.56-2.50 (dd, J = 14.8, 7.7 Hz, 1H), 2.31 (m, 1H), 2.27-2.26 (d, J = 4.9 Hz, 1H), 2.22-2.20 (d, J = 7.4 Hz, 1H), 1.92-1.90 (d, J = 10.3 Hz, 1H), 1.80-1.77 (d, J = 14.1 Hz, 1H), 1.72-1.66 (m, 1H), 1.34-1.32 (d, J = 10.1 Hz, 1H). ¹³C NMR (100 MHz, CDCl₃) and DEPT-135: δ 139.22 (Ar-C), 128.76 (Ar-C), 128.35 (Ar-C), 127.06 (Ar-C), 74.85 (CH), 71.14 (CH), 67.06 (CH), 63.48 (CH), 58.15 (CH₂), 51.41 (CH), 44.08 (CH), 41.16 (CH), 36.83 (CH₂), 35.44 (CH), 24.81 (CH₂). MS (HR-ESI) m/z : calc. 272.1645 (M+H⁺), found 272.1648 (M+H⁺), 273.1684, 274.1718, 294.1483 (M+Na).

3.3.2.3.2.2: 7-Benzyl-7-azatetracyclo[6.2.1.0^{2,6}.0^{4,10}]undecane-5,9-diol (21)

Physical characteristics: A creamy white powder, Mp: 135-140 °C. FT-IR (ATR): V_{\max} (cm⁻¹) = 3357, 2971, 2940, 2852, 1739, 1450, 1366, 1217, 1009, 916, 838, 778, 746, 705. ¹H NMR (400 MHz, CD₃OD): δ 7.32-7.18 (m, 5H), 4.44-4.43 (d, $J = 3.4$ Hz, 1H), 4.34-4.33 (d, $J = 3.4$ Hz, 1H), 4.14-4.13 (d, $J = 3.1$ Hz, 1H), 3.94 (m, 1H), 3.72 (s, 2H), 2.68-2.67 (d, $J = 1.9$ Hz, 2H), 2.21 (s, OH), 2.19-2.18 (m, 1H), 2.09-2.06 (t, $J = 6.9$ Hz, 1H), 2.02 (s, OH), 1.86-1.84 (d, $J = 9.2$ Hz, 1H) 1.64-1.59 (q, $J = 10.6, 5.0$ Hz, 1H), 1.40-1.37 (d, $J = 11$ Hz, 1H), 1.11-1.09 (d, $J = 9.2$ Hz, 1H). ¹³C NMR (100 MHz, CD₃OD and DEPT-135): δ 140.64 (Ar-C), 128.71 (Ar-C), 128.52 (Ar-C), 126.96 (Ar-C), 71.09 (CH), 71.01 (CH), 68.27 (CH), 64.05 (CH), 58.08 (CH₂), 47.12 (CH), 43.84 (CH), 43.32 (CH), 36.87 (CH₂), 30.01 (CH₂). MS (HR-ESI) m/z : calc. 272.1645 (M+H⁺), found 272.1647(M+H⁺), 273.1681, 274.1739.

3.3.2.3.3: Synthetic procedures and characterisation data of compounds 22 and 23



4,10-Dioxapentacyclo[6.3.1.0^{2,7}.0^{3,5}.0^{9,11}]dodecane (**19**, 1 g, 6.09 mmol) was placed in a 30 ml glass reactor vessel. To the same vessel, phenylhydrazine (2 g, 18.49 mmol) and water (10 ml) were added. The cloudy mixture was heated in a microwave reactor (150 W) at 110 °C. The pressure was set at 200 psi and continuously stirred for 60 hours. After completion, the reaction mixture was allowed to cool to room temperature and was extracted with dichloromethane (15 ml x 4). The combined organic fractions were washed with water (50 ml), dried over anhydrous magnesium sulphate, and concentrated under reduced pressure to give a dark crude mixture. The crude mixture was purified by column chromatography on silica gel. Hexane (25%) in ethyl acetate was used as an eluting solvent to afford the diastereomers (64:36) as a dark yellow oil (yield: 0.32g, 20.10%).

Different mobile phases, each with distinctive polarities, were used to separate compounds **22** and **23**, but were unsuccessful. However, the NMR spectra (^1H , ^{13}C and DEPT) showed a mixture of diastereomers, each with different proton integrations. Based on the integration values, the percentages of each compound in the mixture were obtained as 64% for compound **22** (major) and 36% for compound **23** (minor).

3.3.2.3.3.1: 7-Phenyl-7-azatetracyclo[6.2.1.0^{2,6}.0^{4,10}]undecane-5,11-diol (**22**)

Physical characteristics: A dark yellow oil. FT-IR (ATR): V_{max} (cm^{-1}) = 3326, 2971, 2954, 2243, 1739, 1661, 1596, 1497, 1371, 1217, 1023, 907, 727. ^1H NMR (400 MHz, CDCl_3): δ 7.25-7.23 (m, 2H), 6.95-6.93 (d, $J = 8$ Hz, 2H), 6.79-6.75 (t, $J = 7.2$ Hz, 1H), 4.01-4.00 (d, $J = 3.2$ Hz, 1H), 3.96 (m, 1H), 3.93 (m, 1H), 3.65-3.64 (d, $J = 7.4$ Hz, 1H), 2.64-2.58 (dd, $J = 15.8$, 7.7 Hz, 1H), 2.41 (bs, OH), 2.34-2.29 (m, 1H), 2.28 (bs, OH), 2.14-2.12 (d, $J = 10.8$ Hz, 1H), 2.08-2.05 (d, $J = 10.3$ Hz, 1H), 1.98-1.93 (q, $J = 9.5$, 4.1 Hz, 2H), 1.81-1.74 (dt, $J = 15.6$, 5.2 Hz, 1H), 1.45-1.43 (d, $J = 10.2$ Hz, 1H). ^{13}C NMR (100 MHz, CDCl_3) and DEPT-135: δ 149.87 (Ar-C), 129.36 (Ar-C), 118.42 (Ar-C), 116.12 (Ar-C), 75.81 (CH), 74.78 (CH), 63.44 (CH), 61.89 (CH), 51.80 (CH), 44.78 (CH), 41.62 (CH), 37.13 (CH_2), 35.74 (CH), 27.33 (CH_2). MS (HR-ESI) m/z : calc. 258.1489 ($\text{M}+\text{H}^+$), found 258.1492 ($\text{M}+\text{H}^+$), 259.1523, 260.1557.

3.3.2.3.3.2: 7-Phenyl-7-azatetracyclo[6.2.1.0^{2,6}.0^{4,10}]undecane-5,9-diol (**23**)

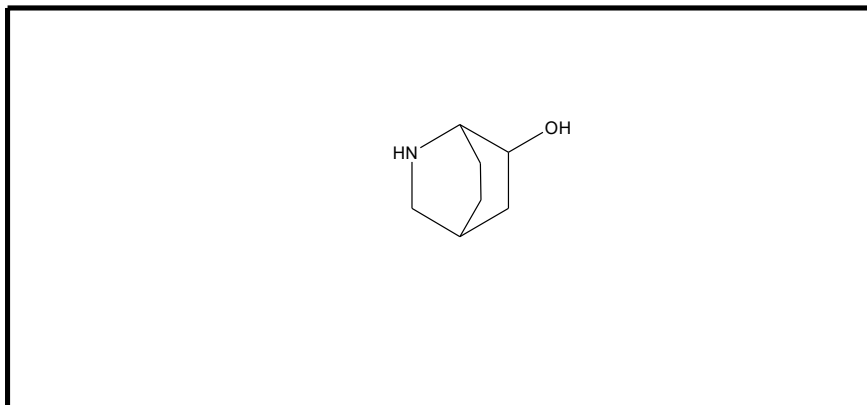
Physical characteristics: A dark yellow oil. FT-IR (ATR): V_{max} (cm^{-1}) = 3326, 2971, 2954, 2243, 1739, 1661, 1596, 1497, 1371, 1217, 1023, 907, 727. ^1H NMR (400 MHz, CDCl_3): δ 7.21-7.19 (d, $J = 6.9$ Hz, 2H), 6.68-6.65 (t, $J = 7.3$ Hz, 1H), 6.62-6.61 (d, $J = 7.9$ Hz, 2H), 4.48-4.47 (d, $J = 5.2$ Hz, 1H), 3.92-3.90 (d, $J = 5.3$ Hz, 1H), 3.63-3.62 (d, $J = 5.4$ Hz, 1H), 3.10-3.05 (q, $J = 10.4$, 5.1 Hz, 1H), 2.94 (s, OH), 2.87 (s, OH), 2.82-2.74 (st, $J = 15.2$, 10, 4.9 Hz, 1H), 2.68-2.67 (t, $J = 4.8$ Hz, 1H), 1.92-1.91 (d, $J = 4.1$ Hz, 2H), 1.74 (m, 1H), 1.7 (m, 1H), 1.67-1.64 (d, $J = 10.2$ Hz, 1H), 1.58-1.51 (dd, $J = 15.5$, 10.1 Hz, 1H). ^{13}C NMR (100 MHz, CDCl_3) and DEPT-135: δ 145.08 (Ar-C), 129.39 (Ar-C), 115.82 (Ar-C), 112.30 (Ar-C), 77.92 (CH), 75.39 (CH), 68.50 (CH), 49.23 (CH), 45.83 (CH), 43.94 (CH), 43.63 (CH), 36.94 (CH_2), 31.35 (CH_2). MS (HR-ESI) m/z : calc. 258.1489 ($\text{M}+\text{H}^+$), found 258.1492 ($\text{M}+\text{H}^+$), 259.1523, 260.1557.

3.3.2.4 Characterisation data of compound **24-27**

The synthesis, isolation and purification of compound (**24-27**) were done by Dr Vitalii A. Palchykov at the Oles Honchar Dnipro National University, Department of Organic Chemistry,

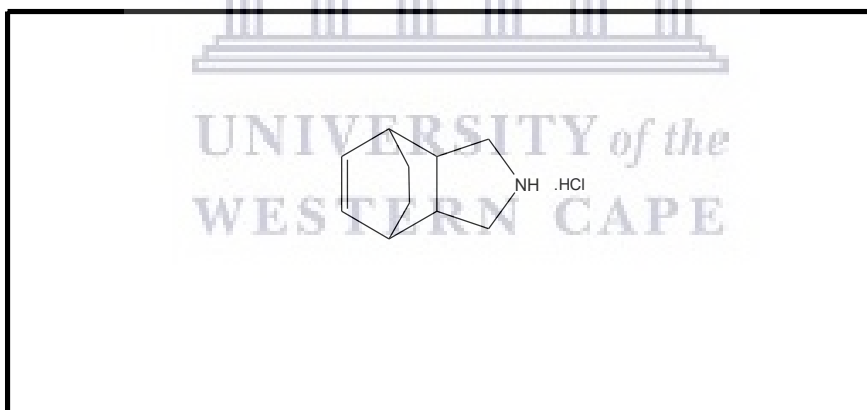
Ukraine. The structures of these compounds were already confirmed and published (Kas'yan & Palchikov, 2010; Palchikov *et al.*, 2014).

3.3.2.4.1: 2-Azabicyclo[2.2.2]octan-6-ol (24)



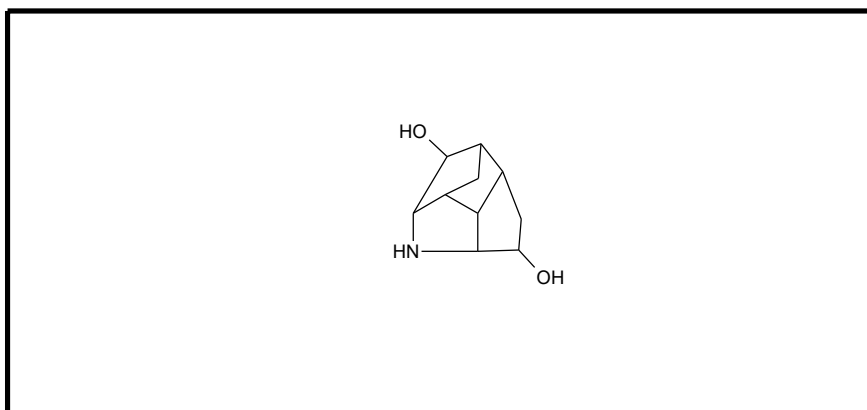
Physical characteristics: A white powder. ^1H NMR (400 MHz, CD_3OD): δ 4.16-3.94 (m, 1H), 3.31-3.21 (m, 1H), 3.07-2.93 (m, 2H), 2.20-2.01 (m, 2H), 1.87-1.37 (m, 5H). ^{13}C NMR (100 MHz, CD_3OD): δ 67.23, 43.95, 35.08, 34.26, 27.28, 23.95, 22.72. MW: 127.18 g/mol.

3.3.2.4.2: 4-Azatricyclo[5.2.2.0^{2,6}]undec-8-ene (25)



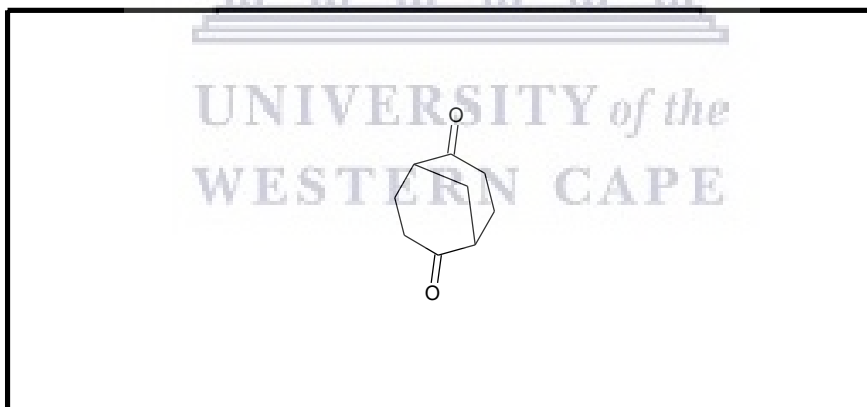
Physical characteristics: A white powder. ^1H NMR (400 MHz, CD_3OD): δ 6.33-6.31 (dd, $J = 4.3, 3.5$ Hz, 2H), 3.46-3.41 (dd, $J = 11.7, 7.6$ Hz, 2H), 2.76-2.71 (dd, $J = 11.4, 6.3$ Hz, 2H), 2.68 (m, 2H), 2.61-2.58 (Q, $J = 6.8, 2.8$ Hz, 2H), 1.58-1.53 (m, 2H), 1.33-1.29 (m, 2H). ^{13}C NMR (100 MHz, CD_3OD): δ 133.78 (C=C), 50.12 (CH), 42.17 (CH_2), 32.35 (CH_2), 23.55 (CH_2). MW: 149.23 g/mol.

3.3.2.4.3: 7-Azatetracyclo[6.3.0.0^{2,6}.0^{3,10}]undecane-5,9-diol (26)



Physical characteristics: A light brown powder. ¹H NMR (400 MHz, DMSO-d₆): δ 5.25 (d, *J* = 3.4 Hz, 1H), 5.20-5.19 (d, *J* = 2.4 Hz, 1H), 4.28-4.27 (d, *J* = 2.3 Hz, 1H), 4.12 (bs, 1H), 3.13-3.12 (d, *J* = 5 Hz, 1H), 2.38 (bs, OH), 2.31-2.29 (d, *J* = 6 Hz, 1H), 2.27-2.23 (t, *J* = 6.5 Hz, 2H), 2.01-1.99 (d, *J* = 9.8 Hz, 1H), 1.87-1.77 (m, 2H), 1.32-1.29 (d, *J* = 9.8 Hz, 1H). ¹³C NMR (100 MHz, DMSO-d₆): δ 72.91, 70.53, 59.92, 58.71, 46.34, 43.27, 42.27, 37.83, 26.76. MW: 181.23 g/mol.

3.3.2.4.4: Bicyclo[3.3.1]nonane-2,6-dione (27)



Physical characteristics: A brown powder. ¹H NMR (400 MHz, DMSO-d₆): δ 2.55-2.53 (m, 2H), 2.47-2.38 (m, 4H), 2.13 (s, 2H), 2.07-1.98 (m, 2H), 1.88-1.83 (m, 2H). ¹³C NMR (100 MHz, DMSO-d₆): δ 213.00, 43.65, 37.15, 31.03, 26.48. MW: 152.19 g/mol.

3.4 Discussion

The Diels-Alder reaction between *p*-benzoquinone and monomerised cyclopentadiene yielded the adduct **1**, an open cage polycyclic molecule, which was used to obtain the cage-like compounds and derivatives thereof (**2-6**). The cycloaddition reaction that resulted in the

formation of **1** was performed in a mixture of hexane (4 parts) and ethylacetate (1 part) to give the *exo*- (minor) and *endo*- (major, +/- 95% yield) isomers after recrystallisation from hexane as 100% yield. In the presence of zinc and acetic acid, the sonication of compound **1** (30 mins) selectively reduced the double bond next to the two ketal groups to afford **2** in substantial yield (71.2%). Further reduction of **2** utilising NaBH₄, a strong reducing agent, promoted the formation of the keto-alcohol **3**. The asymmetric reduction of the diketal groups may be due to the steric hindrance caused by the cage-like structure and/or the weak electrostatic effect as well as dispersion forces resulting from the solvents and reductant (Constantino *et al.*, 2000; Ito *et al.*, 2007; Yang *et al.*, 2018). This might have affected the hydrogen bonding abilities of the unreacted ketal group. The selective reduction could also be attributed to lower concentration of hydrogen bond donors (reductant) in the solvent mixtures. The structures of these compounds (**1**, **2** & **3**) were elucidated and confirmed through spectroscopic data (¹H-, ¹³C-, DEPT-135-NMR and IR). The formation of compound **4** resulted from the reaction between tricyclo[6.2.1.0^{2,7}]undeca-4,9-diene-3,6-dione and cyclopentadiene, in the presence of NaH and CH₃COOH. In the work up reaction leading to compound **4**, 6-(propylamino)tricyclo[6.2.1.0^{2,7}]undec-9-en-3-one was expected as the product. However, pentacyclo[10.2.1.1^{5,8}.0^{2,11}.0^{4,9}]hexadeca-6,13-diene-3,10-dione (**4**) was obtained at a yield of 12.4% and this was possible due to reaction between impurities (cyclopentadiene and tricyclo[6.2.1.0^{2,7}]undeca-4,9-diene-3,6-dione (**1**)) transferred from the intermediate product. The work up allowed further Diels-Alder reaction between the enedione of **1** and cyclopentadiene to afford the double adduct **4**. In addition to the NMR spectra, MS and elemental analysis was used to confirm compound **4**.

For compounds **1-4**, the characteristic vibration bands between 1600 cm⁻¹ and 1700 cm⁻¹ for the carbonyl group were observed in the IR spectra. The appearance of a broad peak at 3398 cm⁻¹ indicates the presence of the hydroxyl group as seen in compound **3**. In the NMR spectra, the bridge protons resonated as a doublet of triplets in the $\delta = 1.42$ -1.53 ppm region and a doublet in the $\delta = 1.26$ -1.41 ppm region for **1-4** (figure 3.1). The formation of two multiplets upfield at $\delta = 2.26$ -2.36 ppm and $\delta = 2.58$ -2.68 ppm confirmed the successful reduction of compound **1** to form **2**. The resonance of an additional CH₂ observed in the upfield region of the DEPT-135 spectra supported the formation of compound **2**. The upfield shift observed in **2** was due to the shielding of the carbon atoms caused by the increased in number of hydrogen atoms formed after selectively reducing the double bond in cyclohexyldione region of the cage molecule. The multiplets at $\delta = 4.28$ -4.33 ppm in the ¹H spectrum and $\delta = 67.74$ ppm in the ¹³C

spectrum confirmed the formation of the keto-alcohol seen in compound **3**. The M+Na peak at m/z 263.1039 and 81.53% of carbon atoms present as per the elemental analysis, suggest the presence of 16 carbon atoms, as seen in **4**. In the elemental analysis, the percentage compositions were found to differ by 1.5-2.3%, and these were attributed to slight impurities present in the final product. Alternatively, the differences can also be linked to incomplete combustion of compound **4** leading to incorrect quantitative analysis of the corresponding atoms. These characteristics together with the NMR (^1H , ^{13}C , DEPT-135 & HSQC) spectra obtained were used to elucidate and confirm the structure of compound **4**. In the ^1H spectrum, the triplet, integrating for four protons, was observed downfield at $\delta = 6.17\text{-}6.18$ ppm and was assigned to the cyclic alkenes moieties. The signals observed at $\delta = 3.34$ ppm and $\delta = 2.86$ ppm were identified as multiplets, each also integrating for four protons and were assigned to the cyclic CH group. In the ^{13}C and DEPT-135, the characteristic carbonyl signal $\delta = 212.66$ ppm was observed downfield. The signal for the cyclic alkenes moieties was also observed downfield at $\delta = 136.36$ ppm while the characteristic signal for the bridge carbons (CH_2) was observed upfield at $\delta = 49.58$ ppm. The symmetrical nature of the structure of **4** accounted for the lower number of signals or peaks observed in the NMR spectra.

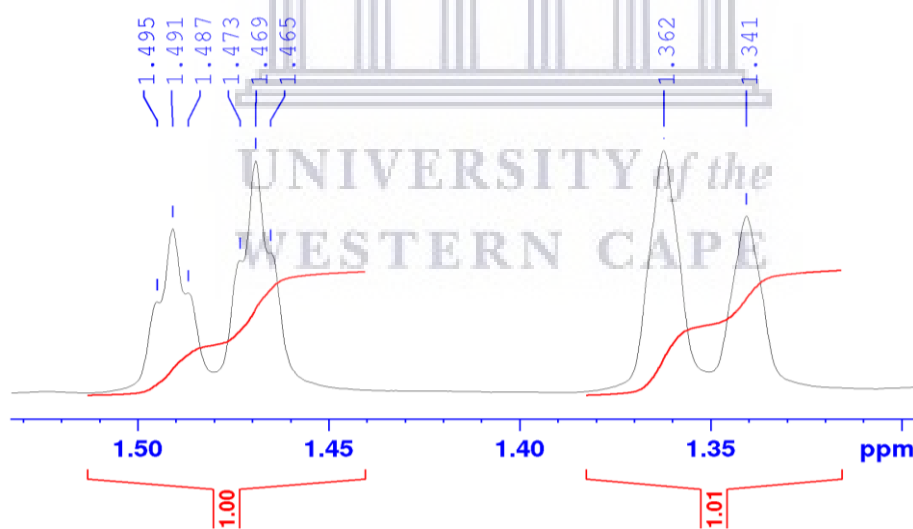


Figure 3.1: The signals of the bridge proton of compound **2** in ^1H NMR at 400 MHz.

Benzylamine (2.7 molar equivalent) or 1-aminopiperidine (1 molar equivalent) were reacted with compound **2** to afford the secondary amine derivatives in yields of 16.2% (**5**) and 36.44% (**6**), respectively. Compound **5** and **6** were obtained from a one-step reaction that involves a Schiff base reaction to form imine derivatives as intermediates. These intermediates were

subsequently reduced by a strong base (NaBH_4) to give the cyclohexylamine derivatives **5** and **6**. In the NMR spectra of compound **5**, the presence of the characteristic signal of the benzyl protons that integrated for five protons were evident downfield at $\delta = 7.25\text{-}7.38$ ppm. The presence of multiplet at $\delta = 3.33$ and singlet at $\delta = 3.89$ ppm with integration of 1H and 2H, respectively, confirmed the formation of amine derivative (figure 3.2). The peak at $\delta = 3.33$ ppm was assigned to the proton at cyclohexyl region while the peak at $\delta = 3.89$ ppm was assigned to the CH_2 group. The downfield assignment of the peaks was due to the electron-withdrawing effect of the nitrogen atom directly attached to the carbons. The ^{13}C and DEPT-135 spectrum showed four CH_2 signals that correspond to the number of carbon atoms with two protons at $\delta = 51.53, 50.26, 38.90$ and 25.14 ppm; aromatic signals at $\delta = 140.54, 128.50, 127.98$ and 127.06 ppm; and a carbonyl signal at $\delta = 213.40$ ppm. In the IR spectra, the characteristic absorption band for N-H and C=O were observed at 1450 and 1685 cm^{-1} , respectively. These characteristics together with the MS spectra peak (M+H) at m/z 268.1700 confirmed the structure of **5**.

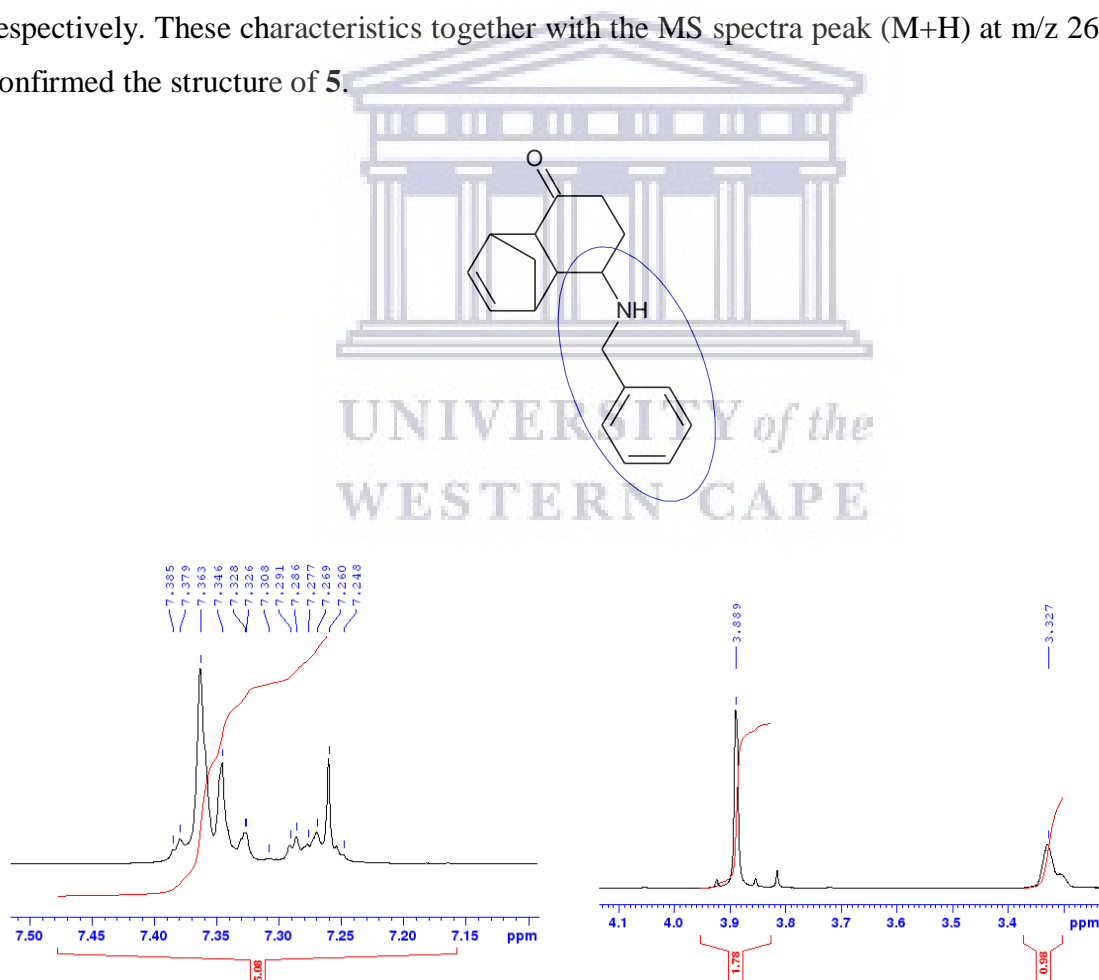


Figure 3.2: Multiplet and singlets of the benzylamine moiety of compound **5** in ^1H NMR at 400 MHz.

As expected, compound **6** showed similarities with compound **5** in the IR spectra, but differs in the NMR spectra and mass spectra. In the ^1H spectrum, the doublet of doublets peaks observed at $\delta = 3.34\text{--}3.39$ ppm ($H_J = 15.1, 6.6\text{ Hz}$) was assigned to the proton in the cyclohexylamine region, and the high coupling constant was due to the electron-withdrawing effect of the nitrogen atom directly linked to the proton. The protons in the piperidyl ring of the conjugate derivative were observed upfield. The peaks in the ring showed: multiplet at $\delta = 2.43\text{--}2.71$ ppm (4H); multiplet at $\delta = 1.56\text{--}1.62$ ppm (4H); and multiplet at $\delta = 1.36\text{--}1.42$ ppm (2H). In the ^{13}C and DEPT-135 spectra, six CH_2 group peaks were observed upfield at $\delta = 57.79, 50.17, 38.83, 26.17, 24.37$ and 24.06 ppm while the peak observed at $\delta = 214.12$ was assigned to the carbonyl moiety present in **6** (figure 3.3).

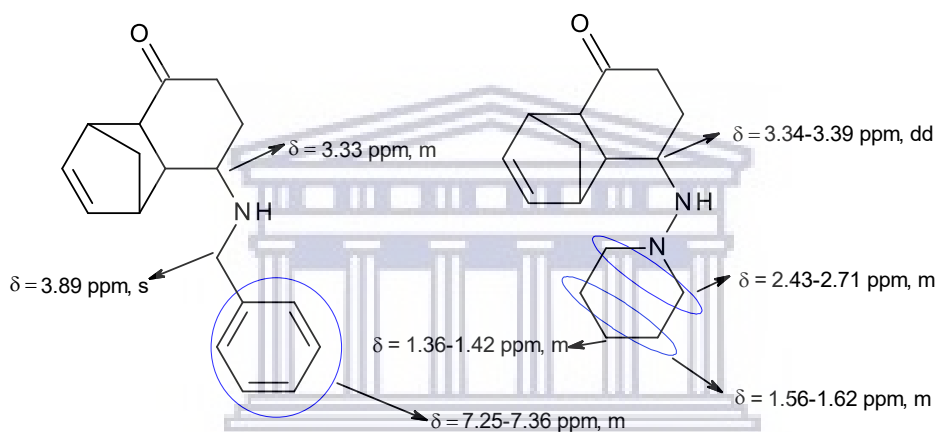


Figure 3.3: ^1H NMR spectrum differences existing between **5** and **6**.

The cyclo-addition reaction between maleic anhydride and monomerised cyclopentadiene resulted in the formation of **7**, an open cage-like molecule. This molecule was conjugated with benzylamine, 1-aminopiperidine, propargylamine, propylamine, phenylhydrazine, ethylenediamine, 1,3-diaminopropane, 1,4-diaminobutane and N,N-methylethylenediamine through aminolysis to afford compounds **8-18** with yields of 6.27-96.5%. Under reflux conditions, the aminolysis of **7** with excess benzylamine afforded the desired compound **8** (82.62%) and the minor dibenzylamide derivative **9** (6.27%) in a ratio of 13:1. A two-step reaction was proposed for compound **9**. In the same reaction leading to the formation of **9** and **10**, it is believed that **7** was hydrolyse, resulting in the formation of Bicyclo[2.2.1]hept-5-ene-2,3-dicarboxylic acid, an intermediate (Rzaeva *et al.*, 2007; Foster *et al.*, 2018). Condensation between dicarboxylic moiety of the intermediate and benzylamine led to the formation of diamide **9** as illustrated in Figure 3.4 (Leggio *et al.*, 2017). Under similar condition, equivalent

molar of 1-aminopiperidine, propargylamine and propylamine were conjugated with compound **7** to afford **10** (47.1%), **11** (75.6%) and **12** (94.6%), respectively.

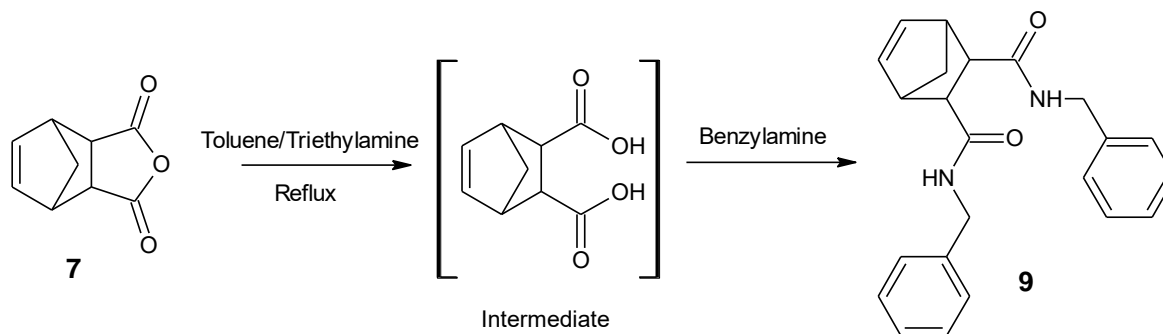


Figure 3.4: Proposed synthetic pathways of compound **9**.

The reaction between compound **7** and ethylenediamine yielded the mono-substituted amine **14** and the di-substituted amine **15**. Although both involve the same single reaction step, two different work-up procedures of the crude mixture afforded compounds **14** and **15**, respectively. Precipitation of the crude mixture with ethylacetate and isolation of the filtrate afforded **14** at a considerable high yield of 89.94%. Re-crystallisation of the crude product in ice-cold methanol afforded **15** at a low yield of 12.32%. Compounds **16-18** differ from compound **14** by the number of carbons between and/or attached to the diamines. Amongst the diamine reactions, the highest yield (96.5%) was observed in the reaction involving N,N-dimethylethylenediamine (**18**). This was expected as the di-methyl substitution protected one of the amines, thus limiting by-product formation. This observation was also evident in **11** (75.58%) and **12** (94.55%). A very important observation was the absence of acid or base catalyst in reactions involving the formation of compound **9** and **13**. This differs from similar reactions reported in the literature (Tarabara *et al.*, 2004; Krishchik *et al.*, 2004; Camm *et al.*, 2007 & Gomez-SanJuan *et al.*, 2013). However, the reactions proceeded to give significant yields of each compound as illustrated in outline 3.3.2.2.6 and 3.3.2.2.7. A plausible explanation would be that the aminolysis of **7** produces water as by-product which is capable of catalysing the reaction.

The structures of compounds **7-18** were elucidated and confirmed by NMR experiments that include: ^1H , ^{13}C , and DEPT-135. The IR and MS spectra were also employed to confirm these structures.

In the IR spectra, the characteristic stretching signals for the carbonyl moiety were observed in the region of $1654\text{-}1766\text{ cm}^{-1}$ for **7-18**. The signal in the region of $800\text{-}920\text{ cm}^{-1}$ and 1729-

1841 cm^{-1} indicates the presence of a five membered heterocyclic ring in all the compounds except **9**. The appearance of stretching absorption bands at 1654 cm^{-1} (strong) and 3304 cm^{-1} (medium), which were attributed to the C=O and N-H group respectively, suggests the presence of the amide moiety in compound **9**. Similarly, the N-H group also exist in the structure of **13**, and was observed as a medium sharp peak at 3282 cm^{-1} . The characteristic medium and broad stretching signal for aliphatic primary amines (NH_2) were observed in the 3372-3386 cm^{-1} range for compounds **14**, **16**, and **17**. The strong sharp absorption bands at 3265 cm^{-1} , as seen in the IR spectrum of compound **11**, supported the presence of aliphatic alkyne in the structure.

In the ^1H NMR spectrum, the bridge protons resonate upfield as a doublet of triplets and a doublet for all the azatricycloundecane derivatives except for compounds **9** and **15** that appeared as two doublets. The doublet of triplets and doublet of compounds **7**, **8**, **10**, **11**, **12**, **13**, **14**, **16**, **17** and **18** were observed in the region of $\delta = 1.55$ -1.81 and 1.45-1.59 ppm, respectively, while the bridge protons of **9** and **15** appeared in the region of $\delta = 1.24$ -1.72 ppm as two doublets. The characteristic peaks for aromatic protons were evident downfield in the spectra of **8**, **9** and **13**. The aromatic protons of compounds **8** and **9** were observed as multiplets in the $\delta = 7.18$ -7.31 ppm region, integrating for five and ten protons, respectively. Unlike **8** and **9**, the aromatic protons of **13** were observed as a doublet of doublets ($\delta = 7.20$ -7.24 ppm), a triplet ($\delta = 6.93$ -6.97 ppm) and a doublet ($\delta = 6.75$ -6.76 ppm). The piperidyl ring of compound **10** was evident in the proton NMR spectra. A triplet ($\delta = 3.07$ -3.10 ppm) and a multiplet ($\delta = 1.61$ -1.67 ppm) were observed and assigned to the piperidyl ring protons, each integrating for four protons. The electron-withdrawing effect of the nitrogen atom in the heterocyclic ring causes a downfield shift of the CH_2 protons adjacent to the heterocyclic nitrogen. The multiplet observed upfield at $\delta = 1.37$ -1.43 ppm was also assigned to the piperidyl protons as its integration accounted for the final two protons. The ^1H spectrum of compound **11** showed a doublet signal at δ 4.09 ppm ($H_J = 2.5$ Hz) and a triplet at δ 2.13 ppm ($H_J = 2.5$ Hz) with integration for two and one protons, respectively. These signals together with the coupling constants observed confirms the presence of the propargyl conjugate in **11**. In comparison, the appearance of a multiplet at $\delta = 1.41$ -1.51 ppm ($H_J = 7.5$ Hz) that integrated for two protons and a triplet at $\delta = 0.87$ -0.84 ppm ($H_J = 7.4$ Hz) that integrated for three protons, as seen in compound **12**, indicate the presence of the propyl conjugate that replaced the propargyl moiety. The protons of compounds **14-18** were all accounted for. In the proton spectra of **14**, the CH_2 protons adjacent to the aliphatic primary amine were observed at $\delta = 2.72$ -2.75 ppm ($H_J = 6.4$ Hz) as a triplet while the CH_2 protons adjacent to the heterocyclic nitrogen were observed at $\delta =$

3.40 ppm ($H_J = 6.4$ Hz) as a doublet. The downfield shift of the former was due to a higher deshielding effect of the heterocyclic nitrogen when compared to the primary amine. In contrast, compound **15** showed no signals between 2.00 ppm and 3.00 ppm. The disappearance of this signals suggest that the ethylenediamine had undergone di-substitution at both amines to afford **15**. Due to the symmetrical nature of the carbons, the signal for the two CH₂ adjacent to the nitrogens was observed as multiplet at $\delta = 3.46$ ppm, integrating for four protons. By comparison to **14**, the appearance of a doublet of doublets at $\delta = 1.65$ -1.71 ppm signal and a doublet of triplets $\delta = 1.59$ -1.64 ppm signal upfield indicate the presence of an additional aliphatic CH₂ which corresponds to the structure of **16**. The structural similarities that also exist between **14**, **17** and **18** allows for spectral comparison and the allocation or assignment of protons. When compared to **14**, two additional CH₂ signals were observed upfield as multiplets, each integrating for two protons, in the spectrum of compound **17**. For compound **18**, the signals for the hydrogens of the two methyl groups were present as a singlet at $\delta = 2.20$ ppm with an integration of six protons. The downfield shift of the CH₃ protons was expected due to the influence of the nitrogen atom deshielding the methyl protons.

In the ¹³C NMR spectra, all carbon signals of compounds **7-18** were observed in the respective regions. DEPT-135 experiments were also conducted for each compound in order to establish the number of methyl, methylene and/or methine signals present. For compound **7**, the carbonyl signal was observed downfield at $\delta = 171.3$ ppm, and this downfield observation was common in the $\delta = 172.8$ -178 ppm region for the spectra of its derivatives (**8-18**). The characteristic ¹³C spectra signals for aromatic carbons were evident in the $\delta = 115.0$ -138.2 ppm region for compound **8**, **9** and **13**. The signal for the methylene carbon between the aromatic carbon and the nitrogen atom was prominent in the DEPT-135 and ¹³C spectra for **8** and **9**. The absence of this signal in the spectra of **13** provides confirmation to the presence of the phenylhydrazine conjugate. The DEPT-135 experiment was also very useful in identifying the methylene carbons of compound **10** as the CH₂ signals found at $\delta = 52.2$, 51.6, 25.9 and 23.1 ppm correspond to the structure. For compound **11**, the quaternary carbon and methylene carbon signals of the propargyl conjugate were observed at $\delta = 71$ ppm and 27.2 ppm, respectively. In contrast, compound **12** showed upfield shift signals at 21.2 ppm and 11.4 ppm for the respective methylene and methyl carbons, thus confirming the presence of the propyl conjugate. Finally, the differences in the structures of compound **14-18** were more pronounced when comparing the methylene carbon signals of amine conjugates in the DEPT-135 spectra for each compound. While compound **14** showed two methylene signals at $\delta = 40.1$ ppm and 41.7 ppm that

correspond to its structure, only one signal at $\delta = 36.4$ ppm was observed in the ^{13}C and DEPT-135 spectrum of **15**. This was due to the symmetric nature that allowed one signal to represent two methylene carbons as reflected in the spectra of **15**. Compared to **14**, compound **16** showed one additional methylene carbon while compound **17** showed two in the respective spectra. The methyl carbons of compound **18** were observed upfield as a single signal at $\delta = 45.4$ ppm due to the symmetric nature of these carbons.

On the basis of the above experiments, it is safe to conclude that the structures and spectra of each compound were in good agreement. The MS spectra showed the respective molecular ion peaks that corresponded to each empirical formula of the compounds (**8-18**). This further confirmed the identity of these compounds.

The epoxidation of dicyclopentadiene using sodium percarbonate in a high-pressure metallic reactor afforded the corresponding diepoxide (**19**) in 54.32% yield. The diepoxide was then conjugated with amines in aqueous medium under microwave condition to afford different rearranged polycyclic amine cages (**20-23**).

A 0.75 molar equivalent of benzylamine was reacted with the diepoxide (**19**) in a microwave system to afford a mixture of diastereomers **20** and **21**. Upon extraction from water and subsequent elution with ethyl acetate, **20** and **21** were separated and obtained in yields of 31.85% and 21.48%, respectively. It is important to point out that several solvents such water, methanol, ethanol and toluene were employed in this reaction. However, only the reaction involving the use of water produced a reasonable yield while the rest showed little or no yield. This was attributed to water's ability to act simultaneously as catalyst and solvent at such a high temperature, thus eliminating or reducing by product (Akiya and Savage, 2002; Medina-Ramos *et al.*, 2014). Hence, allowing the reaction to proceed thus favouring compound **20** and **21** formation. Interestingly, the use of a three molar excess of phenylhydrazine did not afford the final product as a polycyclic cage amine with phenylhydrazine moiety. Instead, aniline analogues (**22** and **23**) were obtained as diastereomers in a yield of 20.1% (64:36). When equal molar of phenylhydrazine was used, very little or no product was observed. In an attempt to separate these isomers, several mobile phases were employed. Unfortunately, the separation of compounds **22** and **23** was not successful. The reasons for the aniline analogue formation could be explained in two ways: (1) it may be that the phenylhydrazine was reductively cleaved by the aqueous medium under high temperature and pressure to form aniline which ultimately reacted with the diepoxide; or (2) the secondary amine adjacent to the phenyl group in the

phenylhydrazine could have conjugated with the diepoxide. Prior to the conjugation, the primary amine may have initially formed the nitro- group and subsequently been eliminated to form the aniline analogues as seen in **22** and **23**

Under conventional technique, the reaction that afforded compounds **20** and **21** occurred in a high-pressure metallic reactor at a temperature greater than 160 °C utilizing water as a solvent (Kas'yan & Palchikov, 2010). Under microwave condition as described earlier, the reaction proceeded at a lower temperature although the yields were much lower than expected. The reason for the poor yield might be explained by the suboptimal isolation and purification techniques employed. It is important to mention that the actual pressure and power during reaction were different from the set figures, and the time of reaction completion was not investigated. However, the advantage of lower temperature could be beneficial in similar reaction where reagents or reactants are prone to degradation by harsh reaction conditions.

Compound **19-23** were characterised and confirmed by MS, IR, and various NMR experiments such as ¹H, ¹³C and DEPT-135. In the IR spectra of **19-23**, there were stretching absorption bands at 690-704, 1217, 1366-1370, 1739 and 2971 cm⁻¹ that suggest the presence of five membered ring and methine group in each of the compounds. The bands in the 1217, 1366-1370 and 1739 cm⁻¹ regions supported the presence of five membered ring while the bands in the region of 690-704 and 2971 cm⁻¹ represent those of methine group. The appearance of a strong stretching absorption signal at 827 cm⁻¹, as seen in the spectra of compound **19**, suggest the presence of an epoxide group(s). Weak broad absorption bands that indicate the presence of an OH group(s) were also observed in the spectra of **20-23**. It is important to note that the epoxide absorption bands were absent in the IR spectra of **20-23**. This clearly indicates that these amines or intermediate amines interacted with both epoxide moieties to afford the respective analogues.

The bridge protons of compound **19** was observed upfield at $\delta = 0.84$ and 1.43 ppm ($H_{J=9.8}$ Hz) as two doublets, each integrating for one proton. The epoxy protons were also observed downfield as a triplet and three doublets with the peaks in the $\delta = 3.39$ - 3.54 ppm ($H_{J=2.2/2.3}$ Hz) region assigned to the norbornanyl epoxide moiety and the peaks in the $\delta = 3.22$ - 3.27 ($H_{J=2.9/3.3}$ Hz) ppm region assigned to the five membered ring epoxide moiety. The structure of **19** was further investigated by analysing the ¹³C and DEPT-135 spectra. The carbons adjacent to the epoxy moiety were observed downfield at $\delta = 48.77$, 49.01 , 58.70 and 61.76 ppm. This was

due to the electron-withdrawing effect of the oxygen group. The presence of two CH₂ signals identified upfield at $\delta = 26.98$ and 29.63 ppm correspond to the structure of compound **19**.

For compound **20** and **21**, the characteristic peaks for the aromatic protons (downfield) and the bridge protons (upfield) were observed in the $\delta = 7.12$ - 7.35 ppm and $\delta = 1.09$ - 1.89 ppm ($H_{20J} = 10$ Hz; $H_{21J} = 9$ Hz) region, respectively. The multiplicity of the aromatic protons showed multiplet peaks while the bridge protons were observed as two doublets. In the proton NMR spectrum of **20**, the two multiplets observed downfield at $\delta = 4.28$ and 3.89 ppm, each integrating for one proton, were assigned to the protons adjacent to the hydroxyl group while the methylene group in between the aromatic and amino moiety showed a doublet of doublets signal in the $\delta = 3.70$ - 3.85 ppm region. These observations together with the appearance of two doublets signals in the $\delta = 2.89$ - 2.90 ppm ($H_J = 1.8$ Hz) and 2.75 - 2.76 ppm ($H_J = 4.8$ Hz) regions, each integrating for one proton, confirmed the presence of the benzylamine conjugate. By comparison, **21** showed two doublets signals downfield in the 4.43 - 4.44 ppm ($H_J = 3.4$ Hz) and 4.33 - 4.34 ppm ($H_J = 3.4$ Hz) region, each integrating for one proton, and these signals were assigned to the protons adjacent to the hydroxyl groups. Although they are not adjacent protons, the coupling constant observed ($J = 3.4$ Hz) indicates close proximity to each other. Based on this information, it was possible to determine the hydroxyl positions in the five-membered cyclic ring. The position of the hydroxyl groups and the orientation of the molecular structure in **21** allow protons adjacent to the hydroxyl moieties to have the same splitting effect on each other, hence the coupling between them while no splitting effects were noticeable in the molecular structure of **20**. The methylene group was observed downfield as a singlet at $\delta = 3.72$ ppm, which showed an integration for two protons. The protons adjacent to the amino group, in the rearranged heterocyclic moiety, were also observed downfield at $\delta = 4.13$ - 4.14 ppm and $\delta = 3.94$ ppm as a doublet and a multiplet, respectively, which also confirmed the benzylamine conjugate.

Compounds **22** and **23** exist as a diastereometric mixture in a 3:2 ratio. The ratio was determined from integrations of part of the benzyl peaks extracted from the ¹H spectrum in the 6-7 ppm region as shown in figure 3.4. The aromatic protons for **22** and **23** gives rise to a multiplet, doublets and triplets in the 6.61-7.25 ppm region. All other protons were assigned accordingly. It is important to note that there was no methylene peak observed in the 3.70-3.85 ppm region in the ¹H spectrum. This confirms the absence of the methylene moiety adjacent to the benzyl group and confirms the presence of aniline moiety within the structures of **22** and **23**. Since the structures are similar to compound **20** and **21**, assignment of protons were done

in the same manner. Based on the splitting behaviour of the protons adjacent to the hydroxyl moieties, as seen in **20** and **21**, each isomer was identified as compound **22** and **23**. The protons directly attached to the hydroxyl moieties were observed at $\delta = 4.01$ and 3.96 ppm as doublets and multiplet, respectively for compound **22** while those of **23** were observed as doublets, each integrating for one protons, at 4.48 ($H_J = 5.2$ Hz) and 3.91 ppm ($H_J = 5.3$ Hz).

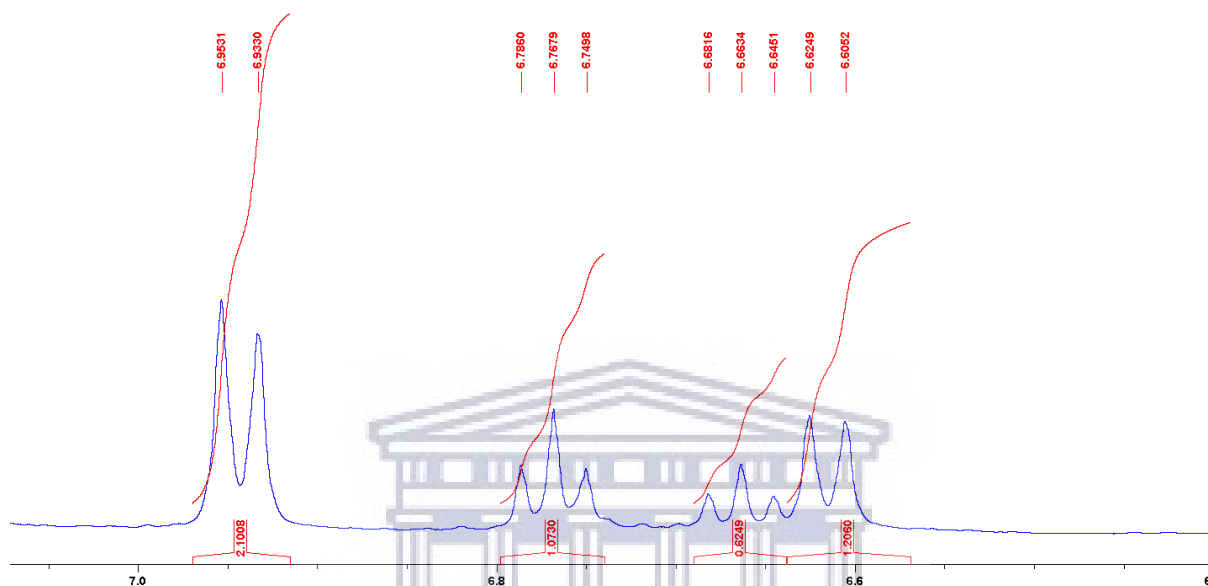


Figure 3.5: Aromatic region of the ^1H spectrum of compound **22** and **23**.

In the ^{13}C and DEPT-135 spectra for **20-23**, the resonances of all the carbons were observed. The aromatic signals were represented in the 112-150 ppm region. Both compounds **20** and **21** showed three methylene signals, while in compounds **22** and **23** only two methylene signals were observed.

Finally, compound **20-23** showed molecular ion peaks (m/z) corresponding to the molecular formula of each compound. The MS spectrum of compound **22** and **23** showed a molecular ion peak m/z at 258.1492 $[\text{M}+\text{H}]^+$ which corresponds to the molecular formula $\text{C}_{16}\text{H}_{19}\text{NO}_2$. This finding also correlates to the NMR spectra observations that indicate the absence of phenylhydrazine or benzylamine analogues, thus confirming the structure of **22** and **23**.

Compounds **24-27** were included in the series due to the structural similarities. They were characterised and confirmed by ^1H and ^{13}C -NMR experiments and the signals observed in each of the compound correspond to those found in the literature (Kas'yan & Palchikov, 2010; Palchikov *et al.*, 2014).

3.5 Conclusion

The norbornane derivatives were successfully synthesised in sufficient yields. The low yields observed in some reactions were due to the susceptibility of certain reactants to degradation by heat and/or under acidic conditions, the separation and purification techniques employed in obtaining final product from the crude mixture, and prolonged reaction times caused by slow reactions. The yields could be improved by either performing reactions in a controlled environment that limits degradation or optimising purification techniques that should minimise product wastage. The synthesised compounds were characterised by MS, IR and NMR techniques. The successful syntheses of the various diamine analogues also provide new opportunities, as linking agents, for conjugation of privileged structures to these norbornane derivatives.

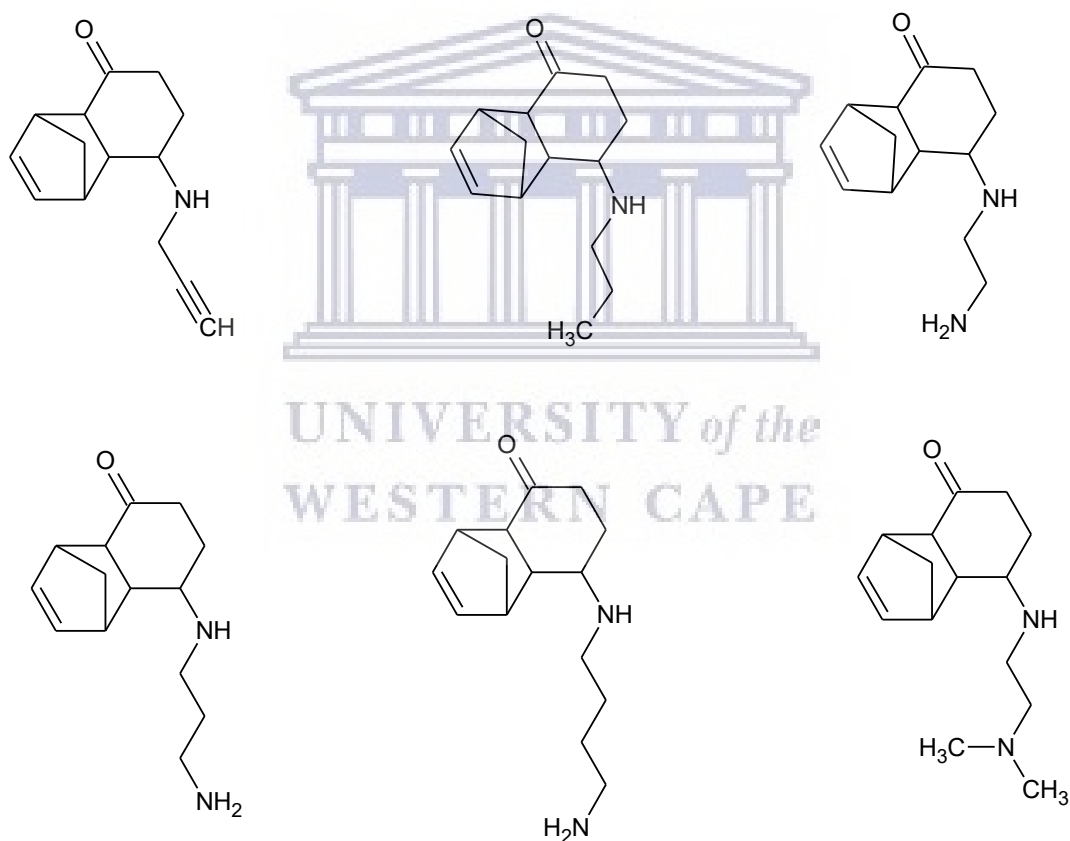


Figure 3.6: Proposed aliphatic amine conjugates.

In the series that include the synthesis of compound **1-6**, conjugates of propargylamine, propylamine, ethylenediamine, 1,3-diaminopropane, 1,4-diaminobutane and N,N-methylethylenediamine were also proposed (figure 3.5). They were subjected to similar reacting conditions as compound **5** and **6**. However, none of the reactions proceed as expected.

It is suggested that the reaction is favourable to the cyclic, heterocyclic or aromatic conjugates or moieties than aliphatic conjugate. The reactivity of the alicyclic conjugates may have been due to the low activation energy required for their reactions when compared to the aliphatic conjugates (Mereshchenko *et al.*, 2015).

Reactions were also conducted under acidic, reflux or dean-stack condition using different solvent such as THF, benzene and ethanol but none of the desired compounds were formed even though one of the starting material (compound **2**) was completely used up in the reaction mixtures. A plausible explanation would be that compound **2** was completely degraded owing to its susceptibility to low pH or thermal energy thus preventing the formations of these conjugates. It is proposed that if subjected to low temperature and high pressure in a microwave system, the formation of these conjugates are possible.

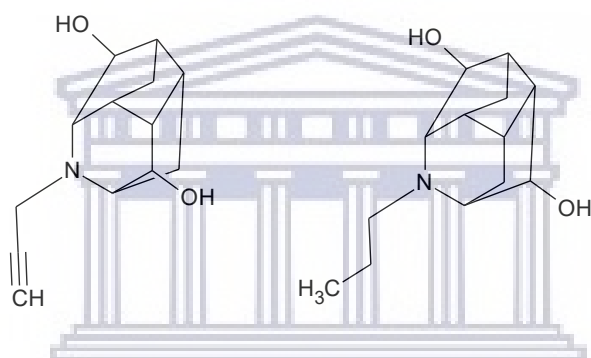


Figure 3.7: Proposed propargylamine and propylamine conjugates of compound **19**.

In the compound **19-23** series, conjugates of propargylamine and propylamine were also proposed (figure 3.6). In this case, products were formed but were insoluble in most organic solvent including DMSO. Therefore, they were not isolated and analysis, and were excluded in the list of series to be evaluated in biological assays as the solubility in DMSO is paramount for activity testing.

In total, 27 compounds were successfully synthesised to be evaluated in cytotoxicity-, neuroprotection-, NMDA receptor inhibition- and VGCC blockage studies.

CHAPTER 4

Biological Studies

4.1 Introduction

The pathways or mechanisms that lead to various neurodegenerative disorders have been a subject of debate for many years. Numerous studies have been proposed, but none could establish a definite mechanism as they are still fragmented and poorly defined. However, it is generally believed that these disorders are a consequence of interrelated processes which eventually lead to neuronal cell death either by necrosis or apoptosis. Of the well known multifactorial processes, the effect of excitotoxicity through calcium overload is prominent. There is then need for compounds or molecules that not only modulate calcium influx under pathological condition, but also have appropriate safety profiles. The objective of this chapter is to evaluate the cytotoxicity, neuroprotection and neuronal calcium inhibition profiles of the norbornane derivatives that were synthesised in the previous chapter. This was achieved by various *in vitro* tests that utilise the human neuroblastoma SH-SY5Y cell-line for biological studies. This cell-line that originates from the peripheral nervous system possesses components of excitatory neurotransmission and contains receptors with high affinity to glutamate as well as other ionotropic receptors (NMDA, AMPA and kainate) that influence the level of intracellular calcium. Moreover, the human neuroblastoma SK-NA-S cell line, a subclone from which SH-SY5Y cells originate, has been shown to contain expression of transcription for ionotropic glutamate receptors (Jantas *et al.*, 2014). These characteristics enable it to be used in neurotoxicity and neuroprotection studies as a human culture model and align with our biological studies. The safety profile of the compounds (**1-27**) in neuronal cells was assessed by performing neurotoxicity assays in order to determine the optimum concentration for the neuroprotection and Ca²⁺ inhibition studies. The neuroprotection studies were performed to investigate the anti-apoptotic abilities of the synthesised compounds against neurotoxin, 1-methy-4-phenylpyridinium (MPP⁺), induced neuronal cell death in human neuroblastoma SH-SY5H cells. Finally, calcium influx studies were performed to determine the Ca²⁺ inhibitory potential of the synthesised compounds on *N*-methyl-D-aspartate receptors (NMDAR) and voltage gated calcium channels (VGCC) as these pharmacological targets play a vital role in calcium overload as observed in numerous neurodegenerative disorders.

4.2 Instrumentation

The readings of spectroscopic emission of light from intracellular Fura-2 (bound/unbound) in the calcium inhibition studies were obtained on a Biotek Synergy™ Mx Monochromator-based fluorescence microplate reader that uses Gen™ 5 data analysis software. The BMG Labtech Omega® POLARstar multimodal plate reader was used in the cell viability studies (neuroprotection and neurotoxicity assays) to measure the spectroscopic absorbance of treated and untreated human neuroblastoma SH-SY5H cells. Black 96-well plates (mfr. No. Greiner 655076, Greiner Bio-one GmbH) were used in the fluorescence measurement experiment while the transparent 96-well plates (mfr. No. Greiner 655101, Greiner Bio-one GmbH) were used in the UV-absorbance assay. Appropriate micropipettes (P2G, P20G, P100G Pipetman micropipettes (Gilson, Inc.)) for each accurate aliquot solution measurement were used to achieve the desired concentrations needed for each experiment during the assay studies. In order to reduce contamination, sample preparations were conducted under sterile condition in a compact laminar flow cupboard (Labotec). Incubation of prepared samples was done in an ESCO CelCulture Air Jacket CO₂ incubator (Apex scientific).

4.3 Cytotoxicity Studies

4.3.1 Background

Cytotoxicity assays are commonly used to measure the toxic potential of substances or chemicals on viable cells without necessarily highlighting their mechanism of action (Cudazzo *et al.*, 2019). Cytotoxicity studies are commonly used to investigate the impact (cytostatic or cytotoxic) of tested agents or substances over certain period of time on the proliferation of specific cancer cell line such as human neuroblastoma SH-SY5Y cells, human embryonic kidney HEK293 cells, human T-cell leukemia Jurkat cells, mouse neuroblastoma N2a cells, mouse neuroblastoma NIH383 fibroblasts, or rat hepatoma H-4-II-E cells. These cell lines have been shown to be sensitive to chemically-induced cytotoxicity (Vinken and Blaauboer, 2017). The choice of markers or approach in cytotoxicity testing or assessment is very important for an accurate or effective toxicological endpoint. Most often, the activity of lactate dehydrogenase is measured in cell culture medium using the NADH-dependent conversion of a dye. This approach evaluates acute toxicity of drugs or chemicals by performing viability or metabolic activity tests based on luminogenic ATP assays (Riebelling *et al.*, 2018; Steinbrecht *et al.*, 2019). Another approach is the measurement of the number of viable cells after treatment in quantitative colorimetric assay such as the 3-(4,5-dimethylthiazol-2-yl)-2,5-

diphenyltetrazolium bromide (MTT) assay, 2-3-bis(2-methoxy-4-nitro-5-sulphophenyl)-2H-tetrazolium-5-carboxanilide sodium salt (XTT) assay, WST-1 assay and 3-(4,5-dimethylthiazol-2-yl)-5-(3-carboxymethoxyphenyl)-2-(4-sulphophenyl)-2H-tetrazolium salt (MTS) assay. The suitability of these colorimetric assays are based on the ability of cellular NAD(P)H-dependent oxidoreductase enzymes located in the cytoplasm to reduce a tetrazolium salt to a coloured formazan salt derivative. The reduction of these tetrazolium salts is a measure of the cell's metabolic state or capacity that corresponds to the number of viable cells (Riebelling *et al.*, 2018). Colorimetric assays have been shown to be an easy and fast method in determining cells viability after incubation with the tested substance (Nery *et al.*, 2014). Of all the colorimetric assays discussed earlier, the MTT assay is undoubtedly the most commonly used one. The MTT cytotoxicity assay is based on the ability of viable cells, *via* mitochondrial enzyme succinate dehydrogenase, to reduce a yellow tetrazolium salt into a blue insoluble formazan that is impermeable to the cell membrane, thus detained inside the cells. However, the addition of organic solvent such as DMSO dissolves the formed formazan and the solubilised formazan is released into the culture medium to allow colorimetric measurement of the cell samples. The ability of the cells to reduce MTT is dependent on the uncompromised mitochondrial activity. Since the integrity and activity of mitochondria are an integral part of a viable cell, it is safe to conclude that the number of surviving cells is directly proportional to the level of formazan product formed (Vinken and Blaauboer, 2017).

For the cytotoxicity studies, the human neuroblastoma SH-SY5Y cell-line was used. This cell line is commonly used as model cell system for studying neuronal cell death. This cell type also expresses growth factor receptors and produces neurotransmitters such as dopamine and noradrenaline in similar manner as the innate human neurons (Ruffels *et al.*, 2004; Gonzalez-Burgos *et al.*, 2017).

The aim of the experiment was to screen the synthesised compounds for potential toxicity against the human neuroblastoma SH-SY5Y cells in order to determine the optimal concentration for neuroprotection and calcium inhibition studies.

4.3.2 Material and methods

4.3.2.1 Cell line and Culture

The human neuroblastoma SH-SY5Y cells were generously donated by the Blackburn Laboratory, University of Cape Town. Cells were grown in Dulbecco's Modified Eagle

Medium (DMEM, Gibco, Life Technologies Corporation, Paisley, UK), supplemented with 10% fetal bovine serum (FBS, Gibco, Life Technologies Corporation, Paisley, UK), 100 U/mL penicillin and 100 µg/mL streptomycin (Lonza Group Ltd., Verviers Belgium). Cultures were incubated at 37 °C in humidified air with 5% CO₂ and a medium change every three days. Cells were sub-cultured when they attained 70 to 80 percent confluency using a solution of 0.25% trypsin EDTA (Lonza Group Ltd., Verviers, Belgium).

4.3.2.2 Screening protocol

Confluent SH-SY5Y cells were seeded in a 96-well microtiter plastic culture plates at a density of 1×10^4 cells/100µL/well. Plated cells, suspended in DMEM (culture media), were incubated for 24 hours in a humidified atmosphere and 5% CO₂ at 37 °C to allow for cell adhesion to the bottom of the microtiter plastic plate. After 24 hours, the culture media were replaced with fresh DMEM (100 µL) that contain increasing concentrations (10 µM, 50 µM and 100 µM) of test compounds (**1-27**), dissolved in DMSO, in each well. The treated group of cells were incubated for 24 hours in a humidified incubator embedded with 5% CO₂ at 37 °C. The control group of cells contained DMEM and DMSO in concentration similar to the highest concentration of the treated group, and were processed and incubated concurrently as the treated group of cells.

4.3.2.3 MTT assay

After incubation of cells, in 96-well plates and exposed to different concentrations (0 µM, 10 µM, 50 µM and 100 µM) of test compounds, for 24 hours, 10 µL of MTT (5mg/ml) solution was added to each well and further incubated for 4 hours at 37 °C. This was followed by addition of 100 µl of DMSO to ensure solubility of the formazan, and absorbance of the sample in each well was measured at 570 nm on a BMG Labtech Omega[®] POLARStar multimodal plate reader. The absorbance data were normalised against those of the control wells with the medium alone (blank).

4.3.2.4 Data analysis

The data of the medium alone (blank) were normalized to the absorbance of the control cells (100%) and the cell viability of the test compounds was expressed as percentage relative to the control cells. The percentage cell viability in test wells were calculated using the formula: % cell viability = (absorbance of treated cells/absorbance of untreated well) x 100. The data analysis was done using the GraphPad Prism version 6.01 for windows (GraphPad software,

LA Jolla California, USA). Statistical significance was performed using the one-way ANOVA analysis. Each test well was done in triplicate and the statistical significance was set at $p < 0.05$.

4.3.2.5 Result and Discussion

Figure 4.1 illustrates the cytotoxic profile of compounds **1-27** and expresses the percentage cell viability of each test compound relative to DMSO only. DMSO only containing wells, without test compound, represents 100% cell viability. These were obtained by screening the test compounds at 10 μM , 50 μM , and 100 μM against the human neuroblastoma SH-SY5Y cells upon 24 hours exposure and subsequently assessed using the MTT assay. After the MTT assay protocol, the absorbance values obtained were analysed and the treated cells were compared to the untreated controls. As expected, the cell viability rate observed in most of the test compounds was inversely proportional to its concentration. This suggests that the percentage cell viability is concentration dependent. In contrast, compound **11** and **15** showed a proportional cell viability rate as low number of viable cells were observed at low concentration (10 μM) and vice versa. This could be due to a number of reasons that include: (1) Incomplete solubilisation of formazan crystal caused by change in pH as the concentration increases. It could be that the compounds (**11** and **15**) altered the pH (increase) level as the concentration increases: (2) Reduced formazan crystal formation caused by slow metabolism of the cells as the concentration increases. It could be that the metabolism of compound **11** and **15** treated cells becomes slower as the concentration increases, thus reducing the ability of the cells to metabolically convert MTT to formazan crystals. Since the accurate measurement of viable cells is solely dependent on the formation of formazan crystals by treated and untreated cells and the solubilisation of formazan crystals, it is suggested that the incomplete solubilisation and formation of formazan crystals had reduced the absorbance value in cells leading to the loss of linearity between absorbance and cells number as evident in figure 4.1. In a number of the treated cell wells, percentage cell viability exceeding 100% (untreated control) were noticeable. This may be due to absorbance readings obtained from over seeded wells relative to the control wells. It may also be that the metabolism of cells in some of the treated wells is faster leading to increase formation of formazan crystals than the untreated controls. Cells treated with compound **7** and **24**, at 100 μM showed the lowest percentage of viable cells with values of 51% and 59%, respectively. These values suggest that compound **7** and **24** have some cytotoxicity towards neuroblastoma cells at 100 μM . At 10 μM and 50 μM , all the tested compounds showed extremely low cytotoxic effect exhibiting percentage cell viability very close to 100% (control).

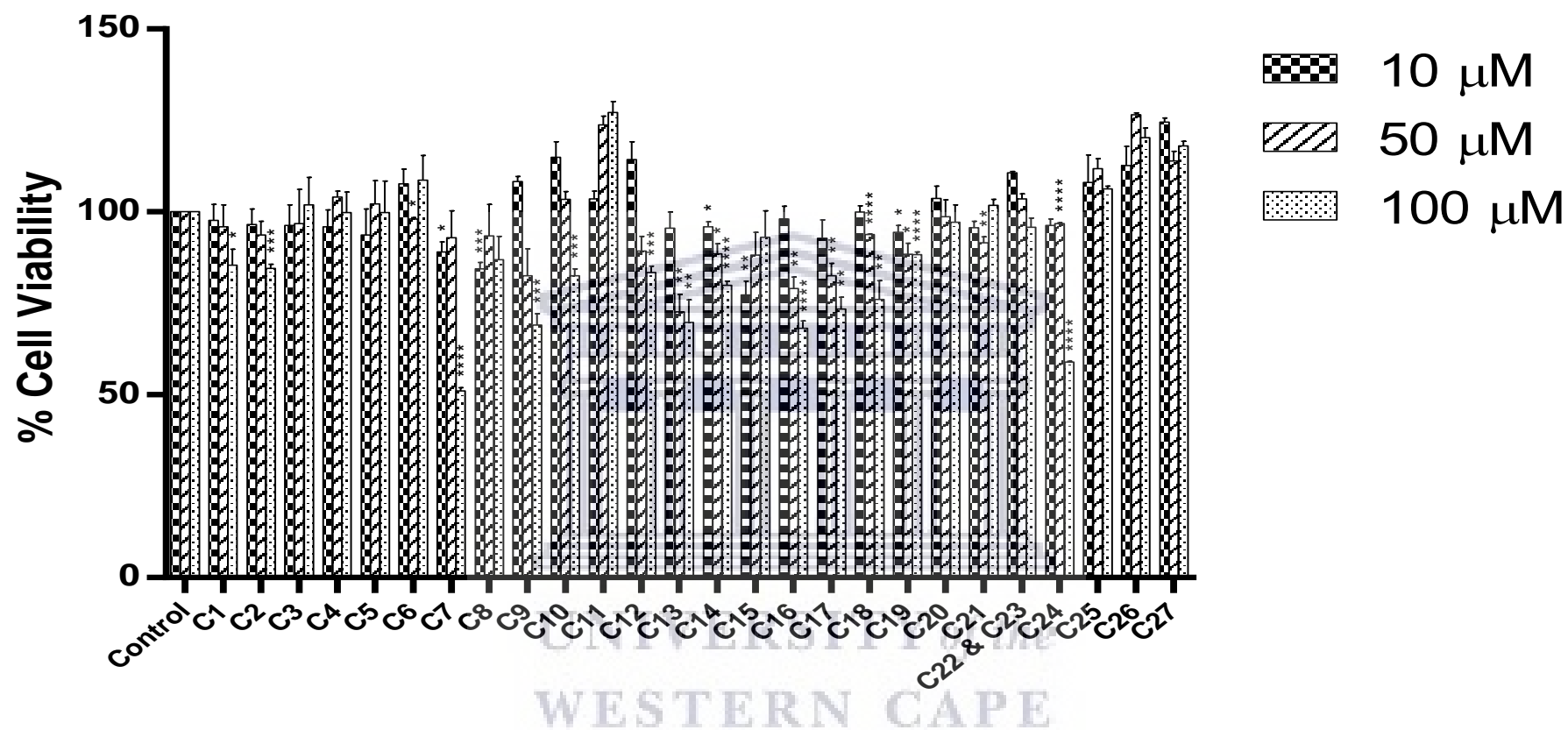


Figure 4.1: Cytotoxicity effect of tested compounds (1-27) on human neuroblastoma SH-SY5Y cells at concentration of 10 μM , 50 μM and 100 μM , after 24 hours exposure. Cell viability of treated cells is expressed as percentage of untreated control cell (100%). Data represent the mean \pm SD of treated cell versus untreated control cell (n = 3; three independent experiments and each experiment done in quadruplicate), was analysed by a one-way ANOVA, and the level of significance expressed as: *P < 0.05, **P < 0.01, ***P < 0.001, ****P < 0.0001.

Due to the good and acceptable cytotoxic profile observed at the lowest concentration (10 μ M) for the synthesised compounds, this concentration was identified and selected for the neuroprotection and calcium influx assays. This is required to avoid potential cytotoxic effect of the synthesised compound on the neuroblastoma cells and to promote accurate cell viability measurements.

4.4 Neuroprotection Studies

4.4.1 Background

Neuroprotection assays are commonly used to investigate or evaluate the ability of compounds to inhibit or halt degeneration of neuronal cells following neurotoxin attack or treatment with agents that induce excitotoxic cell death. In most cases, the aim is to prevent disease progression and secondary injuries by halting or reducing the loss of neurons (Ahsan, 2017; Tripathi and Ayyannan, 2017). For the purpose of assays, induced loss of neurons can be achieved by either administering neurotoxins such 1-methyl-4-phenylpyridinium (MPP^+) and amyloid beta ($A\beta$) or introducing a stressor or oxidant such as hydrogen peroxide (H_2O_2) or endotoxins. The MPP^+ and neuroblastoma SH-SY5Y cells is the most commonly used neurotoxin and cell lines, respectively, in neurotoxin induced and/or neuroprotection assays, particularly for Parkinson's disease models. MPP^+ is an active metabolite derived from 1-methyl-4-phenyl-1,2,3,6-tetrahydropyridine (MPTP) following activation by monoamine oxidase B (MAO-B) in the inner mitochondrial membrane. MPP^+ has been shown to selectively and potently inhibit respiratory complex I of the mitochondrial electron transport chain to cause cascades of events leading to the generation of free radicals that subsequently attack the neuronal cells, thus contributing to neuronal cell death (Cui *et al.*, 2013; Kim *et al.*, 2009; ¹Wang *et al.*, 2016; ²Wang, *et al.*, 2016; Jantas *et al.*, 2014; Zheng *et al.*, 2019). It has also been established that the effective concentration of MPP^+ needed to evoke 50% SH-SY5Y neuronal cell death is 2 mM (Jantas *et al.*, 2014). It was then appropriated to utilise the MPP^+ -induced toxicity model and neuroblastoma cell line to evaluate the neuroprotective characteristics of the synthesised compounds. Although this model is prominent in Parkinson's disease protection research, it can also be applied to other neurodegenerative diseases as other parts of the brain are susceptible to MPP^+ -induced toxicity.

In this experiment, neuroblastoma SH-SY5Y cells were treated with either MPP^+ only or in combination with synthesised compounds **1-27**. After incubation for a specific period of time, the treated cells relative to untreated control (DMSO) were subjected to MTT assay as

described earlier. The percentage cell viability of the treated cell relative to the untreated control that represent 100% cell viability were then analysed.

4.4.2 Material and methods

4.4.2.1 Cell line and Culture

The cell line (human neuroblastoma SH-SY5Y) and culture utilized for the neuroprotection studies were prepared in the same manner as that of the cytotoxicity studies (outlined in 4.3.2.1).

4.4.2.2 Neuroprotection protocol

Once confluent, SH-SY5Y cells were seeded in a 96 well plate at density of 1×10^4 cells/100 μ l/well. Plated cells were allowed to adhere to the bottom of the plastic plate as described in outlined 4.3.2.2. Synthesised compounds (**1-27**) were dissolved in DMSO required to make a final solution of 10 μ M for each compound. This concentration was deemed appropriate as it showed minimal or no cytotoxic effect on cells (figure 4.1), and consequently will not affect the cell viability values. The plated cells were treated with synthesised compounds and 2 mM of MPP⁺, and were incubated for a period of 24 hours. Prior to MPP⁺ exposure or incubation, the cells were pre-treated with 10 μ M of each compound for 2 hours. The untreated control cells which contain DMSO and DMEM were incubated in the same manner as the treated cells. After incubation for the set period of time, both treated and untreated cells were subjected to MTT assay.

4.4.2.3 MTT assay and Data analysis

The cell viability of treated and untreated cells were assessed and analysed by the MTT reduction assay and data analysis previously described in 4.3.2.3 and 4.3.2.4, respectively. Statistical significance was performed using the one-way ANOVA and the t-test (unpaired) analysis. Each test well was done in triplicate and the statistical significance was set at $p < 0.05$.

4.4.2.4 Result and Discussion

The neuroprotective effect of compounds **1-27** on neuroblastoma SH-SY5Y cells after 24 hours exposure to neurotoxin (MPP⁺) was assessed using the MTT cell viability assay. As illustrated in figure 4.1, the test compounds, when used alone at 10 μ M, showed very little or no detrimental effects on the cells as confirmed by the cytotoxicity studies. The neuroprotection

assay was then carried out at this concentration (10 μM) to ensure that the integrity or cell viability is not compromised by the test compounds. However, treatment of neuroblastoma cells with 2 mM of MPP^+ over 24 hours period induced a significant loss in cell viability by 49.9%. This value is similar to the values (about 50 percent loss) reported in literature (Wang and Xu, 2005, Cui *et al.*, 2013).

In order to determine the neuroprotective effects of synthesised compounds, cells pre-treated for 2 hours with test compounds were subjected to the same condition (2000 μM of MPP^+). All compounds (**1-27**) attenuated MPP^+ -induced neuronal cell damage as shown by significant enhancement in cell SH-SY5Y viability of 22.8% to 53.3% when compared to the MPP^+ only treated cell. The increases in cell viability for each compound was statistically significant as shown by all the p values that were smaller than 0.05 when compared to the MPP^+ only treated group of cells (figure 4.2). The highest and lowest neuroprotective activities were observed for compound **8** and **18**, respectively. The selective reduction and double adduct derivative of compound **1** showed improved protection against MPP^+ -induced cell damage as seen in compound **2** and **4**, respectively.

The substitution of the propargylamine moiety (**11**) with the propylamine moieties (**12**) leads to a slight increase in neuroprotective activity while substitution of the phenylhydrazine moiety with the benzylamine moiety improved the percentage cell viability of compound **8** by about 18%. The saturated carbons, in **2** and **12**, offer less rigid structures than the unsaturated carbons of alkenes and alkynes in **1** and **11**. The flexibility of these structures may allow better interactions with the neuronal cell membrane or antioxidant enzymes leading to improved neuroprotective activities.

The increased lipophilicity of compound **4** and amino group of **14** that provide better interaction with protein transporter may have enhanced their transportation into the neuronal cell or binding to dopamine active transporter (compared to **1** and **18**, respectively) thus the improved activity. When one of the carbonyl moieties in **2** was reduced to the hydroxyl moiety (compound **3**), a decrease in protection was observed. The introduction of a hydroxyl moiety improves hydrophilic character of compound **3** that in turns reduce its penetration into the cells leading to reduced neuroprotective activity.

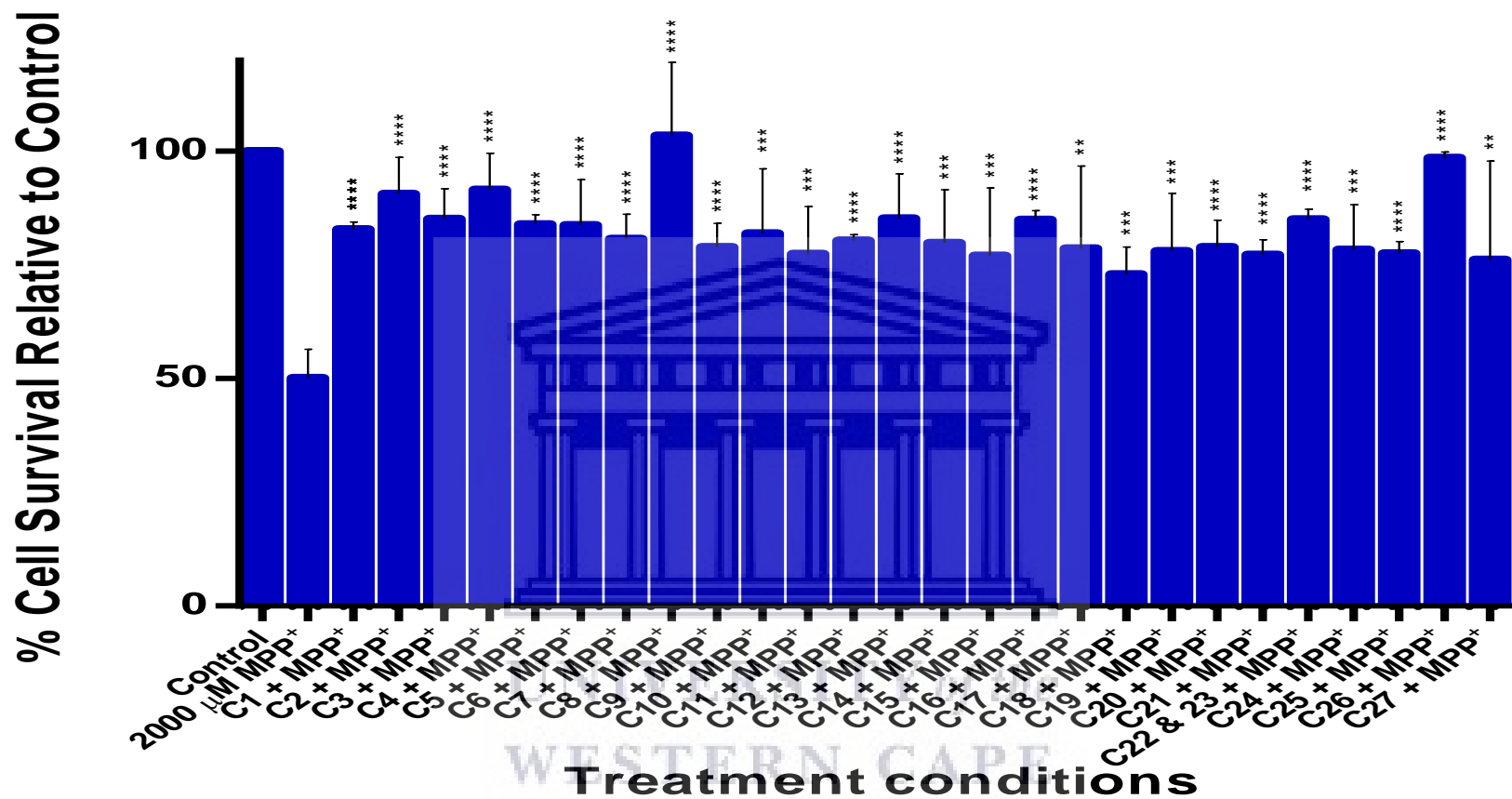


Figure 4.2: Neuroprotective effect of compound 1-27 on MPP⁺-induced toxicity in neuroblastoma SH-SY5Y cells. Cell viability of treated cells is expressed as percentage relative to the untreated control cells (DMSO) expressed as 100% cell viability. Data are represented as percent \pm SD of treated cell versus untreated control cell (n = 3; three independent experiment) and was analysed by a one-way ANOVA statistic. The level of significance is expressed as: *P < 0.05, **P < 0.01, ***P < 0.001, ****P < 0.0001 versus 2000 μ M MPP⁺-treated cells.

Interestingly, compound **26** showed a significant ($p < 0.05$) increase in cell viability of 98.5% upon exposure to MPP⁺-induced toxicity. However, the addition of a benzyl moiety, as seen in **22** & **23**, significantly reduced the percentage cell viability to 85.1% ($p < 0.05$), and the introduction of a linker between the nitrogen group and benzyl moiety, as seen in **20** and **21**, result in cell viability values of 79.0% and 77.2%, respectively, which indicate a further reduction in neuroprotective activity. It is suggested that the reduced activities may be due to the loss of protonated nitrogen group (lacks lone pair electrons) in compounds **20-23**. Similarly, the effect of the nitrogen group was also evident when compound **18** was compared with compound **14**, **16**, and **17**. Replacing the hydrogen atoms on the primary amines (**14**, **16** & **17**) with two methyl groups (**18**) reduced the neuroprotective effects of compound **18** by approximately 6-12% ($p < 0.05$ for compound **16**), indicating the importance of primary or secondary amines for improved activity. There were no significant differences in the activities of compound **14**, **16** and **17**, indicating that a difference in chain length between the heterocyclic five membered ring and the primary amines do not change the neuroprotective activities of these compounds. Ideally, this nitrogen group would offer improved interaction and binding to dopamine active transporter. This prevents MPP⁺ from entering dopaminergic neurons and subsequently improves neuroprotection as observed in compound **16** and **26**. The neuroprotective effect of compound **20** was similar to that of compound **21**. This indicates that changing the position of the hydroxyl moiety is well tolerated as no significant change in activities were observed (figure 4.2). It is important to note that the improved activity of the diastereometric mixture **22** & **23**, over **20** and **21** may suggest additive or synergistic effect rather than improved neuroprotective effect by each compound (**22** or **23**). Successfully separating this mixture and testing each compound would give clarity on their neuroprotective effects. Generally, the benzoquinone moieties (**1-6**) showed better neuroprotection than the furandione moieties (**7-18**) and the diepoxide moieties (**19-27**).

In this study, the norbornane scaffold has been shown to have neuroprotective effects against MPP⁺-induced neuroblastoma cell damage, and the effect of structural modifications were also illustrated. Although the mechanisms of neuroprotection were not discussed, the restoration of cell viability of neuroblastoma SH-SY5Y that range between 72.9% to 100%, after pre-treating for 2 hours with synthesised compounds (**1-27**) and subsequent exposure to MPP⁺, was most probably due to the compounds ability to: inhibit MPP⁺-induced caspase-3 activation; block MPP⁺ transport into the cell *via* dopamine active transporter; reduce Bax/Bcl-2 (pro-apoptotic and anti-apoptotic) ratio evoked by MPP⁺; improve mitochondrial integrity and functions;

and/or protect antioxidant such as catalase and superoxide dismutase (SOD) from MPP⁺ thus limiting reactive oxygen species (Wang and Xu, 2005; Singh *et al.*, 2016; Jung *et al.*, 2006; Lee *et al.*, 2011; Sun *et al.*, 2011; Zhou *et al.*, 2013; Jantas *et al.*, 2014; Jouha *et al.*, 2017). In order to verify or ascertain this mechanism, experiments that include: microscopic assessment of morphological changes, assessment of caspase-3 activity, flow cytometric measurement of mitochondrial transmembrane potential, flow cytometric detection of apoptotic cells, flow cytometric detection of necrotic cells, oxygen consumption assays to determine mitochondrial respiration, mitochondrial cytochrome c release using western blot assay, measurement of intracellular reactive oxygen species, and quantification of immunoblot by densitometric analysis to determine Bax/Bcl-2 ratio will be necessary (Wang and Xu, 2005; Jantas *et al.*, 2014).

4.5 Calcium influx studies

4.5.1 Introduction

Calcium influx studies are designed to evaluate the influence of test compounds on the flux of calcium ions through ionic channels or receptors, NMDA receptors and voltage-gated calcium channels in particular, in response to membrane depolarisation or receptor stimulation. Calcium ions (Ca²⁺) play a very important role as a secondary messenger or signal involved in many neuronal physiological processes including neurotransmission, gene expression, and neuronal development (progenitor proliferation, neuronal migration and differentiation, axon guidance, dendrite growth and cortical development). Despite its physiological importance, conditions that disrupt calcium homeostasis with even little change in intracellular calcium concentration can lead to pathophysiological neuronal processes like neuronal excitability, neuronal dysfunction, apoptosis, neurodegeneration and cell death. Due to its role in excitatory neurons, it is necessary to ensure precise calcium dynamics and maintain intracellular calcium homeostasis at all time for normal neural functions (Heusinkveld & Westerink, 2011; Baykara *et al.*, 2019; Leoni *et al.*, 2019; Wang *et al.*, 2019). The primary source of intracellular calcium influx in excitable neuronal cells is from the depolarisation of the cell membrane that results in the opening of VGCC and the activation of NMDA receptor-gated channels leading to influx of calcium from the neuronal extracellular space. Although intracellular Ca²⁺ release contributes to the intracellular [Ca], its impact is less detrimental to the neuronal cells. Under physiological conditions, neuronal cells are able to exert strong calcium homeostasis control by tightly regulating the balance between Ca²⁺ influx, extrusion, sequestration and buffering

(cytosolic Ca^{2+} binding proteins). However, under pathological conditions, increased or excessive calcium influx triggers a cascade of events that leads to neuronal dysfunction and cell death. To avert this effect, there is need for calcium ion chelating agents, calcium receptor inhibitors or calcium channel blockers that will prevent neurodegeneration by restoring calcium homeostasis (Heusinkveld & Westerink, 2011; Danesi *et al.*, 2018; Bisi *et al.*, 2019; Leoni *et al.*, 2019). The most common methods for assessing real-time change in intracellular Ca^{2+} are the plate reader-based approach or the single cell fluorescence microscopy experiment. The microscopy approach is well known to have higher temporal and spatial resolution and higher sensitivity, and no artifacts associated with changes in volume and osmolarity. However, it is labour intensive and time consuming, and are considered low- or at best medium-throughput. In contrast, plate reader-based approaches have lower sensitivity and are associated with artifacts, but has high throughput and are not labour intensive and time consuming. Despite the limitations, this approach is mostly utilized and preferred by many researchers as they still provide enough information on the kinetic change in intracellular calcium ion concentration. The plate reader approach uses dyes as indicators to measure the concentration of calcium ions that flows into the cells within a set period of time. It can either be single wavelength dye such as Fluo-4 or ratiometric dual wavelength dye such as Fura-2 (Heusinkveld & Westerink, 2011; Meijer *et al.*, 2014). In most case, the ratiometric dual wavelength dye, Fura-2, is preferred due to its ability to determine calcium influx concentration by indicating the fractional contribution of the Ca^{2+} free and Ca^{2+} bound forms of the probe in instances where the concentration of the probes is unknown. In contrast, despite the higher fluorescent yield of a single wavelength dye, they are affected by variability in factors like cell density, loading efficiency of dye, dye concentration and dye leakage which influence the results, and are unable to process probes with unknown calcium concentration. The ratiometric indicators also have the advantage of not needing calibration for each or individual experiment as the use of ratiometric calculation makes the output independent of indicator loading. These advantages, together with the capability to ensure more accurate calibration due to its ability to exhibit an increase in fluorescence upon calcium ion binding with a corresponding shift in the excitations and emissions, favour the use of a ratiometric wavelength indicator over the use of single wavelength indicator (Neher, 1995; Szmackinski & Lakowicz, 1995; Robinson *et al.*, 2004; Kukkonen, 2009). Fura-2 is a ratiometric indicator of Ca^{2+} that exhibit fluorescence at certain wavelength. It is commercially available as an ester in the form of Fura-2/AM (acetoxymethyl). In this form, it is unable to bind to Ca^{2+} and easily diffuses through the cell membrane into the cell. Once inside the cells, the Fura-2/AM is cleaved by intracellular esterase enzymes into the

Ca²⁺-sensitive molecule, an impermeant anionic indicator (Fura-2), which is trapped in the cytoplasm and has strong binding affinity for intracellular Ca²⁺. Generally, a plate reader with the capacity to monitor fluorescence over a period of time, after excitation of samples at 340 nm and 380 nm and subsequent emission at 510 nm, is commonly used to assess or determine the Fura-2 response to intracellular Ca²⁺ by showing a change in the optimal excitation wavelength with a substantial change in emission wavelength. Due to the fact that excitation of Ca²⁺-bound and Ca²⁺-free Fura-2 occurs at 340 nm and 380 nm, respectively, and both are able to fluoresce at approximately 510 nm, one is able to predict increase in concentration of intracellular Ca²⁺ as indicated by reduction in the fluorescence value at 380 nm after stimulation or depolarisation of neuronal cells loaded with Fura-2. The relative calcium influxes or inhibitions by screened molecules or drugs are mostly determined by calculating the 340/380 nm fluorescence intensities ratio (Grynkiewicz *et al.*, 1985; Lev-Ram & Grinvald, 1987; Blatter & Wier, 1990; Henke *et al.*, 1996; Dustin, 2000; Robinson *et al.*, 2004; Hu *et al.*, 2005; Gulaboski *et al.*, 2008; Mauleon *et al.*, 2013). In this view, the ratiometric approach using a fluorescent plate reader was considered appropriate for the calcium influx studies of synthesised compounds (**1-27**). Due to the physiological and pathological similarities that exist between primary neurons and neuroblastoma SH-SY5Y cells, the use of SH-SY-5Y cell to screen known and unknown calcium blockers (receptors or channels) is justified (Warnock *et al.*, 2013).

In these studies, the inhibitory or blocking effects of synthesised compounds (**1-27**) on calcium influx through NMDA receptors and VGCC were explored in order to investigate the neuroprotective potential of tested compounds against calcium (overload) induced neuronal toxicity under neuropathological condition.

4.5.2 NMDA mediated Ca²⁺ influx studies

4.5.2.1 Background

NMDA receptors are ionotropic receptors whose activation or stimulations by an excitatory neurotransmitter account for the majority of intracellular calcium ions in neuronal cells. Glutamate is the principal excitatory neurotransmitter found in the mammalian brain and spinal cord. Under physiological condition, glutamate concentration is tightly controlled and it plays a vital role in calcium signalling, fast synaptic transmission, neuronal plasticity, neuronal outgrowth and survival, memory, behaviour and learning, and critical for neural functioning by activating the ionotropic receptors (NMDA and non-NMDA receptors). However,

glutamine concentration becomes abnormally high under pathological conditions, and become neurotoxic to the neuronal cells as observed in the pathogenesis of many neurodegenerative disorders. Excessive glutamate is believed to over-activate or over-stimulate neuronal glutamate receptors (NMDA and non-NMDA receptors) leading to prolonged and massive influx of calcium ions in the cytoplasm. Of these glutamate receptors, the NMDA receptor is suggested to be the most influential in glutamate-mediated neuronal death during primary cultures of nerve cells. The excess calcium influx or overload disrupts the normal calcium homeostasis and triggers several cascades of events that ultimately induce neuronal cell death either by apoptosis or necrosis. This glutamate-induced neuronal cell death is termed excitotoxicity and it is a prominent feature among neurodegenerative disorders (Jing *et al.*, 2004; Lee *et al.*, 2012; Kim *et al.*, 2013; Taveira *et al.*, 2014; Yang *et al.*, 2014; Pereira *et al.*, 2017; Jeong *et al.*, 2017; Berntsen *et al.*, 2018; Jembrek *et al.*, 2018; Kumar *et al.*, 2019; Smidkova *et al.*, 2019; Park *et al.*, 2020).

It is clear that excessive glutamate induced activation of the NMDA receptor is the main cause of excitotoxic effects in neuronal cells, and reduction of this NMDA-mediated calcium influx is considered as a possible therapeutic or pharmacological target that would slow down or halt the degenerative process in neurological disorders and diseases (Berntsen *et al.*, 2018; Smidkova *et al.*, 2019). The NMDA induced SH-SY5Y cell injury model is believed to mimic glutamate-induced toxicity in human neurons and is generally accepted as activity screening model for the neuroprotective effect of NMDA receptor inhibitors. This supported the selection of neuroblastoma SH-SY5Y cell lines for the NMDA calcium influx studies (Liu *et al.*, 2019).

4.5.2.2 Experiment design

The inhibitory potential of synthesised compounds (**1-27**) against NMDA receptor mediated Ca^{2+} influxes were assessed using a fluorescence dual wavelength ratiometric approach. Fura-2/AM was used as the ratiometric indicator. The fluorescence indicator, suspended in fresh DMEM solution, was loaded on adhered SH-SY5Y neuroblastoma cells that were cultivated and grown in the lab, and calcium containing buffers were subsequently added. DMSO (only) was used as the control while MK-801 and NGP1-01 were designated as the positive controls. The NMDA/glycine buffer solution was used to stimulate or activate NMDA receptors of the SH-SY5Y cells to induce NMDA-mediated calcium influxes. The real-time kinetic changes in intracellular Ca^{2+} were monitored by a fluorescent plate reader that measures change in fluorescence intensities upon activation of the receptors. Since change in fluorescence

intensities corresponds to change in intracellular Ca^{2+} , the inhibitory effects of the synthesised compounds (1-27) and positive controls (MK-801 and NGP1-01), relative to the negative control (DMSO), on NMDA receptor mediated Ca^{2+} influxes can be determined.

4.5.2.3 Material and methods

Solutions were prepared in a controlled environment to minimise contaminants, and were stored at 2-8 °C throughout the experiments. Cells were handled and treated in a lamina air flow sterilised system. Materials, solutions and methods used in this study were outlined as follows:

4.5.2.3.1 Calcium and magnesium free buffer

Appropriate amount of sodium chloride (NaCl, 118 mM), potassium chloride (KCl, 4.7 mM), HEPES (20 mM) and glucose monohydrate (30.9 mM) were correctly weighed in a litre volumetric flask. To the flask, distilled water was added and it was made up to a litre volume to make the final calcium and magnesium free solution. Using a 4 molar concentration of an acid or base (NaOH/HCl), the pH of the final solution was adjusted to 7.4.

4.5.2.3.2 Calcium containing buffer

Calcium chloride dehydrate ($\text{CaCl}_2 \cdot 2\text{H}_2\text{O}$, 2 mM) was dissolved in 200 ml solution aliquots from the calcium and magnesium free buffer solution. The calcium containing final solution was then buffered with an acid or a base, as described earlier, to a pH value of 7.4.

4.5.2.3.3 Stimulation or activation buffer

To 200 ml of calcium and magnesium free buffer, appropriate amount of calcium chloride dihydrate (0.1 mM), NMDA (0.55 mM), and glycine (0.55 mM) were added. The final solution was adjusted to a pH value of 7.4 with an acid or base as described earlier, to obtain the final stimulation buffer solution

4.5.2.3.4 Cell line and culture conditions

The human neuroblastoma SH-SY5Y cells were generously donated by the Blackburn Laboratory, University of Cape Town. Cells were grown in Dulbecco's Modified Eagle Medium (DMEM, Gibco, Life Technologies Corporation, Paisley, UK), supplemented with 10% fetal bovine serum (FBS, Gibco, Life Technologies Corporation, Paisley, UK), 100 U/mL penicillin and 100 µg/mL streptomycin (Lonza Group Ltd., Verviers Belgium). Cultures were

incubated at 37 °C in humidified air with 5% CO₂ and a medium change every three days. Cells were sub-cultured when they attained 70 to 80 percent confluency using a solution of 0.25% trypsin EDTA (Lonza Group Ltd., Verviers, Belgium).

4.5.2.3.5 Cell treatment

Confluent neuroblastoma SH-SY5Y cells were seeded in 100 µL of DMEM at a density of 1 x 10⁵ cells per well in a 96-well black plate. The seeded plate was incubated at 37 °C for 24 hours so as to allow cell adherence to the plate bottom. After 24 hours, 10 µL of Fura-2/AM (5 mM) was suspended in 9990 µL of fresh DMEM to obtain 5 µM final concentrations. The DMEM in each of the seeded wells was replaced with 100 µL of Fura-2/AM in DMEM suspension, and was incubated for 1 hour at 37 °C to allow diffusion of Fura-2/AM into the neuroblastoma cells. After 1 hour, the Fura-2/AM in DMEM suspension was removed from each well, and the wells were washed with Krebs-HEPES solution to remove any extracellular Fura-2/AM. Thereafter, 49 µL of calcium containing buffer was added to the wells and incubated at 37 °C for 30 minutes. The test compounds were added to seeded wells for fluorescence analysis.

4.5.2.3.6 Measurement of intracellular calcium

A stock solution of 0.5 mM of each test compound was prepared in an eppendorf vial by dissolving an appropriate amount in 1 ml DMSO. 1 µL of the test compounds (reference and synthesized (**1-27**) compounds) were pipetted from the stock solutions and added to the treated cells in order to achieve final concentrations of 10 µM in each well. 1 µL of DMSO was used as negative control. Once sample preparation was completed, the 96-well plate was placed in a Synergy™ Mx monochromator-based fluorescent microplate reader (BioTek®, Germany) connected to Gen 5™ data analysis software. In the machine, the plate was further incubated at 37 °C for 30 minutes with intermittent shaking every minute before fluorescence reading. Calcium influx for each cell well was monitored over a period of 35 seconds with 0.5 seconds interval between wells. During fluorescence readings, 10 µL of NMDA/glycine or stimulating buffer was injected into each well after 10 seconds to activate the NMDA receptors for purpose of calcium influx. The sample was exposed to dual wavelengths of 340 and 380nm for the purpose of excitation, and fluorescence from emission at 510 nm was measured. The ratio of fluorescence (340/380) values after stimulation corresponds to the concentration of NMDA-mediated calcium influx within the 35 seconds period. The number of samples for each test compound was greater than eight, and the experiment was conducted in triplicate.

4.5.2.3.7 Data and statistical analysis

The calcium influx of each test compound was expressed as percentage relative to the control (DMSO only) represented as 100% calcium influx. Percentage values were obtained from a fluorescence ratio (340/380 nm) versus time analysis using Microsoft Excel and graphs were generated in GraphPad Prism version 6.01 for windows. Data is expressed as the mean \pm SD. A one-way ANOVA and t-test (unpaired) analysis were done, and the statistical significance was set at $p < 0.05$.

4.5.2.4 Result and discussion

The ability of the synthesised compounds (**1-27**) to block calcium ions influx into neuronal cells was evaluated in this study. MK-801 and NGP1-01 are known NMDA receptor blockers, which were used as reference compounds. While MK-801 is associated with undesirable psychotomimetic side effects (Lipton, 2004), NPG1-01 is described as a polycyclic cage with a safe side effect and toxicity profile (Joubert *et al.*, 2011). The inhibitory effects (figure 4.3) of test compounds at 10 μ M were determined by measuring the increase in intracellular calcium ions through NMDA receptors on SY-SY5Y neuroblastoma cells, loaded with Fura-2, upon NMDA (0.55 mM)/glycine (0.55 mM) activation. Synthesised compounds (**1-27**) were treated in the same manner as the reference compounds. Unsurprisingly, MK-801 and NGP1-01 showed NMDA receptor inhibition of 47.5 and 38.2%, respectively. All synthesised compounds (**1-27**) were able to moderately inhibit NMDA mediated calcium ion influx by 23.5-73% with the strongest inhibition observed for compound **27**. Compound **7** showed the weakest inhibition. Interestingly, the inhibitory activity of compounds **2, 3, 4, 5, 12, 15, 16, 17, 18, 19, 20, 21, 25, 26** and **27** exceeded that of MK-801. This is probably due to the structural similarities between these compounds and MK-801, with functional moiety modifications that are well tolerated, thus allowing better interaction and inhibition at the NMDA receptors.

Norbornane derivative, **1**, demonstrated an inhibitory effect, in NMDA/glycine mediated Ca^{2+} influx, similar to MK-801 but greater than NGP1-01 as evident by the 43.8% inhibition. Reduction of the alkene in the benzoquinone moiety, as observed in **2**, improves the blocking activity by 7.2%. The improved activity, even though minimal, is likely due to less steric hindrance or rigidity in compound **2**, thus allowing it to properly fit the receptor pocket leading to improved inhibition. When one of the carbonyl moieties was selectively reduced to the hydroxyl moiety (**3**), a significant increase to 69.7% NMDA receptor inhibition was observed ($p < 0.05$). The presence of the hydroxyl moiety may have enhanced the hydrogen bonding

interaction between compound **3** and the NMDA receptor and improved activity at the receptor binding site. Surprisingly, the double adduct **4** produces a higher NMDA receptor inhibition (62.3%) than both Diels-adduct **1** and MK-801. This observation is inconsistent with most of the polycyclic molecules like MK-801 or NGP1-01 in terms of binding mechanism. Most polycyclic molecules usually have a bridgehead basic nitrogen atom that interacts at or near the Mg^{2+} binding site of the NMDA receptors. Despite the absence in **4**, an improved blocking of Ca^{2+} influx was still evident. It is possible that the inhibitory effect of **4** against calcium ion influx in NMDA receptor is through an allosteric site rather than the Mg^{2+} binding site. The same mechanism of receptor interaction can be proposed for compound **1**. The possible reason for improved double adduct activity over the Diels-Adduct could be the planar conformation and potential deeper penetration, in the allosteric site, of double adduct **4**. This could be the reason why increased NMDA blocking activity was observed when compared to the Diels-Alder adduct **1**. The incorporation of a benzylamine moiety at one of the carbonyl moieties significantly improved the activity of **2** from 51% to 65.3% NMDA receptor inhibition as observed in **5**. The improvement is attributed to the presence of the basic nitrogen atom and aromatic moiety that enhance binding to the NMDA receptor *via* the Mg^{2+} binding site and the hydrophobic pocket of the receptor, respectively, leading to improved blocking activity at the NMDA receptor. However, replacing the benzylamine moiety with the 1-aminopiperidine moiety diminishes the inhibitory activity, as evident in **6** (26.5%), thus suggesting the importance of the aromatic ring in hydrophobic NMDA receptor interactions for this particular series. The reduction of the ring size from a 6-membered ring (benzoquinone moiety) to a 5-membered heterocyclic ring (furanone moiety) significantly reduces the ability of **7** to attenuate NMDA receptor mediated calcium ion influx demonstrated by the 23.5% inhibition ($p < 0.05$). Substitution of the oxygen atom in the 5-membered heterocyclic ring with a less electronegative atom (nitrogen), as seen in **25**, resulted in increased NMDA receptor inhibitory activity (55.5%). Addition of the benzylamine moiety to form compound **8** reduces the inhibition to 43.3%. This is because the basic nitrogen atom influence on the receptor (NMDA) was eliminated by the methylenebenzyl conjugate leading to diminished activity. Similar inhibitory effects were observed for compound **10** (43.7%), **11** (43.8%), and **13** (45.1%). This shows that changing the CH_2 to NH group and/or incorporation of aromatic or alkyne moieties in these group compounds do not influence their inhibitory activities.

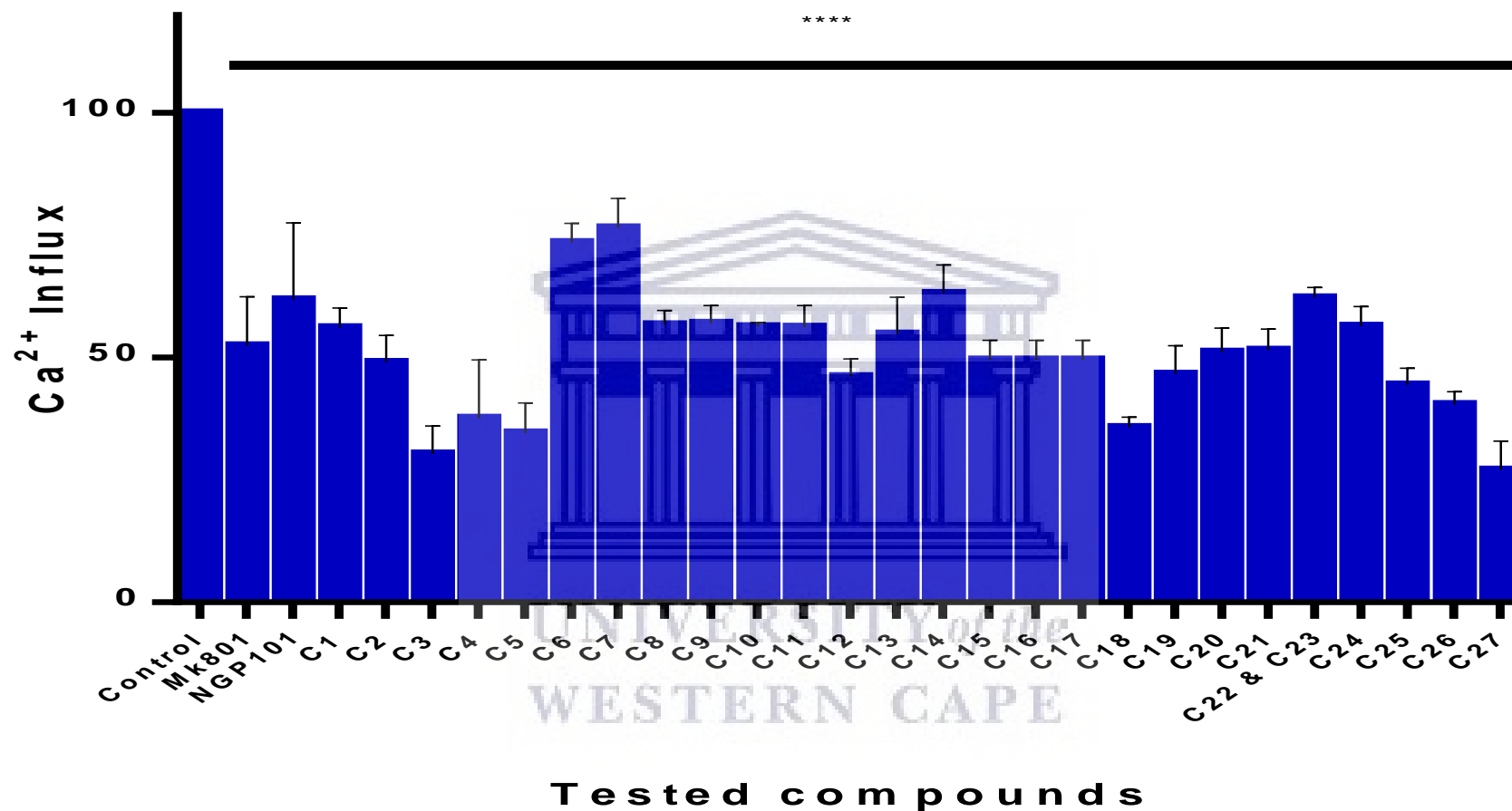


Figure 4.3: Inhibitory effects of synthesised (1-27) and reference compounds on NMDA/glycine calcium influx. MK-801 and NGP1-01 were used as reference compounds and data are expressed as percentage Ca²⁺ influx relative to 100% control untreated cells (DMSO only). The level of significance expressed as: *P < 0.05, **P < 0.01, ***P < 0.001, ****P < 0.0001.

However, the replacement of the alkyne moiety in **11** with the alkane moiety in **12** improved the NMDA receptor blocking activity by 10.2%. This is attributed to the flexibility of the alkane moiety that in turn produces better receptor interaction than the alkyne moiety.

The replacement of either the heterocyclic ring, in **10**, or aromatic ring, in **8** and **13**, with aliphatic amines resulted in moieties that displayed little or no change in blocking activity. Compound **14**, a diamine conjugate, showed a reduced inhibitory activity (36.2%) when compared with **8**, **10** or **13**. Interestingly, the di-substituted derivative of the diamine moiety (**15**) and dimethylation of the primary amine (**18**) potentiate their ability to attenuate calcium ion influx. Compound **15** and **18** showed inhibition of 50.4% and 64.3%, respectively. This deviates from the norm for polycyclic derivatives such as memantine, as described earlier and suggest an allosteric binding site that favours hydrophobic interaction rather than the Mg^{2+} binding site. It is also possible that the two methyl groups on compound **18** prolonged and enhanced its interaction with the NMDA receptor and consequentially increased the affinity leading to improved activity. The effects of different chain lengths were noticeable in the aliphatic amine groups. Increase in chain length from the ethyl moiety to a propyl moiety (**16**) improved the inhibitory activity by 14.2%. It is suggested that the elongated chain may have provided deeper penetration into the receptor pocket resulting in enhanced activity. However, an additional methylene group in the flexible side chain, as seen in **17**, offered no change in activity when compared with **16**.

NMDA receptor inhibition was also observed for the diepoxide compound **19** (53.3%). The activity at the NMDA receptor site could be explained by the susceptibility of the diepoxide to hydrolyse under physiological conditions or medium leading to the formation of hydroxyl moieties in both epoxy groups. The formed hydroxyl moieties would easily promote hydrogen bond interaction with the NMDA receptor binding sites. All the closed cages (**20**, **21**, **22**, **23** & **26**) derived from compound **19** showed good to excellent inhibition of NMDA mediated calcium influx. Among this group, compound **26** showed the highest inhibition (59.5%). This was expected as the basic amino functionality and the hydroxyl moieties would have enhanced NMDA receptor interaction leading to a slight increase in activity when compared to compound **19**. However, when the aniline analogue was incorporated in compound **26**, a diminished activity was observed as evident in calcium inhibition value of 37.8% for the diastereomers (**22** and **23**). The addition of a methylene moiety between the aromatic ring and the heterocyclic moiety, in **20**, significantly enhances the NMDA receptor inhibitory effects (48.8%). It was suggested that the linker (CH_2) may have allowed the aromatic ring to extend deeper into the

hydrophobic pocket of the NMDA receptor thus improving hydrophobic interaction and activity. A similar inhibitory effect was also observed for compound **21**. This indicates that the inhibitory effect of compound **20** or **21** is not affected by changing the position of the hydroxyl moiety.

The importance of the basic amino functionality and hydroxyl moiety to promote binding to Mg^{2+} site and hydrogen bond interaction, respectively was also noticeable in compound **24**. This suggests that the presence of the norbornane analogue with a basic amine group and hydroxyl or carbonyl moieties in the molecular structure may just prove sufficient for calcium influx attenuation. This proposition was corroborated by the activity of compound **9** with its NMDA receptor inhibition similar to compound **24**.

Interesting, the enlargement of the ring size from a 6-membered ring to an 8-membered ring was well tolerated at the NMDA receptor as demonstrated by the excellent inhibition (73%) for compound **27**. Due to the absence of a basic amine bridgehead or hydroxyl moiety, the strong inhibition was proposed to be either enhanced hydrophobic interaction with the NMDA receptor as a result of bulkiness or strong affinity at the receptor allosteric site. A particular trend was noticeable in the activity of the dione cyclic ring as NMDA receptor inhibition of 8-membered > 6-membered > 5-membered.

In this NMDA mediated calcium influx study, the inhibitory effects of the synthesised compounds (**1-27**), with reference to MK-801 and NGP1-01 were established, and the proposed structure activity relationships of each structure were highlighted. The percentage inhibitions of the reference compounds (MK-801 and NGP1-01) were inconsistent with those reported in Geldenhuys *et al.* (2007) as complete NMDA receptor inhibitions, close to 100%, were observed. However, the author conducted its calcium influx studies using a synaptoneurosomes, and tested the compounds (pre-incubated with nitrendipine) at 100 μ M. In this study, the difference in the type of cells (neuroblastomas SH-SY5Y cells) and test concentration (10 μ M), and the lack of pre-treatment with a calcium channel blocker (nitrendipine) may have influenced the results for MK-801 (47.5%) and NGP1-01 (38.2%). Nonetheless, all test compounds were screened in the same manner, thus the values for the reference compounds were acceptable for comparison or screening studies. Some of the norbornane derivatives (**5, 6, 9, 13, 14, 16, 17, 24, 25 & 26**) share similar characteristics like basic amino functionality, hydroxyl moiety or hydrophobic moiety with polycyclic cages such as memantine or NGP1-01 (known blockers), which enhanced their calcium inhibition *via* the

Mg²⁺ binding site and/or hydrophobic pocket of the NMDA receptor. While some derivatives showed satisfactory inhibition by means of hydrophobic or allosteric interactions with the NMDA receptor; others showed inhibition greater than MK-801 and NGP1-01. These calcium current inhibitions are expected to be beneficial through prevention of NMDA/glycine induced excitotoxicity, a prominent phenomenon in most neurodegenerative disorders. Albeit, the evaluation of more norbornane derivatives and the IC₅₀ determination of active compounds are needed so that the structure activity relationship is well understood. It should also be noted that this study focused on inhibition of NMDA mediated calcium influx. It will be interesting to explore their neuroprotective effect against NMDA-induced toxicity. Information on the blocking mechanism could be vital as one would be able to identify if the mode of binding is by “trapping” like MK-801 and phenylcyclidine or “foot in the door” like memantine. This is clinically relevant as it provides information on the psychotomimetic side effect profile. Nonetheless, this study predicted the potential calcium blocking effects of norbornane derivatives that could be beneficial in slowing down or halting excitotoxic induced neuronal death through impediment of glutamate or NMDA/glycine mediated calcium overload.

4.5.3 Voltage gated Ca²⁺ influx studies

4.5.3.1 Background

The detrimental effects of intracellular Ca²⁺ overload mediated by NMDA receptors on neuronal cells have already been discussed. Similarly, voltage-gated calcium channels are calcium-conducting channels (Pchitskaya *et al*, 2018) that also contribute to the increased calcium influx in response to membrane depolarisation or indirect activation by glutamate. These additional sources of calcium mediated by VGCC, L-type calcium channels in particular, contribute to intracellular calcium overload and play an important role in inducing excitotoxicity and apoptosis (Joubert *et al*, 2011; Luoma, 2011). Under physiological conditions, influx of Ca²⁺ mediated by VGCC regulates numerous intracellular functions including contraction, secretion, nerve and cardiac excitability, pacemaker activity, neurohormone secretion, neurotransmitter release, cell differentiation, enzyme and allosteric protein modulation, and gene expression (Figure 4.4; Snutch, 2009; Seko *et al*, 2003; Kumar *et al*, 2019). However, deviation from its physiological role *via* alteration in L-type VGCC activities has been linked to aging and age-related neurodegenerative disorders (Seko *et al*, 2003; Kumar *et al*, 2019). Increase in intracellular Ca²⁺ and disruption of calcium homeostasis by A β peptide accumulation in Alzheimer’s disease through L-type VGCC activation has been reported. In

Parkinson's diseases, the enhanced role of L-type VGCC in driving the pacemaking activity of ageing substantia nigra pars compacta neurons (adult mice) and subsequently making the dopaminergic neurons prone to degeneration has been reported (Kochegarov, 2003; Hurley & Dexter, 2012; Espinosa-Parrilla *et al.*, 2015; Pchitskaya *et al.*, 2018). Under these pathological conditions and Ca^{2+} dysregulation, the extremely sensitive neurons are further subjected to calcium homeostasis defects that are consequently destructive, thus promoting neuronal cell death (Pchitskaya *et al.*, 2018).

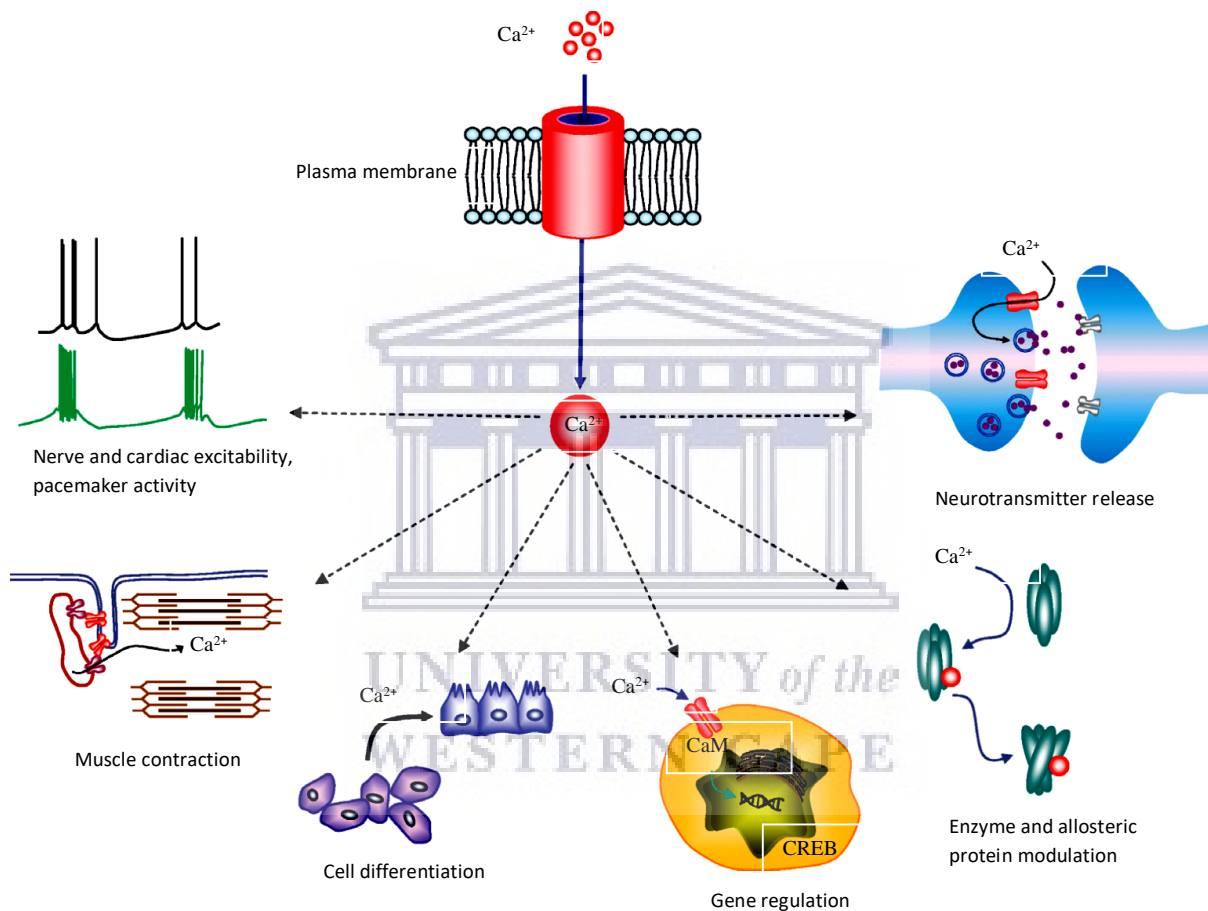


Figure 4.4: Physiological functions of the Voltage-gated calcium channels.

Restoring calcium homeostasis *via* VGCC blockers or modulators could be therapeutically beneficial to patients with neurodegenerative diseases. Currently, calcium ion blockers such as izradipine and dihydropyridines have been shown to protect neurons in an animal model of PD and in hypertensive patients, respectively. This protective effect may be attributed to their ability to prevent Ca^{2+} overload through L-type VGCC due to excessive excitation leading to reduced neuronal damage and improved behaviour (Kochegarov, 2003; Espinosa-Parrilla *et al.*, 2015; Pchitskaya *et al.*, 2018). Luoma *et al.* (2011) have also shown and reported the

neuroprotective effects of L-type calcium channel inhibitors while investigating the activity of progesterone.

Due to the similarities that exist between human neurons and the SH-SY5Y neuroblastoma cell line and the usage thereof by most researchers in pharmacological disease models of most neurodegenerative diseases, the SH-SY5Y cell line was also used for this VGCC mediated calcium influx study.

4.5.3.2 Experiment design

The ability of the synthesised compounds (**1-27**) to block VGCC mediated Ca^{2+} influx was evaluated utilising the ratiometric fluorescent method. Fura-2/AM was the preferred indicator due to its dual wavelength excitation reading system. The fluorescence indicator, suspended in fresh DMEM solution, was loaded on adhered SH-SY5Y neuroblastoma cells that were cultivated and grown in the lab, and calcium containing buffers were subsequently added. DMSO (only) was used as the positive control while nimodipine and NGP1-01 were used as the reference compounds. A depolarising buffer solution containing 770 mM of K^+ was used to activate or open the voltage-gated calcium channel through depolarised membrane potential, leading to movement or influx of calcium ions against concentration (ions) gradient (from extracellular space inside the neuroblastoma SH-SY5Y cell). The real-time kinetic changes in intracellular Ca^{2+} after membrane depolarisation were monitored utilising a fluorescent plate reader that measures change in fluorescence intensities. The change in fluorescence intensities correlates with the change in intracellular Ca^{2+} upon VGCC mediated membrane depolarisation, and the inhibitory effects of the synthesised compounds (**1-27**) and reference controls (nimodipine and NGP1-01), relative to the negative control (DMSO) were determined in this manner.

4.5.3.3 Material and methods

Solutions were prepared in a controlled environment, and were stored at 2-8 °C throughout the experiments. Cells were handled and treated in a laminar air flow sterilised system. Materials, solutions and methods used in this study were outlined as follows:

4.5.3.3.1 Calcium free buffer

Sodium chloride (NaCl, 118 mM), potassium chloride (KCl, 4.7 mM), HEPES (20 mM), magnesium chloride (MgCl_2 , 1.18 mM) and glucose monohydrate (30.9 mM) were weighed in

a 1 L volumetric flask The contents in the flask were dissolved and made up to one litre volume using distilled water. The resulting solution was adjusted to a pH of 7.4 by titrating with either 4 molar concentrations of HCl or NaOH.

4.5.3.3.2 Calcium containing buffer

Sodium chloride (NaCl, 118 mM), potassium chloride (KCl, 4.7 mM), HEPES (20 mM), calcium chloride dihydrate ($\text{CaCl}_2 \cdot 2\text{H}_2\text{O}$, 2 mM), magnesium chloride hexahydrate (1.18 mM) and glucose monohydrate (30.9 mM) were correctly weighed in a 200 ml volumetric flask. Distilled water was added and made up to 200 ml. The pH of the solution was adjusted to 7.4 by the addition of either HCl or NaOH.

4.5.3.3.3 Depolarisation buffer

Sodium chloride (NaCl, 5.4 mM), potassium chloride (KCl, 770 mM), sodium hydrogen carbonate (NaHCO_3 , 10 mM), calcium chloride dihydrate ($\text{CaCl}_2 \cdot 2\text{H}_2\text{O}$, 1.4 mM), magnesium sulphate (MgSO_4 , 0.9 mM), glucose monohydrate (5.5 mM), potassium dihydrogen phosphate, (KH_2PO_4 , 0.6 mM), sodium hydrogen phosphate (Na_2HPO_4 , 0.6 mM), and HEPES (20 mM) were correctly weighed and dissolved in 50 ml of distilled water in a 200 ml volumetric flask. The solution was made up to 200 ml with distilled water, and the pH was then adjusted to 7.4.

4.5.3.3.4 Cell line and culture conditions

The human neuroblastoma SH-SY5Y cells were generously donated by the Blackburn Laboratory, University of Cape Town. Cells were grown in Dulbecco's Modified Eagle Medium (DMEM, Gibco, Life Technologies Corporation, Paisley, UK), supplemented with 10% fetal bovine serum (FBS, Gibco, Life Technologies Corporation, Paisley, UK), 100 U/mL penicillin and 100 $\mu\text{g}/\text{mL}$ streptomycin (Lonza Group Ltd., Verviers Belgium). Cultures were incubated at 37 °C in humidified air with 5% CO_2 and a medium change every three days. Cells were sub-cultured when they attained 70 to 80 percent confluency using a solution of 0.25% trypsin EDTA (Lonza Group Ltd., Verviers, Belgium).

4.5.3.3.5 Cell treatment

Confluent neuroblastoma SH-SY5Y cells were treated in the same manner as that of the NMDA mediated Ca^{2+} influx studies (outlined in 4.5.2.3.5). Thereafter, the test compounds were added to seeded wells for fluorescence analysis.

4.5.3.3.6 Measurement of intracellular calcium

A stock solution of 0.5 mM for each test compounds was prepared in an eppendorf vial by dissolving an appropriate amount in 1 ml DMSO. 1 μ L of the test compounds (reference and synthesized (**1-27**) compounds) were pipetted from the stock solutions and added to the treated cells in order to achieve final concentrations of 10 μ M in each well. 1 μ l of DMSO was used as negative control. Once sample preparation was completed, the 96-well plate was placed in the fluorescence plate reader, a Synergy™ Mx monochromator-based fluorescent microplate reader (BioTek®, Germany) connected to Gen 5™ data analysis software. In the machine, the plate was further incubated at 37 °C for 30 minutes with intermittent shaking every minute before fluorescence reading. Calcium influx for each well was monitored over a period of 35 seconds with 0.5 seconds interval between wells. During fluorescence reading, 10 μ L of the depolarisation buffer was injected into each well after 10 seconds to activate voltage-gated calcium channel mediated calcium influx. Samples were exposed to dual wavelengths of 340 and 380 nm for the purpose of excitation, and fluorescence from emission at 510 nm was measured. The ratio of fluorescence (340/380) values after stimulation corresponds to the concentration of VGCC-mediated calcium influx within the 35 second period. The number of samples for each test compound was greater than 8, and experiments were conducted in triplicate.

4.5.3.3.7 Data and statistical analysis

The calcium influx of each test compound was expressed as percentage relative to the control (DMSO only) represented as 100% calcium influx. Percentage values were obtained from a fluorescence ratio (340/380 nm) versus time analysis using Microsoft Excel and graphs were generated in GraphPad Prism version 6.01 for windows. Data is expressed as the mean \pm SD. A one-way ANOVA and t-test (unpaired) analysis were done, and the statistical significance was set at $p < 0.05$.

4.5.3.4 Result and discussion

In this study, the inhibitory activities of synthesised compounds were evaluated and compared with known VGCC blockers, nimodipine and NGP1-01. Using a fluorescence (Fura-2) based assay, the ability of test compounds (10 μ M; synthesised and reference) to attenuate VGCC mediated calcium ion influx in response to membrane depolarisation (KCl, 770 mM) in human SH-SY5Y neuroblastoma cells were evaluated (Figure 4.5). As expected, nimodipine and

NGP1-01 showed VGCC inhibition of 34.1 and 34.2 % at 10 μ M, respectively. In comparison to the reference compounds (nimodipine and NGP1-01), compounds **1**, **2**, **3**, **4**, **6**, **7**, **8**, **9**, **10**, **11**, **12**, **13**, **14**, **15**, **16** & **17** demonstrated moderate to good inhibition activities while compounds **5** and **18-27** exhibit little or no VGCC inhibition.

Norbornane derivative, **1**, slightly attenuated VGCC mediated Ca^{2+} influx in neuroblastoma cells by 15%. However, the inhibitory activity was increased, as observed in **2** (25.4%), by selectively reducing the double bond in the benzoquinone moiety. This may indicate that the less sterically hindered cyclohexane ring is important for VGCC inhibitory activity as it allows it to interact better with the voltage-gated calcium channels. Reduction of one of the carbonyl moieties in **2** to a hydroxyl moiety further improved the VGCC inhibition of compound **3** (32.8%), which is similar to the inhibitory activities of nimodipine and NGP1-01. It was suggested that the hydroxyl moiety could have provided better interaction with the channels through hydrogen bonding leading to enhance activity. Interestingly, the double adduct **4** (50.3%), when compared to **1**, demonstrated significantly improved VGCC inhibition that exceeded the activities of nimodipine and NGP1-01. The double adduct is more lipophilic than the Diels-adduct, and it is suggested that this hydrophobic characteristic of **4** may have allowed improved interaction with the VGCC that translated to increased VGCC inhibitory activities. The introduction of the benzylamine moiety to compound **2**, drastically diminished the inhibitory activity of **5** (8.4%, $p < 0.05$). However, replacement with the 1-aminopiperidine moiety improved the inhibitory effects, as seen in compound **6**.

The inhibitory effects of compound **7** in VGCC mediated calcium ions influx was moderate (23.1%) when compared to known blockers (nimodipine and NGP1-01). The introduction of the benzylamine moiety increased the activity of compound **8** (37.2%). The replacement of the benzylamine moiety with 1-aminopiperidine and phenylhydrazine moieties lead to calcium inhibitions of 29.9% (**10**) and 26.8% (**13**), respectively. Further structure modifications with propargylamine (**11**) and propylamine (**12**) had very little effect on the inhibitory activities as indicated by blockage of 30.2% and 28%, respectively. These activities were considered good when compared to the known VGCC blockers, nimodipine and NGP1-01. The replacement and elimination of the oxygen atom with the nitrogen atom and carbonyl moieties in the heterocyclic ring of **7** lead to diminished inhibitory activity in compound **25** (7.9%). This suggests that the carbonyl moieties may be necessary for VGCC inhibition in this series of compounds.

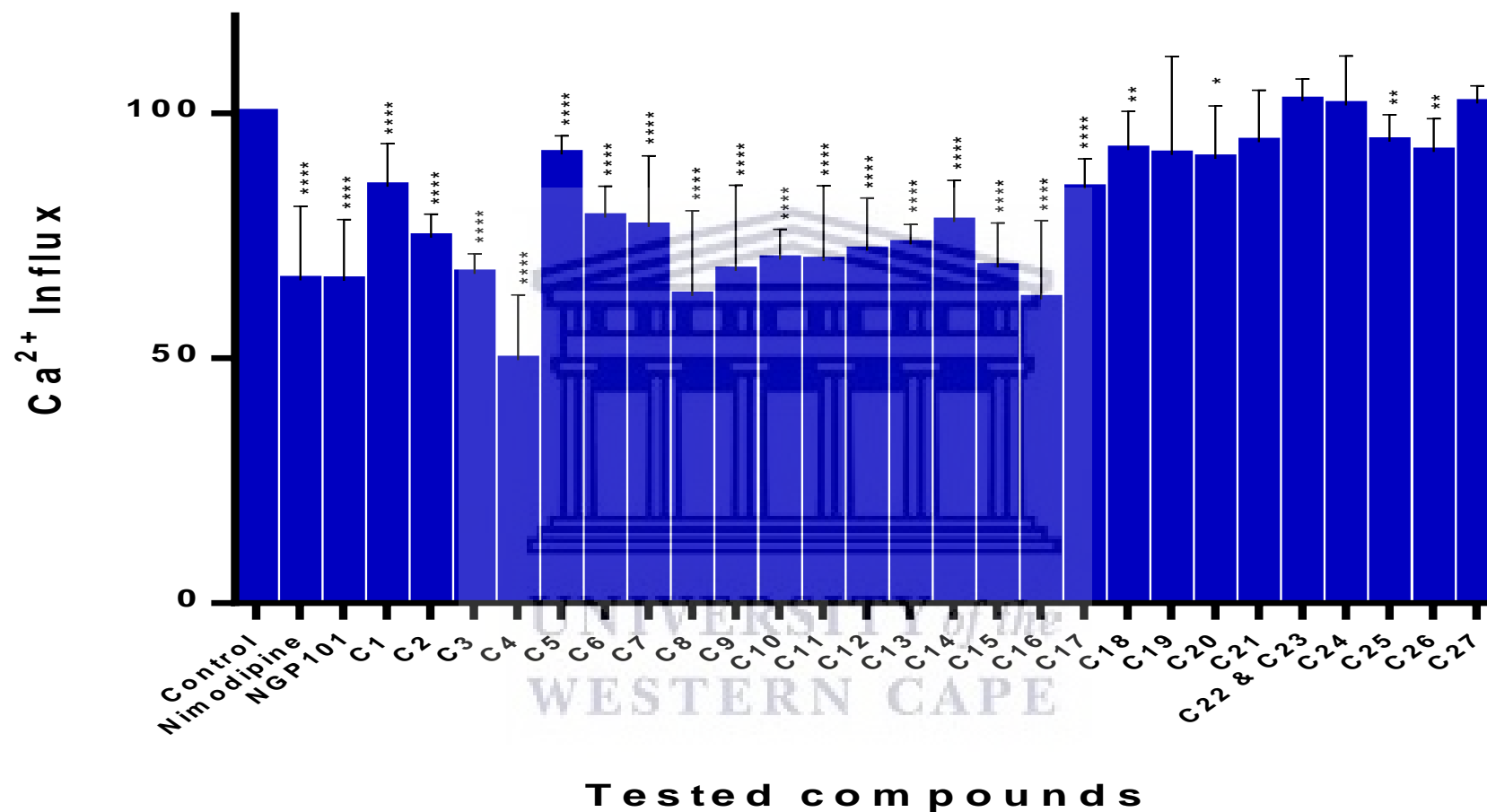


Figure 4.5: Inhibitory effects of synthesised (1-27) and reference compounds on VGCC mediated calcium influx. Nimodipine and NGP1-01 were used as reference compounds and data are expressed as percentage Ca²⁺ influx relative to 100% control untreated cells (DMSO only). The level of significance expressed as: *P < 0.05, **P < 0.01, ***P < 0.001, ****P < 0.0001.

The inclusion of aliphatic amines, as seen in **14**, demonstrated VGCC inhibition of 22.2%. The inhibitory activity was similar to compound **7** but weaker than compound **8** (benzylamine moiety). The weaker inhibitory effect was largely due to reduced lipophilicity introduced by the basic nitrogen atom (aliphatic amines). The di-substituted derivatives (**15**) showed improved VGCC inhibition (31.4%). The enhanced activity, over **14**, may be due to the hydrophobic or lipophilic nature of compound **15**, which could have improved interaction with the voltage gated calcium channels. In comparison to **14**, increasing the carbon linker between the primary amine and heterocyclic ring from two to three resulted in improved VGCC inhibition of **16** (37.9%). However, further increase in the linker drastically diminished the activity of **17**. Also, the dimethylation of the primary amines, as observed in **18**, reduced the inhibitory activity to 8.5%. This activity was inconsistent with the good VGCC inhibitory activities demonstrated by compound **10** and **15** where the structures also lacked the primary or secondary amine. In comparison to **14**, compound **18** (dimethyl moiety) was expected to demonstrate improved activity, like the di-substituted derivative (**15**) and aminopiperidine moiety (**10**), due to its improved hydrophobicity. It was proposed that the dimethyl moiety, as seen in **18**, lack the hydrophobic character possessed by compound **10** or **15** leading to less hydrophobic interaction(s) with VGCC and subsequent reduction in VGCC inhibition. It is also likely that the dimethyl substitution resulted in lesser hydrogen bond interaction between the voltage gated channels and compound **18**, leading to a weaker inhibitory activity than compound **14**.

Unfortunately, the closed cage molecules (**20-23** & **26**) and norbornane derivative (**24**) showed very little or no inhibitory activities on VGCC mediated calcium influx in a neuroblastoma cell. The lack of activity may be attributed to the absence of carbonyl moieties which may be necessary for VGCC inhibition in this group of compounds. Compounds **20** and **21** showed weak calcium inhibition of 9.2% and 5.9%, respectively. However, conversion of the benzylamine moiety to the aniline moieties (**22** & **23**), with weaker basicity, resulted in complete loss of inhibitory activity. No inhibitory activity was observed for compound **27** even though it exhibits the characteristic carbonyl moieties. The lack of VGCC inhibitory activities is likely due to the enlarged ring size that is unable to fit the voltage gated calcium channel. Also evident is the influence of the dione ring size on the VGCC inhibitory activities of these group of compounds as a particular trend was observed: 5-membered ring > 6-membered > 8-membered ring.

In this VGCC mediated calcium influx study, the inhibitory effects of synthesised (**1-27**) and reference (nimodipine and NGP1-01) compounds were determined. The impact or influence of structural modifications on inhibition of VGCC mediated Ca^{2+} influxes were highlighted. The majority of these norbornane derivatives demonstrated inhibitory activities similar to or exceeding nimodipine or NGP1-01. The structure activity relationship of these groups of compounds illustrated the importance of carbonyl moieties and hydrophobicity on VGCC inhibition. In some instances, the hydroxyl moiety demonstrated improved activity, but only in the presence of a carbonyl moiety. It is well known that voltage gated calcium channels are also activated during glutamate/glycine induce toxicity. Calcium ions contributed through this channel potentiate calcium overload and exacerbate neuronal cell death. It is reasonable to conclude that inhibition of this channel could potentially reduce calcium overload in pathological condition thus halting or reducing excitotoxic mediated cell death, which was explored using norbornane derivatives and structurally related moieties.

4.6 Conclusion

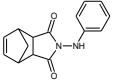
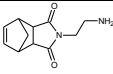
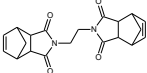
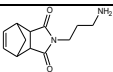
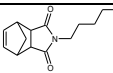
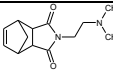
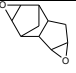
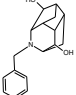
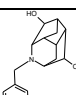
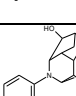
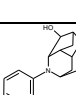
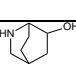
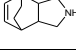
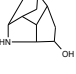
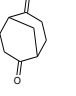
The cytotoxicity and neuroprotection profiles of norbornane derivatives and related moieties were successfully evaluated in this study. Where necessary, the activities of synthesised compounds (**1-27**) were compared with reference compounds with known activities, and consequences of structure modifications were illustrated, enabling the determination of structure activity relationships of the synthesised compounds. Due to the primary role of excitotoxicity in neurodegenerative disorders, finding therapeutic agents, with very little or no cytotoxic effects, which potentially attenuate channels or receptor mediated calcium influx while also being neuroprotective against neurotoxins such as MPP^+ is highly necessary. The activities of all test compounds in a SH-SY5Y neuroblastoma cell line (10 μM) are summarised in table 4.1. The table illustrates the following: the average mean of percentage cell viability at different concentration in cytotoxicity study; the average mean of percentage cell viability after co-treatment of synthesised compounds with MPP^+ in the neuroprotection study; and the average mean percentage of VGCC and NMDA receptor mediated calcium inhibition.

When screened at different concentrations, synthesised compounds showed satisfactory cytotoxic profiles as demonstrated by the high percentage (close to 100) of cell viability observed at 10 μM . Similarly, increasing the concentration to 50 μM was well tolerated in the study. However, at 100 μM , compound **7** and **24** were toxic to the SH-SY5Y neuroblastoma

cell as evident by the almost 50% loss in cell viability. To avoid or minimise compound induced cell death, further experiments or studies were conducted at 10 μ M utilising the same cell line.

Table 4: Biological profiles of test compounds

Compounds	Structures	Cytotoxicity % viability			Neuroprotection % viability 10 μ M	NMDA %Inhibition 10 μ M	VGCC %Inhibition 10 μ M
		10 μ M	50 μ M	100 μ M			
MK-801		-	-	-	-	48	-
Nimodipine		-	-	-	-	-	34
NGP1-01		-	-	-	-	38	34
1		97	96	85	83	44	15
2		97	94	85	91	51	23
3		97	97	102	85	70	33
4		95	104	100	92	62	50
5		94	102	100	84	65	8
6		108	98	109	84	27	21
7		89	93	51	81	23	23
8		84	93	87	103	43	37
9		108	83	69	79	43	32
10		115	103	83	82	44	30
11		104	124	127	77	44	30
12		114	89	83	80	54	28

13		96	73	70	85	45	27
14		96	89	80	80	37	22
15		77	88	93	77	50	31
16		98	79	68	85	50	38
17		93	83	73	79	50	15
18		100	94	76	73	64	7
19		94	88	88	78	53	8
20		104	99	97	79	49	9
21		96	92	102	77	48	6
22							
23		111	104	96	85	38	-3
24		96	97	59	78	44	-2
25		108	112	106	78	56	6
26		113	127	120	99	60	8
27		125	114	118	76	73	-2

The neuroprotective properties of the norbornane scaffolds, co-treated with MPP⁺, were established, and the cell viabilities were compared with viability of MPP⁺ infected neuronal cells. All synthesised compounds appeared to show very good neuroprotection profiles in the presence of neurotoxins. Although few structure activity relationships were highlighted, the mechanisms of protection were not determined as it is outside the scope of this study. Nonetheless, the impact of primary amines or basic nitrogen atom and hydrophobicity on

neuroprotection for these series of compounds were discussed to assert their importance. Various mechanisms of neuroprotection have been proposed or suggested but would require additional experiment work to support or confirm them.

In the calcium influx studies, most of the synthesised compounds showed good inhibition of NMDA receptor mediated calcium flux when compared to activities of known NMDA receptor blockers (MK-801 and NGP1-01). For those with basic amino functionality and hydrophobic moieties, structure activity relationships were consistent with those of polycyclic cage amines such as NGP1-01. In contrast, the activities of compounds without these functional groups were attributed to either binding to an allosteric site or hydrophobic interactions with the receptor. The overall NMDA inhibition results demonstrated the importance of basic amino functionality, hydroxyl moieties, carbonyl moieties and/or hydrophobic moieties in this series of compounds. In the VGCC inhibition studies, compounds **2, 3, 4, 6, 7, 8, 9, 10, 11, 12, 13, 14, 15** and **16** showed good inhibitory activities when compared to the reference compounds. In few cases, compounds (**4, 8** and **16**) showed better inhibition than the well know calcium blockers (nimodipine and NGP1-01). The structure activity relationship of these proposed VGCC inhibitors (**1-27**) revealed the importance of hydrophobic and carbonyl moieties, which are well tolerated and accommodated in the hydrophobic pockets of voltage gated calcium channels, despite the presence of polar group such as amines and amides. These results were consistent with the finding of VGCC inhibitors reported in the literature (Bisi *et al.*, 2019). Interestingly, compounds (**2, 3, 4, 6, 7, 8, 9, 10, 11, 12, 13, 14, 15** and **16**) were able to attenuate calcium ion influx in the NMDA receptor and voltage gated calcium channels. In addition to the dual inhibitions, they also displayed good neuroprotective and cytotoxicity profiles. These characteristics potentially classify these compounds as possible neuroprotective agents with a good safety profile. However, investigations at different concentrations for IC₅₀ determination are required for optimal assessment of these activities. Despite the unavailability of IC₅₀ data, findings were considered satisfactory since the synthesised compounds (**1-27**) were treated in the same manner as the reference compounds with known activities. In these studies, compounds with NMDA receptor inhibition, VGCC inhibition, neuroprotection against MPP⁺ and/or good cytotoxic profiles were identified as promising therapeutic candidates in the treatment or prevention of neurodegenerative disorders.

CHAPTER 5

Conclusion

5.1 Introduction

The progressive loss of neuronal cells is a feature common to most neurodegenerative disorders. As a result, physiological functions of the brain and/or spinal cord are lost leading to characteristic symptoms that defines each neurodegenerative disease. These disorders, amidst others, include: Alzheimer's disease (AD), Parkinson's disease (PD), amyotrophic lateral sclerosis (ALS) and Huntington's disease. Devising strategies and treatments to combat these disorders have been challenging therapeutically. Firstly, the mechanism of neurodegeneration is still not well elucidated as various degenerative process are being proposed by countless studies. However, it is generally believed that neuronal cell death is caused by interrelated processes that include, amongst others; excitotoxicity, oxidative stress, neuroinflammation, mitochondrial dysfunction and protein aggregation (Swart *et al.*, 2014; Gan *et al.*, 2018). This cascade of events leads to apoptosis or necrosis. Despite the vast knowledge, no adequate treatment has been discovered as current treatment only offer symptomatic relief. As such, a multi-target approach that addresses these processes is required to not only effectively treat the symptoms, but also stop the degenerative process (Dey and Nath De, 2015; Eberhart and Topka, 2016). Secondly, the complexity of the brain makes it almost impossible to develop a clinically acceptable therapeutic agent without affecting its physiological functions. In most cases, the same neurotransmitters or neuronal enzymes to be regulated or inhibited are required for the normal physiological functions of the brain. Therefore, a balancing act between treatment of neurodegenerative disorders and ensuring normal function of the brain is crucial.

Of the proposed mechanisms of neurodegeneration, the effect of excitotoxicity caused by either extracellular and/or intracellular stimuli is prominent, as implicated in the pathology of several neurological disorders (Abeti and Abramov, 2015). MPP^+ , a neurotoxic cation, induces excitotoxicity in dopaminergic neurons by attacking mitochondria through its interaction with mitochondrial complex 1 of the electron transport chain, leading to a cascade of events that mediate neuronal cell death. Glutamate, a main excitatory neurotransmitter, induces excitotoxicity by overestimating NMDA receptors to allow a massive influx of calcium ions *via* NMDA receptor channels and associated gated channels (voltage gated calcium channels),

leading to several interrelated processes that eventually result to cell death. Agents or molecules with ability to control the activity of glutamate on NMDA receptors or to block MPP^+ and mitochondrial complex 1 interactions are supposed to be therapeutic in the effective treatment of these disorders. While memantine is a non-competitive NMDA receptor blocker, NGP1-01, a polycyclic closed cage amine, has been shown to not only block NMDA receptor channels, but also voltage gated calcium channels. Additional advantages of NGP1-01 are its ability to inhibit MPP^+ -induced toxicity. With this as background, we proposed and synthesised a series of opened-and rearranged- cage compounds that are structurally similar to MK-801 and NGP1-01, and evaluated their activities against NMDA/glycine- and MPP^+ -induced toxicity in neuroblastomas SH-SY5Y cells.

5.2 Synthesis

Three series with a total number of 29 compounds were proposed and 23 compounds (**1-23**) that includes by products were successfully synthesised, isolated and purified. Additional compounds (**24-27**) that were synthesised, isolated, and purified by Dr Vitalii A. Palchykov were included in biological assays.

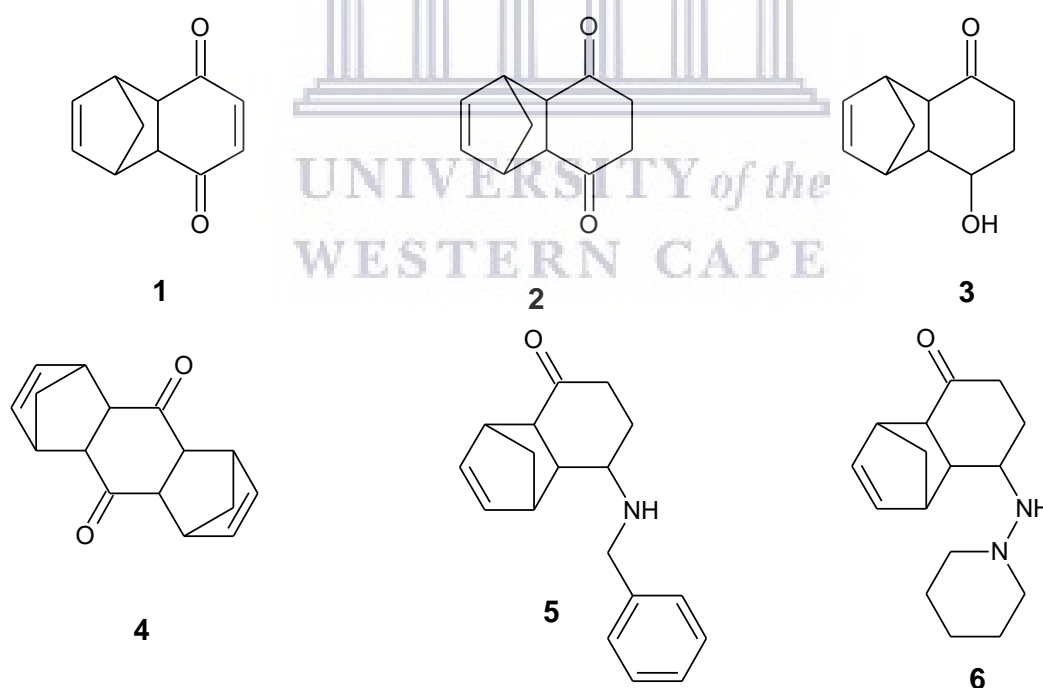


Figure 5.1: Structures of series 1.

In the first series (**1-6**; figure 5.1), the cycloaddition reaction of benzoquinone and monomerised cyclopentadiene yielded the adduct **1** with a 100% yield of isomer mixtures ((exo

(minor): endo (major, +/- 95%). This open-cage like molecule was sonicated in a mixture of zinc and acetic acid to form its respective reduced derivative as observed in compound **2**. Using a strong reducing agent (NaBH₄), compound **2** was further reduced to the keto-alcohol **3**. A one-step synthesis consisting of Schiff base and reductive reactions of compound **2**, afforded compounds **5** and **6** in the presence of benzylamine and 1-aminopiperidine, respectively. The dimeric adduct **4** was obtained from impurities (cyclopentadiene and **1**) that were transferred from the intermediate product. The structures of these compounds (**1-6**) were elucidated and confirmed by various experiments that include NMR, MS or IR. The characteristic signal for the bridge in each compound was observed upfield, while the signals of the conjugated moieties were identified downfield for compound **5**. Certain functional groups, carbonyl moieties in particular, that support structural confirmation were identified in all the compounds. The molecular mass data obtained from a high resolution mass spectrometer confirmed the molecular structure of some of the compounds.

Compounds containing propylamine, propargylamine, ethylenediamine, 1,3-diaminopropane, 1,4-diaminobutane and N,N-methylethylenediamine were also proposed. Unfortunately, the syntheses were unsuccessful. Reactions were conducted both at room temperature and under reflux conditions. However, none of the reactions proceeded neither at room temperature nor high temperature (reflux). Ideally, these type of reactions would proceed under reflux conditions but the thermolabile vulnerability of compound **2** (intermediate) prevented the formation of these conjugates. In this series, alicyclic conjugates (benzylamine and 1-aminopiperidine) easily reacted with the diketal **2** to form **5** and **6**, whereas the aliphatic conjugates were practically unreactive under the same reaction condition. Generally, by comparison, alicyclic conjugate reactions are known to require lower activation energy than their aliphatic counterparts, which was why the reactions proceeded at room temperature (Mereshchenko *et al.*, 2015). The reaction between the diketal and aliphatic moieties could succeed if the activation energy is improved. However, the conditions would exclude the use of thermal energy due to the thermal instability of diketal **2**.

In the second series (**7-18**, figure 5.2), the cycloaddition reaction, under reflux, between maleic anhydride and monomerised dicyclopentadiene yielded a furandione derivative (**7**). Under similar reaction conditions, aminolysis of compound **7** with benzylamine, 1-aminopiperidine, propargylamine, propylamine, phenylhydrazine, ethylenediamine, 1,3-diaminopropane, 1,4-diaminobutane and N,N-methylethylenediamine resulted in respective pyrrolidinedione conjugates (**8-18**). The structures of these opened cages were also confirmed using various

experiments that include NMR, MS and IR. The characteristic peaks for each compound in these experiments were observed and correctly assigned.

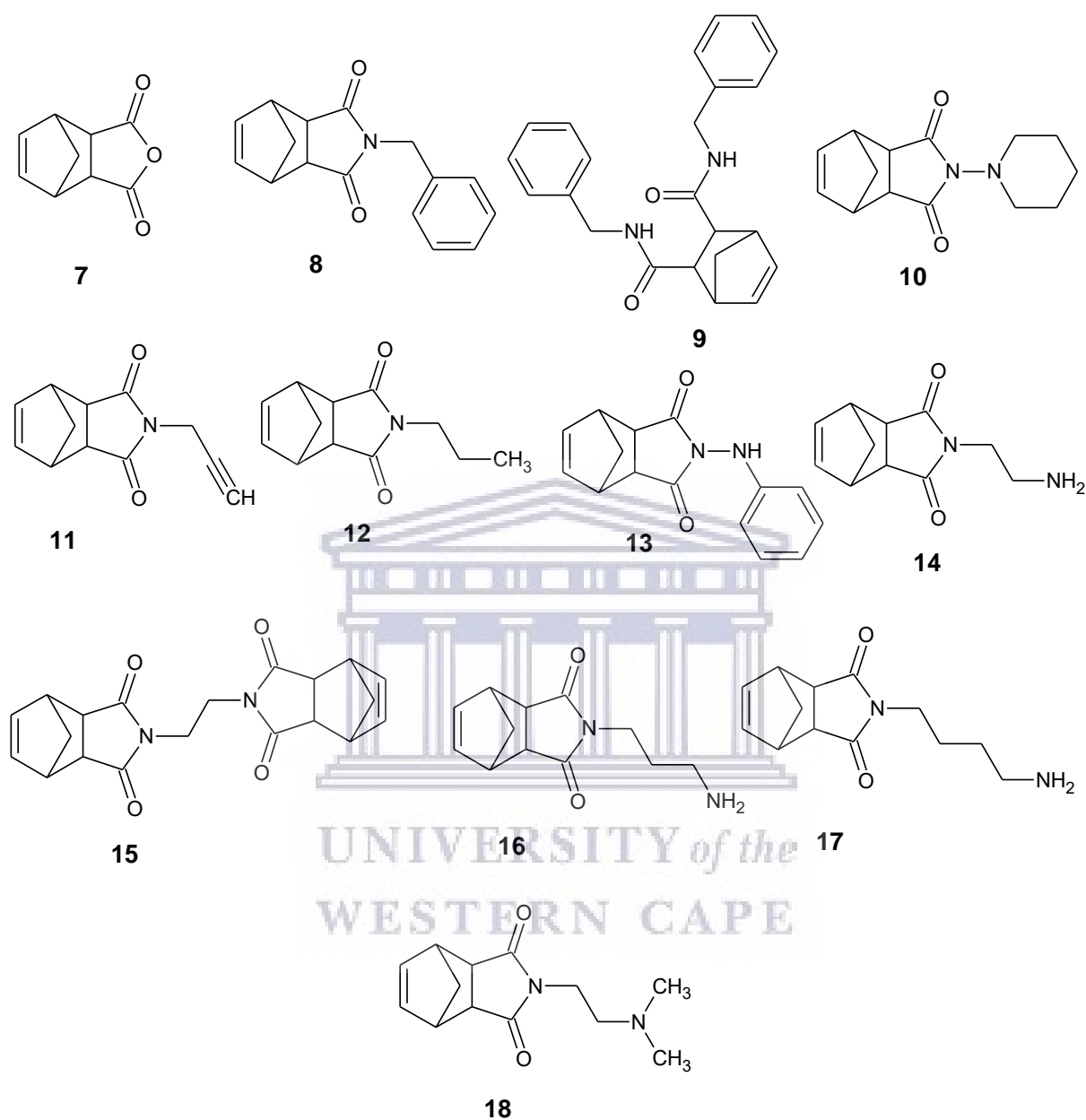


Figure 5.2: Structures of series 2.

Unlike the diketal **2**, furandione **7** was thermostable and the reaction proceeded under thermal or reflux conditions to afford the respective pyrrolidinedione derivatives (**8-18**). The reaction that led to the formation of compound **8** also afforded the dibenzylamide derivate **9** as a by-product in 6.27% yield. A change in the reaction conditions may improve the yield of compound **9**. Interestingly, changing the work up procedure of compound **14** by re-crystallising the crude mixture in ice-cold methanol resulted in the isolation of **15**, however at a lower yield

(12.32%) when compared to 89.94% of compound **14**. It is suggested that the polar protic nature of methanol favour crystal formation (**15**) when compared to ethyl acetate, an aprotic organic solvent (Braybrook *et al.*, 2002; Sathyanarayanamoorthi *et al.*, 2010; Yang *et al.*, 2014). The low yield was attributed to the relative solubility of the compound **15** in methanol. It is believed that changing the solvent may significantly improve the yield.

In the third series (**19-23**; figure 5.3), di-epoxidation of dicyclopentadiene resulted in the formation of compound **19**. Under microwave condition, benzylamine was incorporated into the epoxy derivative to afford the rearranged cage-like molecules (**20** and **21**). Interestingly, the reaction involving phenylhydrazine under similar condition afforded the aniline derivatives (**22** and **23**). These rearranged cage like molecules emerged as a diastereomeric mixture in the respective crude products. The benzylamine derivatives (**20** and **21**) were easily separated with 100% ethyl acetate using column chromatography. The aniline derivatives (**22** and **23**) were practically inseparable despite exploring different mobile phases. The structure of these compounds (**19-23**) were elucidated and confirmed by various experiments that include NMR, MS and IR.

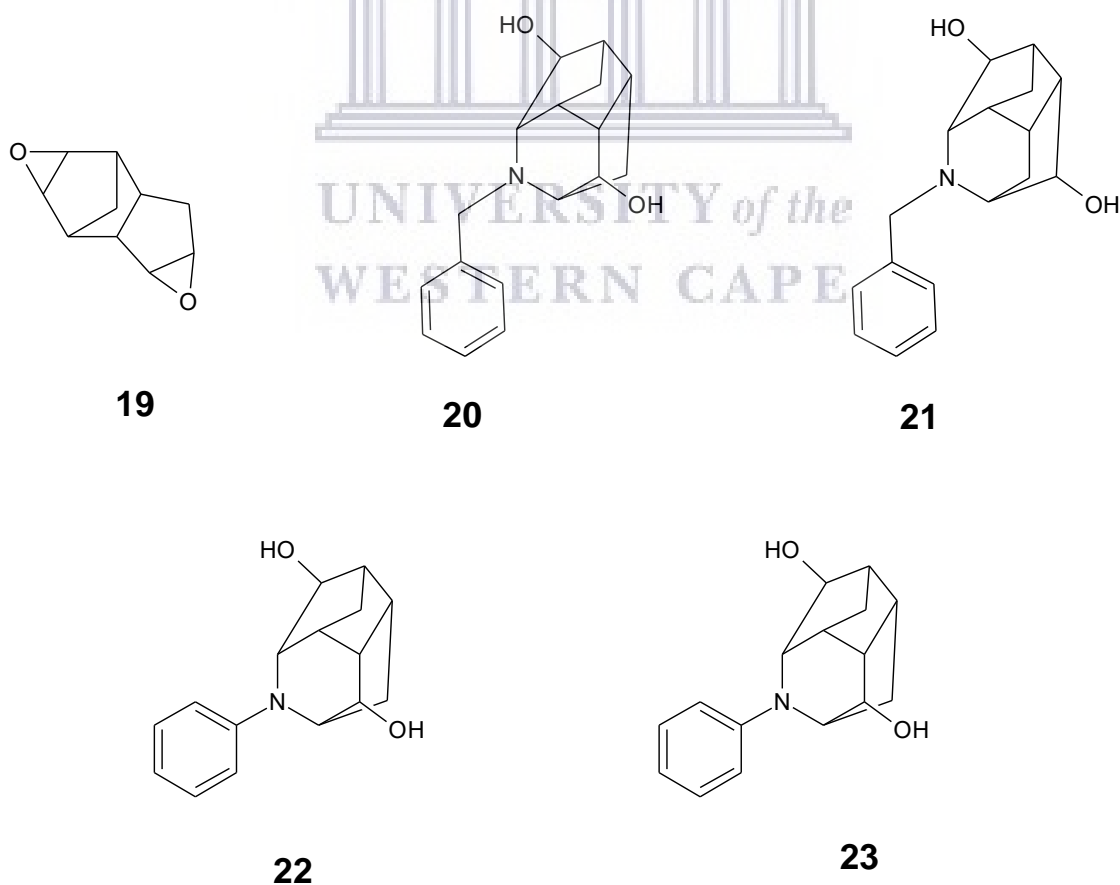


Figure 5.3: Structures of series 3.

The aliphatic conjugates (propylamine and propargylamine) were also proposed. However, the products formed were insoluble in conventional solvents such as DMSO, water, acetone, methanol and benzene. Due to their poor solubility, particularly in DMSO, these conjugates were excluded in the series as the biological testing would be affected.

Compound **24-27** (figure 5.4) were acquired and included in the series because of the structural similarities between the acquired (**24-27**) and synthesised (**1-23**) compounds. The structures were elucidated and confirmed by ^1H and ^{13}C -NMR, and the peaks observed correspond to those found in the literature (Kas'yan & Palchikov, 2010; Palchikov *et al.*, 2014).

Once the structures were characterised and confirmed, the synthesised (**1-23**) and acquired (**24-27**) compounds were screened for potential neurotoxic and neuroprotection effects.

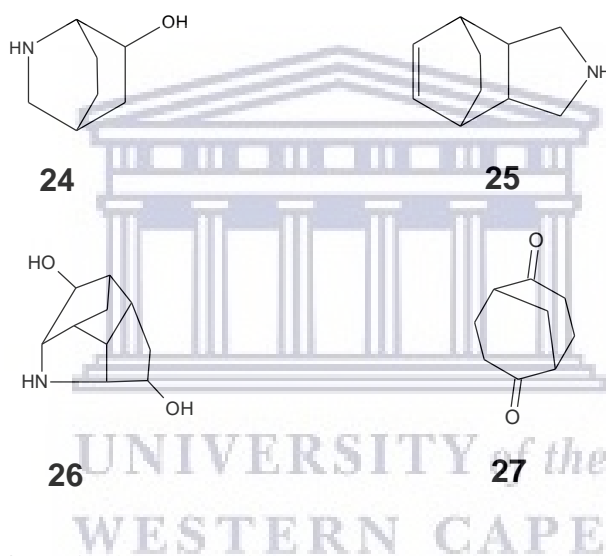


Figure 5.4: Structures of acquired compounds.

5.3 Biological studies

The cytotoxic profiles, neuroprotective effects and calcium inhibitory profiles of the synthesised compounds (**1-27**) were successfully evaluated in the biological studies (table 4.1). The human neuroblastoma SH-SY5Y cell line was used throughout the biological studies as it possesses components and characteristics which are typical of human neuronal cells. Firstly, the cytotoxicity of the synthesised polycyclic compounds was determined at different concentrations in human neuroblastoma cells to establish the optimal concentration for neuroprotection and Ca^{2+} inhibition studies. Once the optimal concentration was identified, the anti-apoptotic effects of these compounds against MPP^+ induced neurotoxicity were successfully assessed. The abilities of the synthesised compounds to attenuate calcium influx

through NMDA receptor and voltage gated calcium channels on human neuroblastoma cells were also successfully evaluated.

In the cytotoxicity study, compounds **1-27** were tested at 10 μM , 50 μM and 100 μM in neuroblastoma SH-SY5Y cells. After a 24-hour exposure time and MTT cell viability assessments, all of the compounds except **11** and **15** displayed cell viability rates that are inversely proportional to their concentration. Generally, all tested compounds demonstrated extremely low cytotoxic effects at 10 μM and 50 μM as evident by the cell viability percentages that are close to 100%. Even at 100 μM , some of these compounds still displayed reasonably good cytotoxic profiles towards the human neuroblastoma cells. However, compound **7** and **24** demonstrated toxicities toward SH-SY5Y cells as they showed cell viability percentages of 51% and 59% respectively, at 100 μM . In light of these observations, the neuroprotection and calcium inhibition studies were carried out at 10 μM . This concentration was deemed optimal as it facilitates accurate cell viability measurements.

In the neuroprotection study, neuroprotective effects of the synthesised compounds **1-27**, on neuroblastoma cells, after exposure to neurotoxin (MPP⁺) were successfully demonstrated. After 24 hours, cell viability testing was performed using the MTT assay. Compared to MPP⁺ only treated cells with a cell viability of 49.9%, all compounds (**1-27**) reasonably attenuated MPP⁺-induced neurotoxicity as demonstrated by the significant enhancement of cell viability that is between 22.8% to 53.3%. The highest and lowest neuroprotective effects were observed for compound **8** (103.5%) and **18** (73.9%), respectively. Notably, less rigid compounds (**2** & **12** compared to **1** & **11**, respectively) and more lipophilic structures (**1** compared to **8**) demonstrated enhanced neuroprotective effects. The important role of lipophilicity was also evident in the reduced neuroprotective effect demonstrated by the hydroxyl moiety of compound **3** when compared to compound **2**. It was also evident that primary (**14**, **16** & **17**) or secondary (**24**, **25** & **26**) amines are important for neuroprotective effects. And generally, the benzoquinone moieties displayed better neuroprotective effects than the furandione or diepoxide derivatives.

In the calcium influx studies, two major calcium entry pathways; namely the NMDA receptor and voltage gated calcium channels, were explored. Elevated intracellular calcium ions were assessed by calculating the ratio of calcium-bound and calcium-unbound in a Fura-2 loaded human neuroblastomas cell line.

In the NMDA receptor mediated calcium influx study, the ability of the synthesised compounds (**1-27**) to inhibit NMDA receptor channels after NMDA/glycine stimulation were successfully demonstrated. Their activities were compared to known NMDA receptor antagonists or blockers (NGP1-01 and MK-801). All compounds (**1-27**) demonstrated NMDA receptor inhibitions in range of 23.5-73% at 10 μ M with compound **27** and **7** showing the strongest and weakest inhibitions, respectively. Surprisingly, many of these compounds (**2, 3, 4, 5, 12, 15, 16, 17, 18, 19, 20, 21, 25, 26** and **27**) displayed inhibitory effects that exceed that of MK-801. Structure activity relationship suggested that the NMDA receptor inhibition of this group of compounds is influenced by the structure's rigidity and lipophilicity and the presence of a basic nitrogen atom, hydroxyl moiety and aromatic moiety. Some of these compounds (**5, 6, 9, 13, 14, 16, 17, 24, 25 & 26**) exhibit similar characteristic functional groups such as basic amino functionality, hydroxyl moiety or hydrophobic moiety as memantine or NGP1-01, which was why they were able to effectively block or inhibit the NMDA receptor. The comparison of the dione cyclic ring demonstrated that the NMDA receptor inhibition increases with ring size in the following manner; 8-membered > 6-membered > 5-membered. Interestingly, compounds **2, 4** and **27** differ in these functional characteristics, but still significantly inhibit NMDA receptor better than NGP1-01 and MK-801. This suggest allosteric interaction rather than interaction at the Mg^{2+} binding sites of the NMDA receptors. Altogether, the inhibitory effects of these compounds on NMDA receptors are expected to protect the neuronal cells from calcium overload mediated by glutamate-induced excitotoxicity.

In the voltage mediated calcium influx study, the inhibitory effects of synthesised compounds (**1-27**) on voltage gated calcium channels, expressed in human neuroblastomas SH-SY5Y cell, were successfully determined. In comparison to nimodipine and NGP1-01, which are known voltage gated calcium channels blockers, compounds **1, 2, 3, 4, 6, 7, 8, 9, 10, 11, 12, 13, 14, 15, 16 & 17** displayed moderate to good VGCC inhibition at 10 μ M. Those with good activity demonstrated inhibition similar to or exceeding nimodipine or NGP1-01. Interestingly, compounds **4** (50.3%), **8** (37.2%) and **16** (37.9%) demonstrated calcium inhibition that exceed nimodipine (34.1%) and NGP1-01 (34.2%). The strongest inhibition was observed with compound **4** (50.3%) while compounds **22, 23, 24 & 27** showed no VGCC inhibitory activity. The structure activity relationship of these groups of compounds suggest the importance of hydrophobicity and a carbonyl moiety that is necessary for interaction with the hydrophobic pocket of VGCC to mediate the inhibition of the channel. In some instances, polar groups like amines (**14, 16, & 17**) and amides (**9**) were well tolerated as demonstrated by their good

inhibitory effects. Unlike the NMDA inhibitory activities, the influence of the dione ring size were inversely proportional to the VGCC inhibitory activities. In general, the calcium inhibitory effects demonstrated by these compounds could potentially protect neurons from the adverse effects of calcium overload, a crucial event in apoptotic cell death.

Interestingly, some of these compounds (**2**, **3**, **4**, **6**, **7**, **8**, **9**, **10**, **11**, **12**, **13**, **14**, **15** and **16**) demonstrated calcium inhibition at both NMDA receptor and voltage gated calcium channels. Also, they displayed good cytotoxic profiles and attenuated MPP⁺-induced neurotoxicity. These characteristics support the hypothesis of this study, that these compounds can potentially act as multitarget-directed neuroprotective agents with good safety profiles.

5.4 Conclusion and recommendations

In this study, a total of 27 compounds that include novel opened cage- and rearranged cage-like molecules were successfully synthesised, purified and characterised. The synthesis of compounds in series 1 were limited to six due to the susceptibility of compound **2** to degradation at high temperature, and the aliphatic amines were unreactive at room temperature. In series 3, the aliphatic amine derivatives were insoluble in DMSO and were excluded from the study. Some of the reactions afforded products and by products with low yields that were attributed to suboptimal reaction conditions and separation techniques. All synthesised compounds showed reasonable cytotoxic profiles in human neuroblastoma cells. Compounds (**1-27**) exerted protection against MPP⁺-induced toxicity. This is significant as they potentially exhibit neuroprotective effects against a major neurotoxin peculiar to Parkinson's disease. The compounds were able to display mono- or dual- inhibition at NMDA receptor and/or voltage gated calcium channels. The inhibitions are expected to potentially protect neuronal cells from calcium overload-mediated apoptosis. The compounds demonstrated more calcium flux inhibition at the NMDA receptors than in voltage gated calcium channels. This is significant as the NMDA receptors are known to play a crucial role in calcium overload during glutamate-induced excitotoxicity that result in neuronal cell death. This observation was attributed to the structure similarities that exist between the synthesised compounds (**1-27**) and NGP1-01 or memantine. Despite limitations, the results in this study provide information on the synthesis and biological evaluation of the proposed structures (opened- and rearranged-cage) and set the foundation for the exploration of these group of compounds as possible neuroprotective agents with good safety profiles.

Nonetheless, the following recommendations and further studies are suggested to better understand the neuroprotective effects of these norbornane derivatives:

- Synthesis of structurally related derivatives with various functional moieties and optimising the reaction conditions that would lead to the formation of aliphatic conjugates of series 1. A microwave reaction in a monitored closed system, conducted at high pressure, high power (watt) and low temperature could for example afford the desired compounds. The additional derivatives could assist in understanding the structure activity relationship of this group of compounds;
- Optimisation of the reaction conditions of series 3. Investigation and determination of optimum temperature and completion time could improve the yield of this series.
- The determination of the IC_{50} of all the synthesised compounds (**1-27**) in the cytotoxicity, neuroprotective and calcium inhibition studies. This is necessary to accurately compare the cytotoxicity and neuroprotective activities of the synthesised compound among themselves and with known inhibitors or blockers;
- The investigation of the mechanism of neuroprotection for synthesised compounds (**1-27**) in the MPP^+ -induced neurotoxicity study would be beneficial for further drug design and optimisation. In order to achieve these objectives, experiments such as dopamine active transporter assay, microscopic assessment of morphological changes, evaluation of caspase-3 activity, flow cytometry measurement of mitochondrial transmembrane potential, flow cytometry detection of apoptotic and necrotic cells, oxygen consumption assay, western blot assay, ROS measurement, and quantification of immunoblot by densitometry analysis should be conducted;
- The determination of the mode of NMDA receptor blockage or inhibition by the synthesised compounds (**1-27**) needs to be clarified. Binding affinity studies such as radioligand ($[^3H]$ -(+)-MK-801) binding assay and docking studies are necessary to establish if these compounds bind to the PCP binding or allosteric binding sites of the NMDA receptors. It will also provide information on the type of binding, which could be either by trapping like MK-801 or foot in the door like memantine. Additionally, it could also provide information on potential side effects and clinical tolerability.

The compounds designed and synthesised in this study displayed neuroprotective effects by attenuating MPP^+ -induced neurotoxicity and inhibited calcium influx through NMDA receptor and voltage gated calcium channels while demonstrating good cytotoxicity profiles. It thus provides a good basis for further exploration of these derivatives and could assist in the

development of potential neuroprotective agents with good safety profiles that will not only provide symptomatic relief, but also halt or slow down the neurodegenerative processes. It will also assist us in understanding how these receptors and channels are involved in the neurodegenerative process and could contribute to the successful design of neuroprotective agents.



References

- Abderemane-Ali, F., Findeisen, F., Rossen, N. & Minor, D. (2019)** A selectivity filter gate controls voltage-gated calcium channel calcium-dependent inactivation. *Neuron*, 101, 1134-1149.
- Abeti, R. & Abramov, A. (2015)** Mitochondrial Ca²⁺ in neurodegenerative disorders. *Pharmacological Research*, 99, 377-381.
- Adam, O. & Jankovic, J. (2008)** Symptomatic treatment of Huntington's disease. *Neurotherapeutics: The Journal of the American Society for Experimental NeuroTherapeutics*, 5, 181-197.
- Aepkers, M. & Wunsch, B. (2005)** Structure-affinity relationship studies of non-competitive NMDA receptor antagonists derived from dexoxadrol and etoxadrol. *Bioorganic & Medicinal Chemistry*, 13, 6836-6849.
- Aghajyanov, M., Chavyshyan, V., Matinyan, S., Danielyan, M. & Yenkovyan, K. (2019)** Alzheimer's disease-like pathology-triggered oxidative stress, alterations in monoamines levels, and structural damage of locus coeruleus neurons are partially recovered by a mix proteoglycans of embryonic genesis. *Neurochemistry International*, 131, 104531. Available at <https://doi.org/10.1016/j.neuint.2019.104531>: accessed February 10, 2020.
- Ahmad, K., Baig, M., Gupta, G., Kamal, M., Pathak, N. & Choi, I. (2016)** Identification of common therapeutic targets for selected neurodegenerative disorders: An in silico approach. *Journal of Computational Science*, 17, 292-306.
- Ahsan, M. (2017).** Anticonvulsant activity and neuroprotection assay of 3-substituted-*N*-aryl-6,7-dimethoxy-3a,4-dihydro-3*H*-indeno[1,2-*c*]pyrazole-2-carboxamide analogues. *Arabian Journal of Chemistry*, 10, S2762-S2766.
- Akaishi, T., Takahashi, T., Abe, M, Aoki, M. & Ishii, T. (2019)** Consideration of gravity as a possible etiological factor in amyotrophic lateral sclerosis. *Medical Hypotheses*, 132, 109369. Available at <https://doi.org/10.1016/j.mehy.2019.109369>: accessed February 12, 2020.
- Akiya, N. & Savage, P. (2002)** Roles of water for chemical reactions in high-temperature water. *Chemical Reviews*, 102, 2725-2750.

Amidfar, M., Woelfer, M., Reus, G., Quevedo, J., Walter, M. & Kim, Y. (2019) The role of NMDA receptor in neurobiology and treatment of major depressive disorders: evidence from translational research. *Progress in Neuropsychopharmacology & Biological psychiatry*, 94, 109668. Available at <https://doi.org/10.1016/j.pnpbp.2019.109668>: accessed February 23, 2020.

Aminoff, M. 2019 Chapter 28: Pharmacologic Management of Parkinsonism & Other Movement Disorders. In: Katzung, B. Eds. *Basic & Clinical Pharmacology*, 14e, New York, NY: McGraw-Hill. Available at <http://accesspharmacy.mhmedical.com/content.aspx?bookid=2249§ionid=175219763>: accessed July 13, 2019.

Amo, T., Oji, Y., Saiki, S. & Hattori, N. (2019) Metabolomic analysis revealed mitochondrial dysfunction and aberrant choline metabolism in MPP⁺-exposed SH-SY5Y cells. *Biochemical and Biophysical Research Communications*, 519, 540-546.

Anekonda, T., Quinn, J., Harris, C., Frahler, K., Wadsworth, T. & Woltjer, R. (2011) L-type voltage-gated calcium blockade with izradipine as a strategy for Alzheimer's disease. *Neurobiology of Disease*, 41, 62-70.

Arbo, B., Riberiro, M. & Garcia-Segura, L. (2019) Development of new treatment for Alzheimer's diseases based on the modulation of translocator protein (TSPO). *Ageing Research Reviews*, 54, 100943. Available at <https://doi.org/10.1016/j.arr.2019.100943>: accessed February 11, 2020.

Arikkath, J., Felix, R., Ahern, C., Chen, C., Mori, Y., Song, I., Shin, H., Coronado, R. & Campbell, K. (2002) Molecular characterisation of a two-domain form of the neuronal voltage-gated P/Q-type calcium channel $\alpha_12.1$ subunit. *FEBS Letters*, 532, 300-308.

Arundine, M. & Tymianski, M. (2003) Molecular mechanism of calcium-dependent neurodegeneration in excitotoxicity. *Cell Calcium*, 34, 325-337.

Bains, S. & Shaw, C. (1997) Neurodegenerative disorders in humans: the role of glutathione in oxidative stress-mediated neuronal death. *Brain Research Reviews*, 25, 335-358.

Bano, D. & Ankarcrona, M. (2018) Beyond the critical point: An overview of excitotoxicity, calcium overload and the downstream consequences. *Neuroscience letters*, 663, 79-85.

Barbado, M., Fablet, K., Ronjat, M & De Waard, M. (2009) Gene regulation by voltage-dependent calcium channels. *Biochimica et Biophysica Acta*, 1793, 1096-1104.

Barygin, O., Gmiro, V., Kim, K., Magazanik, L. & Tikhonov, D. (2009) Blockade of NMDA receptor channels by 9-aminoacridine and its derivatives. *Neuroscience Letters*, 451, 29-33.

Baykara, M., Ozcan, M., Bilgen, M. & Kelestimur, H. (2019) Effects of gadolinium and gadolinium chelates on intracellular calcium signalling in sensory neurons. *Neuroscience Letters*, 707, 134295. Available at <https://doi.org/10.1016/j.neulet.2019.134295>: accessed **January 21, 2020**.

Bayram-Weston, Z., Jones, L., Dunnett, S. & Brooks, S. (2012) Light and electron microscopic characterization of the evolution of cellular pathology in YAC128 Huntington's disease transgenic mice. *Brain Research Bulletin*, 88, 137-147.

Berntsen, H., Bjorklund, C., Strandabo, R., Haug, T., Moldes-Anaya, A., Fuentes-Lazaro, J., Verhaegen, S., Paulsen, R., Tasker, R. & Ropstad, E. (2018) PFOS-induced excitotoxicity is dependent on Ca²⁺ influx via NMDA receptors in rat cerebella granule neurons. *Toxicology and Applied Pharmacology*, 357, 19-32.

Bhat, A., Dar, K., Anees, S., Zargar, M., Masood, A., Sofi, M. & Ganie, S. (2015) Oxidative stress, mitochondrial dysfunction and neurodegenerative diseases; a mechanistic insight. *Biomedicine & Pharmacotherapy*, 74, 101-110.

Bhurtel, S. Katila, N., Srivastav, S., Neupane, S. & Choi, D. (2019) Mechanistic comparison between MPTP and rotenone neurotoxicity in mice. *Neurotoxicology*, 71, 113-121.

Bienat, C., Banister, S., Hoban, J., Tsanaktsidis, J., Metaxas, A., Windhorst, A. & Kassiou, M. (2014) Structure-activity relationship of N-substituted 4-(trifluoromethoxy) benzamidines with affinity for GluN2B-containing NMDA receptors. *Bioorganic & Medicinal Chemistry Letters*, 24, 828-830.

Bisi, A., Arribas, R., Micucci, M., Budriesi, R., Feoli, A., Castellano, S., Belluti, F., Gobbi, S., De los Rios, C. & Rampa, A. (2019) Polycyclic maleimide-based derivatives as first dual modulators of neuronal calcium channels and GSK-3 β for Alzheimer's diseases treatment. *European Journal of Medicinal Chemistry*, 163, 394-402.

Blatter, L. & Wier, W. (1990) Intracellular diffusion, binding, and compartmentalization of the fluorescent calcium indicators indo-1 and fura-2. *The Biophysical Journal*, 58, 1491-1499.

Blatzheim, K. (2009) Interdisciplinary palliative care, including massage, in treatment of amyotrophic lateral sclerosis. *Journal of bodywork & movement Therapies*, 13, 328-335.

Boll, M., Bayliss, L., Vargas-Canas, S., Burgos, J., Montes, S., Penaloza-Solano, G., Rios, C. & Alcaraz-Zubeldia, M. (2014) Clinical and biological changes under treatment with lithium carbonate and valproic acid in sporadic amyotrophic lateral sclerosis. *Journal of the Neurological Sciences*, 340, 103-108.

Bolshakov, K. Kim, K., Potapjeva, N., Gmiro, V., Tikhonov, D., Usherwood, P., Mellor, I. & Magazanik, L. (2005) Design of antagonists for NMDA and AMPA receptors. *Neuropharmacology*, 49, 144-155.

Bondy, S. (2016) Anthropogenic pollutants may increase the increase the incidence of neurodegenerative disease in an aging population. *Toxicology*, 341-343, 41-46.

Bourinet, E. & Zamponi, G. (2017) Block of voltage-gated calcium channels by peptide toxins. *Neuropharmacology*, 127, 109-115.

Boussicault, L., Kacher, R., Lamaziere, A., Vanhoutte, P., Caboche, J., Betuing, S. & Potier, M. (2018) CYP46A1 protects against NMDA-mediated excitotoxicity in Huntington's disease: Analysis of lipid raft content. *Biochimie*, 153, 70-79.

Braybrook, A., Heywood, B. & Karatzas, P. (2002) An experimental investigation of crystal/solvent interactions in the copper (II) acetate monohydrate/propan-1-ol system. *Journal of Crystal Growth*, 244, 327-332.

Breyer, A., Elstner, M., Gillessen, T., Weiser, D. & Elstner, E. (2007) Glutamate-induced cell death in neuronal HT22 cells is attenuated by extracts from St. John's wort (*Hypericum perforatum* L.). *Phytomedicine*, 14, 250-255.

Brooks, S., Jones, L. & Dunnett, S. (2012) Comparative analysis of pathology and behavioural phenotypes in mouse models of Huntington's disease. *Brain Research Bulletin*, 88, 81-93.

Brown, A. & Sheares, V. (2007) Amorphous unsaturated aliphatic polyesters derived from dicarboxylic monomers synthesized by Diels–Alder chemistry. *Macromolecules*, 40, 4848-4853.

Brown, D., Shorter, J. & Wobst, H. (2020) Emerging small-molecule therapeutic approaches for amyotrophic lateral sclerosis and frontotemporal dementia. *Bioorganic & Medicinal*

Chemistry Letters, 30, 126942. Available at <https://doi.org/10.1016/j.bmcl.2019.126942>: accessed February 12, 2020.

Browne, E. & Abbott, B. (2016) Recent progress towards an effective treatment of amyotrophic lateral sclerosis using the SOD1 mouse model in a preclinical setting. *European Journal of Medicinal Chemistry*, 121, 918-925.

Browne, E., Parakh, S., Duncan, L., Langford, S., Atkin, J. & Abbott, B. (2016) Efficacy of peptide nucleic acid and selected conjugates against specific cellular pathologies of amyotrophic lateral sclerosis. *Bioorganic & Medicinal Chemistry*, 24, 1520-1527.

Cai, M. & Yang, E. (2019) Complementary and alternative medicines for treating amyotrophic lateral sclerosis: a narrative review. *Integrative Medicine Research*, 8, 234-239.

Cai, Y., Zhang, X., Zhou, X., Wu, X., Li, Y., Yao, J. & Bai, J. (2017) Nicotine suppresses the neurotoxicity by MPP⁺/MPTP through activating $\alpha 7$ nAChR/PI3K/Trx-1 and suppressing ER stress. *NeuroToxicology*, 59, 49-55.

Camm, K., Castro, N., Liu, Y., Czechura, P., Snelgrove, J. & Fogg, D. (2007). Tandem ROMP-hydrogenation with a third-generation Grubbs catalyst. *Journal of American Chemical Society*, 129, 4168-4169.

Carri, M., Ferri, A., Cozzolino, M., Calabrese, L. & Rotilo, G. (2003) Neurodegeneration in amyotrophic lateral sclerosis: the role of oxidative stress and altered homeostasis of metals. *Brain Research Bulletin*, 61, 2003, 365-374.

Carroll, J., Lerch, J., Franciosi, S., Spreeuw, A., Bissada, N., Henkelman, R. & Hayden, M. (2011) Natural history of disease in the YAC128 mouse reveals a discrete signature of pathology in Huntington disease. *Neurobiology of Disease*, 43, 257-265.

Cassidy, L., Fernandez, F., Johnson, J., Naiker, M, Owoola, A. & Broszczak, D. (2020) Oxidative stress in Alzheimer's disease: A review on emergent natural polyphenolic therapeutics. *Complementary Therapies in Medicine*, 49, 102294. Available at <https://doi.org/10.1016/j.ctim.2019.102294>: accessed February 10, 2020.

Celsi, F., Pizzo, P., Brini, M., Leo, S., Fotino, C., Pinton, P. & Rizzuto, R. (2009) Mitochondria, calcium and cell death: A deadly triad in neurodegeneration. *Biochimica et Biophysica Acta*, 1787, 335-344.

Chaffey, H. & Chazot, P. (2008) NMDA receptor subtypes: Structure, function and therapeutic. *Current Anaesthesia & Critical Care*, 19, 183-201.

Chen, J. & Dashipour, K. (2017) Chapter 59: Parkinson's Disease. In Di Piro, P., Talbert, R., Yee, G., Matzke, G., Wells, B. & Posey, L. Eds. *Pharmacotherapy: A Pathophysiologic Approach*, 10e, New York, NY: McGraw-Hill. Available at <http://accesspharmacy.mhmedical.com/content.aspx?bookid=1861§ionid=134127873>: accessed July 13, 2019.

Chen, L. Liu, C. & Liu, L. (2008) Changes in osmolality modulate voltage-gated calcium channels in trigeminal ganglion neurons. *Brain Research*, 1208, 56-66.

Chen, Y., Ji, Y., Jin, X., Sun, X., Zhang, X., Chen, Y., Shi, L., Cheng, H., Mao, Y., Li, X., Hou, Y., Zhang, D. Zhao, S., Ma., J. & Huang, S. (2019) Mitochondrial abnormalities are involved in periodontal ligament fibroblast apoptosis induced by oxidative stress. *Biochemical and Biophysical Research Communications*, 509, 483-490.

Christel, C. & Lee, A. (2012) Ca²⁺-dependent modulation of voltage-gated Ca²⁺ channels. *Biochimica et Biophysica Acta*, 1820, 1243-1252.

Ciosi, M., Maxwell, A., Cumming, S., Moss, D., Aishammari, A., Flower, M., Durr, A., Leavitt, B., Roos, R., Holmans, P., Jones, L., Langbehn, D., Kwak, S., Tabrizi, S. & Monckton, D. (2019) A genetic association study of glutamine-encoding DNA sequence structures, somatic CAG expansion, and DNA repair gene variants, with Huntington disease clinical outcomes, *EbioMedicine*, 48, 568-580.

Colacurcio, D. & Nixon, R. (2016). Disorders of lysosomal acidification- The emerging of v-ATPase in aging and neurodegenerative diseases. *Ageing Research Reviews*, 32, 75-88

Commins, S. & Kirby, B. (2019) The complexities of behavioural assessment in neurodegenerative disorders: A focus on Alzheimer's disease. *Pharmacological Research*, 147, 104363. Available at <https://doi.org/10.1016/j.phrs.2019.104363>: accessed February 10, 2020.

Constantino, M., Beatriz, A. & Jose da Silva, G. (2000) A model synthesis of the bicyclic core structure of the furanoheliangolide sesquiterpenes. *Tetrahedron Letters*, 41, 7001-7004.

Costa, B., Irvine, M., Fang, G., Eaves, R., Mayo-Martin, M., Laube, B., Jane, D. & Monaghan, D. (2012) structure-activity relationships of allosteric NMDA receptor inhibitors based on 2-naphthoic acid. *Neuropharmacology*, 62, 1730-1736.

Croese, T. & Furlan, R. (2018) Extracellular vesicles in neurodegenerative diseases. *Molecular Aspects of Medicine*, 60, 52-61.

Cudazzo, G., Smart, D., McHugh, D. & Vanscheeuwijck, P. (2019) Lysosomotropic-related limitations of the BALB/c 3T3 cell-based neutral red uptake assay and an alternative testing approach for assessing e-liquid cytotoxicity. *Toxicology in Vitro*, 61, 104647. Available at <https://doi.org/10.1016/j.tiv.2019.104647>: accessed November 18, 2019.

Cui, W., Zhang, Z., Li, W., Hu., S., Mak, S., Zhang, H., Han, R., Yuan, S., Li, S., Sa, F., Xu, D., Lin, X., Zuo, Z., Rong, J., Ma, E., Choi, T., Lee, S. & Han, Y. (2013) The anti-cancer agent SU4312 unexpectedly protects against MPP⁺-induced neurotoxicity via selective and direct inhibition of neuronal NOS. *British Journal of Pharmacology*, 168, 1201-1214.

Cury, R., de Jesus Carvalho, M., Lasteros, F., Dias, A., dos Santos Ghilardi, M, Paiva, A., Coutinho, A, Buchpiguel, C., Teixeira, M., Barbosa, E. & Fonoff, E. (2018) Effects of subthalamic stimulation on olfactory function in Parkinson's disease. *World Neurosurgery*, 114, e559-e564.

Danesi, C., Achuta, V., Corcoran, P., Peteri, U., Turconi, G., Matsui, N., Albayrak, I., Rezov, V., Isaksson, A. & Castren, M. (2018) Increased calcium influx through L-type calcium channels in human and mouse neural progenitors lacking fragile x mental retardation protein. *Stem Cell Reports*, 11, 1449-1461.

Daniele, S., Giacomelli, C. & Martini, C. (2018) Brain ageing and neurodegenerative disease: The role of cellular waste management. *Biochemical Pharmacology*, 158, 207-216.

Dejmek, M., Hrebabecky, H., Sala, M., Dracinsky, M., Prochazkova, E., Leyssen, P., Neyts, J., Balzarini, J. & Nencka, R. (2014) From norbornane-based nucleotide analogs locked in South conformation to novel inhibitors of feline herpes virus. *Bioorganic & Medicinal Chemistry*, 22, 2974-2983.

Deng, H., Wang, P. & Jankovic, J. (2018) The genetics of Parkinson's disease. *Ageing Research Reviews*, 42, 72-85.

Derakhshankhah, H., Sajadimajd, S., Jafari, S., Izadi, Z., Sarvari, S., Sharifi, M., Falahati, Moakedi, F., Muganda, W., Muller, M., Raoufi, M., Presley, J. (2020) Novel therapeutic strategies for Alzheimer's disease: Implications from cell-based therapy and

nanotherapy. *Nanomedicine: Nanotechnology, Biology, and Medicine*, 24, 102149. Available at <https://doi.org/10.1016/j.nano.2020.102149>: accessed February 10, 2020.

Deschepper, M., Hoogendoorn, B., Brooks, S., Dunnett, S. & Jones, L. (2012) Proteomic changes in the brains of Huntington's disease mouse models reflect pathology and implicate mitochondrial changes. *Brain Research Bulletin*, 88, 210-222.

Dey, A. & Nath De, J. (2015) Neuroprotective therapeutics from botanicals and photochemicals against Huntington's disease and related neurodegenerative disorders. *Journal of Herbal Medicine*, 5, 1-19.

Di Domenico, F., Tramutola, A. & Butterfield, D. (2017) Role of 4-hydroxy-2-nonenal (HNE) in the pathogenesis of Alzheimer disease and other selected age-related neurodegenerative disorders. *Free Radical Biology and Medicine*, 111, 253-261.

Dickson, D. (2018) Neuropathology of Parkinson disease. *Parkinsonism and Related Disorders*, 46, s30-s33.

Diels, O. & Alder, K. (1928) Synthesen in der hydroaromatischen reihe. *Justus Liebigs Annalen der Chemie*, 460 (1), 98-122.

Dolphin, A. (2013) The $\alpha_2\delta$ subunits of voltage-gated calcium channels. *Biochimica et Biophysica Acta*, 1828, 1541-1549.

Dong, Y., Lin, H., Rattelle, A., Panzer, J., Lynch, D. (2018) 6.06 Excitotoxicity. *Comprehensive Toxicology (Third Edition)*, 6, 70-100.

Drygalski, K, Fereniec, E., Korycinski, K., Chomentowski, A., Kielczewska, A., Odrzygocz, C & Modzelewska, B. (2018) Resveratrol and Alzheimer's disease. From molecular pathophysiology to clinical trials. *Experimental Gerontology*, 113, 36-47.

Du Plessis, S., Bossert, M., Vink, M., Van den Heuvel, L., Bardien, S., Emsley, R., Buckle, C., Seedat, S. & Carr, J. (2018) Reward processing dysfunction in ventral striatum and orbitofrontal cortex in Parkinson's disease. *Parkinsonism and Related Disorders*, 48, 82-88.

Duque, M., Camps, P., Profire, L., Montainer, S., Vazquez, S., Sureda, F., Mallol, J., Lopez-Querol, M., Naesens, L., De Clercq, E., Prathalingam, S. & Kelly, J. (2009) Synthesis and pharmacological evaluation of 2-oxaadamant-1-yl)amines. *Bioorganic & Medicinal Chemistry*, 17, 3198-3206.

Duque, M., Camps, P., Torres, E., Valverde, E., Sureda, F., Lopez-Querol, M., Camins, A., Prathalingam, R., Kelly, J. & Vazquez, S. (2010) New oxapolycyclic cage amines with NMDA receptor antagonist and trypanocidal activities. *Bioorganic & Medicinal Chemistry*, 18, 46-57.

Dustin, L. (2000) Ratiometric analysis of calcium mobilization. *Clinical and Applied Immunology Reviews*, 1, 5-15.

Dwivedi, N., Shah, J., Mishra, V., Tambuwala, M. & Kesharwani, P. (2019) Nanoneuromedicine for management of neurodegenerative disorder. *Journal of Drug Delivery Science and Technology*, 49, 477-490.

Eberhardt, O. & Topka, H. (2016) The preclinical stage of movement disorders. *Basal Ganglia*, 6, 35-44.

Eftekhazadeh, B., Hyman, B. & Wegmann, S. (2016) Structural studies on the mechanism of protein aggregation in age related neurodegenerative diseases. *Mechanisms of Ageing and Development*, 156, 1-13.

Egunlusi, A., Malan, S. & Joubert, J. (2015) Tricycloundecane derivatives as potential N-methyl-d-aspartate (NMDA) receptor and voltage-gated calcium channel modulators. *ChemMedChem*, 10 (7), 1259-1266.

Eira, J., Silva, C.S., Sousa, M.M. & Liz, M.A. (2016) The cytoskeleton as a novel therapeutic target for old Neurodegenerative disorders. *Progress in Neurobiology*, 141, 61-82.

Eisinger, R., Hess, C., Martinez-Ramirez, D., Almeida, L., Foote, K., Okun, M. & Gunduz, A. (2017) Motor subtype changes in early Parkinson's disease. *Parkinsonism and Related Disorders*, 43, 67-72.

Elfawy, H. & Das, B. (2019) Crosstalk between mitochondrial dysfunction, oxidative stress, and age related neurodegenerative disease: Etiologies and therapeutic strategies. *Life Sciences*, 218, 165-184.

Ellwardt, E. & Zipp, F. (2014) Molecular mechanism linking neuroinflammation and neurodegeneration in MS. *Experimental Neurology*, 262, 8-17.

Espinosa-Parrilla, J., Martinez-Moreno, M., Casull, X., Mahy, N & Rodriguez, M. (2015) The L-type voltage-gated calcium channel modulates microglial pro-inflammatory activity. *Molecular and Cellular Neuroscience*, 64, 104-115.

Fang, T., Al Khleifat, A., Meurgey, J., Jones, A., Leigh, P., Bensimon, G. & Al-Chalabi, A. (2018) Stage at which riluzole treatment prolongs survival in patients with amyotrophic lateral sclerosis: a retrospective analysis of data from a dose-ranging study. *The Lancet Neurology*, 17, 416-422.

Findling, R., Goldman, R., Chiu, Y., Silva, R., Jin, F., Pikalov, A. & Loebel, A. (2015) Pharmacokinetics and Tolerability of Lurasidone in Children and Adolescents with psychiatric disorders. *Clinical Therapeutics*, 37 (12), 2788-2797.

Fish, P., Steadman, D., Bayle, E. & Whiting, P. (2019) New approaches for the treatment of Alzheimer's disease. *Bioorganic & Medicinal Chemistry Letters*, 29, 125-133.

Flores-Soto, M., Chaparro-Huerta, V., Escoto-Delgadillo, M., Vazquez-Valls, E., Gonzalez-Castaneda, R. & Beas-Zarate, C. (2012) Structure and function of NMDA-type glutamate receptor subunits, *Neurologia*, 27, 301-310.

Foster, J., Varlas, S., Blackman, L., Arkinstall, L. & O'Reilly, R. (2018) Ring-Opening metathesis polymerization in aqueous media using a macroinitiator approach. *Angewandte Chemie, International Edition*, 57, 10672-10676.

Fratiglioni, L. & Qiu, C. (2009) Prevention of common neurodegenerative disorders in the elderly. *Experimental Gerontology*, 44, 46-50.

Fukuoka, M., Takahashi, M., Fujita, H., Chiyo, T., Popiel, H., Watanabe, S., Furuya, H., Murata, M., Wada, K., Okada, T., Nagai, Y. & Hohjoh, H. (2018) Supplemental treatment for Huntington's disease with *miR-132* that is deficient in Huntington's disease brain. *Molecular Therapy: Nucleic Acids*, 11, 79-90.

Gamez, J., Salvado, M., De la Ossa, M. & Badia, M. (2016) Lithium for treatment of amyotrophic lateral sclerosis: Much ado about nothing. *Neurologia*, 31 (8), 550-561.

Gan, L., Cookson, M., Petrucelli, L. & La Spada, A. (2018) Converging pathways in neurodegeneration, from genetics to mechanisms. *Nature Neuroscience*, 21, 1300-1309.

Garcia-Blanco, A., Baquero, M., Vento, M., Gil, E., Bataller, L. & Chafer-Pericas, C. (2017) Potential oxidative stress biomarkers of mild cognitive impairment due to Alzheimer disease. *Journal of the Neurological Sciences*, 373, 295-302.

Garcia de Yebenes, J., Landwehrmeyer, B., Squitieri, F., Reilman, R., Rosser, A., Barker, R., Saft, C., Magnet, M., Sword, A., Rembratt, A. & Tedroff, J. (2011) Pridopidine for the

treatment of motor function in patients with Huntington's disease (MermaiHD): a phase 3, randomised, double-blind, placebo-controlled trial. *The Lancet of Neurology*, 10, 1049-1057.

Garcia-Moreno, J., de la Riva, M., Martinez-Lara, E., Siles, E. & Canuelo, A. (2019) Tyrosol, a simple phenol from EVOO, targets multiple pathogenic mechanisms of neurodegeneration in a *C. elegans* model of Parkinson's disease. *Neurobiology of Aging*, 82, 60-68.

Geldenuys, W., Terre'Blanche, G., Van der Schyf, C. & Malan, S. (2003) Screening of novel pentacyclo-undecylamines for neuroprotective activity. *European Journal of Pharmacology*, 458, 73-79.

Geldenuys, W., Malan, S., Murugesan, T., Van der Schyf, C. & Bloomquist, J. (2004) Synthesis and biological evaluation of pentacyclo[5.4.0.0^{2,6}.0^{5,9}]undecane derivatives as potential therapeutic agents in Parkinson's disease. *Bioorganic & Medicinal Chemistry*, 12, 1799-1806.

Geldenuys, W., Malan, S., Bloomquist, J. & Van der Schyf, C. (2007) Structure-activity relationships of pentacycloundecylamines at the N-methyl-D-aspartate receptor. *Bioorganic & Medicinal Chemistry*, 15, 1525-1532.

Geldenuys, W., Bezuidenhout, L. & Dluzen, D. (2009) Effect of a novel dopamine uptake inhibitor upon extracellular dopamine from superfused murine striatal tissue. *European Journal of Pharmacology*, 619, 38-43.

Ghani, M., Lang, A., Zinman, L., Nacmias, B., Sorbi, S., Bessi, V., Tedde, A., Tartaglia, M., Surace, E., Sato, C., Moreno, D., Xi, Z., Hung, R., Nalls, M., Singleton, A., George-Hyslop, P. & Rogaeva, E. (2015) Mutation analysis of patients with neurodegenerative disorders using NeuroX array. *Neurobiology of Aging*, 36, 545 (e9-14).

Ghavami, S., Shojaei, S., Yeganeh, R., Ande, S., Jangamreddy, J., Mehrpour, M., Christoffersson, J., Chaabane, W., Moghadam, A., Kashani, H., Hashemi, M., Owji, A. & Los, M. (2014) Autophagy and apoptosis dysfunction in neurodegenerative disorders. *Progress in Neurobiology*, 112, 24-49.

Godinho, B., Malhotra, M., O'Driscoll, C. & Cryan, J. (2015) Delivering a disease-modifying treatment for Huntington's disease. *Drug Discovery Today*, 20, 50-64.

Gold, M., Koczulla, A., Mengel, D., Koepke, J., Dodel, R., Dontcheva, G., Habib, P. & Bach, J. (2015) Reduction of glutamate-induced excitotoxicity in murine primary neurons involving calpain inhibition. *Journal of the Neurological Sciences*, 359, 356-362.

Gomez-SanJuan, A., Sotomayor, N. & Lete, E. (2013). RCM approach to complex polycyclic α -hydroxy γ -lactams: synthesis of indolizinones and pyrroloazepinones. *European Journal of Organic Chemistry*, 2013 (29), 6722-6732.

Gonzalez-Burgos, E., Fernandez-Moriano, C., Lozano, R., Iglesias, I. & Gomez-Serranillos, M. (2017) Ginsenosides Rd and Re co-treatments improve rotenone-induced oxidative stress and mitochondrial impairment in SH-SY5Y neuroblastoma cells. *Food and Chemical Toxicology*, 109, 38-47.

Gibbs, S. & Braun, J. (2008) Emerging roles of J proteins in neurodegenerative disorders. *Neurobiology of Disease*, 32, 196-199.

Gieling, R. & Klunder, A. (2004) Immobilized cyclopentadiene in the Diels Alder/retro-Diels Alder concept. *ARKIVOC*, 2, 91-108.

Grobler, E., Grobler, A., Van der Schyf, C. & Malan, S. (2006) Effect of polycyclic cage amines on the transmembrane potential of neuronal cells. *Bioorganic & Medicinal Chemistry*, 14, 1176-1181.

Gryniewicz, G., Poenie, M., & Tsien, R. (1985) A new generation of Ca^{2+} indicators with greatly improved fluorescence properties. *Journal of Biological Chemistry*. 260, 3440-3450.

Gulaboski, R., Pereira, C., Natalia, M., Cordeiro, D., Silva, A., Hoth, M. & Bogeski, I. (2008) Redox properties of the calcium chelator Fura-2 in mimetic biomembranes. *Cell Calcium*, 43, 615-621.

Gusella, J. (2019) CAG repeat not polyglutamine length determines timing of Huntington's disease onset. *Cell*, 178, 887-900.

Haeberlein, S. & Lipton, S. (2009) Excitotoxicity in neurodegenerative disease. *Encyclopaedia of Neuroscience*, 77-86.

Hanamsagar, R. & Bilbo, S. (2016) Sex differences in neurodevelopmental and neurodegenerative disorders: Focus on microglial function and neuroinflammation during development. *Journal of Steroid Biochemistry & Molecular Biology*, 160, 127-133.

Hao, J., Mdzinarishvili, A., Abbruscato, T., Klein, J., Geldenhuys, W., Van der Schyf, C. & Bickel, U. (2008) Neuroprotection in mice by NGP1-01 after transient focal brain ischemia. *Brain Research*, 1196, 113-120.

Hasegawa, M., Nonaka, T. & Masuda-Suzukake, M. (2017) Prion-like mechanisms and potential therapeutic targets in neurodegenerative disorders. *Pharmacology & Therapeutics*, 172, 22-33.

Havekes, R., Heckman, P., Wams, E., Stasiukonyte, N., Meerlo, P. & Eisel, U. (2019) Alzheimer's disease pathogenesis: The role of disturbed sleep in attenuated brain plasticity and neurodegenerative processes. *Cellular signalling*, 64, 109420. Available at <https://doi.org/10.1016/j.cellsig.2019.109420>: accessed February 10, 2020.

Henke, W., Cetinsoy, C., Jung, K. & Loening, S. (1996) Non-hyperbolic calcium calibration curve of Fura-2: implications for the reliability of quantitative Ca^{2+} measurements. *Cell Calcium*, 20 (3), 287-292.

Hernandez, A., Gonzalez-Alzaga, B., Lopez-Flores, I. & Lacasana, M. (2016) Systematic reviews on neurodevelopmental and neurodegenerative disorders linked to pesticide exposure: Methodological features and impact on risk assessment. *Environment International*, 92-93, 657-679.

Heusinkveld, H., Wahle, T., Campbell, A., Westerink, R., Tran, L., Johnston, H., Stone, V., Cassee, F. & Schins, R. (2016) Neurodegenerative and neurological disorders by small inhaled particles. *NeuroToxicology*, 56, 94-106.

Heusinkveld, H. & Westerink, R. (2011) Caveats and limitations of plate reader-based high-throughput kinetic measurements of intracellular calcium levels. *Toxicology and Applied Pharmacology*, 255, 1-8.

Heyes, S., Pratt, W., Rees, E., Dahimene, S., Ferron, L. Owen, M. & Dolphin, A. (2015) Genetic disruption of voltage-gated calcium channels in psychiatric and neurological disorders. *Progress in Neurobiology*, 134, 36-54.

Hickey, S., Ashton, T., Boer, G., Bader, C., Thomas, M., Elliott, A., Schmuck, C., Yu, H., Li, J., Nation, R., Cooper, M., Plush, S., Brooks, D. & Pfeffer, F. (2018) Norbornane-based cationic antimicrobial peptidomimetics targeting the bacterial membrane. *European Journal of Medicinal Chemistry*, 160, 9-22.

Hrebabecky, H., Dejmek, M., Sala, M., Mertlikova-Kaiserova, H., Dracinsky, M., Leyssen, P., Neyts, J., Nencka, R. (2012) Synthesis of novel thienonorbornylpurine derivatives. *Tetrahedron*, 68, 3195-3204.

Hristov, K., Mangalanathan, U., Casciola, M., Pakhomova, O. & Pakhomov, A. (2018) Expression of voltage-gated calcium channels augments cell susceptibility to membrane disruption by nanosecond pulsed electric field. *BBA-Biomembranes*, 1860, 2175-2183.

Hu, Z., Yu, L. & Yu, Z. (2005) Theoretical analysis on ratiometric fluorescent indicators caused biased estimates of intracellular free calcium concentration, *Journal of Photochemistry and Photobiology B. Biology*, 78, 179-187.

Hurley, M. & Dexter, D. (2012) Voltage-gated calcium channels and Parkinson's disease. *Pharmacology & Therapeutics*, 133, 324-333.

Ichikawa, O., Okazaki, K., Nakahira, H., Maruyama, M., Nagata, R., Tokuda, K., Horisawa, T. & Yamazaki, K. (2012) Structural insight into receptor-selectivity for lurasidone. *Neurochemistry International*, 61, 1133-1143.

Ingram, R., Kang, H., Lightman, S., Jane, D., Bortolotto, Z., Collingridge, G., Lodge, D., Volianskis, A. (2018) Some distorted thoughts about ketamine as a psychedelic and a novel hypothesis based on NMDA receptor-mediated synaptic plasticity. *Neuropharmacology*, 142, 30-40.

Ito, F., Petroni, J., de Lima, D., Beatriz, A., Marques, M., de Moraes, M., Costa-Lotufo, L., Montenegro, R., Magalhaes, H. & do O Pessoa, C. (2007) Synthesis and biological evaluation of rigid polycyclic derivatives of the Diels-Alder Adduct tricyclo[6.2.1.0^{2,7}]undeca-4,9-diene-3,6-dione. *Molecules*, 12, 271-282.

Jaeschke, R., Sowa-Kucima, M., Panczyszyn-Trzewik, P., Misztak, P., Styczen, K. & Datka, W. (2016) Lurasidone: The 2016 update on the pharmacology, efficacy and safety profile. *Pharmacological Reports*, 64 (4), 748-755

Jantas, D., Greda, A., Golda, S., Korostynski, M., Grygier, B., Roman, A., Pilc, A. & Lason, W. (2014) Neuroprotective effects of metabotropic glutamate receptor group II and III activators against MPP(+)-induced cell death in human neuroblastoma SH-SY5Y cells: The impact of cell differentiation state. *Neuropharmacology*, 83, 36-53.

Jembrek, M., Radovanovic, V., Vlainic, J., Vukovic, L. & Hanzic, N. (2018) Neuroprotective effect of zolpidem against glutamate-induced toxicity is mediated via the PI3K/Akt pathway and inhibited by PK11195. *Toxicology*, 406-407, 58-69.

Jeong, I., Yang, J., Hong, Y., Kim, H., Hahn, S. & Yoon, S. (2017) Dapoxetine induced neuroprotective effects against glutamate-induced neuronal cell death by inhibiting calcium signalling and mitochondrial depolarization in cultured rat hippocampal neurons. *European Journal of Pharmacology*, 805, 36-45.

Jha, S., Jha, N., Kumar, D., Ambasta, R. & Kumar, P. (2017) Linking mitochondrial dysfunction, metabolic syndrome and stress signalling in neurodegeneration. *Biochimica et Biophysica Acta*, 1863, 1132-1146.

Jiang, T., Sun, Q. & Chen, S. (2016) Oxidative stress: A major pathogenesis and potential therapeutic target of antioxidative agents in Parkinson's disease and Alzheimer's diseases. *Progress in Neurobiology*, 147, 1-19.

Jiang, S., Zheng, R., Zeng, J., Li, X., Han, Z. & Hou, S. (2010) Reversible inhibition of intracellular calcium influx through NMDA receptors by imidazoline I₂ receptor antagonists. *European Journal of Pharmacology*, 629, 12-19.

Jing, G., Grammatopoulos, T., Ferguson, P., Schelman, W. & Weyhenmeyer, J. (2004) Inhibitory effects of angiotensin on NMDA-induced cytotoxicity in primary neuronal cultures. *Brain Research Bulletin*, 62, 397-403.

Jirgensons, A., Kauss, V., Kalvinsh, I., Gold, M., Danysz, W., Parsons, C. & Quack, G. (2000) Synthesis and structure-affinity relationships of 1,3,5-alkylsubstituted cyclohexylamines binding at NMDA receptors PCP site. *European Journal of Medicinal Chemistry*, 35, 555-565.

Jonson, I., Ougland, R., Klungland, A. & Larsen, E. (2013) Oxidative stress causes DNA triplet expansion in Huntington's disease mouse embryonic stem cells. *Stem Cell Research*, 11 (3), 1264-1271.

Joubert, J., Van Dyk, S., Green, I. & Malan, S. (2011) Synthesis, evaluation and application of polycyclic fluorescent analogues as *N*-methyl-D-aspartate receptor and voltage gated calcium channels ligands. *European Journal of Medicinal Chemistry*, 46, 5010-5020.

Jouha, J., Loubidi, M., Bouali, J., Hamri, S., Hafid, A., Suzenet, F., Guillaumet, G., Dagci, T., Khouili, M., Aydin, F., Saso, L. & Armagan, G. (2017) Synthesis of new heterocyclic compounds based in pyroazolopyridine scaffold and evaluation of their neuroprotective potential in MPP⁺-induced neurodegeneration. *European Journal of Medicinal Chemistry*, 129, 41-52.

Jovanovic-Tucovic, M., Harhaji-Trajkovic, L., Dulovic, M., Tovilovic-Kovacevic, G., Zogovic, N., Jeremic, M., Mandic, M., Kostic, V., Trajkovic, V. & Markovic, I. (2019) AMP-activated protein kinase inhibits MPP⁺- induced oxidative stress and apoptotic death of SH-SY5Y cells through sequential stimulation of Akt and autophagy. *European Journal of Pharmacology*, 863, 172677. Available at <https://doi.org/10.1016/j.ejphar.2019.172677>: accessed March 12, 2020.

Ju, T., Chen, H., Chen, Y., Chang, C., Chang, C. & Chern, Y. (2014) AMPk- α 1 functions downstream of oxidative stress in mediate neuronal atrophy in Huntington's disease. *Biochimica et Biophysica Acta*, 1842, 1668-1680.

Jung, T., Lee, J., Shim, W., Kang, E., Kim, J., Ahn, C., Lee, H. & Cha, B. (2006) Adiponectin protects human neuroblastomas SH-SY5Y cells against MPP⁺-induced cytotoxicity. *Biochemical and Biophysical Research Communications*, 343, 564-570.

Juntas-Morales, R., Pageot, N., Bendarraz, A., Alphantery, S., Sedel, F., Seigle, S., Camu, W. (2020) High-dose pharmaceutical grade biotin (MD1003) in amyotrophic lateral sclerosis: A pilot study. *EClinicalMedicine*, 19, 100254. Available at <https://doi.org/10.1016/j.eclinm.2019.100254>: accessed February 12, 2020.

Kas'yan, L. & Palchikov, V. (2010) Cage-like Amino Alcohols. Synthesis, Reactions and Application. *Russian Journal of Organic Chemistry*, 46 (1), 1-42.

Katz, M, Jensen, C., Student, J., Johnson, G. & Coates, J. (2017) Cervical spinal cord and motor unit pathology in a canine model of SOD1-associated amyotrophic lateral sclerosis. *Journal of the Neurological Sciences*, 378, 193-203.

Kavitha, R., Kumar, J., Egbuna, C. & Ifemeje, J. (2020) Chapter 10 – Phytochemicals as therapeutic interventions in neurodegenerative diseases. *Phytochemicals as lead compounds for New Drug Discovery*, pages 161-178.

Kelani, M., Kruger, H., Govender, T., Maguire, G., Nacker, T. & Onajole, O. (2020) Serendipitous discovery of new pentacycloundecane molecules. *Journal of molecular Structure*, 1204, 127497. Available at <https://doi.org/10.1016/j.molstruc.2019.127497>: accessed March 04, 2020.

Kennedy, L., Shelbourne, P. & Dewar, D. (2005) Alterations in dopamine and benzodiazepine receptor binding precede overt neuronal pathology in mice modelling early Huntington diseases pathogenesis. *Brain Research*, 1039, 14-21.

Kim, H., Kim, Y., Jang, J., Choi, Y., Baek, J., Hong, J., Choi, Y., Shin, H., Choi, B. (2013) Neuroprotective effects of *Polygonum multiflorum* extract against glutamate-induced oxidative toxicity in HT22 hippocampal cells. *Journal of Ethnopharmacology*, 150, 108-115.

Kim, I., Koppula, S., Park, P., Kim, E., Kim, C., Choi, W., Lee, K. & Choi, D. (2009) *Chrysanthemum morifolium* Ramat (CM) extract protects human neuroblastoma SH-SY5Y cells against MPP⁺-induced cytotoxicity. *Journal of Ethnopharmacology*, 126, 447-454.

Kochegarov, A. (2003) Pharmacological modulators of voltage-gated calcium channels and their therapeutical application. *Cell Calcium*, 35, 145-162.

Kostic, M., Zivkovic, N., Cvetanovic, A., Stojanovic, I. & Colic, M. (2017) IL-17 signalling in astrocytes promotes glutamate excitotoxicity: Indications for the link between inflammatory and neurodegenerative events in multiple sclerosis. *Multiple Sclerosis and Related Disorders*, 11, 12-17.

Krishchik, O., Tarabara, N., Kas'yan, A., Shishkina, S., Shishkin, O., Isaev, A. & Kas'yan, L. (2004). Reaction of endic anhydride with hydrazines and acylhydrazines. *Russian Journal of Organic Chemistry*, 40 (8), 1140-1145.

Krull, O. & Wunsch, B. (2004) Synthesis and structure/NMDA receptor affinity relationships of 1-substituted tetrahydro-3-benzazepines. *Bioorganic & Medicinal Chemistry*, 12, 1439-1451.

Kukkonen, J. (2009) An easy ratiometric compensation for the extracellular Ca²⁺ indicator-caused fluorescence artefact. *Analytical Biochemistry*, 390, 212-214.

Kumar, A., Davuluri, G., Welch, N., Kim, A., Gangadhariah, M., Allawy, A., Priyadarshini, A., McMullen, M., Sandler, Y., Willard, B., Hoppel, C., Nagy, L. & Dasarathy, S. (2019) Oxidative stress mediates ethanol-induced skeletal muscle mitochondrial

dysfunction and dysregulated protein synthesis and autophagy. *Free Radical Biology and Medicine*, 145, 284-299.

Kumar, M., John, M., Mayadevi, M., James, J. & Omkumar, R. (2019) Alteration in the phosphorylation status of NMDA receptor GluN2B subunit by activation of both NMDA receptor and L-type voltage gated calcium channel. *Neuroscience letters*, 709, 134343. Available at <https://doi.org/10.1016/j.neulet.2019.134343>: accessed January 24, 2020.

Kumar, V., Sami, N., Kashav, T., Islam, A., Ahmad, F. & Hassan, M. (2016) Protein aggregation and neurodegenerative diseases: From theory to therapy. *European Journal of Medicinal Chemistry*, 124, 1105-1120.

Kushnir, A. & Marx, S. (2018) Chapter 2: Voltage-gated calcium channels. **In Zipes, D, Jalife, J. & Stevenson, W. Ed.** *Cardiac Electrophysiology: From cell to Bedside*, 7th Edition, Elsevier Inc., Philadelphia, 12-24.

Lai, T., Zhang, S. & Wang, Y. (2014) Excitotoxicity and stroke: Identifying novel targets for neuroprotection. *Progress in Neurobiology*, 115, 157-188.

Landolfi, A., Troisi, J., Savanelli, M. C., Vitale, C., Barone, P. & Amboni, M. (2017) Bisphenol A glucuronidation in patients with Parkinson's disease. *NeuroToxicology*, 63, 90-96.

Lazniewska, J. & Weiss, N. (2017) Glycoylation of voltage-gated calcium channels in health and disease. *Biochimica et Biophysica Acta*, 1859, 662-668.

Lee, D., Kim, C. & Lee, Y. (2011) Astaxanthin protects against MPTP/MPP⁺-induced mitochondrial dysfunction and ROS production *in vivo* and *in vitro*. *Food and Chemical Toxicology*, 49, 271-280.

Lee, J., Yon, J., Lin, C., Jung, A., Jung, K. & Nam, S. (2012) Combined treatment with capsaicin and resveratrol enhances neuroprotection against glutamate-induced toxicity in mouse cerebral cortical neurons. *Food and Chemical Toxicology*, 50, 3877-3885.

Lee, M., Ban, J., Kim, K., Jeon, G., Im, W., Sung, J & Kim, M. (2016) Adipose-derived stem cell exosomes alleviate pathology of amyotrophic lateral sclerosis *in vitro*. *Biochemical and Biophysical Research Communications*, 479, 434-439.

Leggio, A., Bagala, J., Belsito, E., Comande, Greco, M. & Liguori, A. (2017) Formation of amides: one-pot condensation of carboxylic acids and amines mediated by TiCl₄. *Chemistry Central Journal*, 11, 87.

Leist, M. & Nicotera, P. (1998) Apoptosis, excitotoxicity, and neuropathology. *Experimental Cell Research*, 239, 183-201.

Leoni, A., Frosini, M., Locatelli, A., Micucci, M., Carotenuto, C., Durante, M., Cosconati, S. & Budriesi, R. (2019) 4-Imidazo[2,1-*b*]thiazole-1,4-DHPs and neuroprotection: preliminary study in hits searching. *European Journal of Medicinal Chemistry*, 169, 89-102.

Lesyk, R., Zimenkovsky, B., Atamanyuk, D., Jensen, F., Kiec-Kononowicz, K. & Gzella, A. (2006) Anticancer thiopyrona[2,3-*d*][1,3]thiazol-2-ones with norbornane moiety. Synthesis, cytotoxicity, physico-chemical properties, and computational studies. *Bioorganic & Medicinal Chemistry*, 14, 5230-5240.

Lev-Ram, V. & Grinvald, A. (1987) Activity-dependent calcium transients in central nervous system myelinated axons revealed by the calcium indicator Fura-2. *The Biophysical Journal*, 52, 571-576.

Liddle, R. (2018) Parkinson's disease from the gut. *Brain Research*, 1693 (Pt B), 201-206.

Lin, G., Sun, Y., Long, J., Sui, X., Yang, J., Wang, Q., Wang, S., He, H., Luo, Y., Qiu, Z. & Wang, Y. (2020) Involvement of the NrF2-Keap1 signalling pathway in protection against thallium-induced oxidative stress and mitochondrial dysfunction in primary hippocampal neurons. *Toxicology Letters*, 319, 86-73.

Lipscombe, D. Andrade, A. & Allen, S. (2013) Alternative splicing: functional diversity among voltage-gated calcium channels and behavioural consequences. *Biochimica et Biophysica Acta*, 1828, 1522-1529.

Lipton, S. (2004) Failures and successes of NMDA receptors Antagonists: Molecular basis for the use of open-channel blockers like memantine in the treatment of acute and chronic neurologic insults. *The Journal of the American Society for Experimental NeuroTherapeutics*, 1, 101-110.

Liu, J., Fan, Y., Kim, D., Zhong, T., Yi, P., Fan, C., Wang, A., Yang, X., Lee, S., Ren, X. & Xu, Y. (2019) Neuroprotective effect of catechins derivatives isolated from Anhua dark tea

on NMDA-induced excitotoxicity in SH-SY5Y cells. *Fitoterapia*, 137, 104240. Available at <https://doi.org/10.1016/j.fitote.2019.104240>: accessed January 23, 2020.

Liu, Z., Qiu, X., Shingung, M., Guo, B., Hu, S., Wang, J., Luo, F., Xu, D., Sun, Y., Zhang, G., Cui, G., Wang, Y., Zhang, Z. & Han, Y. (2020) Multifunctional memantine nitrate significantly protects against glutamate-induced excitotoxicity *via* inhibiting calcium influx and attenuating PI3K/Akt/GSK3beta pathway. *Chemico-Biological Interactions*, 109020. Available at <https://doi.org/10.1016/j.cbi.2020.109020>: accessed March 12, 2020.

Lockman, J., Geldenhuys, W., Jones-Higgins, M., Patrick, J., Allen, D. & Van der Schyf, C. (2012) NGP1-01, a multi-targeted polycyclic cage amine, attenuates brain endothelial cell death in iron overload conditions. *Brain Research*, 1489, 133-139.

Ludtmann, M. & Abramov, A. (2018) Mitochondrial calcium imbalance in Parkinson's disease. *Neuroscience Letters*, 663, 86-90.

Luo, Y., Wang, Q. & Zhang, Y. (2016) A systems pharmacology approach to decipher the mechanism of danggui-shaoyao-san decoction for the treatment of neurodegenerative diseases. *Journal of Ethnopharmacology*, 178, 66-81.

Luoma, J., Kelley, B. & Mermelstein, P. (2011) Progesterone inhibition of voltage-gated calcium channels is a potential neuroprotective mechanism against excitotoxicity. *Steroids*, 76, 845-855.

Lutnant, I., Schepmann, D. & Wunsch, B. (2016) Benzimidazolone bioisosteres of potent GluN2B selective NMDA receptor antagonist. *European Journal of Medicinal Chemistry*, 116, 136-146.

Maccioni, R., Munoz, J. & Barbeito, L. (2001) The molecular bases of Alzheimer's Disease and other neurodegenerative disorders. *Archives of Medical Research*, 32, 367-381.

Malhotra, R. (2018) Neurodegenerative disorders and sleep. *Sleep Medicine Clinics*, 13 (1), 63-70.

Mao, C., Yang, Y., Chen, J., Wang, F., Chen, J., Zhang, J., Zhang, H., Zhaung, S., Xiong, Y., Gu, C., Yuan, W., Huang, J., Fay, A., Zhong, C. & Liu, C. (2018) Poor nighttime sleep is positively associated with dyskinesia in Parkinson's disease patients. *Parkinsonism and Related Disorders*, 48, 68-73.

- Matej, R., Tesar, A. & Rusina, R. (2019)** Alzheimer's disease and other neurodegenerative dementias in comorbidity: A clinical and neuropathological overview. *Clinical Biochemistry*, 73, 26-31.
- Mathis, S., Goizet, C., Soulages, A., Vallat, J. & Masson, G. (2019)** Genetics of amyotrophic lateral sclerosis: A review. *Journal of the Neurological Sciences*, 399, 217-226.
- Mattson, M. (2019)** Chapter 11 - Excitotoxicity. In *Stress: Physiology, Biochemistry, and Pathology*. Handbook of Stress Series, 3, 125-134.
- Mauleon, G., Lo, J., Peterson, B., Fall, C. & Eddington, D. (2013)** Enhanced loading of Fura-2/AM calcium indicator dye in adult rodent brain slices via a microfluidic oxygenator. *Journal of Neuroscience Methods*, 216, 110-117.
- Mazibuko, Z., Choonara, Y., Kumar, P., Du Toit, L., Modi, G., Naidoo, D. & Pillay, V. (2015)** A Review of the Potential Role of Nano-Enabled Drug Delivery Technologies in Amyotrophic Lateral Sclerosis: Lessons Learned from Other Neurodegenerative Disorders. *Journal of Pharmaceutical Sciences*, 104, 1213-1229.
- McDonough, S. (2007)** Gating modifier toxins of voltage-gated calcium channels. *Toxicon*, 49, 202-212.
- Mdzinarishvili, A., Geldenhuys, W., Abbruscato, T., Bickel, U., Klein, J. & Van der Schyf, C. (2005)** NGP1-01, a lipophilic polycyclic cage amine, is neuroprotective in focal ischemia. *Neuroscience Letters*, 383, 49-53.
- Medina-Ramos, W., Mojica, M., Cope, E., Hart, R., Pollet, P., Eckert, C. & Liotta, C. (2014)** Water at elevated temperatures (WET): reactant, catalyst, and solvent in the selective hydrolysis of protecting groups. *Green Chemistry*, 16, 2147-2155.
- Mehta, A., Prabhakar, M., Kumar, P., Deshmukh, R. & Sharma, P. (2013)** Excitotoxicity: Bridge to various triggers in neurodegenerative disorders. *European Journal of Pharmacology*, 698, 6-18.
- Meijer, M., Hendriks, H., Heusinkveld, H., Langeveld, W. & Westerink, R. (2014)** Comparison of plate reader-based methods with fluorescence microscopy for measurements of intracellular calcium levels for the assessment of *in vitro* neurotoxicity. *NeuroToxicology*, 45, 31-37.

Mellone, M. & Gardoni, F. (2013) Modulation of NMDA receptor at the synapse: Promising, therapeutic interventions in disorders of the nervous system. *European Journal of Pharmacology*, 719, 75-83.

Mereshchenko, A., Ivanov, A., Baranovskii, V., Mloston, G., Rodina, L., & Nikolaev, V. (2015) On the strong difference in reactivity of acyclic and cyclic diazodiketones with thioketones: experimental results and quantum-chemical interpretation. *Beilstein Journal of Organic Chemistry*, 11, 504-513.

Mestre, T. & Ferreira, J. (2012) An evidence-based approach in the treatment of Huntington's disease. *Parkinsonism and Related Disorders*, 18, 316-320.

Migliore, L. & Coppede, F. (2009) Environmental-induced oxidative stress in neurodegenerative disorders and aging. *Mutation Research/Genetic Toxicology and Environmental mutagenesis*, 674, 73-84

Miller, N., Chou, K., Bohnen, N., Muller, M. & Seidler, R. (2018) Dopaminergic polymorphisms associated with medication responsiveness of gait in Parkinson's disease. *Parkinsonism and Related Disorders*, 48, 54-60.

Moraes, B., Coelho, P., Fao, L., Ferreira, I. & Rego, A. (2020) Modified glutamatergic postsynapse in neurodegenerative disorders. *Neuroscience*. Available at <https://doi.org/10.1016/j.neuroscience.2019.12.002>: accessed February 26, 2020.

Moreau, A. & Kullmann, D. (2013) NMDA receptor-dependent function and plasticity in inhibitory circuits. *Neuropharmacology*, 74, 23-31.

Moreira, P., Zhu, X., Wang, X., Lee, H., Nunomura, A., Petersen, R., Perry, G. & Smith, M. (2012) Mitochondria: A therapeutic target in neurodegeneration. *Biochimica et Biophysica Acta*, 1802 (1), 212-220.

Mufson, E., Ikonovic, M., Counts, S., Perez, S., Malek-Ahmadi, M., Scheff, S. & Ginsberg, S. (2016) Molecular and cellular pathophysiology of preclinical Alzheimer's disease. *Behavioural Brain Research*, 311, 54-69.

Mulpuri, S., Shin, J., Shin, B., Greiner, A. & Yoon, D. (2011) Synthesis and characterization of substituted polynorbornene derivatives. *Polymers*, 52, 4377-4386.

Musgrove, R., Jewell, S., Di Monte, D. (2015) Chapter 10 – overview of Neurodegenerative disorders and susceptibility factors in neurodegenerative processes. **In Aschner, M. & Costa,**

L. Ed. Environmental Factors in neurodevelopmental and Neurodegenerative Disorders, Academic Press, London, 172-210.

Nagasawa, M., Sakimura, K., Mori, K., Bedell, M., Copeland, N., Jenkins, N. & Mishina, M. (1996) Gene structure and chromosomal localisation of the mouse NMDA receptor channel subunits. *Molecular Brain Research*, 36, 1-11.

Nanou, E. & Catterall, W. (2018) Calcium channels, synaptic plasticity, and neuropsychiatric disease, *Neuron*, 98, 466-481.

Neal, M. & Richardson, J. (2018) Time to get personal: A framework for personalised targeting of oxidative stress in neurotoxicity and neurodegenerative disease. *Current Opinion in Toxicology*, 7, 127-132.

Neher, E. (1995) The use of Fura-2 for estimating Ca buffers and Ca fluxes. *Neuropharmacology*, 24 (11), 1423-1442.

Nery, E., Jastrzebska, E., Zukowski, K., Wroblewski, W., Chudy, M. & Ciosek, P. (2014) Flow-through sensor array applied to cytotoxicity assessment in cell cultures for drug-testing purposes. *Biosensors and Bioelectronics*, 51, 55-61.

Neumaier, F., Dibue-Adjei, M., Hescheler, J. & Schneider, T. (2015) Voltage-gated calcium channels: Determinants of channel function and modulation by inorganic cations. *Progress in Neurobiology*, 129, 1-36

Nido, G., Dolle, C., Flonas, I., Tuppen, H., Alves, G., Tysines, O., Haugarvoll, K. & Tzoulis, C. (2018) Ultradeep mapping of neuronal mitochondrial deletions in Parkinson's disease. *Neurobiology of Aging*, 63, 120-127.

Nieto-Rostro, M., Sandhu, G., Bauer, C., Jiruska, P., Jefferys, J. & Dolphin, A. (2014) Altered expression of the voltage-gated calcium channel subunit $\alpha_2\delta-1$: A comparison between two experimental models of epilepsy and a sensory nerve ligation model of neuropathic pain. *Neuroscience*, 283, 124-137.

Nirale, P., Paul, A. & Yadav, K. (2020) Nanoemulsions for targeting the neurodegenerative diseases: Alzheimer's, Parkinson's and Prion's. *Life Sciences*, 245, 117394. Available at <https://doi.org/10.1016/j.lfs.2020.117394>: accessed February 12, 2020.

Nomura, E., Ohta, T., Tadokoro, K., Shang, J., Feng, T., Liu, X., Shi, X., Matsumoto, N., Sasaki, R., Tsunoda, K., Sato, K., Takemoto, M., Hishikawa, N., Yamashita, T.,

Kuchimaru, T., Kizaka-Kondoh, S. & Abe, K. (2019) Imaging hypoxic stress and the treatment of amyotrophic lateral sclerosis with dimethylallylglycine in mice model. *Neuroscience*, 415, 31-43.

Obata, T. (2019) Glutaminergic tonic action potentiates MPP⁺-induced hydroxyl radical production in rat striatum. *Neuroscience Letters*, 705, 51-53.

Oosterloo, M., Bijlsma, E., Van Kuijk, S., Minkels, F. & de Die-Smulders, C. (2019) Clinical and genetic characteristics of late-onset Huntington's disease. *Parkinsonism and Related Disorders*, 61, 101-105.

Ossola, B., Schendzielorz, N., Chen, S., Bird, G., Tuominen, R., Mannisto, P. & Hong, J. (2011) Amantadine protects dopamine neurons by a dual action: reducing activation of microglia and inducing expression of GDNF in astroglial. *Neuropharmacology*, 61, 574-582.

Ozben, T. & Ozben, S. (2019) Neuro-inflammation and anti-inflammatory treatment options for Alzheimer's disease. *Clinical Biochemistry*, 72, 87-89.

Palchikov, V., Tarabara, I., Krishchik, O., Omelchenko, I., Shishkina, S., Shishkin, O. & Kasyan, L. (2014) *exo*-2,3-Epoxybicyclo[2.2.1]heptan-*endo*-5,6-dicarboximides: versatile starting materials for the preparation of oxazaheterocyclic cage compounds. *Monatshefte für Chemie*, 145, 1155-1163.

Park, E., Lee, G., Choi, S., Choi, S., Chae, S., Kang, S. & Park, H. (2010) correlation between extracellular glutamate release and neuronal cell death in an eleven vessel occlusion model in rat. *Brain Research*, 1342, 160-166.

Park, H., Kwak, M. & Baek, S. (2020) Neuroprotective effects of *Dendropanax morbifera* leaves on glutamate-induced oxidative cell death in HT22 mouse hippocampal neuronal cells. *Journal of Ethnopharmacology*, 251, 112518. Available at <https://doi.org/10.1016/j.jep.2019.112518>: accessed January 23, 2020.

Pchitskaya, E., Popugaeva, E. & Bezprozvanny, I. (2018) Calcium signalling and molecular mechanisms underlying neurodegenerative diseases. *Cell Calcium*, 70, 87-94.

Pena-Bautista, C., Vento, M., Baquero, M. & Chafer-Pericas, C. (2019) Lipid peroxidation in neurodegeneration. *Clinica Chimica Acta*, 497, 178-188.

Peng, Z., Luchtman, D., Wang, X., Zhang, Y. & Song, C. (2019) Activation of microglia synergistically enhances neurodegeneration caused by MPP⁺ in human SH-SY5Y cells. *European Journal of Pharmacology*, 850, 64-74.

Pereira, E., Braga-de-souza, S., Santos, C., Santos, L., Cerqueira, M., Ribeiro, P., Fernandez, L., Silva, V. & Costa, S. (2017) *Amburana cearensis* seed extracts protect PC-12 cells against toxicity induced by glutamate. *Brazilian Journal of Pharmacognosy*, 27, 199-205.

Pezzi, J., Boshcman Ens De Bem, C., da Rocha, T., Schumacher-Schuh, A., Chaves, M., Rieder, C., Hutz, M., Fiegenbaum, M. & Camozzato, A. (2017) Association between DNA methyltransferase gene polymorphism and Parkinson's disease. *Neuroscience Letters*, 639, 146-150.

Piedras-Renteria, E., Barrett, C., Cao, Y. & Tsien, R. (2007) Voltage-gated calcium channels, calcium signalling, and channelopathies. *New Comprehensive Biochemistry*, 41, 127-166.

Prins, L., du Preez, J., van Dyk, S. & Malan, S. (2009) Polycyclic cage structures as carrier molecules for neuroprotective non-steroidal anti-inflammatory drugs. *European Journal of Medicinal Chemistry*, 44, 2577-2582.

Procaccini, C. Santopaolo, M., Faicchia, D., Colamatteo, A., Formisano, L., de Candia, P., Galgani, M., De Rosa, V. & Matarese, G. (2016) Role of metabolism in neurodegenerative disorders. *Metabolism Clinical and Experimental*, 65 (9), 1376-1390.

Prolla, T. & Mattson, M. (2001) Molecular mechanisms of brain aging and neurodegenerative disorders: lessons from dietary restriction. *Trends in Neurosciences*, 24 (11), 21-31.

Qureshi, I.A. & Mehler, M.F. (2013) Epigenetic mechanisms governing the process of neurodegeneration. *Molecular Aspects of Medicine*, 34 (4), 875-882.

Regan, M., Grant, T., McDaniel, M., Karakas, E., Zhang, J., Traynelis, S., Grigorieff, N. & Furukawa, H. (2018) Structural mechanism of functional modulation by gene splicing in NMDA receptors. *Neuron*, 98, 521-528.

Reid, W. & Bellinger, O. (1984) Das Verhalten von (1 α ,2 α ,5 α ,6 α)-3,4-Bis(trimethylsiloxy)tricyclo[4.2.1.0^{2,5}]nona-3,7-dien gegenüber Oxidationsmitteln. *Liebigs Annalen de Chemie*, 1778-1784.

Riebell, C., Piret, J., Trouiller, B., Nelissen, I., Saout, C., Toussaint, O. & Haase, A. (2018) A guide to nanosafety testing: Considerations on cytotoxicity testing in different cell models. *NanoImpact*, 10, 1-10.

Rivero-Segura, N., Coronado-Mares, M., Rincon-Heredia, R., Perez-Torres, I., Montiel, T., Pavon, N., Cabrera-Reyes, E., Massieu, L. & Cerbon, M. (2019) Prolactin prevents mitochondrial dysfunction induced by glutamate excitotoxicity in hippocampal neurons. *Neuroscience Letters*, 701, 58-64.

Robinson, J. Jenkins, N., Holman, N., Roberts-Thomson, S. & Monteith, G. (2004) Ratiometric and nonratiometric Ca^{2+} in a breast cancer cell line using a fluorescence microplate reader. *Journal of Biochemical and Biophysical Methods*, 58, 227-237.

Rodriguez-Martinez, E., Martinez, F., Espinosa-Garcia, M., Maldonado, P. & Rivas-Arancibia, S. (2013) Mitochondrial dysfunction in the hippocampus of rats caused by chronic oxidative stress. *Neuroscience*, 252, 384-395.

Roppongi, T., Tohgo, T., Nakamura, S., Asami, T., Yoshimi, A., Shiozaki, K., Kato, D., Kawanishi, C. & Hirayasu, Y. (2007) Perospirone in treatment of Huntington's disease: A first case report. *Progress in Neuro-Psychopharmacology & Biological Psychiatry*, 31, 308-310.

Ross, C. & Tabrizi, S. (2011) Huntington's disease: from molecular pathogenesis to clinical treatment. *The Lancet of Neurology*, 10, 83-98.

Ruffels, J., Griffin, M. & Dickenson, J. (2004) Activation of ERK1/2, JNK and PKB by hydrogen peroxide in human SH-SY5Y neuroblastoma cells: role of ERK1/2 in H_2O_2 -induced cell death. *European Journal of Pharmacology*, 483, 163-173.

Rzaeva, A., Ramazanova, E., Ataev, M. & Shabanov, A. (2007) Diels-Alder reaction at a cathode. *Azerbaidzhanskii Khimicheskii Zhurnal*, 1, 78-80.

Sala, M., Hrebabecky, H., Dracinsky, M., Masojidkova, M., De Palma, A., Neyts, J. & Holy, A. (2009) Norbornane as the novel pseudoglycone moiety in nucleosides. *Tetrahedron*, 65, 9291-9299.

Sala, M., De Palma, A., Hrebabecky, H., Dejmek, M., Dracinsky, M., Leyssen, P., Neyts, J., Mertlikova-Kaiserova, H. & Nencka, R. (2011) SAR studies of 9-norbornylpurines as Cocksackoevirus B3 Inhibitors. *Bioorganic & Medicinal Chemistry Letters*, 21, 4271-4275.

Sala, M., Hrebabecky, H., Leyssen, P., Dejmek, M., Dracinsky, M., De Palma, A., Neyts, J. & Nencka, R. (2012) Novel substituted 9-norbornylpurines and their activities against RNA viruses. *Bioorganic & Medicinal Chemistry Letters*, 22, 1963-1968.

Sas, K., Robotka, H., Toldi, J. & Vecsei, L. (2007) Mitochondria, metabolic disturbances, oxidative stress and the kynurenine system, with focus on neurodegenerative disorders. *Journal of the Neurological Sciences*, 257, 221-239.

Saravi, S. & Dehpour, A. (2016) Potential role of organochlorine pesticides in the pathogenesis of neurodevelopmental, neurodegenerative, and neurobehavioral disorders: A review. *Life Sciences*, 145, 255-264.

Sathyanarayanamoorthi, V., Mahalakshmi, S. & Kannappan, V. (2010) Polarizable continuum studies on auxin derivatives. *Journal of Molecular Liquids*, 154, 88-93.

Seko, T., Kato, M., Kohno, H., Ono, S., Hashimura, K., Takimizu, H., Nakai, K., Maegawa, H., Katsube, N., Toda, M. (2003) Structure-activity study of L-amino acid-based N-type calcium channel blockers. *Bioorganic & Medicinal Chemistry*, 11, 1901-1913.

Shinoda, Y., Nakajima, Y., Iguchi, H., Tatsumi, S., Kitaoka, M., Nakajima, M., Takahashi, T., Fujiwara, Y. & Furuichi, T. (2016) Galacto-*N*-biose is neuroprotective against glutamate-induced excitotoxicity *in vitro*. *European Journal of Pharmacology*, 791, 711-717.

Shishido, T., Nagano, Y., Araki, M., Kurashige, T., Obayashi, H., Nakamura, T., Takahashi, T., Matsumoto, M. & Maruyama, H. (2019) Synphillin-1 has neuroprotective effects on MPP⁺-induced Parkinson's disease model cells by inhibiting ROS production and apoptosis. *Neuroscience Letters*, 690, 145-150.

Simms, B. & Zamponi, G. (2014) Neuronal voltage-gated calcium channels: Structure, function, and dysfunction. *Neuron*, 82, 24-45.

Singh, A., Verma, P., Balaji, G., Samantaray, S. & Mohanakumar, K. (2016) Nimodipine, an L-type calcium channel blocker attenuates mitochondrial dysfunctions to protect against 1-methyl-4-phenyl-1,2,3,6-tetrahydropyridine-induced Parkinsonism in mice. *Neurochemistry International*, 99, 221-232.

Singh, A., Agarwal, S. & Singh, S. (2020) Age related neurodegenerative Alzheimer's disease: Usage of traditional herbs in therapeutics. *Neuroscience Letters*, 717, 134679. Available at <https://doi.org/10.1016/j.neulet.2019.134679>: accessed February 11, 2020.

Sivandzade, F., Prasad, S., Bhalerao, A. & Cuccullo L. (2019) NRF2 and NF- κ B interplay in cerebrovascular and neurodegenerative disorders: Molecular mechanisms and possible therapeutics approaches. *Redox Biology*, 21, 101059. Available at <https://doi.org/10.1016/j.redox.2018.11.017>: accessed February 15, 2020.

Smidkova, M., Hajek, M., Adla, S., Slavikova, B., Chodounska, H., Matousova, M., Mertlikova-Kaiserova, H. & Kudova, E. (2019) Screening of novel $3\alpha5\beta$ -neurosteroids for neuroprotective activity against glutamate- or NMDA induced excitotoxicity. *Journal of Steroid of Biochemistry and Molecular Biology*, 189, 195-203.

Snutch, T. (2009) Voltage-gate calcium channels. *Encyclopedia of Neuroscience*, 427-441.

Sonkusare, S. & Ramarao, K. (2005) Dementia of Alzheimer's disease and other neurodegenerative disorders-memantine, a new hope. *Pharmacological Research*, 51, 1-17.

Sorolla, M., Reverter-Branchat, G., Tamarit, J., Ferrer, I., Ros, J. & Cabisco, E. (2008) Proteomic and oxidative stress analysis in human brain samples of Huntington disease. *Free Radical Biology & Medicine*, 45, 667-678.

Steinbach, R., Batyrbekova, M., Gaur, N., Voss, A., Stubendorff, B., Mayer, T., Gaser, C., Witte, O., Prell, T. & Grosskreutz, J. (2020) Applying the D50 disease progression model to gray and white matter pathology in amyotrophic lateral sclerosis. *NeuroImage: Clinical*, 25, 102094. Available at <https://doi.org/10.1016/j.nicl.2019.102094>: accessed February 11, 2020.

Steinbrecht, S., Konig, R., Schmidtke, K., Herzog, N., Scheibner, K., Kruger-Genge, A., Jung, F., Kammerer, S. & Kupper, J. (2019) Metabolic activity testing can underestimate acute drug cytotoxicity as revealed by HepG2 cell clones overexpressing cytochrome P450 2C19 and 3A4. *Toxicology*, 412, 37-47.

Steventon, S. & Mitchell, S. (2018) Phenylalanine hydroxylase: A biomarker of disease susceptibility in Parkinson's disease and amyotrophic lateral sclerosis. *Medical Hypotheses*, 119, 29-33.

Stringer, J. Ed. Chapter 20: Drug used in Parkinson's disease. In: *Basic Concepts in Pharmacology: What You need to know for Each Drug class*, 5th edition, New York, NY:

McGraw-Gill. Available at <http://accesspharmacy.mhmedical.com/content.aspx?bookid=2147§ionid=161351745>: accessed July 13, 2019.

Stroebel, D., Casado, M. & Paoletti, P. (2018) Triheteromeric NMDA receptors: from structure to synaptic physiology. *Current Opinion in Physiology*, 2, 1-12.

Sun, F., Zhang, L., Zhang, R. & Li, L. (2011) Tetrahydroxystilbene glucoside protects human neuroblastoma SH-SY5Y cells against MPP⁺-induced cytotoxicity. *European Journal of Pharmacology*, 660, 283-290.

Swalley, S. (2020) Expanding therapeutic opportunities for neurodegenerative diseases: A perspective on the important role of phenotypic screening. *Bioorganic & medicinal Chemistry*, 28, 115239. Available at <https://doi.org/10.1016/j.bmc.2019.115239>: accessed March 10, 2020.

Swart, C., Haylett, W., Kinnear, C., Johnson, G., Bardien, S. & Loos, B. (2014) Neurodegenerative disorders: Dysregulation of carefully maintained balance? *Experimental Gerontology*, 58, 279-291.

Szmacinski, H. & Lakowicz, J. (1995) Possibility of simultaneously measuring low and high calcium concentrations using Fura-2 and lifetime-based sensing. *Cell Calcium*, 18, 64-75.

Tarabara, I., Kas'yan, A., Yarovoi, M., Shishkina, S., Shishkin, O. & Kas'yan, L. (2004). Reaction of Bicyclo[2.2.1]hept-5-ene-2,3-dicarboximides with aromatic azides. *Russian Journal of Organic Chemistry*, 40 (7), 992-998.

Taveira, M., Sousa, C., Valentao, P., Ferreres, F., Teixeira, J. & Andrade, P. (2014) Neuroprotective effect of steroidal alkaloids on glutamate-induced toxicity by preserving mitochondrial membrane potential and reducing oxidative stress. *Journal of Steroid Biochemistry and Molecular Biology*, 140, 106-115.

Temme, L., Bechthold, E., Schreiber, J., Gawaskar, S., Schepmann, D., Robaa, D., Sippl, W., Seebohm, G. & Wunsch, B. (2020) Negative allosteric modulators of the GluN2N NMDA receptor with phenylethylamine structure embedded in ring-expanded and ring contracted scaffolds. *European Journal of Medicinal Chemistry*, 190, 112138. Available at <https://doi.org/10.1016/j.ejmech.2020.112138>: accessed February 27, 2020.

Tomycz, N. D. (2016) The proposed use of cervical spinal cord stimulation for the treatment and prevention of cognitive decline in dementias and neurodegenerative disorders. *Medical Hypotheses*, 96, 83-86.

Tripathi, R. & Ayyannan, S. (2017) Anticonvulsant activity, organotypic hippocampal neuroprotection assay and in-silico sodium channel blocking potential of 2-amino-6-nitrobenzothiazole derived semicarbazones. *Biomedicine & Pharmacotherapy*, 95, 1451-1460.

Tuluc, P., Yarov-Yarovoy, V., Benedetti, B. & Flutcher, B. (2016) Molecular interactions in the voltage sensor controlling gating properties of Cav calcium channels. *Structure*, 24, 261-271.

Tovar, K. & Westbrook, G. (2017) Modulating synaptic NMDA receptor. *Neuropharmacology*, 112, 29-33.

Tuovinen, N., Seppi, K., De Pasquale, F., Muller, C., Nocker, M., Schocke, M., Gizewski, E., Kremser, C., Wenning, G., Poewe, W., Djamshidian, A., Scherfler, C. & Seki, M. (2018) The reorganisation of functional architecture in the early-stages of Parkinson's disease. *Parkinsonism and Related Disorders*, 50, 61-68.

Vadakkan, K. (2016) Neurodegenerative disorders share common features of "loss of function" states of a proposed mechanism of nervous system functions. *Biomedicine & Pharmacotherapy*, 83, 412-430.

Valionyte, E., Yang, Y., Roberts, S., Kelly, J., Lu, B. & Luo, S. (2020) Lowering mutant Huntingtin levels and toxicity: Autophagy-Endolysosome pathways in Huntington's disease. *Journal of Molecular Biology*. Available at <https://doi.org/10.1016/j.jmb.2019.11.012>: accessed February 14, 2020.

Valor, L. (2015) Epigenetic-based therapies in the preclinical and clinical treatment of Huntington's disease. *The International Journal of Biochemistry & Cell Biology*, 67, 45-48.

Van Der Burg, J., Bjorkqvist, M. & Brundin, P. (2009) Beyond the brain: widespread pathology in Huntington's disease. *The Lancet of Neurology*, 8, 765-774.

Van der Schyf, C. & Geldenhuys, W. (2009) Polycyclic compounds: ideal drug scaffolds for the design of multiple mechanism drugs? *Neurotherapeutic: The Journal of the American Society for Experimental NeuroTherapeutics*, 6, 175-186.

Van Eijk, R., Nikolakopoulos, S., Ferguson, T., Liu, D., Eijkemans, M. & van den Berg, L. (2018) Increasing the efficiency of clinical trials in neurodegenerative disorders using group sequential trial designs. *Journal of Clinical Epidemiology*, 98, 80-88.

Vincenzetti, S., Nasuti, C., Fedeli, D., Ricciutelli, M., Pucciarelli, S. & Gabbianelli. (2016) Proteomic analysis for early neurodegenerative biomarker detection in an animal model. *Biochimie*, 121, 79-86.

Vinceti, M., Filippini, T., Malagoli, C., Violi, F., Mandrioli, J., Consonni, D., Rothman, K. & Wise, L. (2019) Amyotrophic lateral sclerosis incidence following exposure to inorganic selenium in drinking water: A long-term follow-up. *Environmental Research*, 179, 108742. Available at <https://doi.org/10.1016/j.envres.2019.108742>: accessed February 11, 2020.

Vinken, M. & Blauboer, B. (2017) *In vitro* testing of basal cytotoxicity: Establishment of an adverse outcome pathway from chemical insult to cell death. *Toxicology in Vitro*, 39, 104-110.

Vranova, H., Henykova, E., Mares, J., Kaiserova, M., Mensikova, K., Vastic, M., Hlustik, P., Zapletalova, J., Stmad, M., Stejskal, D. & Kanovsky, P. (2016) Clusterin CSF levels in differential diagnosis of neurodegenerative disorders. *Journal of the Neurological Sciences*, 361, 117-121.

Walter, C., Clemens, L., Muller, A., Fallier-Becker, P., Proikas-Cezanne, T., Riess, O., Metzger, S. & Nguyen, H. (2016) Activation of AMPK-induced autophagy ameliorates Huntington disease pathology *in vitro*. *Neuropharmacology*, 108, 24-38.

Wang, H., Wang, Y., Zhao, L., Cui, Q., Wang, Y. & Du, G. (2016) Pinocembrin attenuates MPP⁺-induced neurotoxicity by the induction of heme oxygenase-1 through ERK1/2 pathway. *Neuroscience Letters*, 612, 104-109.

Wang, H., Zhao, P., Huang, Q., Chi, Y., Dong, S. & Fan, J. (2019) Bisphenol-A induces neurodegeneration through disturbance of intracellular calcium homeostasis in human embryonic stem cells-derived cortical neurons. *Chemosphere*, 229, 618-630.

Wang, M., Dolphin, A. & Kitmitto, A. (2004) L-type voltage-gated calcium channels: understanding function through structure. *FEBS Letters*, 564, 245-230.

Wang, X., Wang, W., Li, L., Perry, G., Lee, H. & Zhu, X. (2014) Oxidative stress and mitochondrial dysfunction in Alzheimer's disease. *Biochimica et Biophysica Acta*, 1842, 1240-1247.

Wang, X. & Xu, J. (2005) Salvianic acid: A protects human neuroblastoma SH-SY5Y cells against MPP⁺-induced cytotoxicity. *Neuroscience Research*, 51, 129-138.

Wang, Y., Miao, Y., Mir, A., Cheng, L., Wang, L., Zhan, L., Cui, Q., Zhao, W. & Wang, H. (2016) Inhibition of beta-amyloid-induced neurotoxicity by pinocembrin through Nrf2/HO-1 pathway in SH-SY5Y cells. *Journal of the Neurological Sciences*, 368, 223-230.

Wang, Y., Yu, X., Zhang, P., Ma, Y., Wang, L., Xu, H. & Sui, D. (2018) Neuroprotective effects of pramipexole transdermal patch in the MPTP-induced mouse model of Parkinson's disease. *Journal of Pharmacological Sciences*, 138, 31-37.

Wang, Y., Zhang, M., Li, Z., Yue, J., Xu, M., Zhang, Y., Yung, K. & Li, R. (2019) Fine particulate matter induces mitochondrial dysfunction and oxidative stress in human SH-SY5H cells. *Chemosphere*, 218, 577-588.

Warnock, A., Tan, L., Li, C., Haack, K., Narayan, S. & Bennett, M. (2013) Amlodipine prevents apoptotic cell death by correction of elevated intracellular calcium in a primary neuronal model of batten disease (CLN3 disease). *Biochemical and Biophysical Research Communications*, 436, 645-649.

Wilson, H., Giordano, B., Turkheimer, F., Chaudhuri, K. & Politis, M. (2018) Serotonergic dysregulation is linked to sleep problems in Parkinson's disease. *NeuroImage Clinical*, 18, 630-637.

Wu, Y., Chen, M. & Jiang, J. (2019) Mitochondrial dysfunction in neurodegenerative diseases and drug targets via apoptotic signalling. *Mitochondrion*, 49, 35-45.

Xu, D., Chen, H., Mak, S., Hu, S., Tsim, K., Hu, Y., Sun, Y., Zhang, G., Wang, Y., Zhang, Z. & Han, Y. (2016) Neuroprotection against glutamate-induced excitotoxicity and induction of neurite outgrowth by T-006, a novel multifunctional derivative of tetramethylpyrazine on neuronal cell models. *Neurochemistry International*, 99, 194-205.

Yacoubian, T. (2017) Chapter 1 - Neurodegenerative disorders: why do we need new therapies? **In Adejare, A. Ed.** *Drug Discovery Approaches for the treatment of Neurodegenerative Disorders Alzheimer's Disease*, Academic Press, London, 1-16.

Yamashita, T. & Kwak, S. (2014) The molecular link between inefficient GluA2 Q/R site-RNA editing and TDP-43 pathology in motor neurons of sporadic amyotrophic lateral sclerosis patients. *Brain Research*, 1584, 28-38.

Yang, D., Yang, Y. & Liu, Y. (2014) Study on the modulation of spectral properties of the formylperylene-methanol clusters by excited-state hydrogen bonding strengthening. *Spectrochimica Acta Part A: Molecular and Biomolecular Spectroscopy*, 117, 379-388.

Yang, E., Park, G. & Song, K. (2013) Neuroprotective effects of liquiritigenin isolated from licorice roots on glutamate-induced apoptosis in hippocampal neuronal cells. *NeuroToxicology*, 39, 114-123.

Yang, L., Lv, X., Du, X., Wu, D. & Wang, M. (2020) Causal effects of serum metabolites on amyotrophic lateral sclerosis: A Mendelian randomization study. *Progress in Neuropsychopharmacology & Biological Psychiatry*, 97, 10971. Available at <https://doi.org/10.1016/j.pnpbp.2019.109771>: accessed February 12, 2020.

Yang, P., Sheng, D., Guo, Q., Wang, P., Xu, S., Qian, K., Li, Y., Cheng, Y., Wang, L. Lu, W. & Zhang, Q. (2020) Neuronal mitochondria-targeted micelles relieving oxidative stress for delayed progression of Alzheimer's disease. *Biomaterials*, 238, 119844. Available at <https://doi.org/10.1016/j.biomaterials.2020.119844>: accessed February 16, 2020.

Yang, R., Cui, H., Wang, H., Wang, Y., Liu, J., Li, Y. & Lu, Y. (2014) *N*-Stearoyltyrosine protects against glutamate-induced oxidative toxicity by an apoptosis-inducing factor (AIF)-mediated caspase-independent cell death pathway. *Journal of Pharmacological Sciences*, 124, 169-179.

Yang, Y., Jiang, S., Yan, J., Li, Y., Xin, Z., Lin, Y. & Qu, Y. (2015) An overview of the molecular mechanisms and novel roles of Nrf2 in neurodegenerative disorders. *Cytokine & Growth Factor Reviews*, 26, 47-57.

Yang, Z., Cheng, W. & Li, Z. (2018) Iridium catalysed highly efficient transfer hydrogenation reduction of aldehydes and ketones in water. *Catalysis Communications*, 117, 38-42.

Youdim, M., Geldenhuys, W. & Van der Schyf, C. (2007) Why should we use multifunctional neuroprotective and neurorestorative drugs for Parkinson's disease? *Parkinsonism and Related Disorders*, 13, S281-S291.

Yu, A. & Lau, Y (2018) Glutamate and glycine binding to the NMDA receptor. *Structure*, 26, 1035-1043.

Zadori, D., Klivenyi, P., Szalardy, L., Fulop, F., Toldi, J. & Vecsei, L. (2012) Mitochondrial disturbances, excitotoxicity, neuroinflammation and kynurenines: Novel therapeutic strategies for neurodegenerative disorders. *Journal of the Neurological Sciences*, 322, 187-191.

Zambrano, P., Suwalsky, M., Jemiola-Rzeminska, M. & Strzalka, K. (2018) Studies on the interaction of NMDA receptor antagonist memantine with cell membranes: A mini-review. *Chemico-Biological Interactions*, 283, 47-50.

Zhang, C., Liang, W., Wang, H., Yang, Y., Wang, T., Wang, S., Wang, X., Wang, Y. & Feng, H. (2019) γ -Oryzanol mitigates oxidative stress and prevent mutant SOD1-related neurotoxicity in *Drosophila* and cell models of amyotrophic lateral sclerosis. *Neuropharmacology*, 160, 107777. Available at <https://doi.org/10.1016/j.neuropharm.2019.107777>: accessed February 12, 2020.

Zhang, J., Chang, S., Xu, P., Miao, M., Wu, H., Zhang, Y., Zhang, T., Wang, H., Zhang, J., Xie, C., Song, N., Luo, C., Zhang, X. & Zhu, S. (2018) Structural basis of the proton sensitivity of human GluN1-GluN2A NMDA receptors. *Cell Reports*, 25, 3582-3590.

Zhang, M., Hubbard, J., Rudnicki, S., Johansen, C., Dalton, K., Heiman-Patterson, T, Forshe, D. & Wills, A. (2013) Survey of current enteral nutrition practices in treatment of amyotrophic lateral sclerosis. *E-SPEN Journal*, 8, e25-e28.

Zhao, H., Sun, P., Fan, T., Yang, X., Zheng, T. & Sun, C. (2019) The effect of glutamate-induced excitotoxicity on DNA methylation in astrocytes in a new *in vitro* neuron-astrocyte-endothelium co-culture system. *Biochemical and Biophysical Research Communications*, 508, 1209-1214.

Zhao, S., Jia, Y. & Song, Y. (2013) Highly efficient and selective oxidation of various substrates under mild conditions using a lanthanum-containing polyoxometalate as catalyst. *Applied Catalysis A: General*, 453, 188-194.

Zheng, C., Zhou, M., Sun, J., Xiong, H, Peng, P., Gu, Z. & Deng, Y. (2019) The protective effects of liraglutide on AD-like neurodegeneration induced by oxidative stress in human neuroblastoma SH-SY5Y cells. *Chemico-Biological Interactions*, 310, 108688. Available at <https://doi.org/10.1016/j.cbi.2019.06.001>: accessed November 05, 2019.

Zhou, J., Sun, Y., Zhao, X., Deng, Z. & Pu, X. (2013) 3-O-demethylswertipunicoside inhibits MPP⁺-induced oxidative stress and apoptosis in PC12 cells. *Brain Research*, 1508, 63-62.

Zito, K. & Scheuss, V. (2009) NMDA receptor function and physiological modulation. Encyclopaedia of Neuroscience, 1157-1164.



UNIVERSITY *of the*
WESTERN CAPE

List of figures

Figure 1.1: Polycyclic NMDA receptor antagonist.....	5
Figure 1.2: Analogues of opened cage norbornane scaffolds.....	6
Figure 1.3: Re-arrange closed cage analogue.....	7
Figure 2.1: Pathological formation Lewy bodies from seeded protein aggregation derived from distorted α -synuclein.....	16
Figure 2.2: Illustration of the sequence of neurons observed in parkinsonism.....	16
Figure 2.3: Dopamine replacement therapy drugs.....	17
Figure 2.4: Dopamine agonists and anticholinergic drugs.....	18
Figure 2.5: Different therapeutic strategies that enhance dopamine activities in Parkinson's disease.....	19
Figure 2.6: Acetylcholinesterase inhibitors.....	20
Figure 2.7: Secretase inhibitors.....	21
Figure 2.8: The connectivity of the brain to the muscles <i>via</i> lateral cortical spinal pathway in the spinal cord.....	23
Figure 2.9: Drugs used in the management of ALS.....	24
Figure 2.10: Potential therapeutic targets or approaches in the management of Huntington's disease (HD).....	26
Figure 2.11: Drugs used in the management of HD.....	27
Figure 2.12: Factors that mediate glutamate induced excitotoxicity leading to loss of neurons in specific part of the and their corresponding neurodegenerative disorders.....	31
Figure 2.13: The role of calcium in excitotoxicity.....	32
Figure 2.14: Schematic representation of the structure of an NMDA-type glutamate receptor and its pharmacological regulation sites.....	35
Figure 2.15: Schematic representation of the transmembrane topology of a Glu1 (A) and a Glu2 (B) subunits	36

Figure 2.16: Subunit composition and transmembrane topology of voltage-gated calcium channel subunits.....	38
Figure 2.17: Diagram showing the multi-heteromeric nature of voltage-gated Ca ²⁺ channels.	39
Figure 2.18: Competitive NMDA receptor antagonists.....	40
Figure 2.19: Uncompetitive NMDA receptor antagonists.....	42
Figure 2.20: Allosteric modulators of NMDA receptors.....	43
Figure 2.21: L-type calcium channel antagonists.....	44
Figure 2.22: Polycyclic cages.....	46
Figure 2.23: (2-oxadamant-1-yl)amine derivatives.....	47
Figure 2.24: Opened polycyclic cages with norbornane scaffolds.....	49
Figure 2.25: Antipsychotic agents.....	50
Figure 2.26: An anticancer agent.....	50
Figure 3.1: Doublet of doublets signal of the bridge proton of compound 2 in ¹ H NMR at 400 MHz.....	81
Figure 3.2: Multiplet and singlets of the benzylamine moiety of compound 5 in ¹ H NMR at 400 MHz.....	82
Figure 3.3: ¹ H NMR spectrum differences existing between 5 and 6	83
Figure 3.4: Proposed synthetic pathways of compound 9	84
Figure 3.5: Aromatic region of the ¹ H spectrum of compound 22 and 23	90
Figure 3.6: Proposed aliphatic amine conjugates.....	91
Figure 3.7: Proposed propargylamine and propylamine conjugates of compound 19	92
Figure 4.1: Cytotoxicity effect of tested compounds (1-27) on human neuroblastoma SH-SY5Y cells.....	98
Figure 4.2: Neuroprotective effect of compound 1-27 on MPP ⁺ -induced toxicity in neuroblastoma SH-SY5Y cells.....	102

Figure 4.3: Inhibitory effects of synthesised (1-27) and reference compounds on NMDA/glycine calcium influx.....	112
Figure 4.4: Physiological functions of the Voltage-gated calcium channels.....	116
Figure 4.5: Inhibitory effects of synthesised (1-27) and reference compounds on VGCC mediated calcium influx.....	121
Figure 5.1: Structures of series 1.....	128
Figure 5.2: Structures of series 2.....	130
Figure 5.3: Structures of series 3.....	131
Figure 5.4: Structures of acquired compounds.....	132



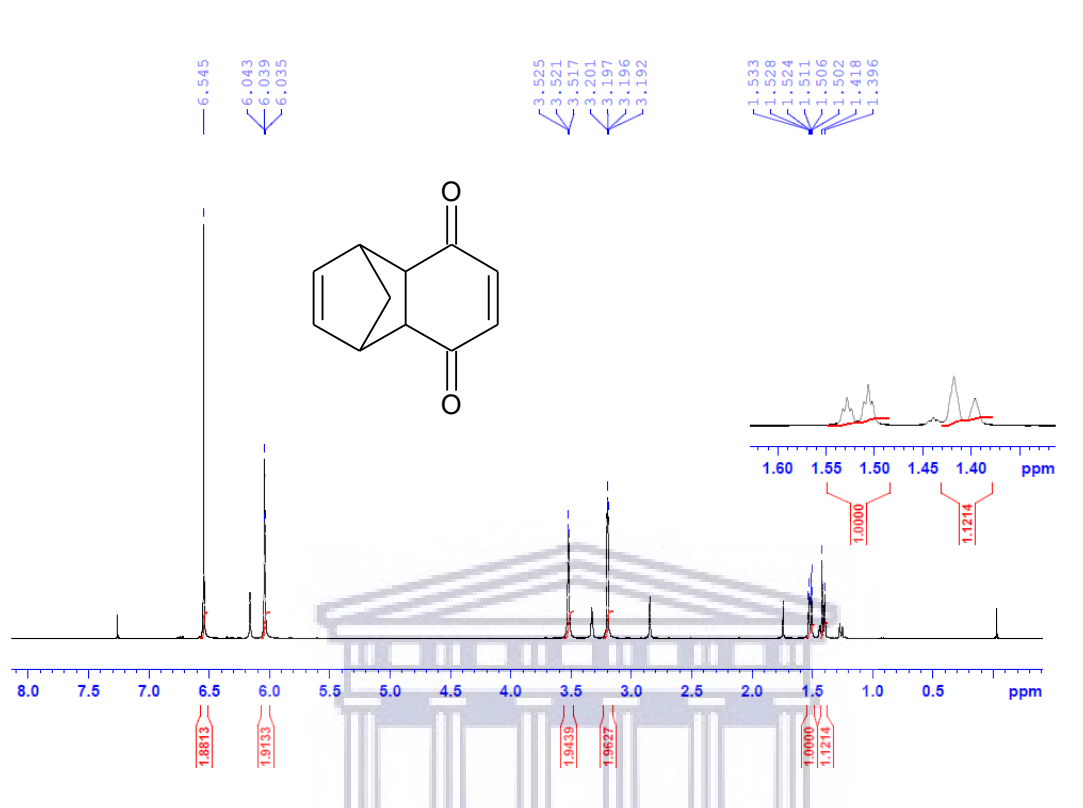
List of tables

Table 1: Sex differences in incidence and outcomes of neurological conditions commonly see in humans.....	12
Table 4: Biological profiles of test compounds.....	124

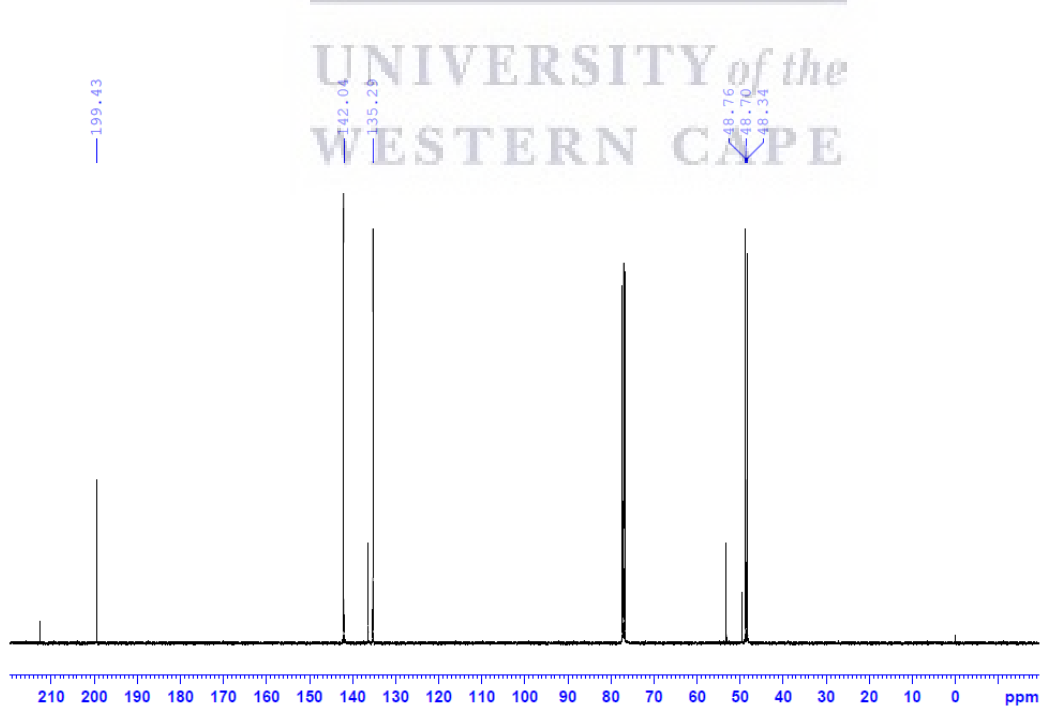


Spectra

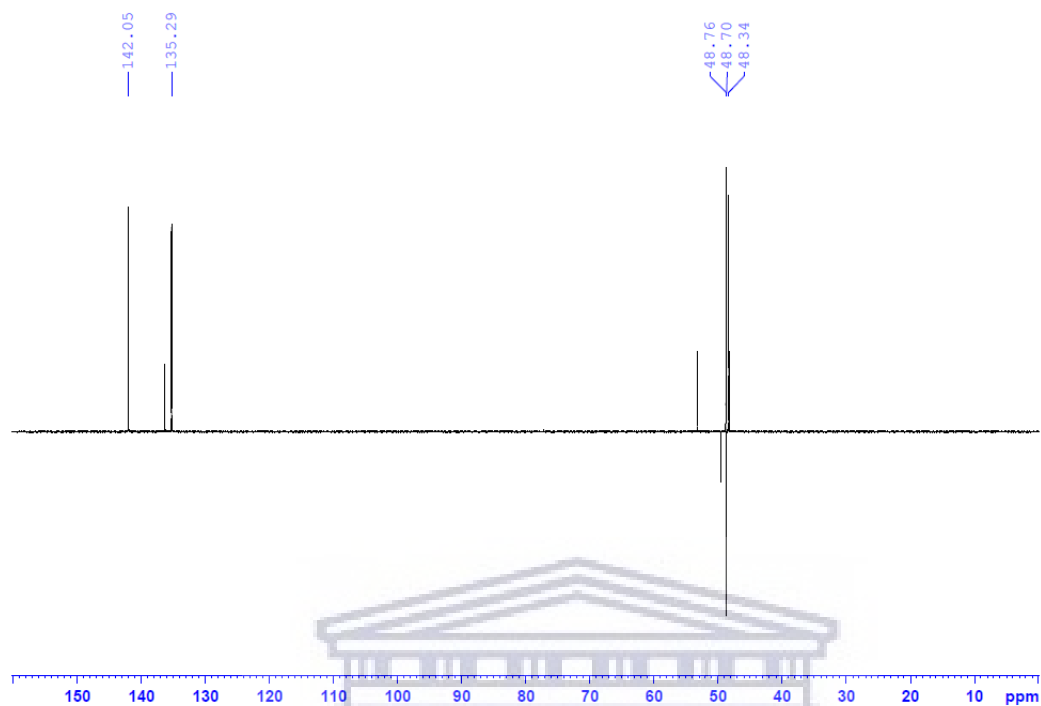
^1H spectrum of compound 1



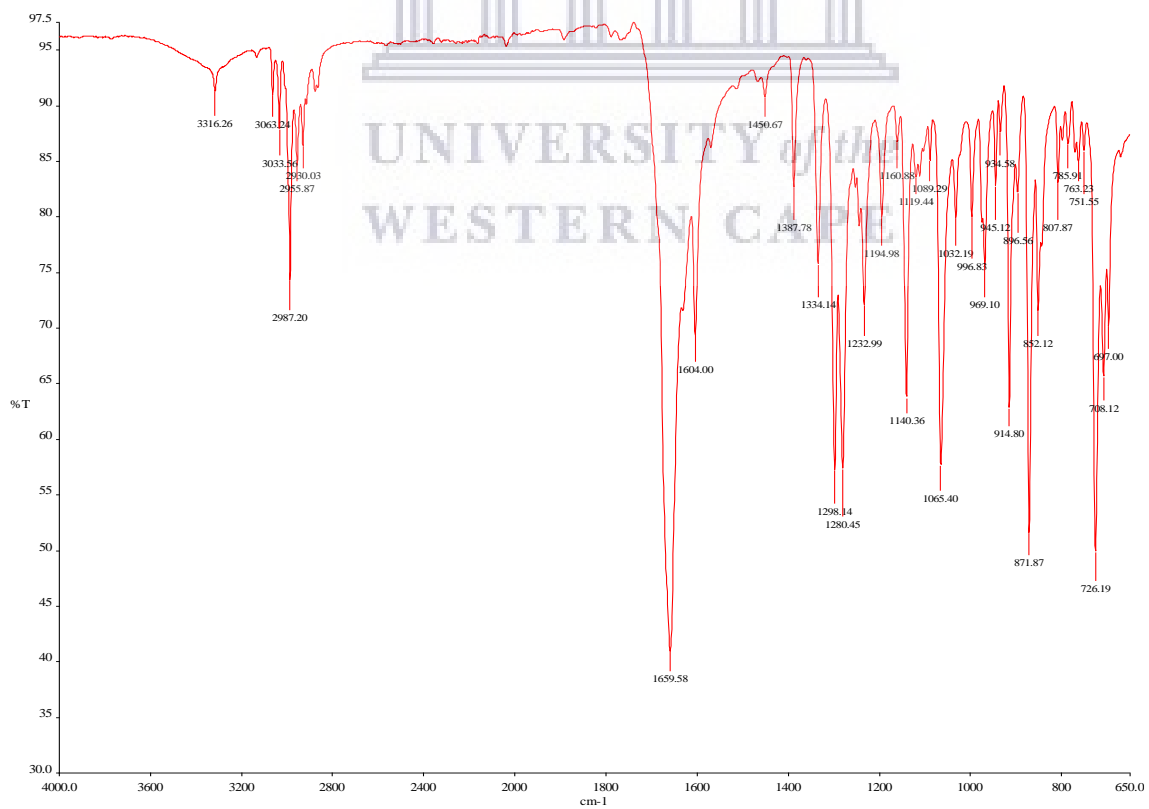
^{13}C spectrum of compound 1



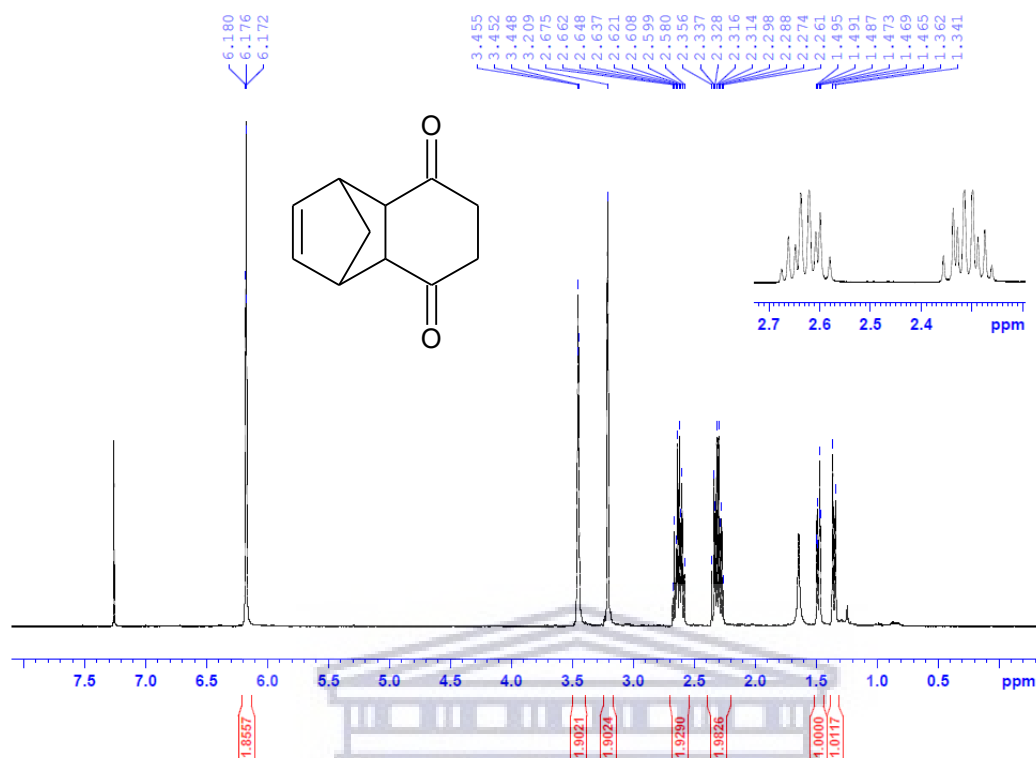
DEPT-135 spectrum of compound 1



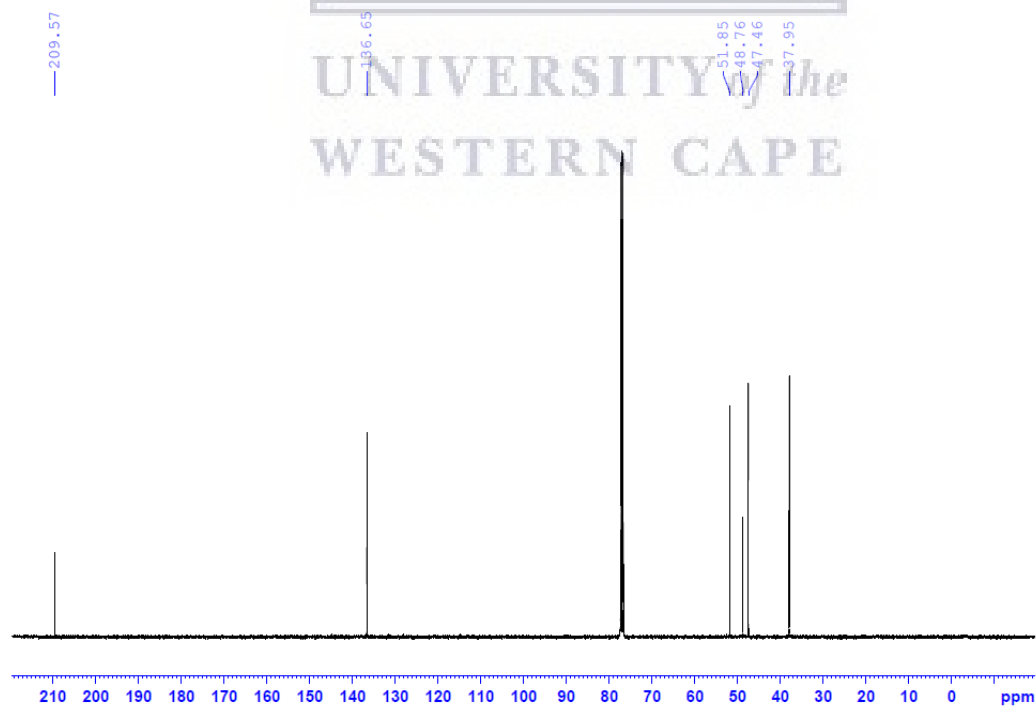
IR spectrum of compound 1



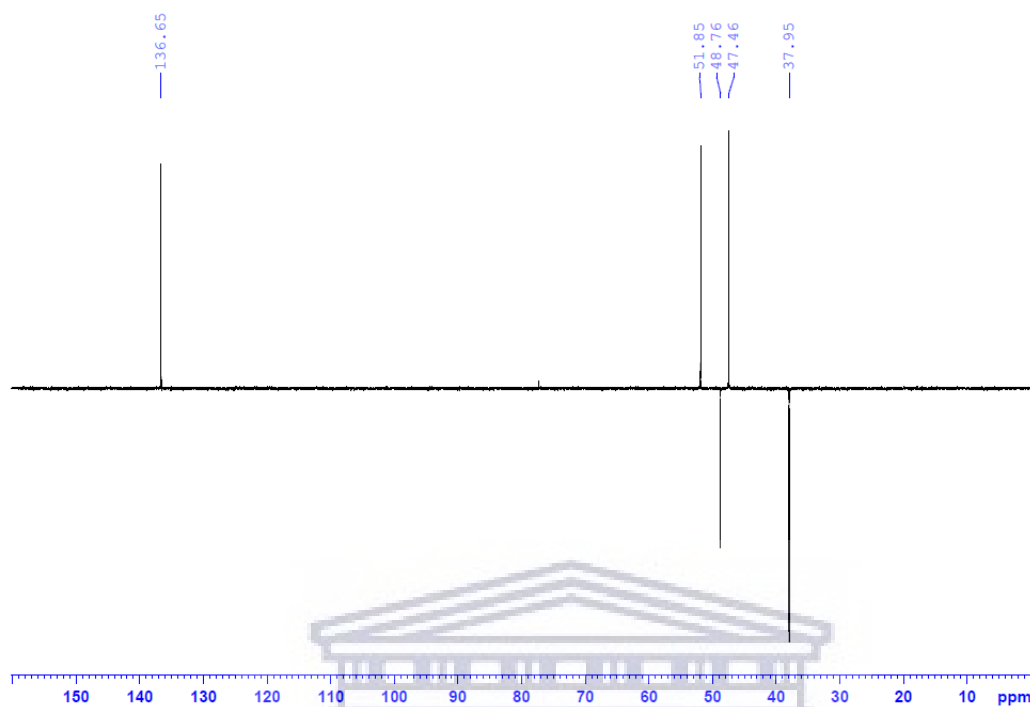
^1H spectrum of compound 2



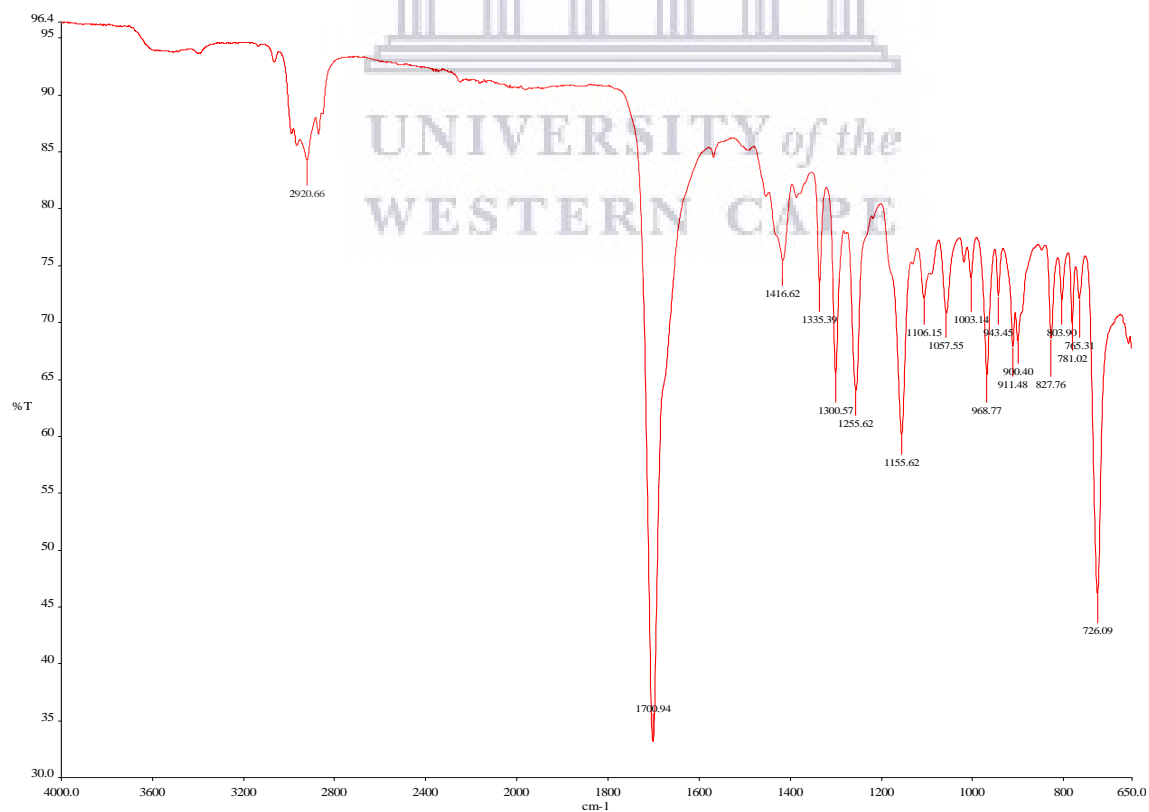
^{13}C spectrum of compound 2



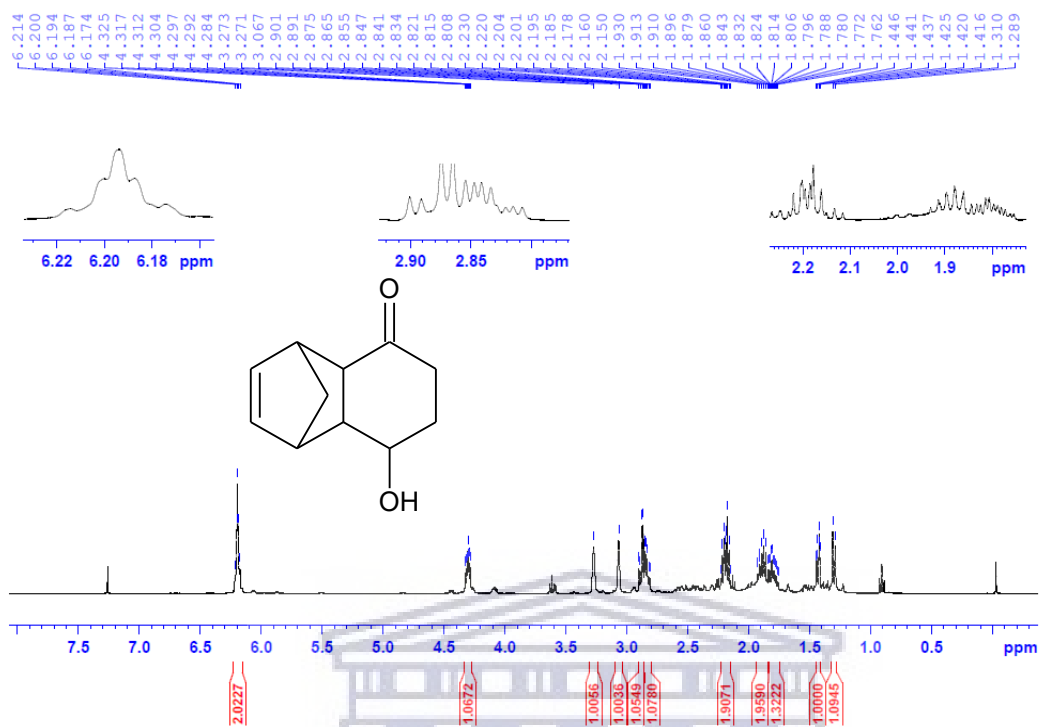
DEPT-135 spectrum of compound 2



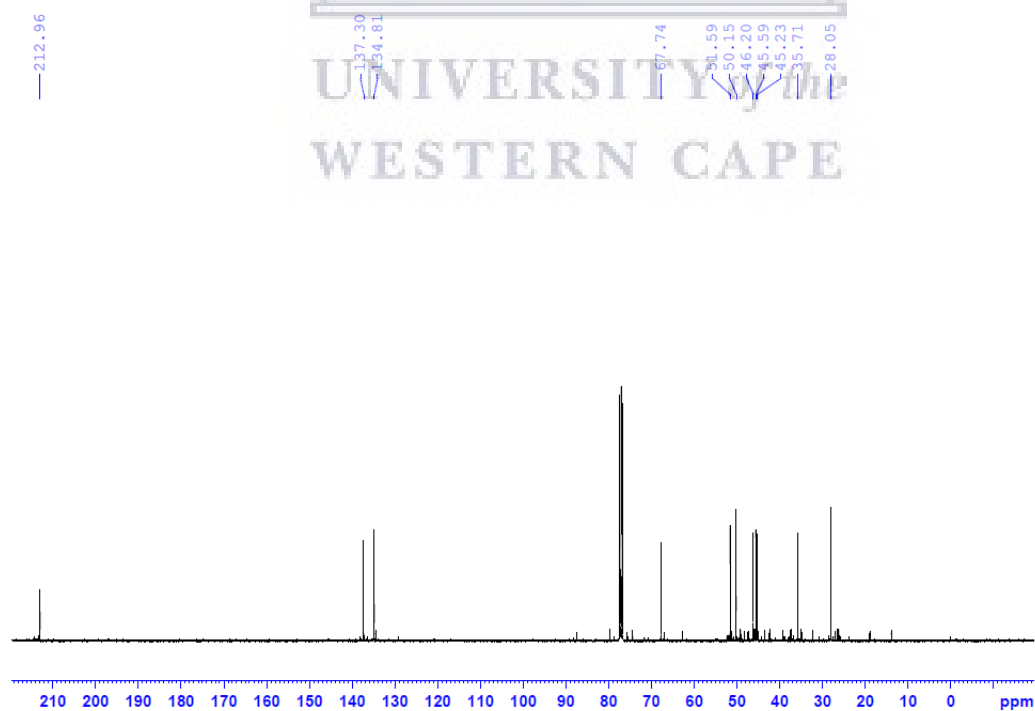
IR spectrum of compound 2



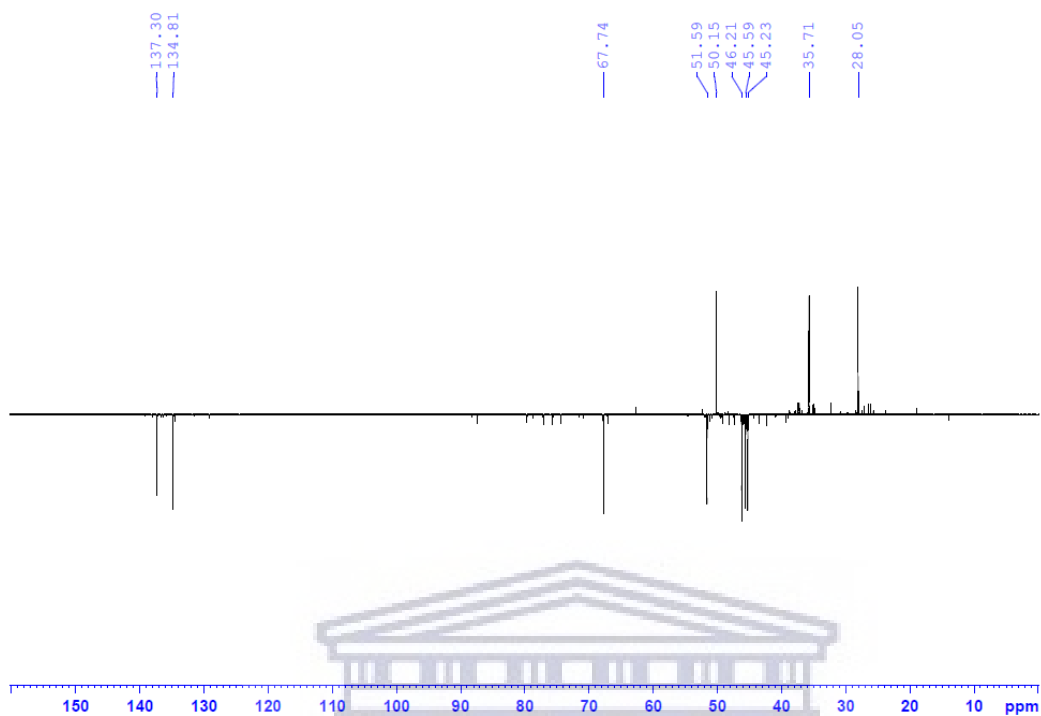
¹H spectrum of compound 3



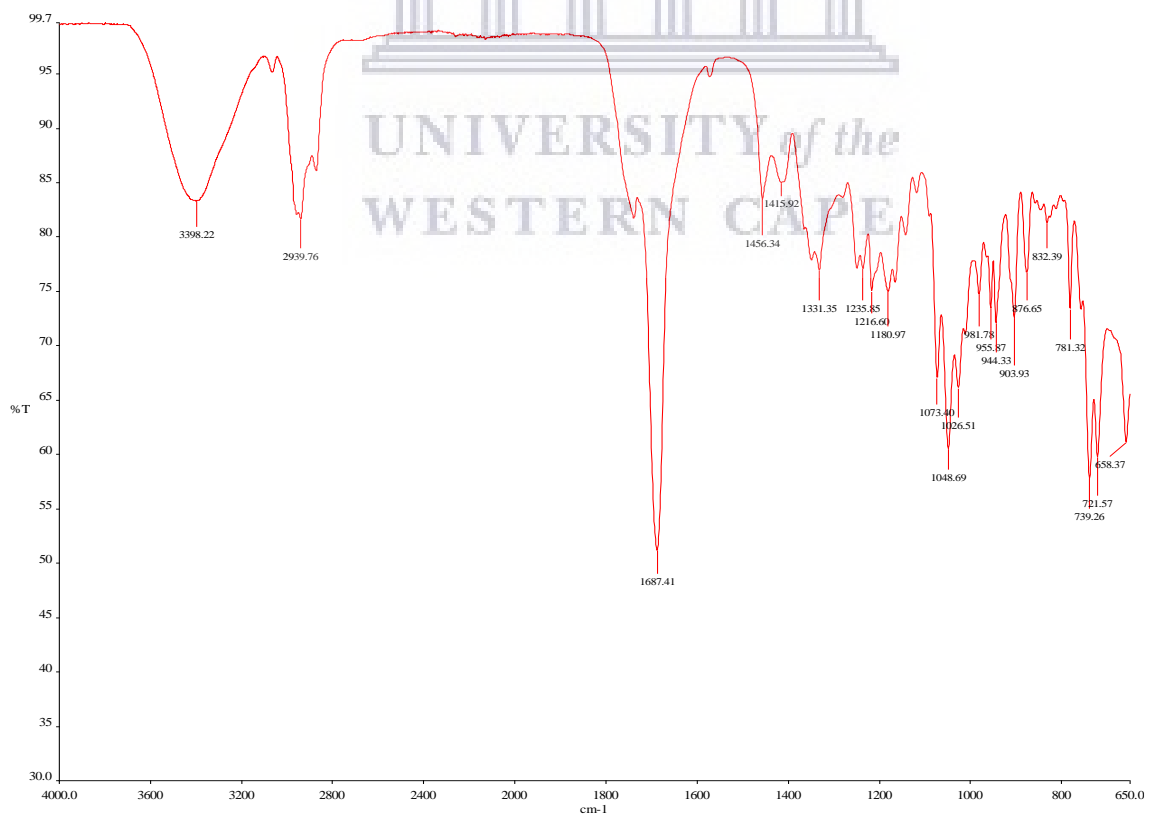
¹³C spectrum of compound 3



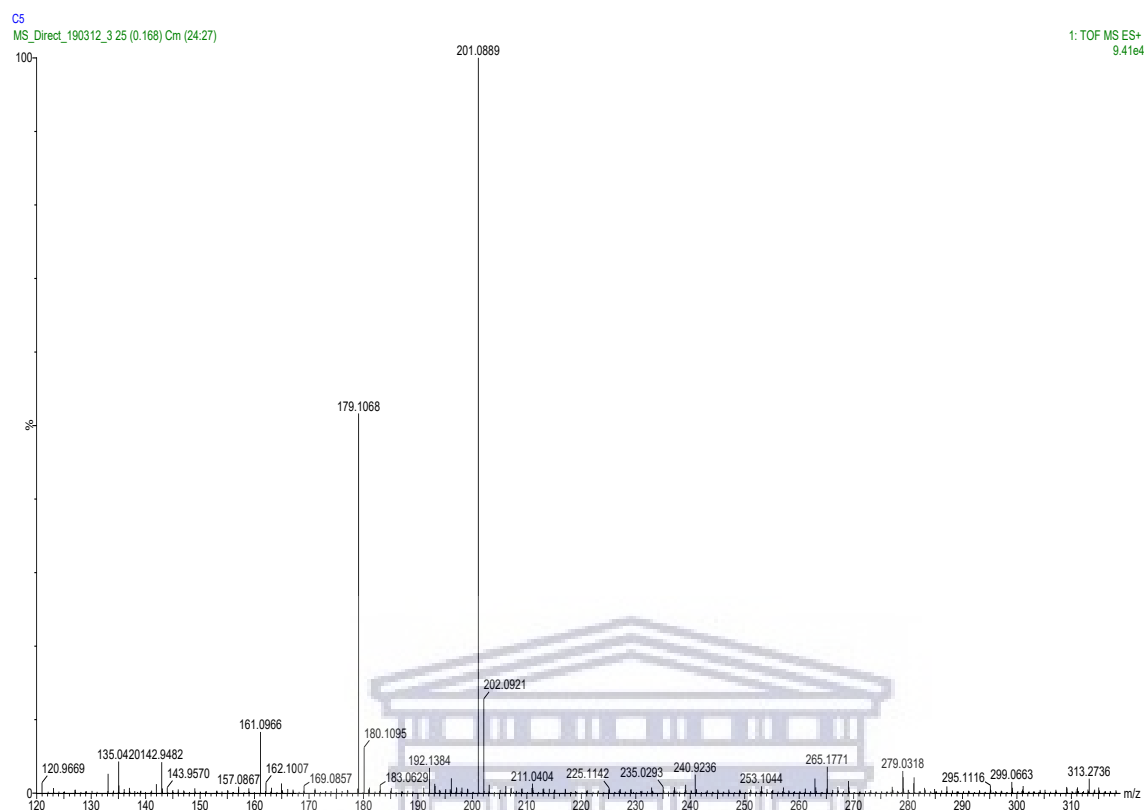
DEPT-135 spectrum of compound 3



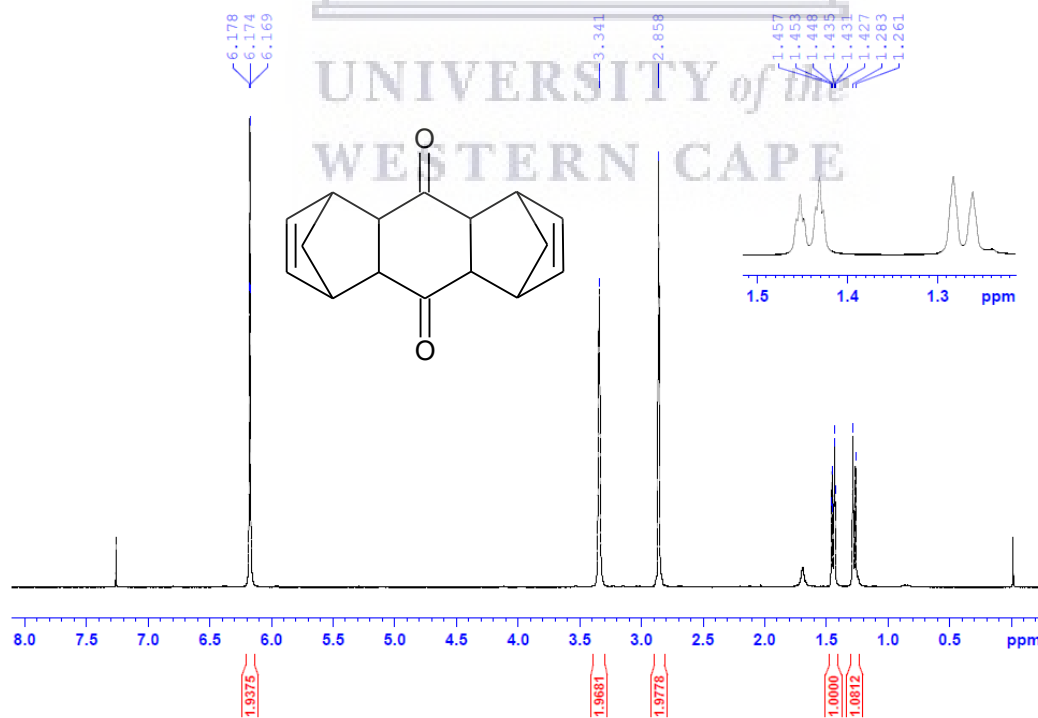
IR spectrum of compound 3



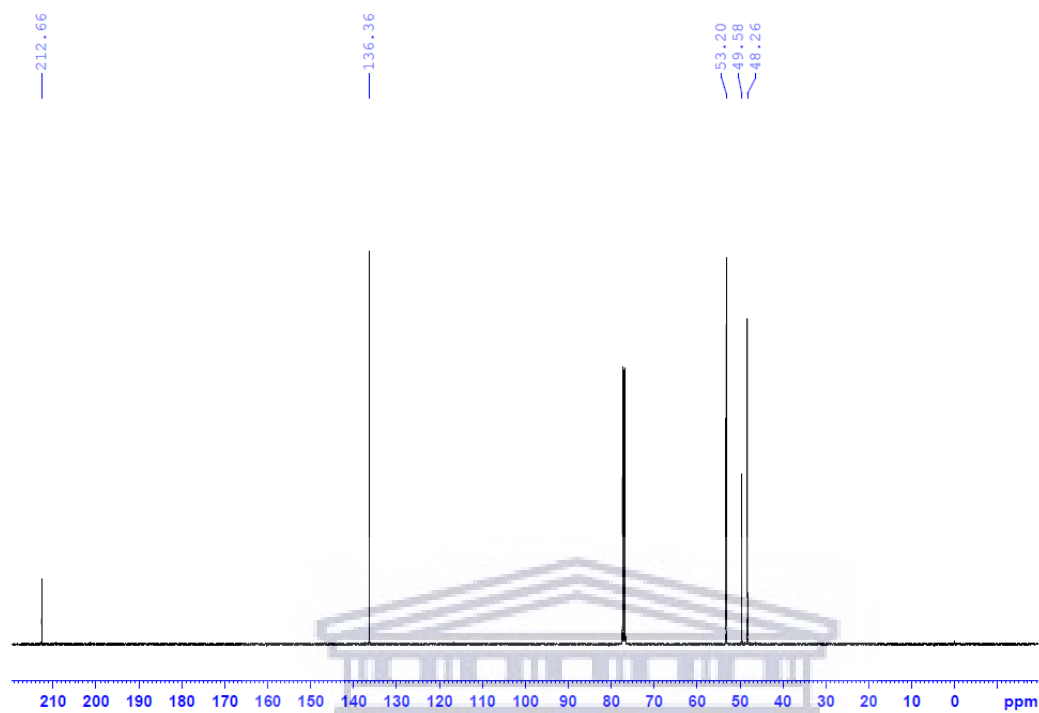
MS spectrum of compound 3



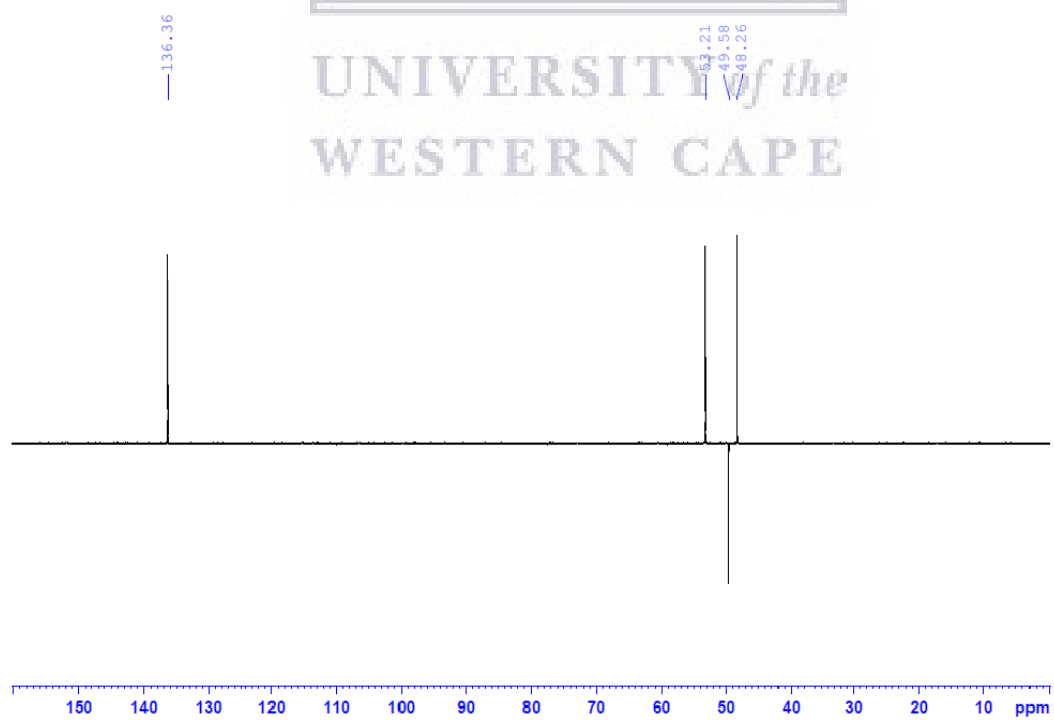
¹H spectrum of compound 4



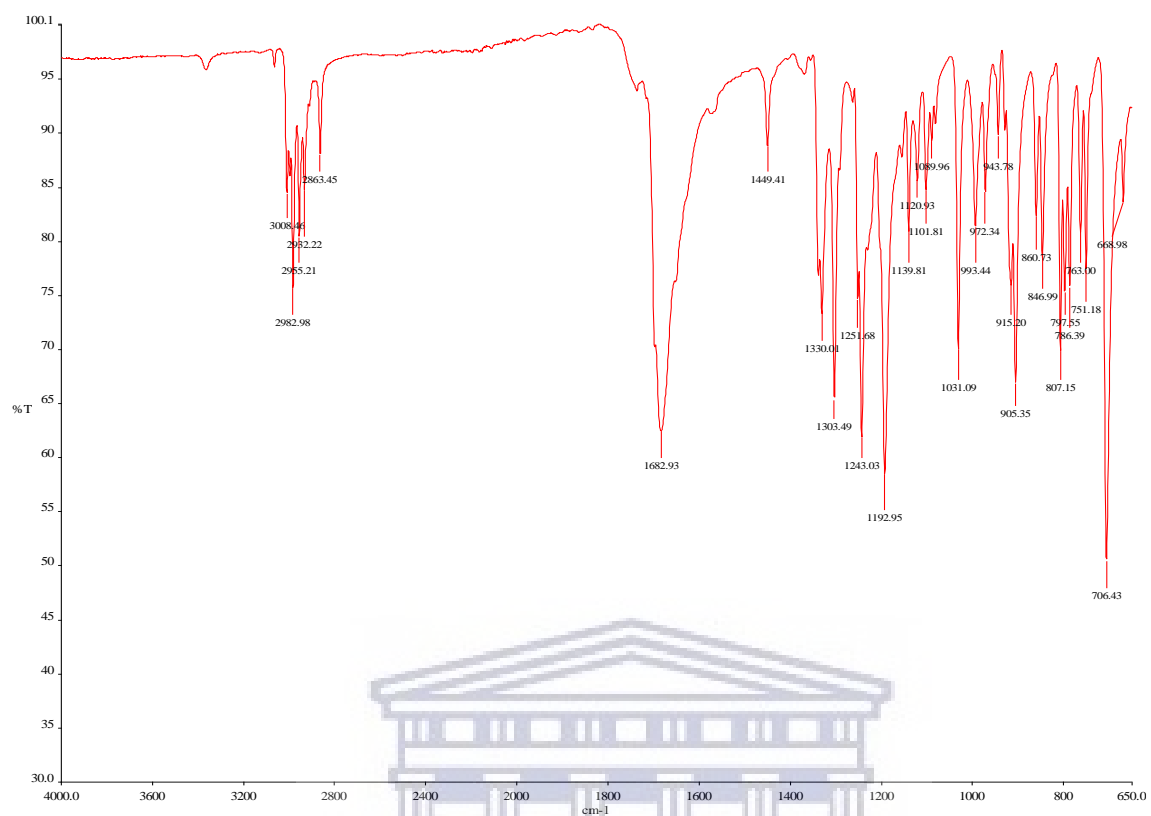
^{13}C spectrum of compound 4



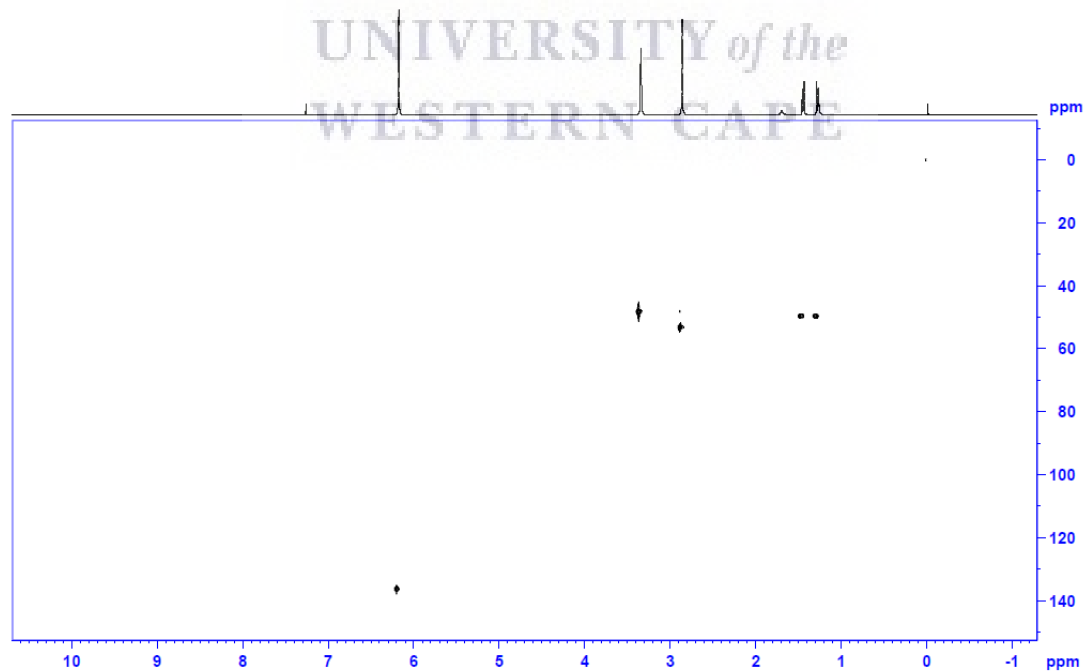
DEPT-135 spectrum of compound 4



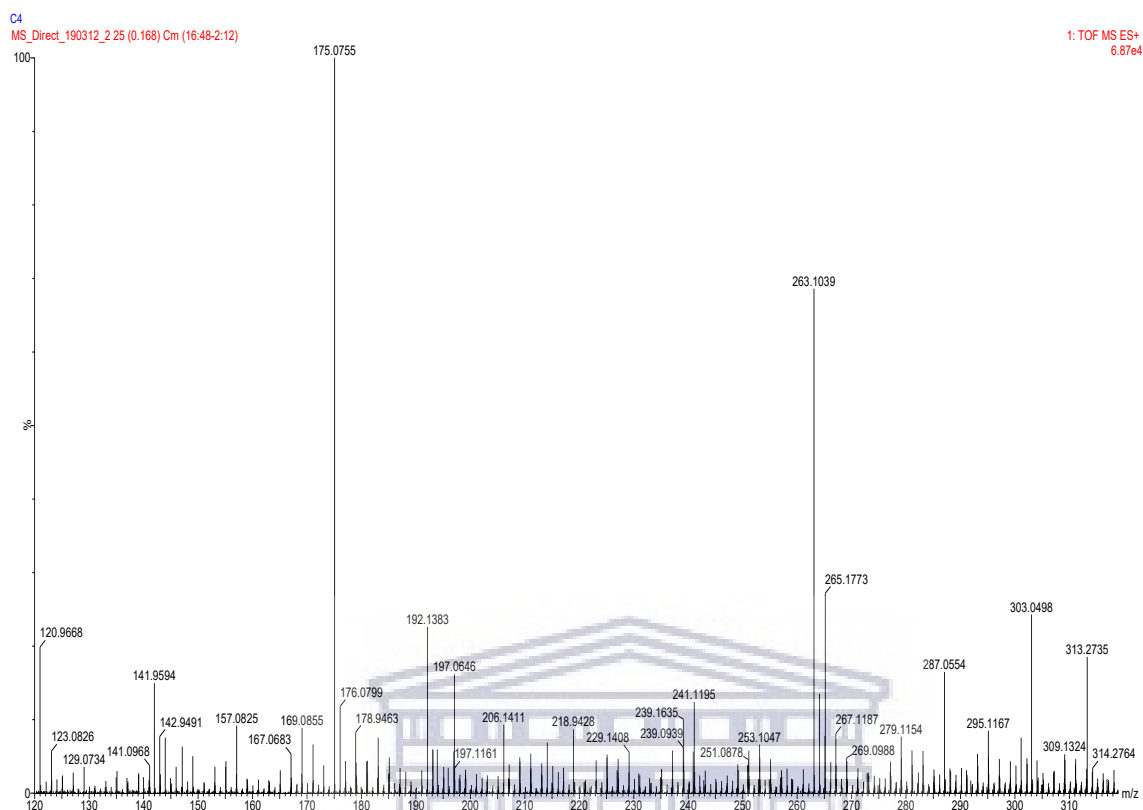
IR spectrum of compound 4



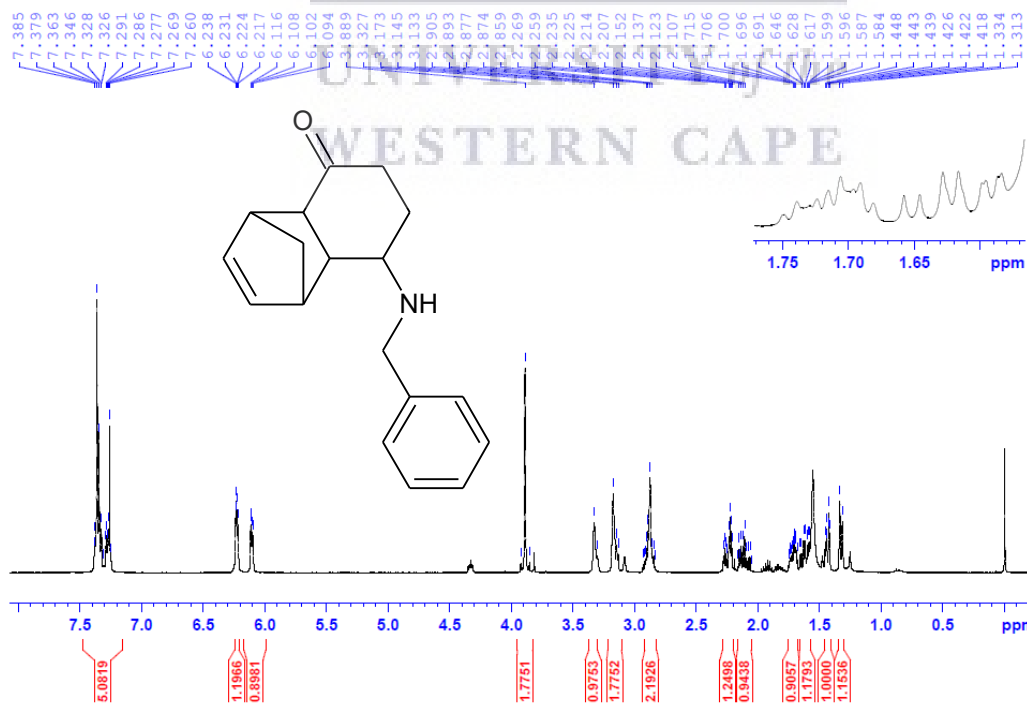
HSQC spectrum of compound 4



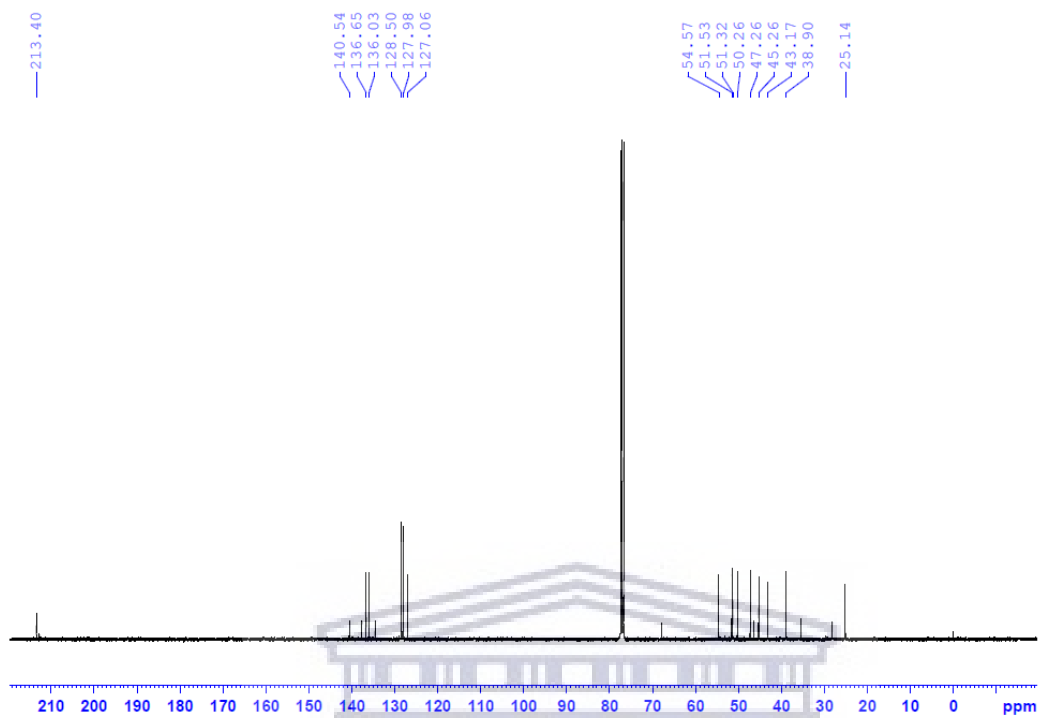
MS spectrum of compound 4



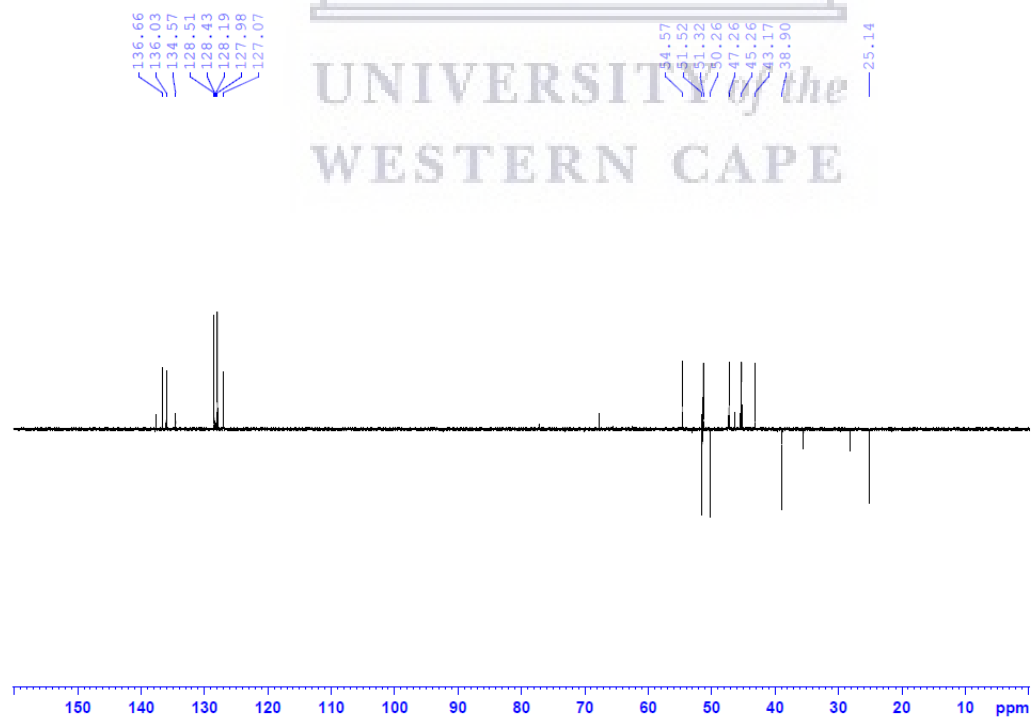
¹H spectrum of compound 5



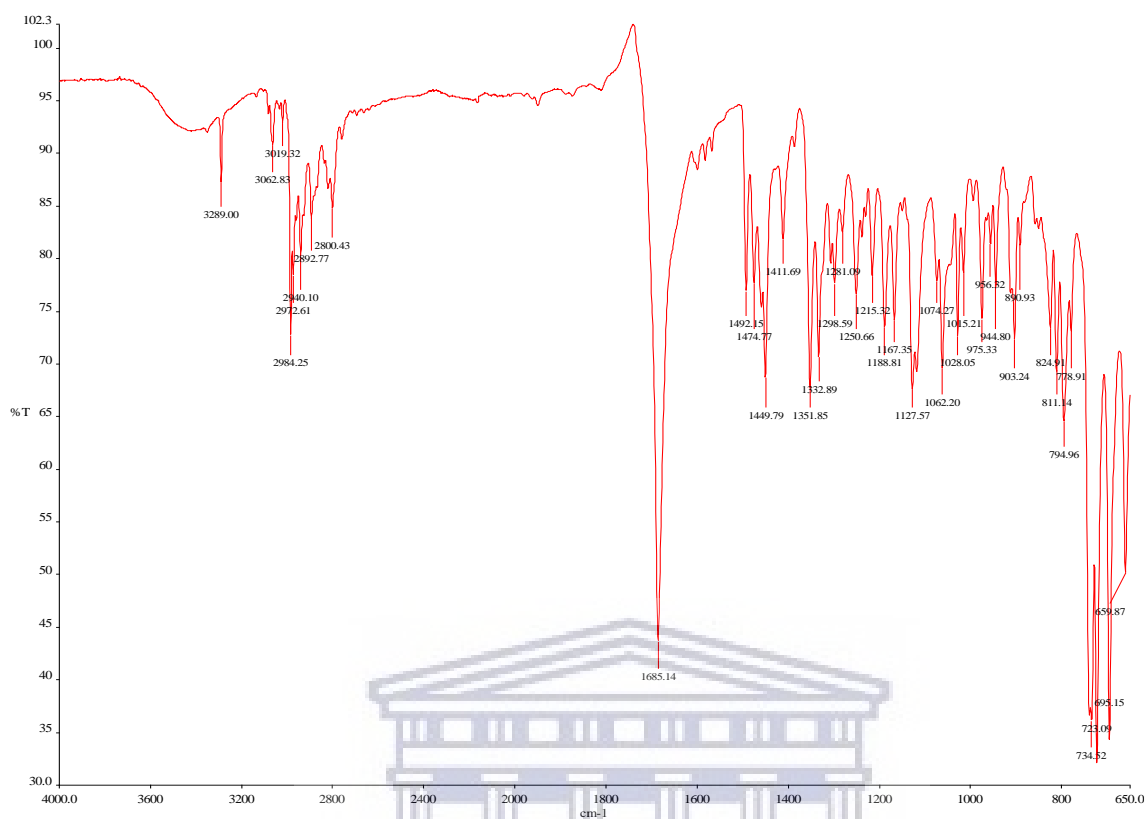
^{13}C spectrum of compound 5



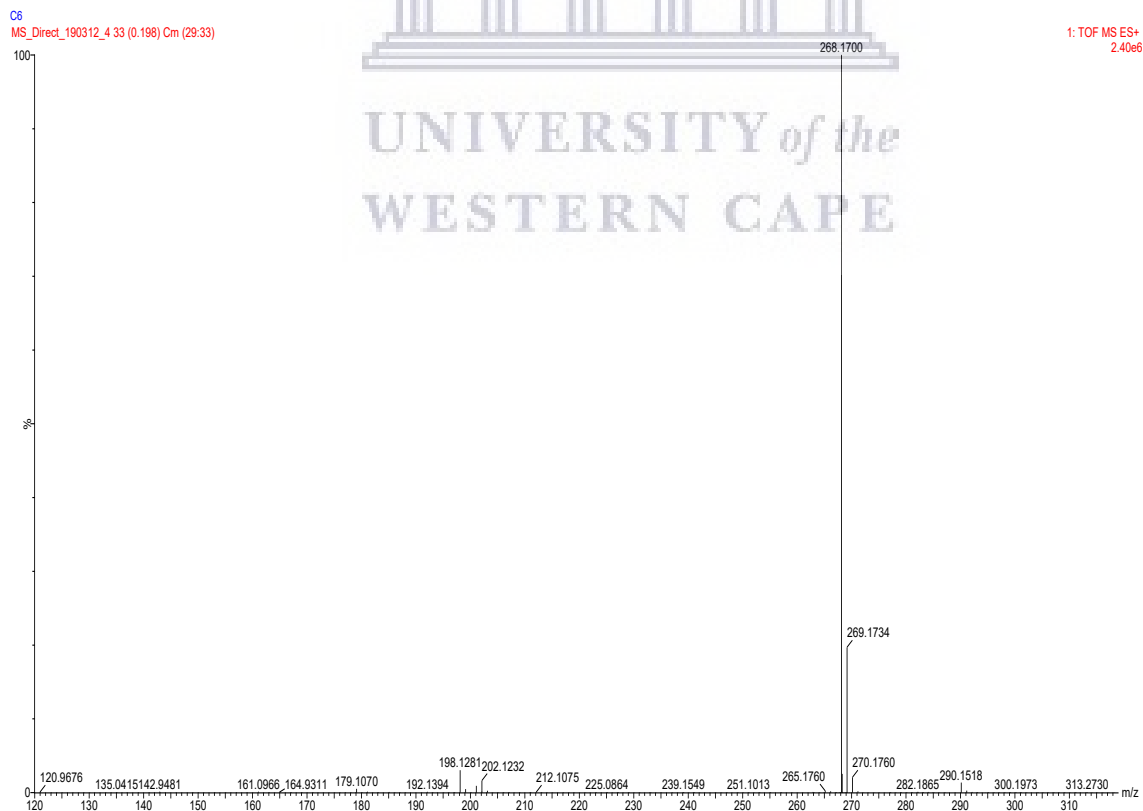
DEPT-135 spectrum of compound 5



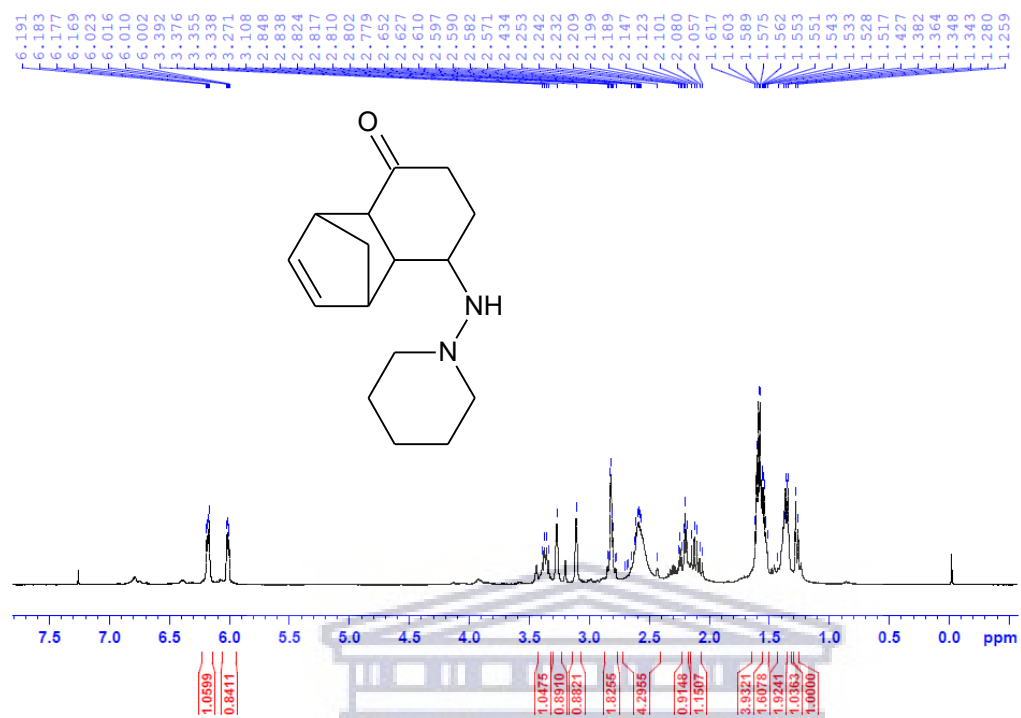
IR spectrum of compound 5



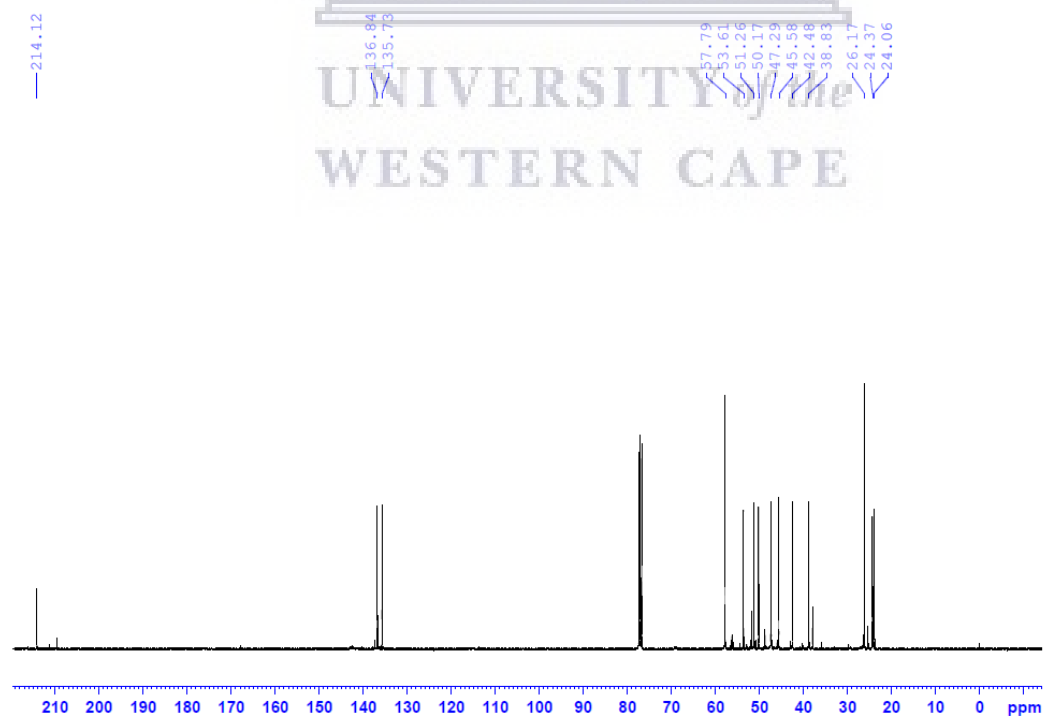
MS spectrum of compound 5



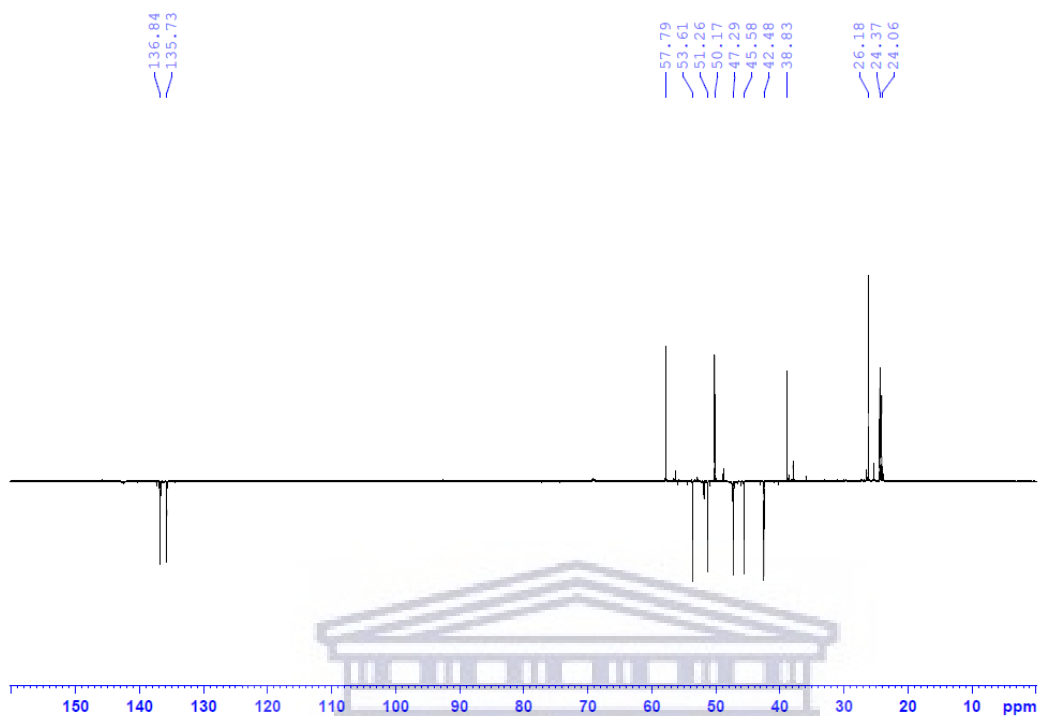
¹H spectrum of compound 6



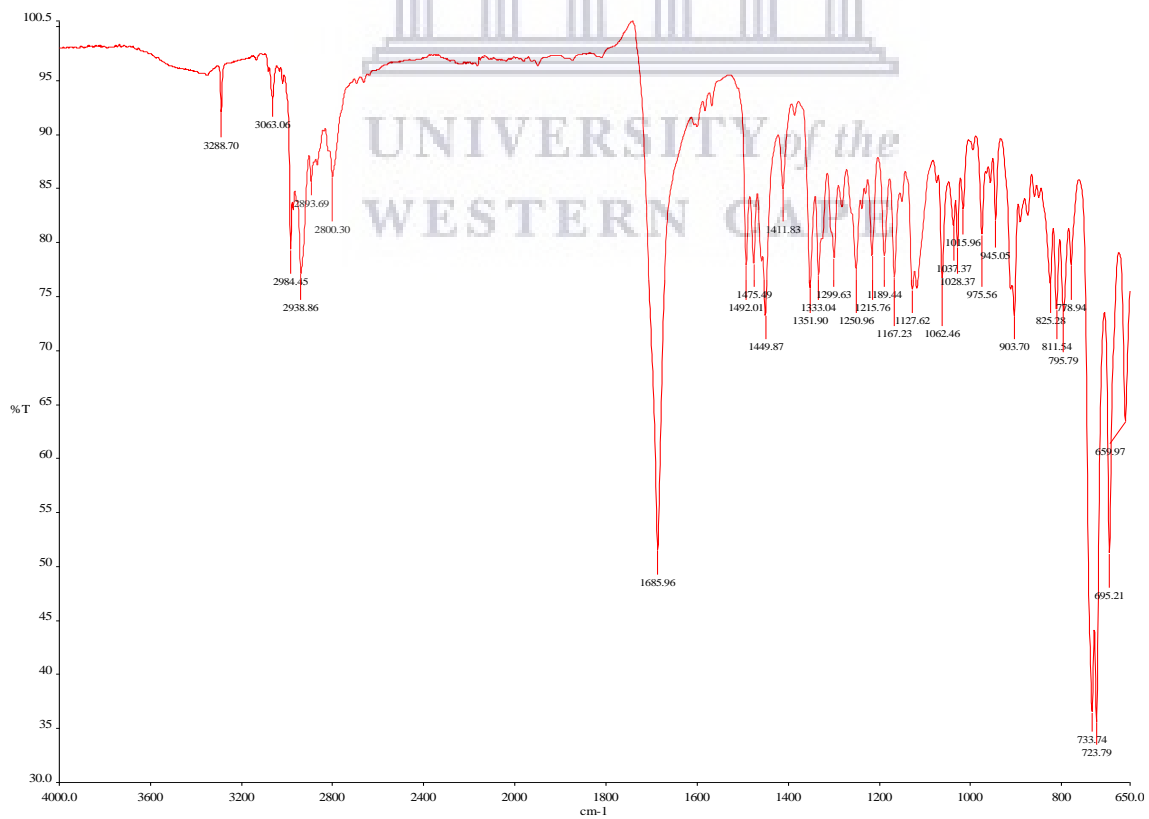
¹³C spectrum of compound 6



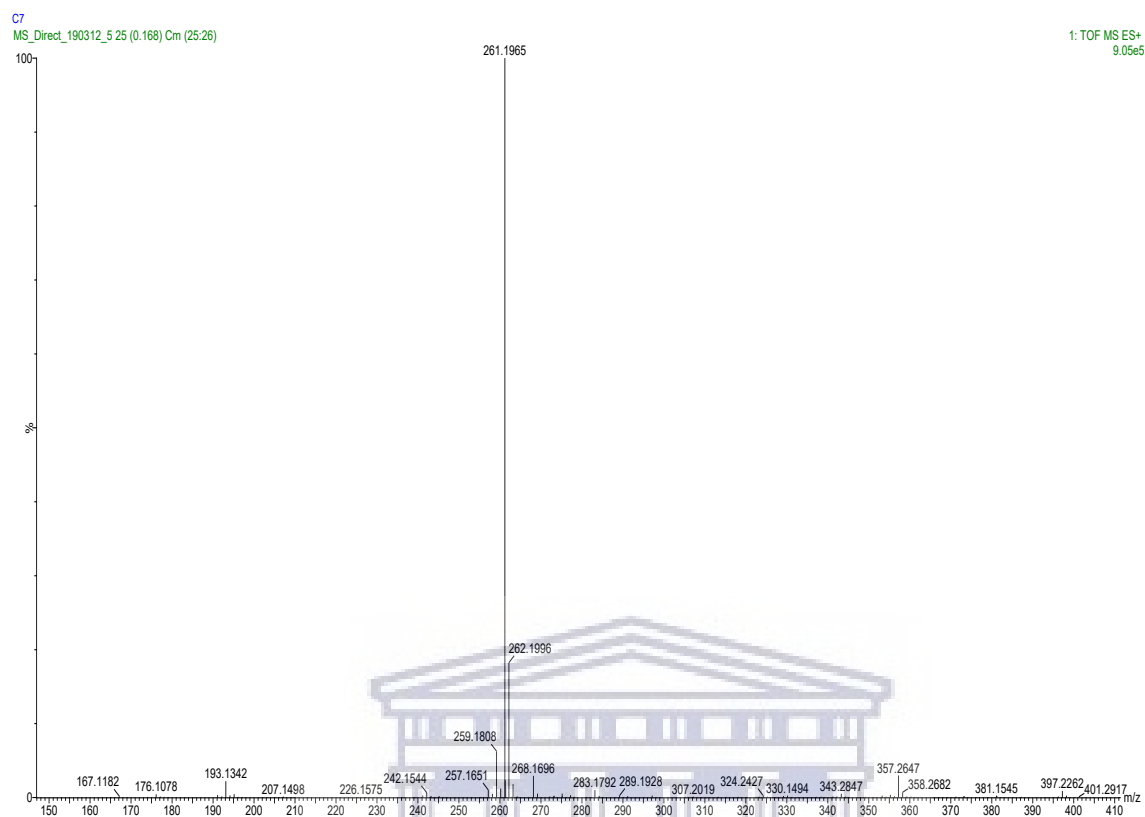
DEPT-135 spectrum of compound 6



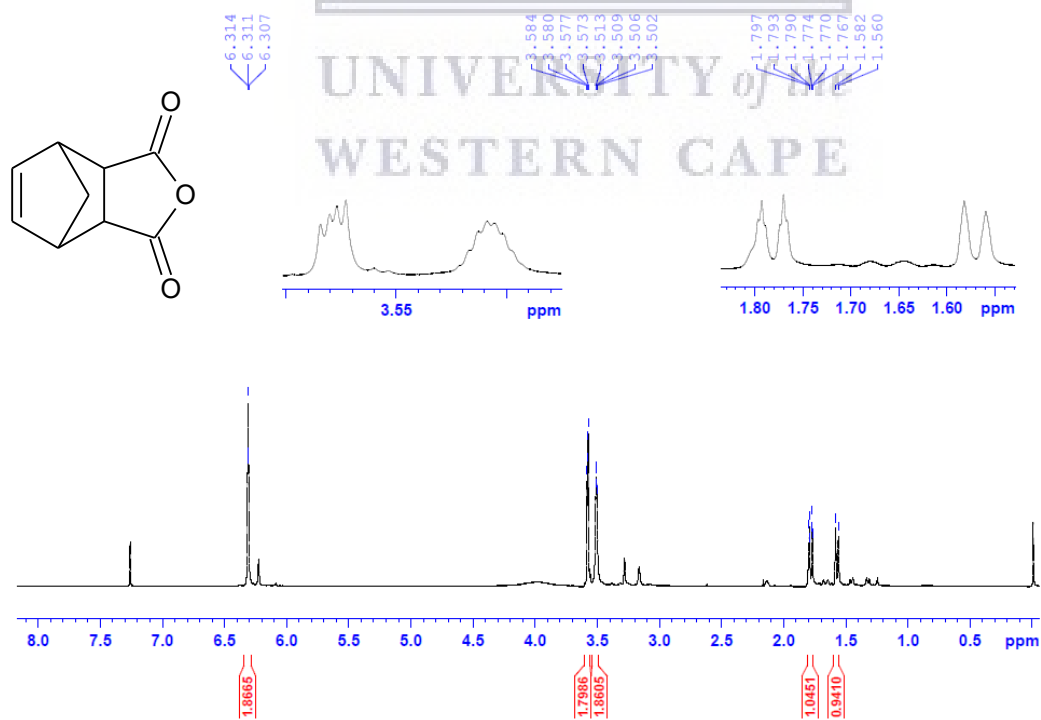
IR spectrum of compound 6



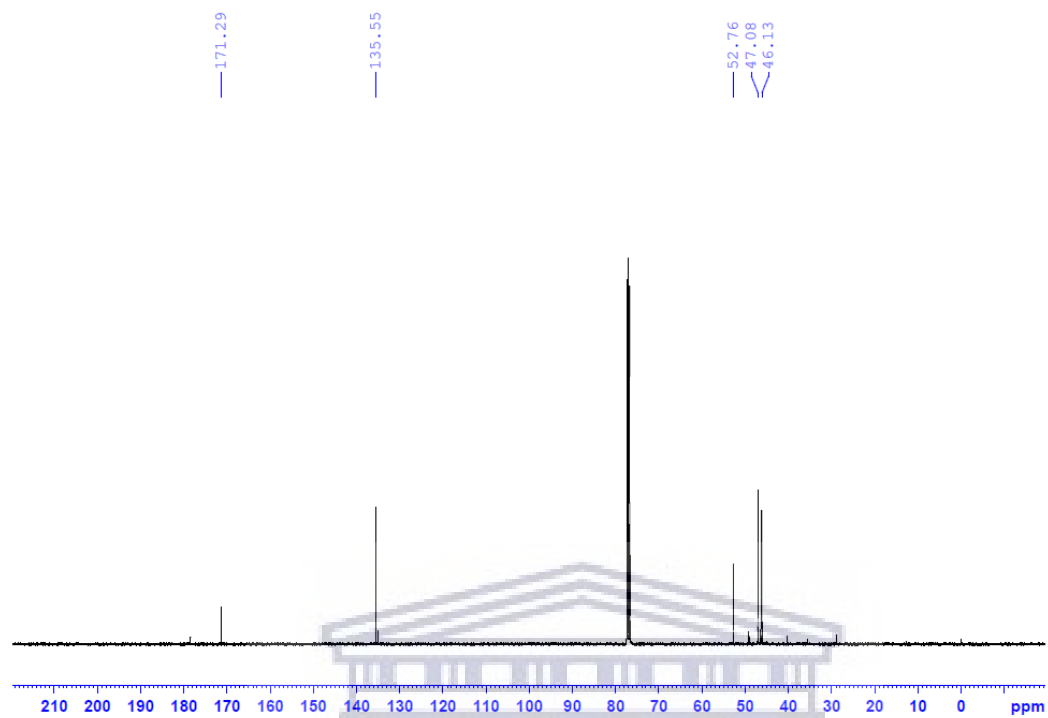
MS spectrum of compound 6



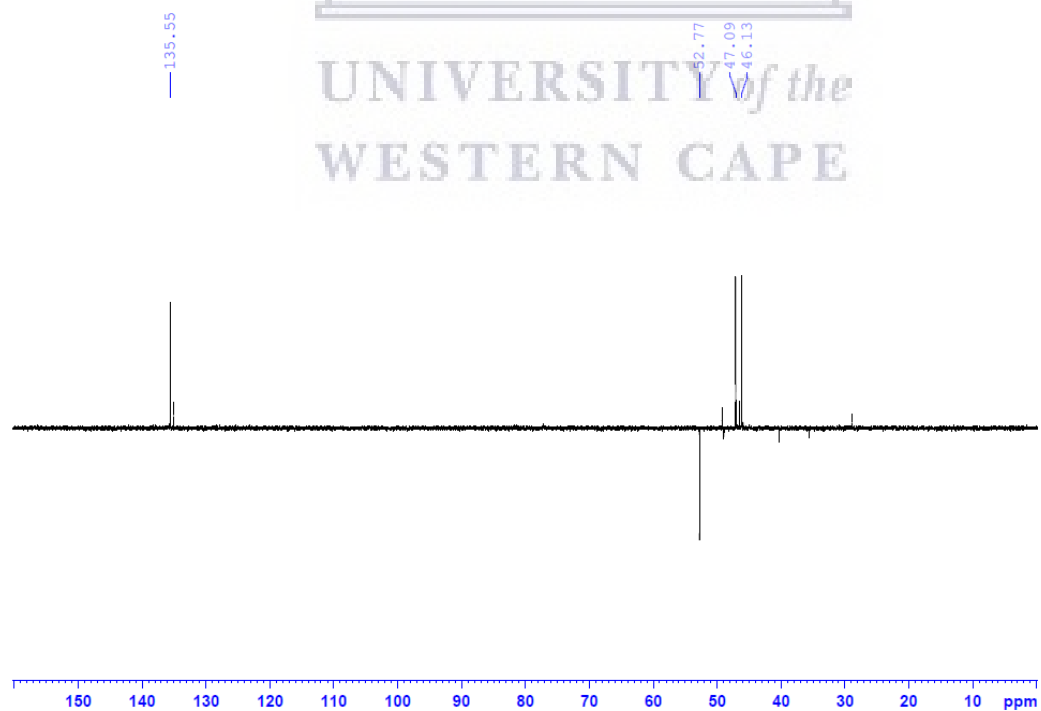
¹H spectrum of compound 7



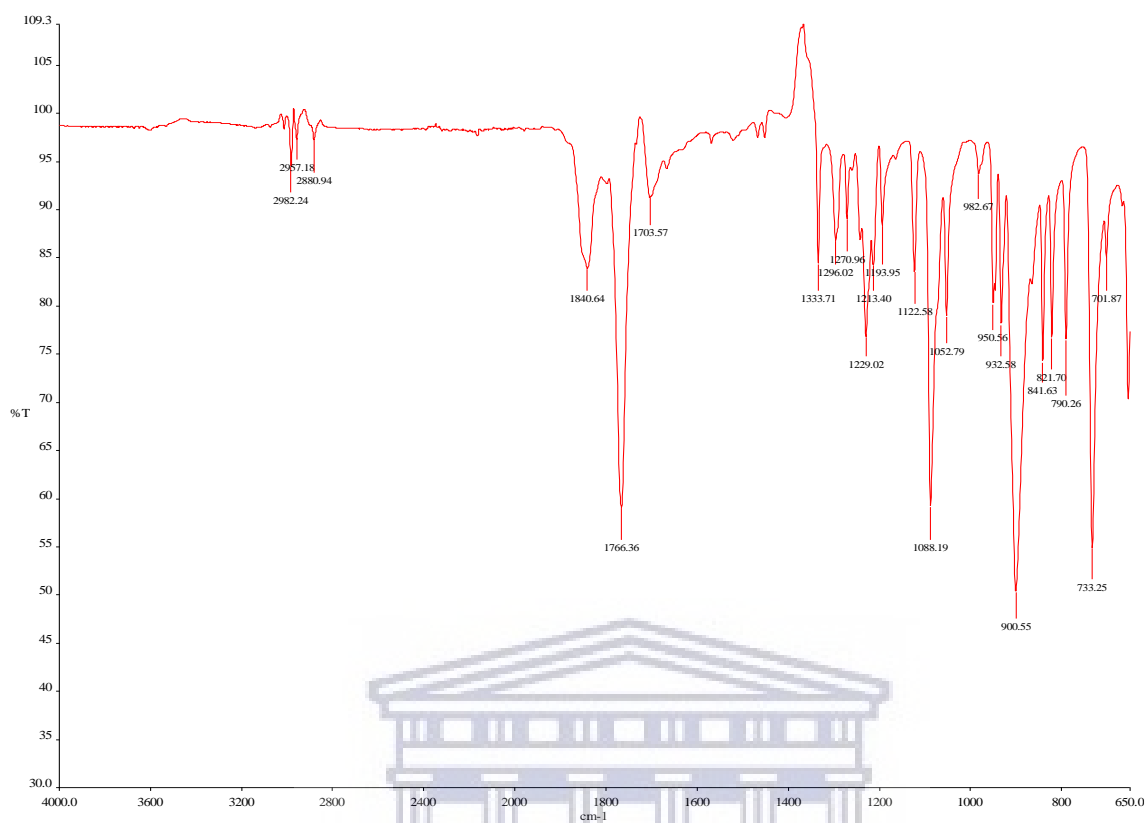
^{13}C spectrum of compound 7



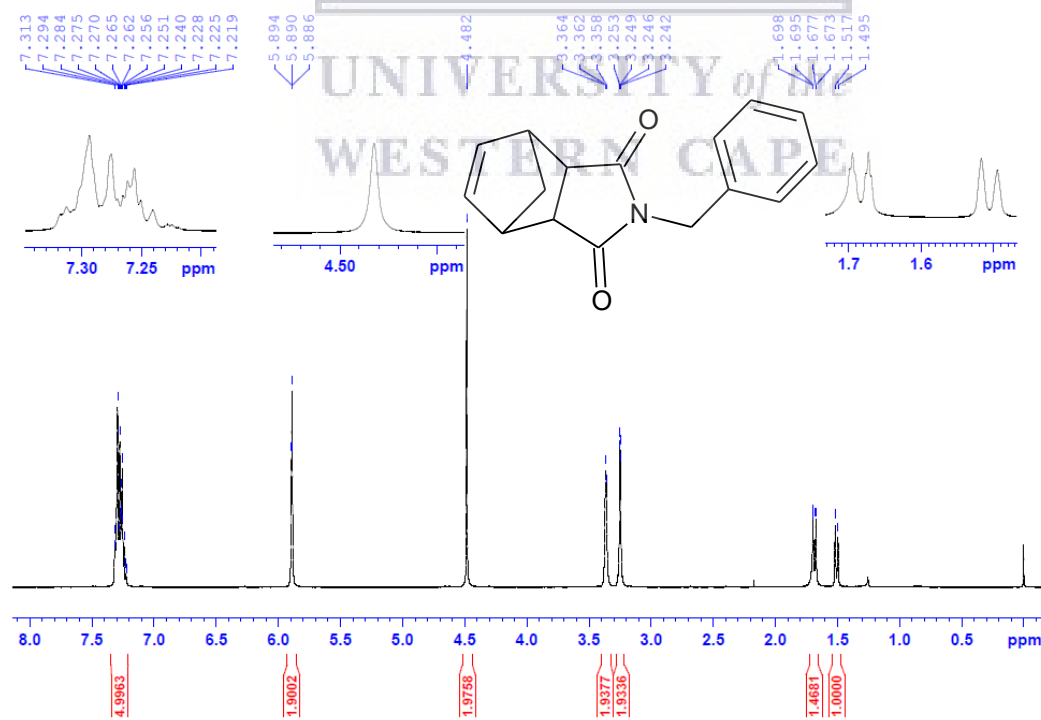
DEPT-135 spectrum of compound 7



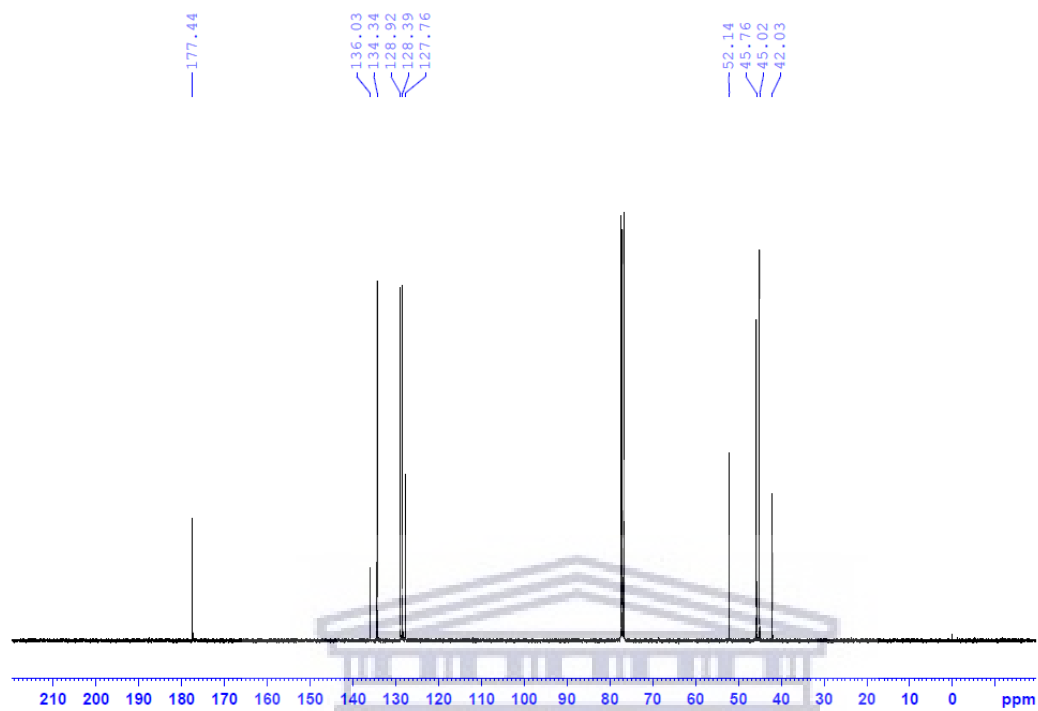
IR spectrum of compound 7



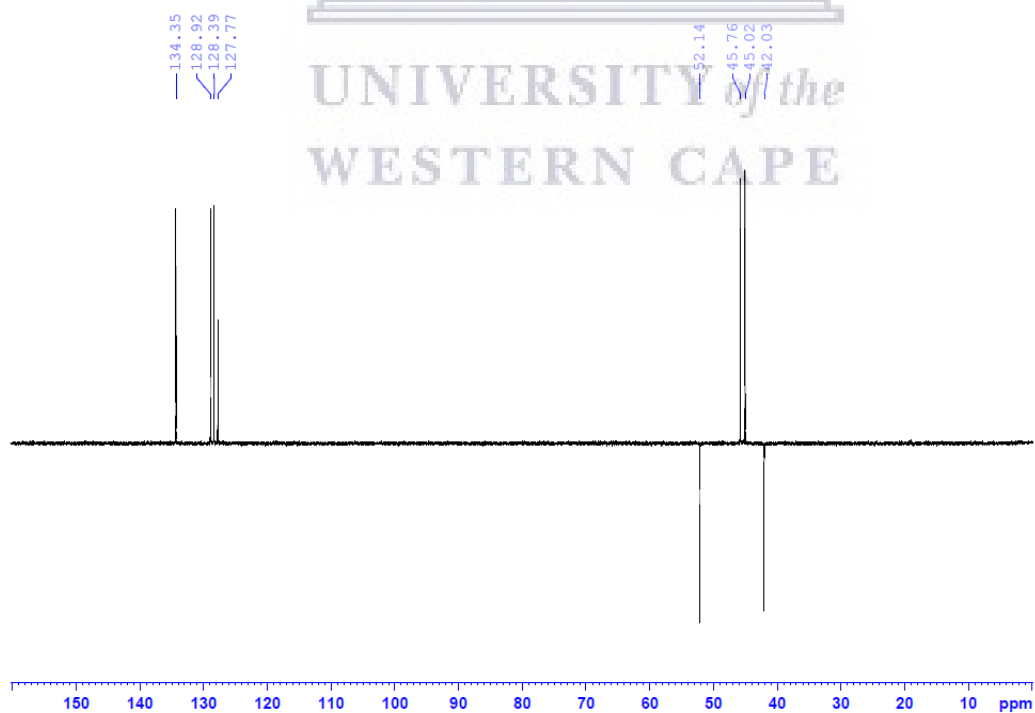
¹H spectrum of compound 8



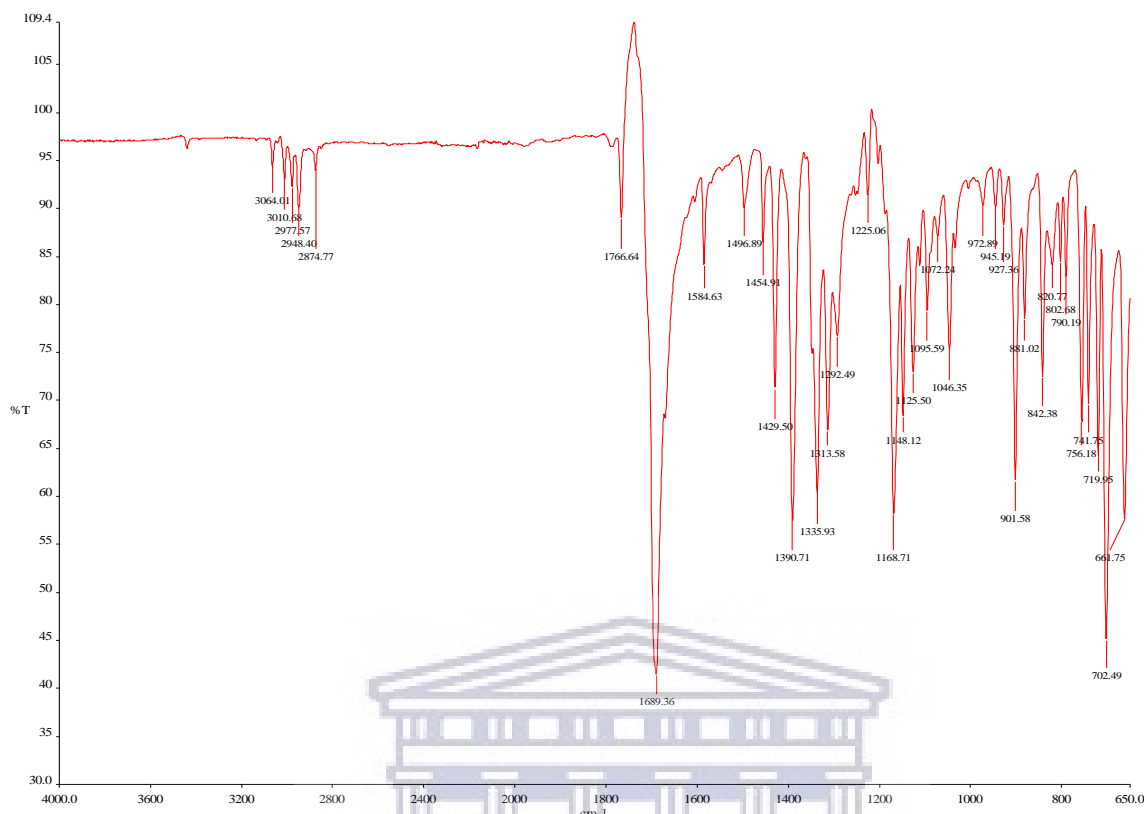
^{13}C spectrum of compound 8



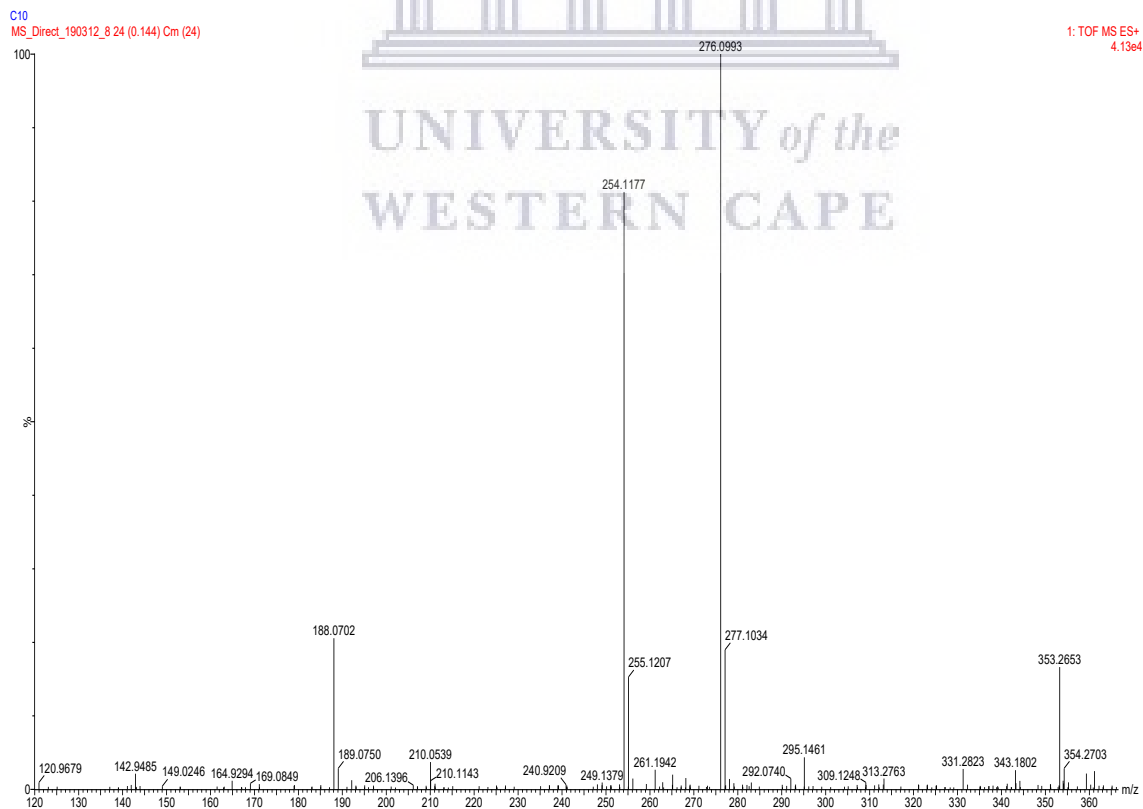
DEPT-135 spectrum of compound 8



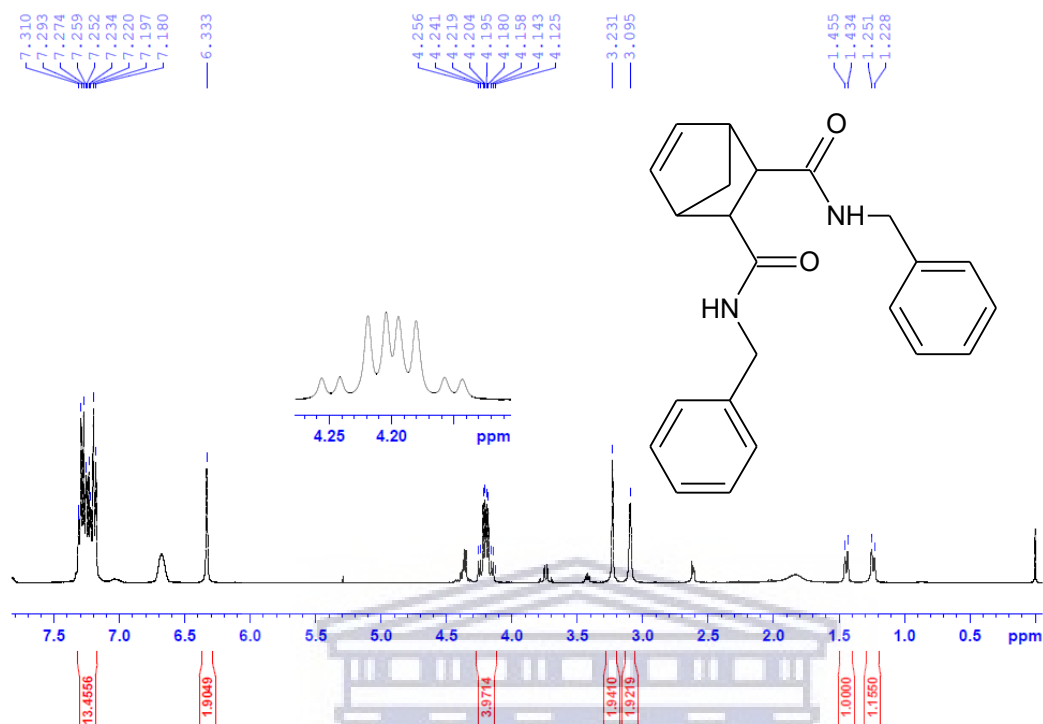
IR spectrum of compound 8



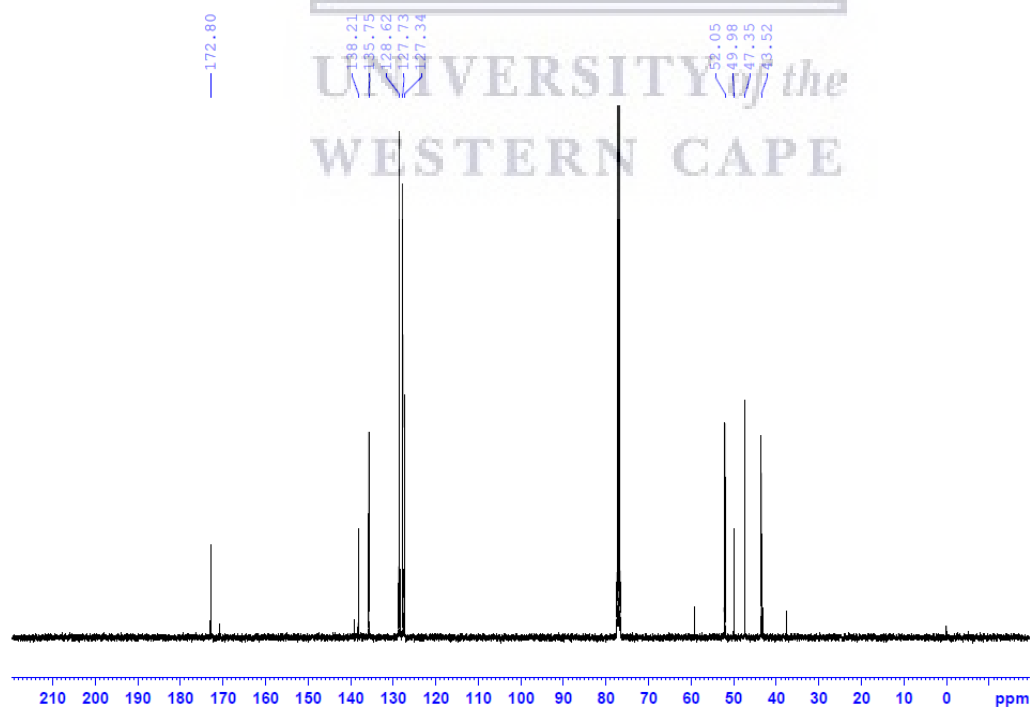
MS spectrum of compound 8



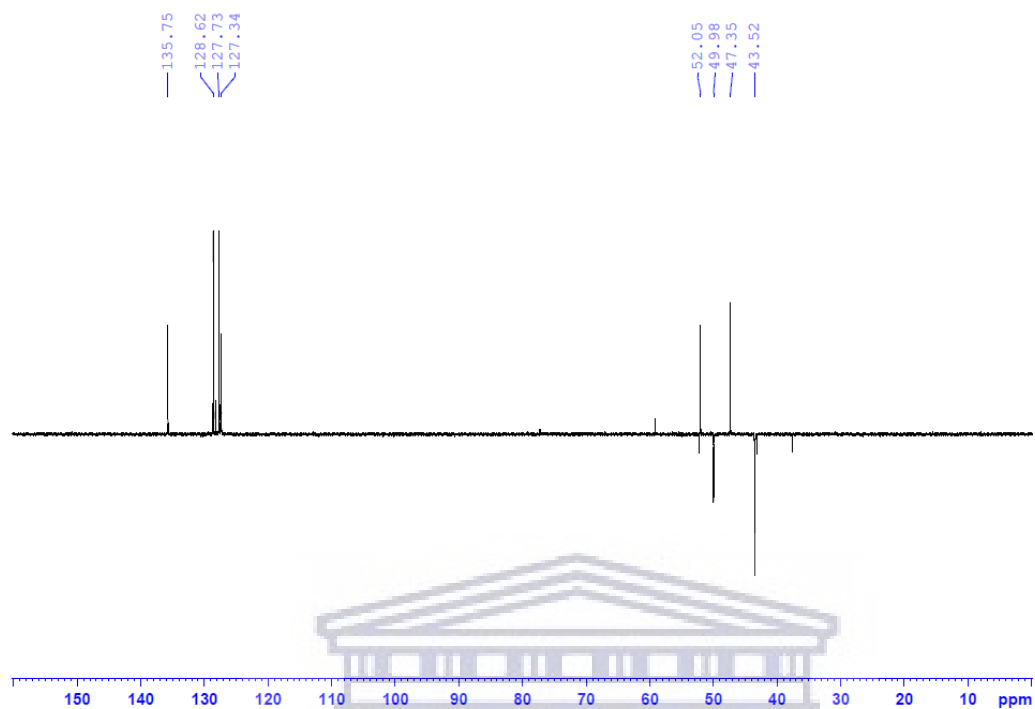
^1H spectrum of compound 9



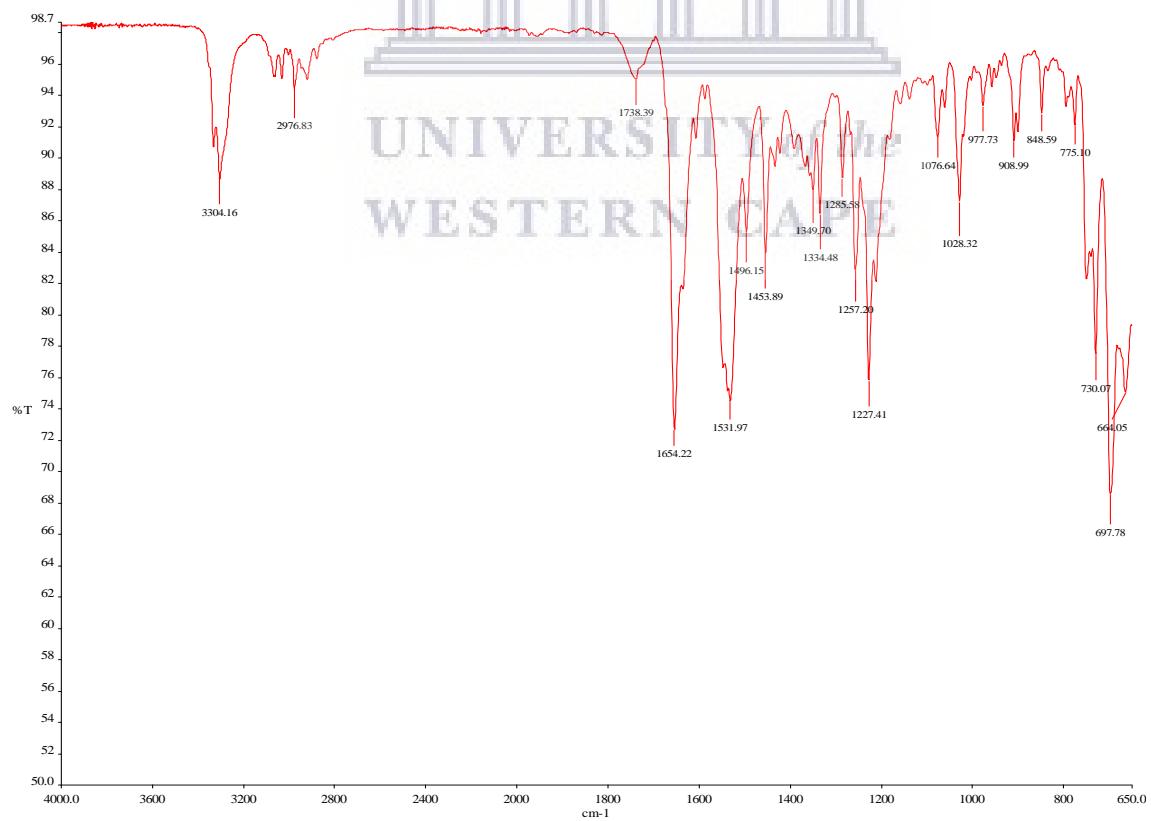
^{13}C spectrum of compound 9



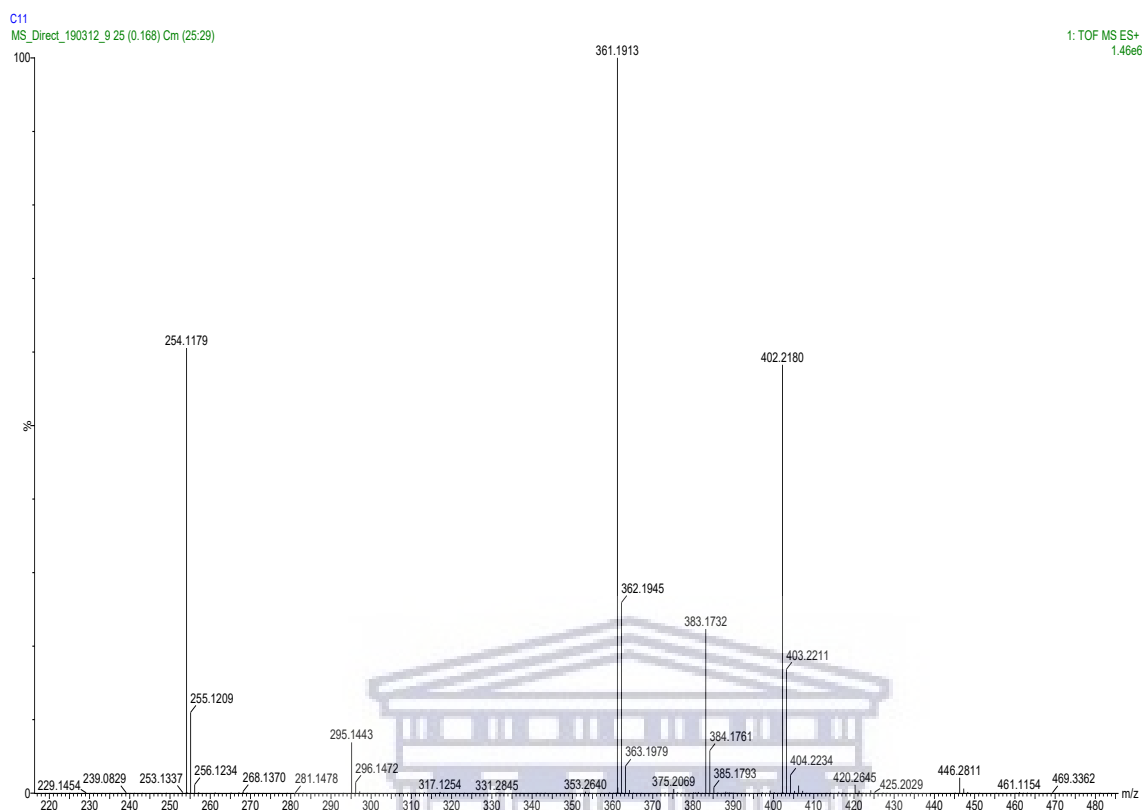
DEPT-135 spectrum of compound 9



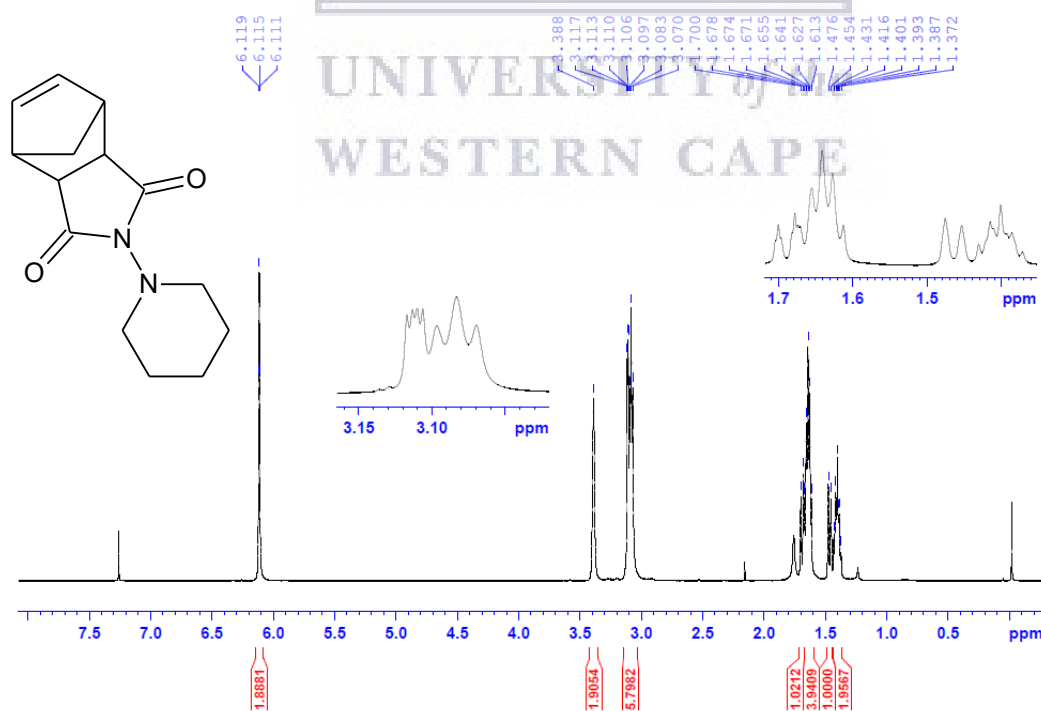
IR spectrum of compound 9



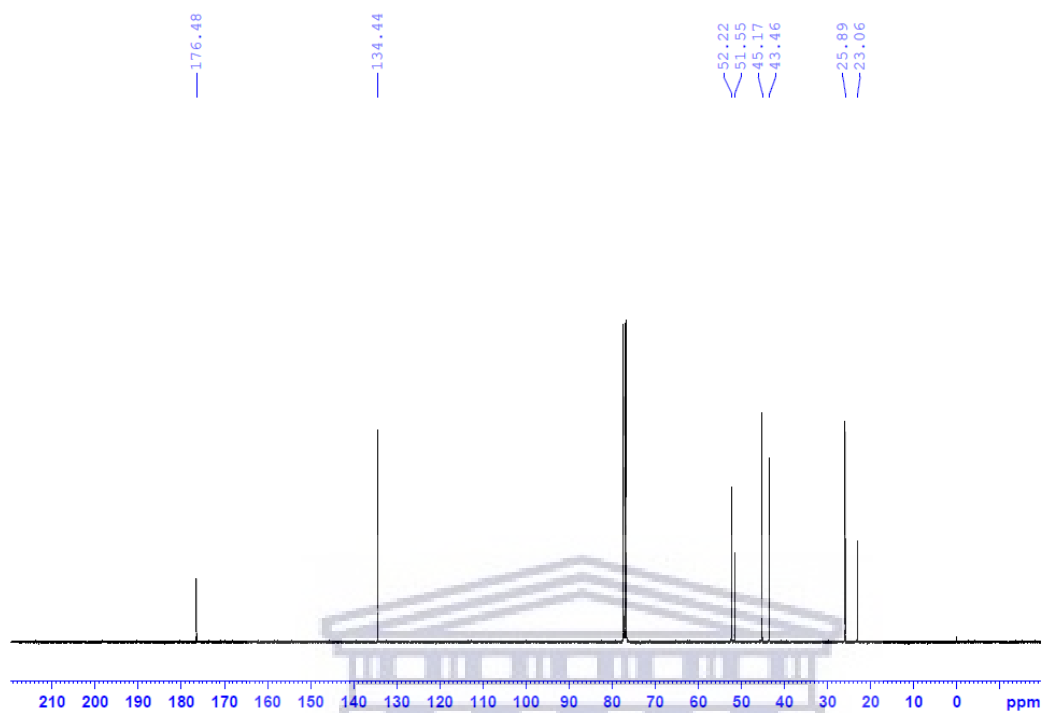
MS spectrum of compound 9



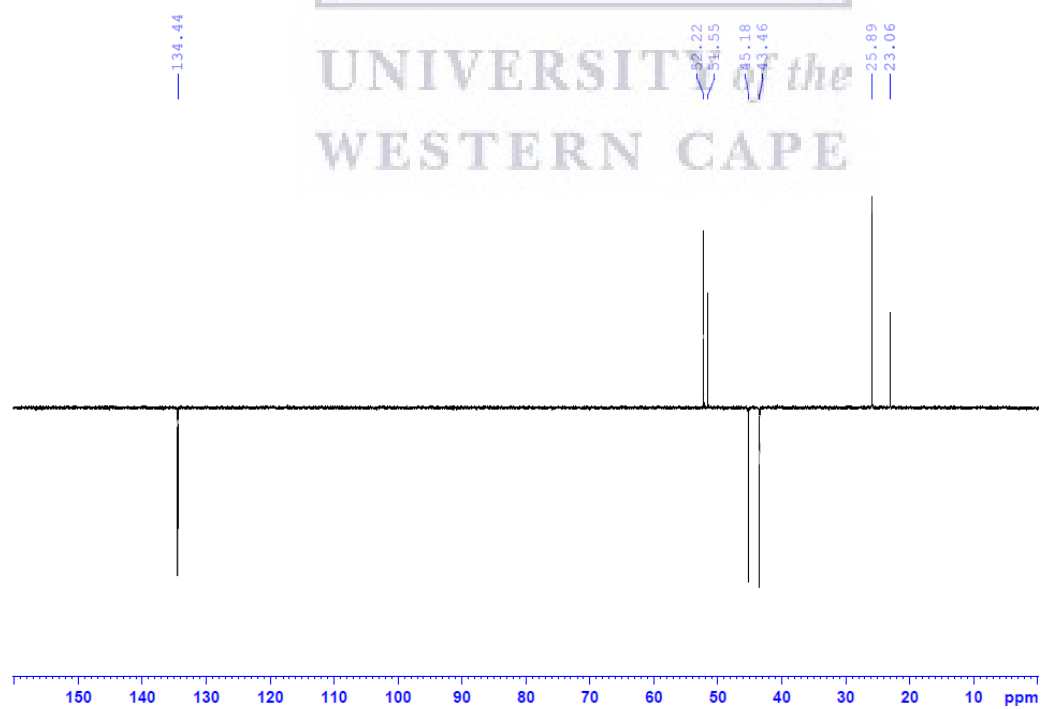
¹H spectrum of compound 10



^{13}C spectrum of compound 10



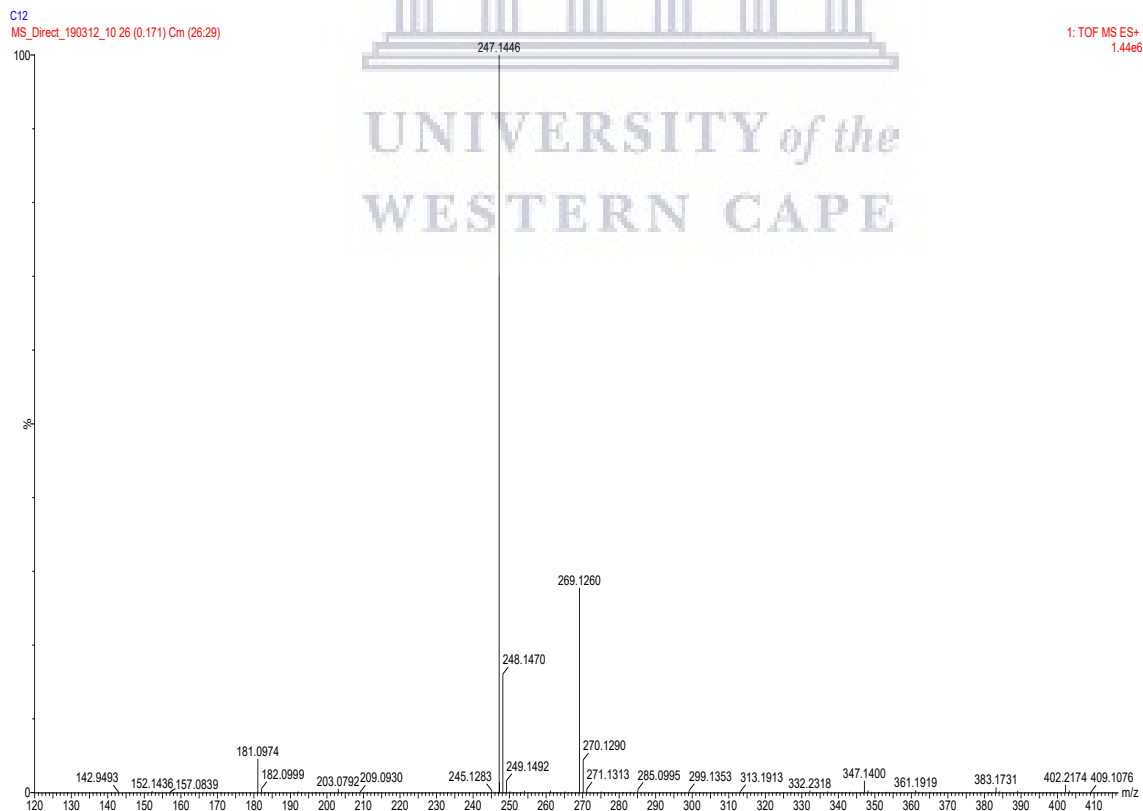
DEPT-135 spectrum of compound 10



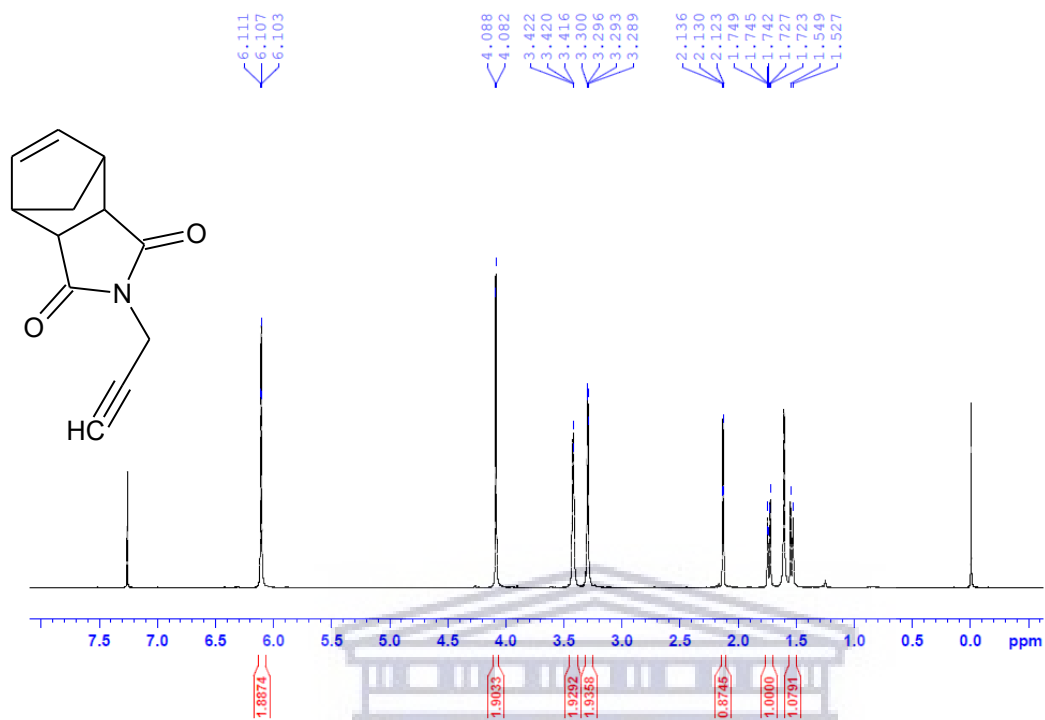
IR spectrum of compound 10



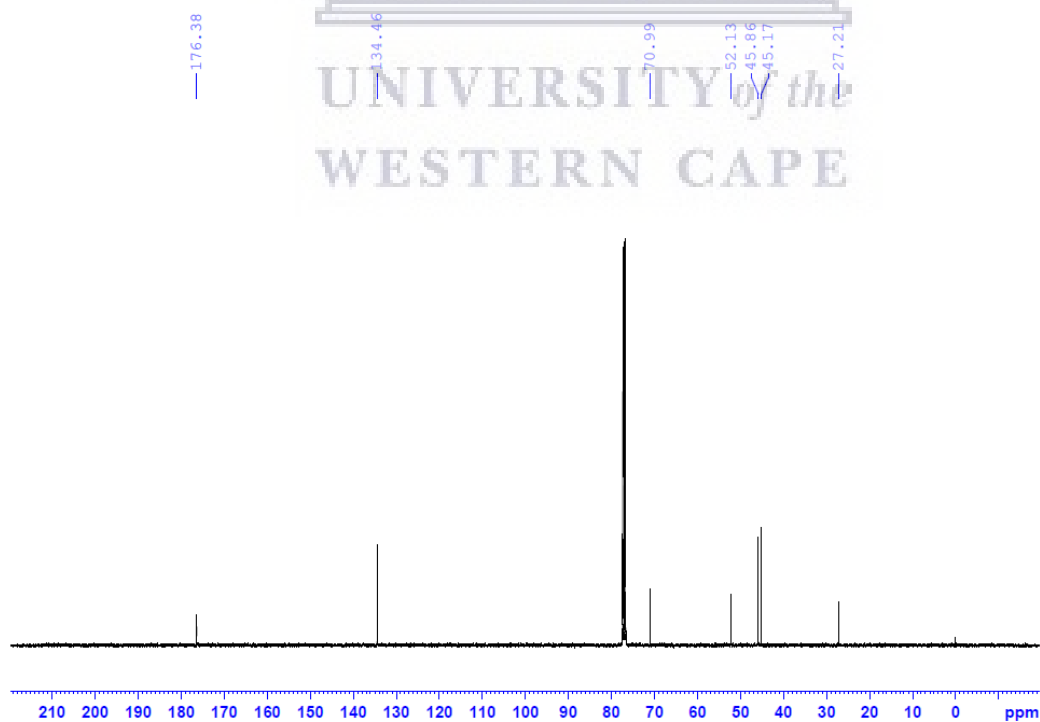
MS spectrum of compound 10



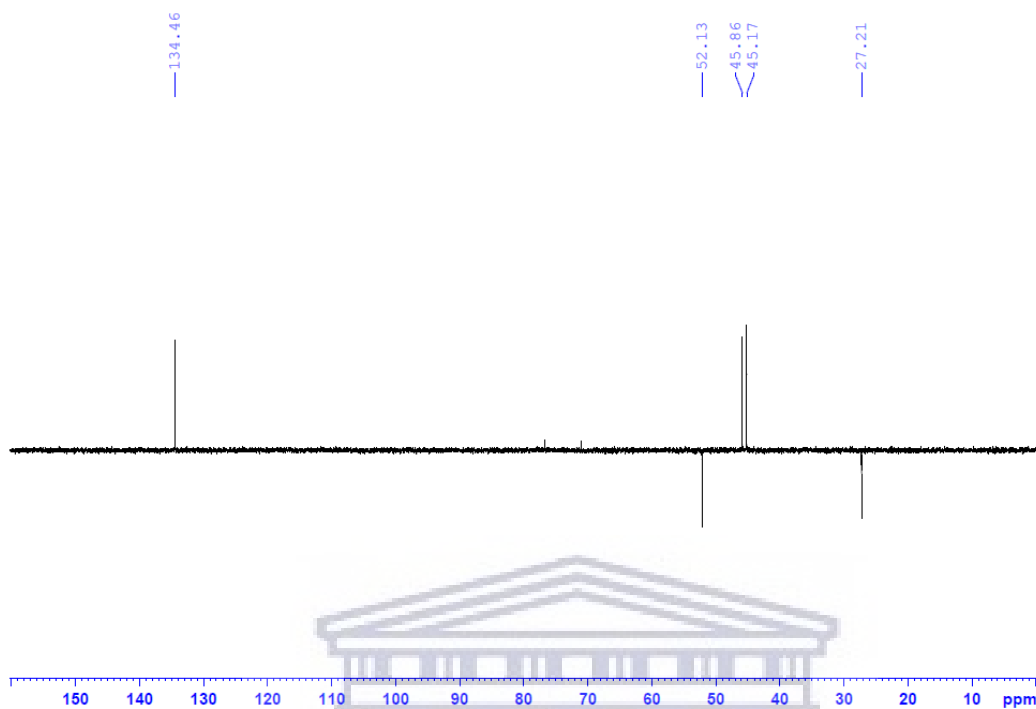
¹H spectrum of compound 11



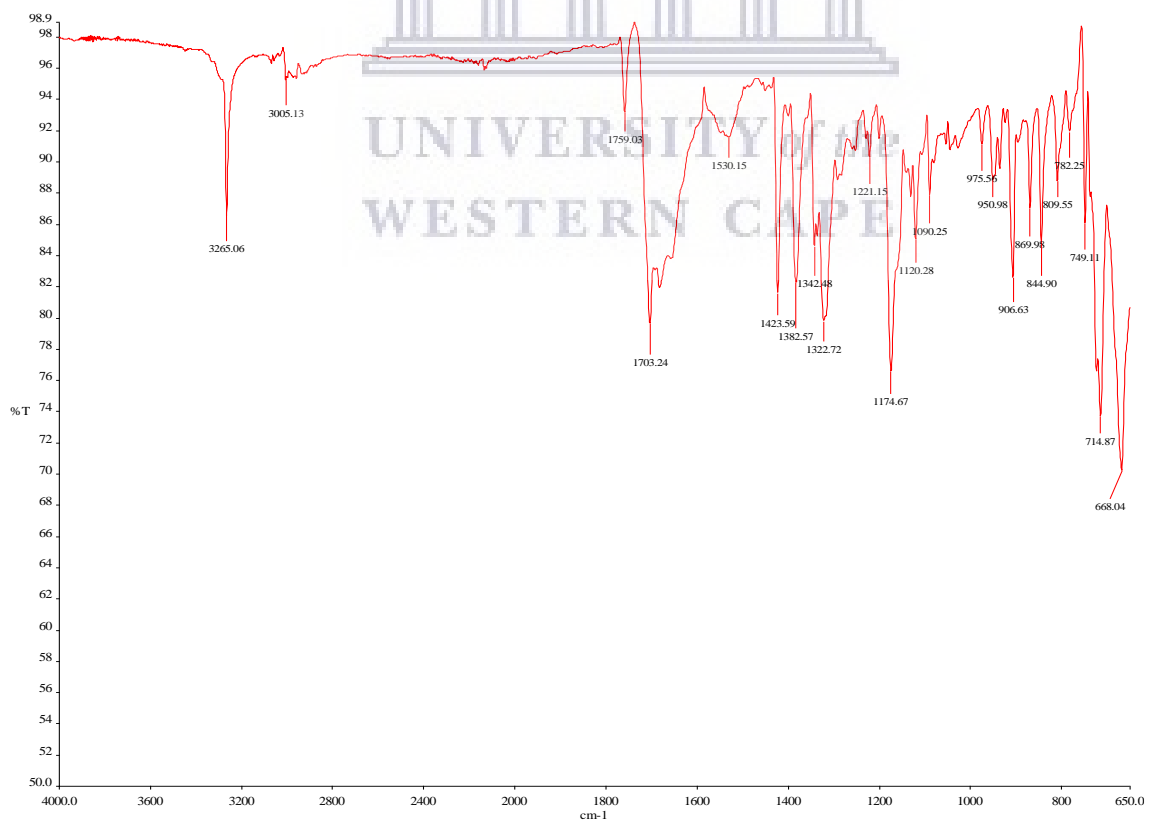
¹³C spectrum of compound 11



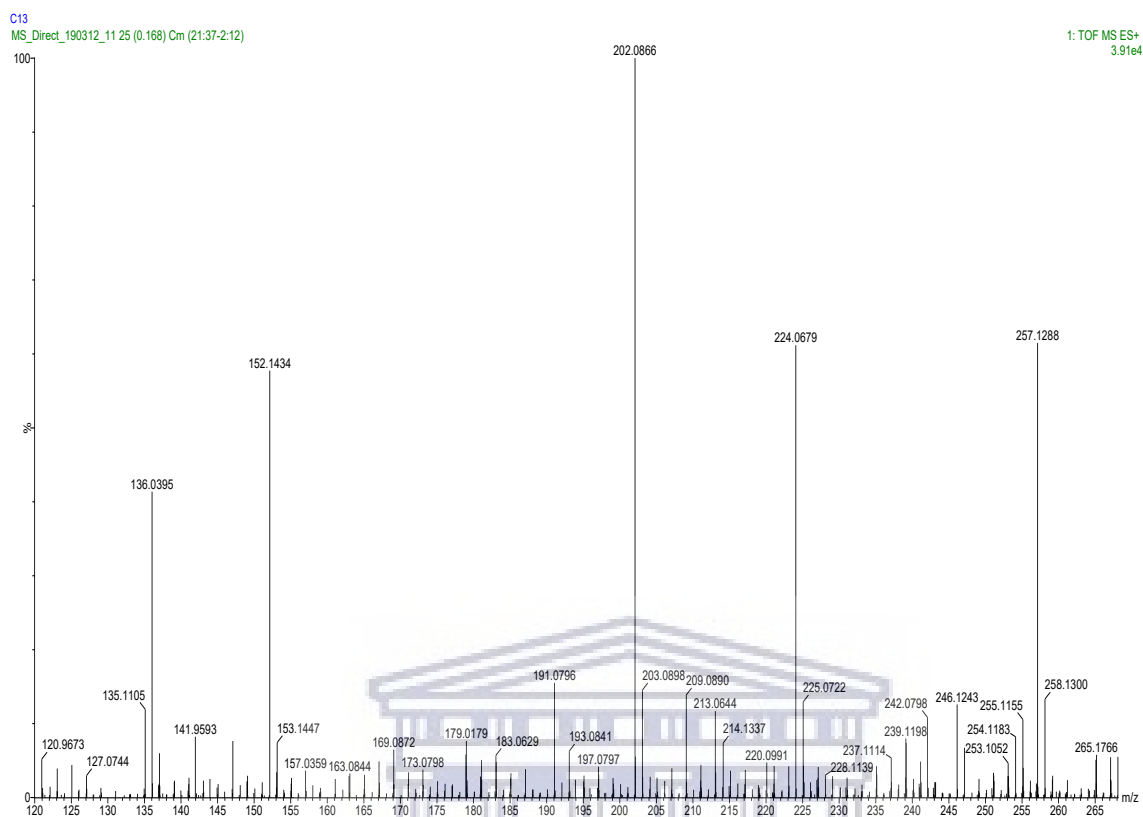
DEPT-135 spectrum of compound 11



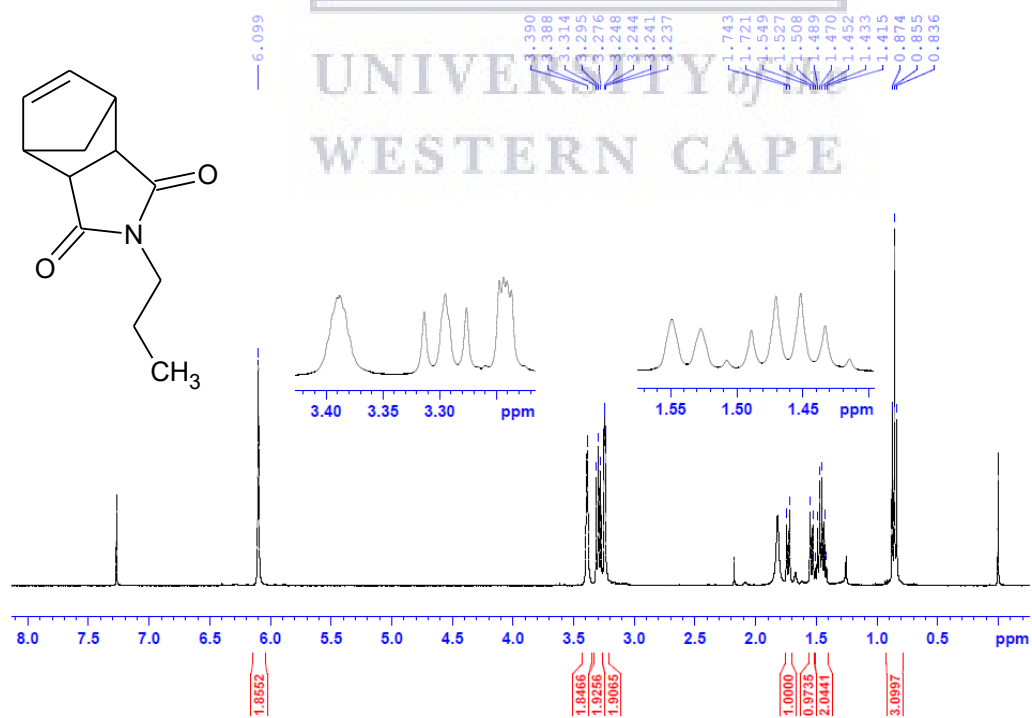
IR spectrum of compound 11



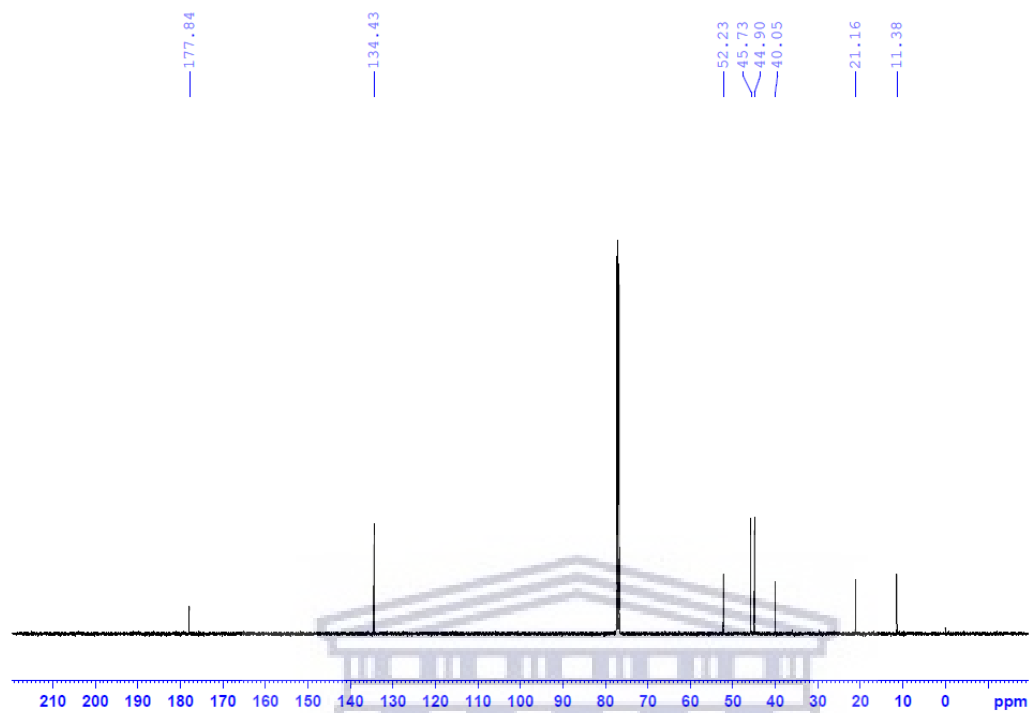
MS spectrum of compound 11



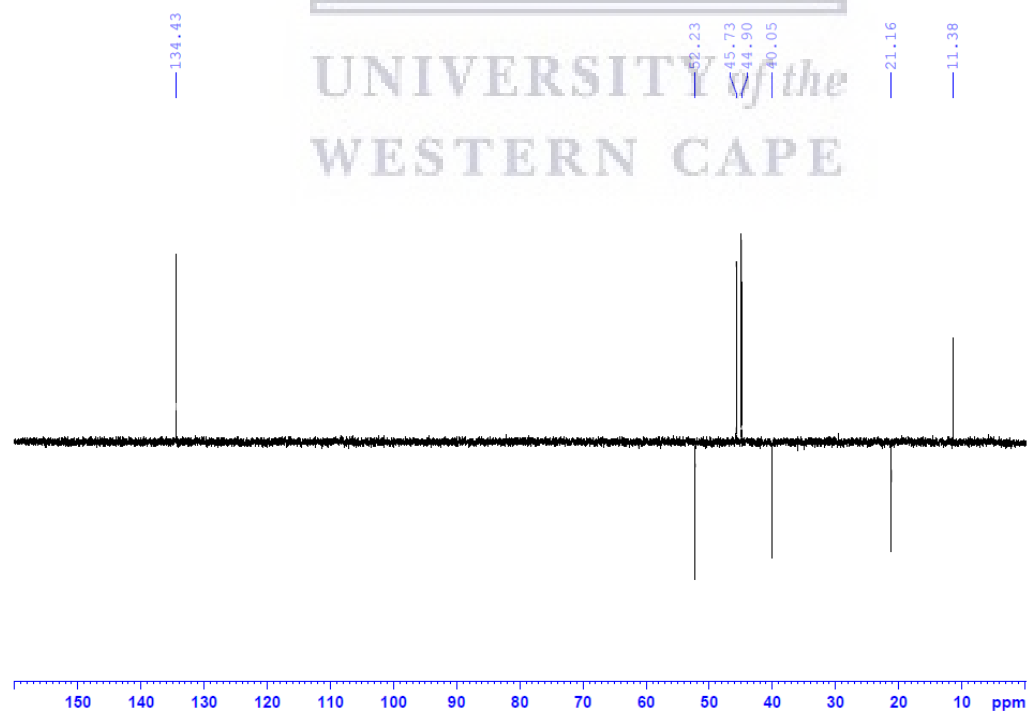
¹H spectrum of compound 12



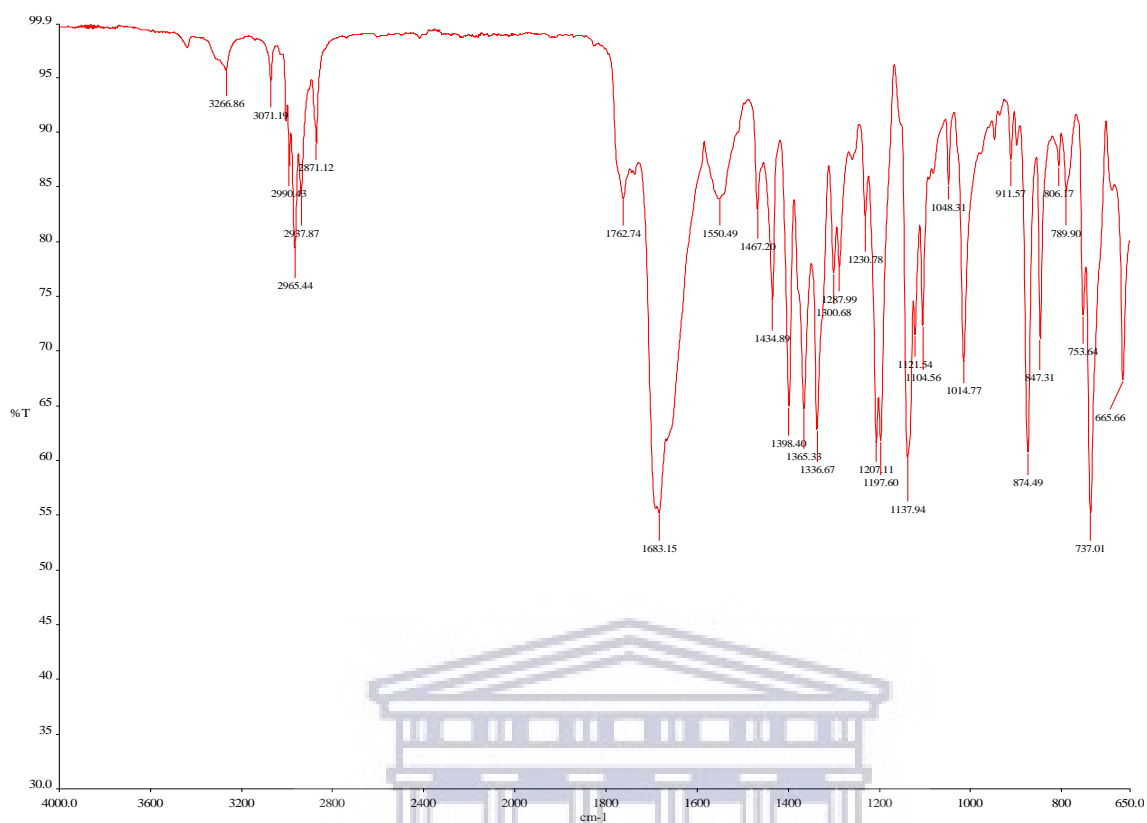
^{13}C spectrum of compound 12



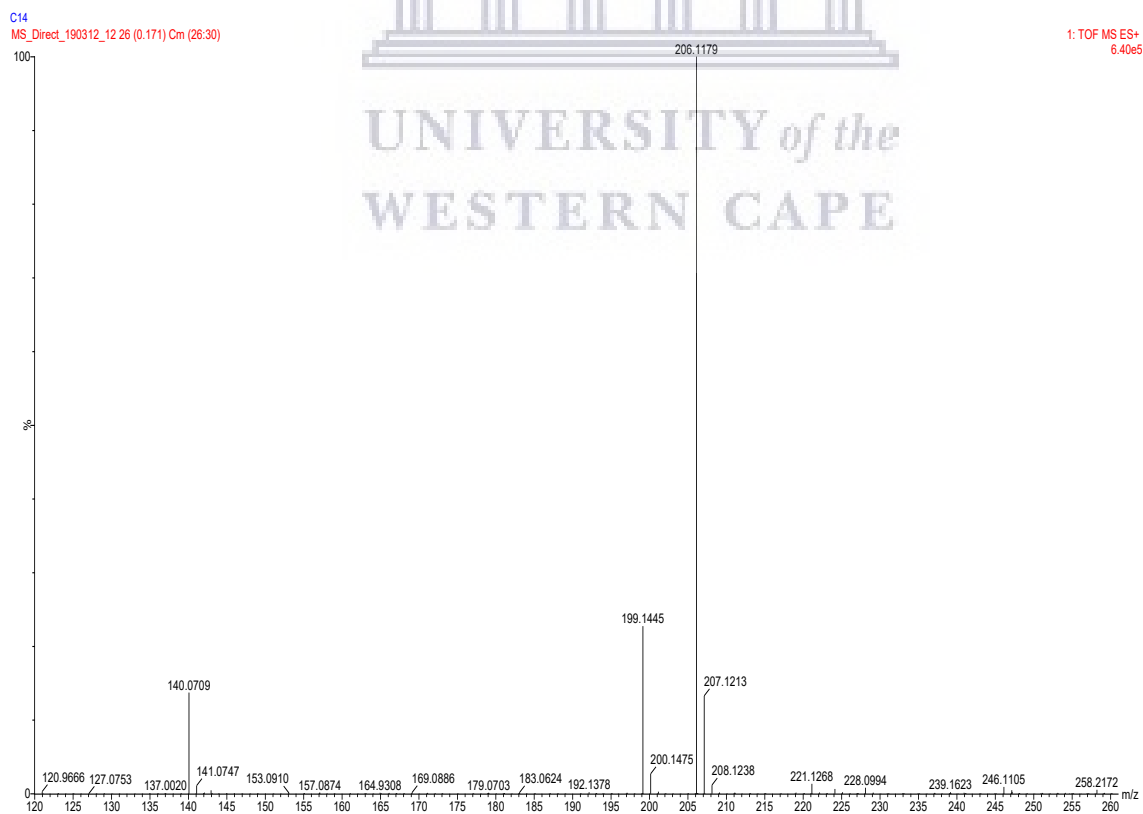
DEPT-135 spectrum of compound 12



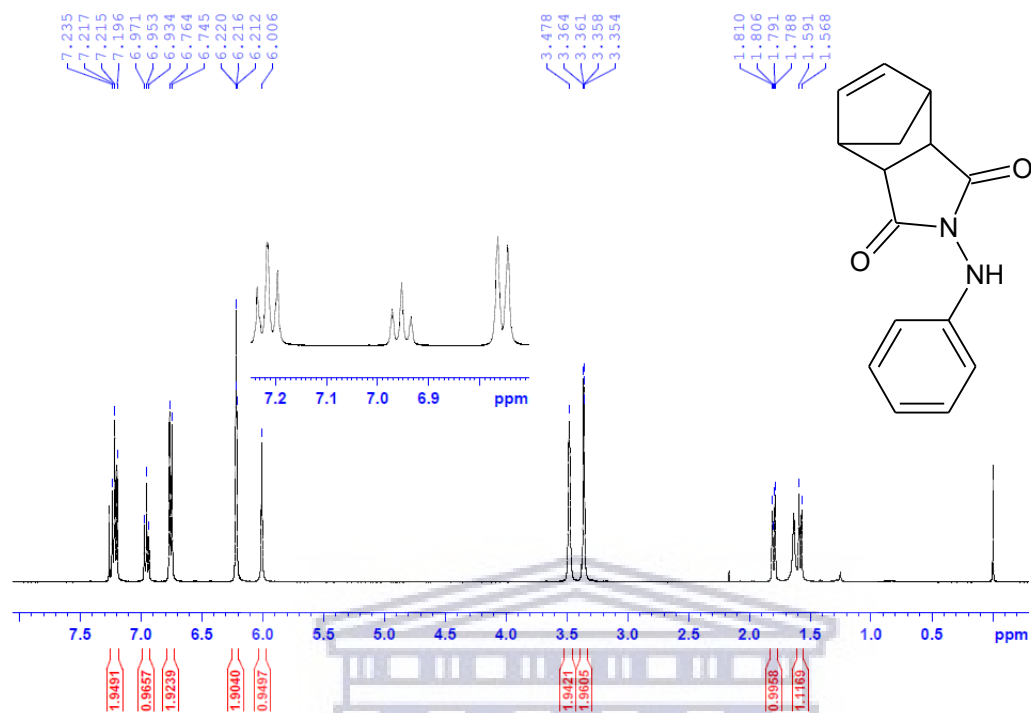
IR spectrum of compound 12



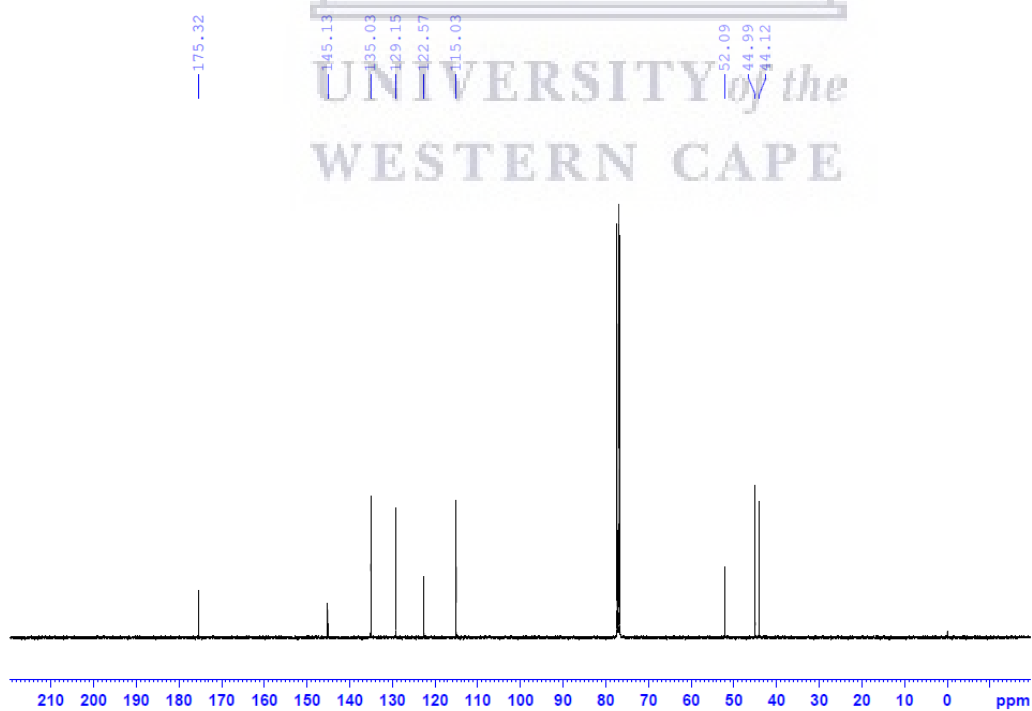
MS spectrum of compound 12



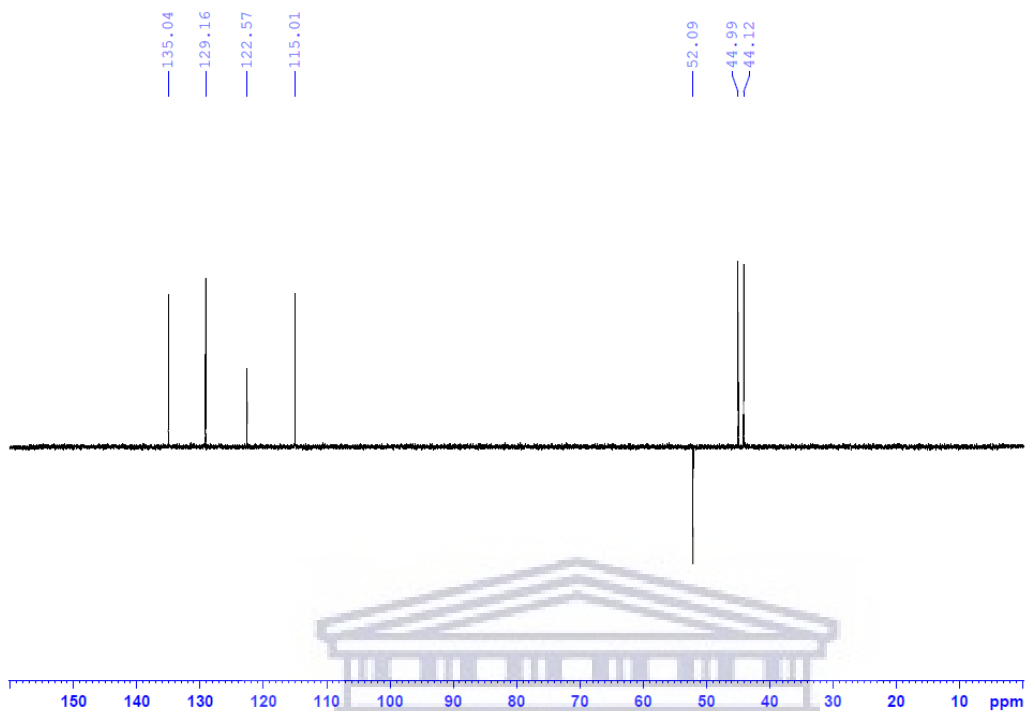
¹H spectrum of compound 13



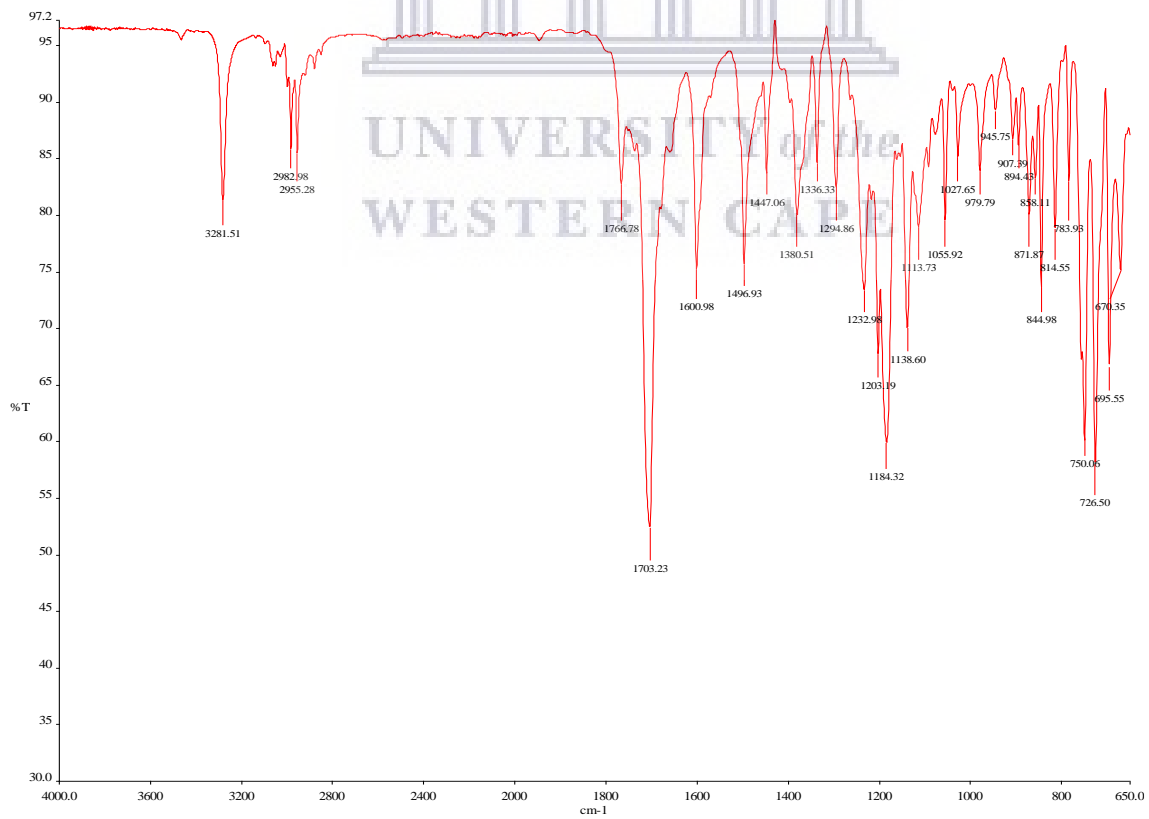
¹³C spectrum of compound 13



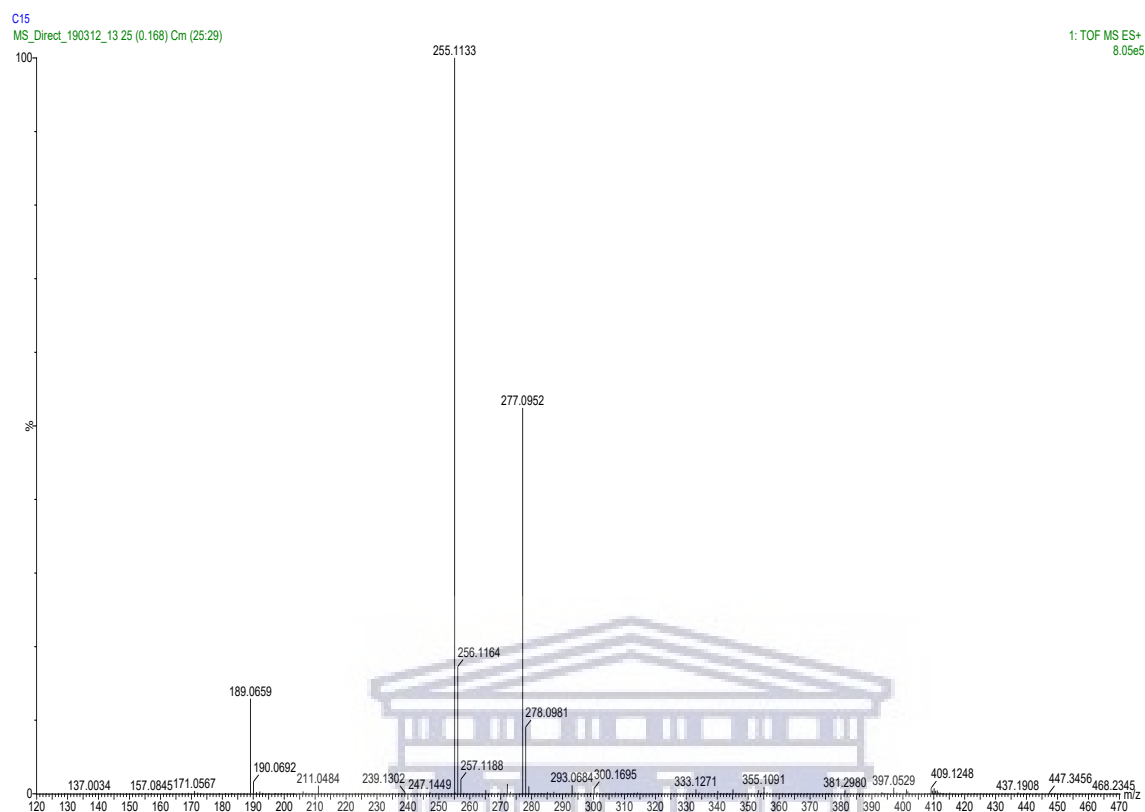
DEPT-135 spectrum of compound 13



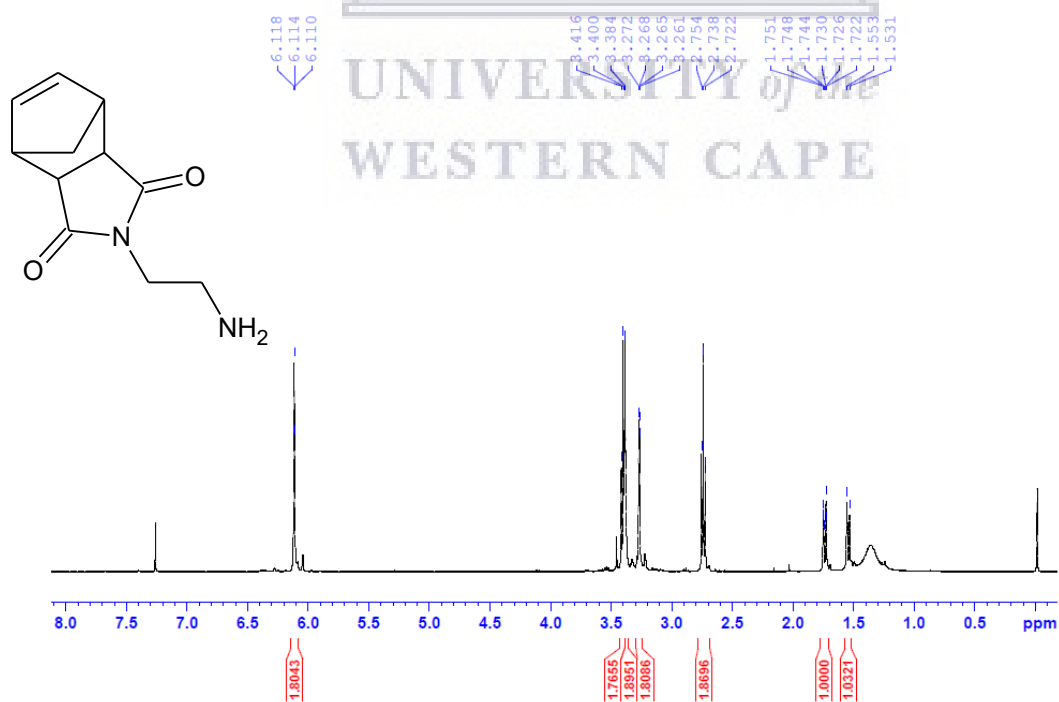
IR spectrum of compound 13



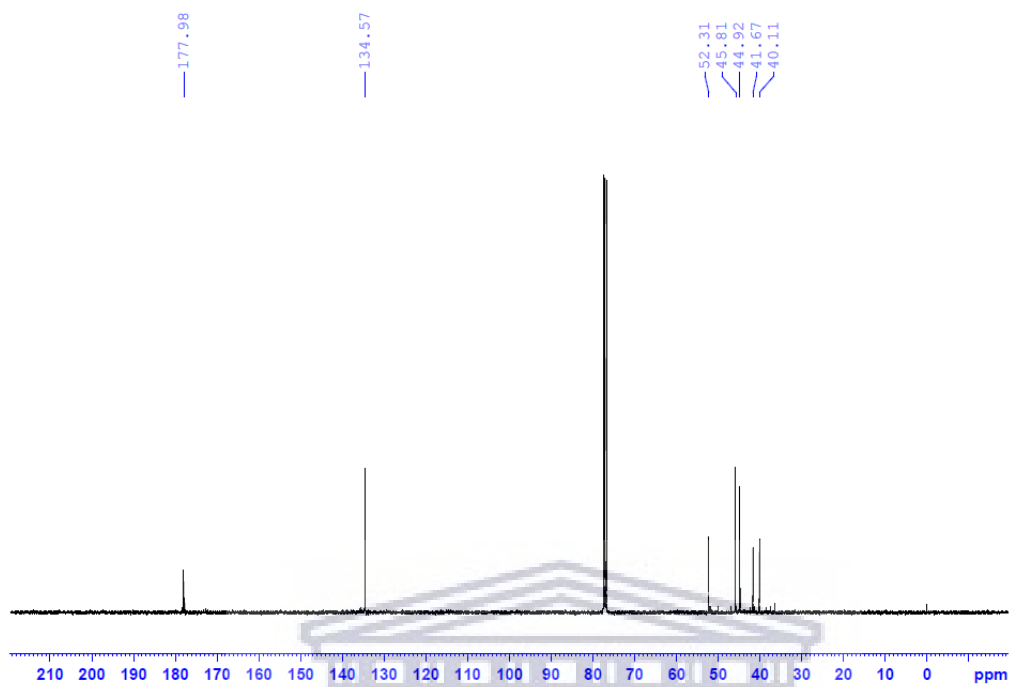
MS spectrum of compound 13



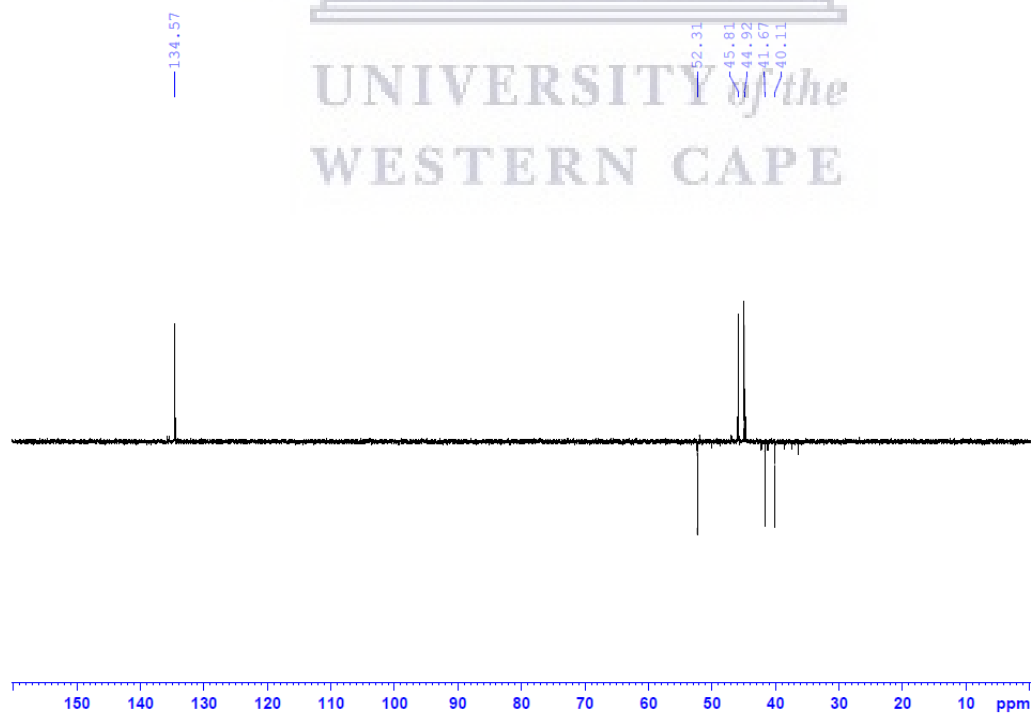
¹H spectrum of compound 14



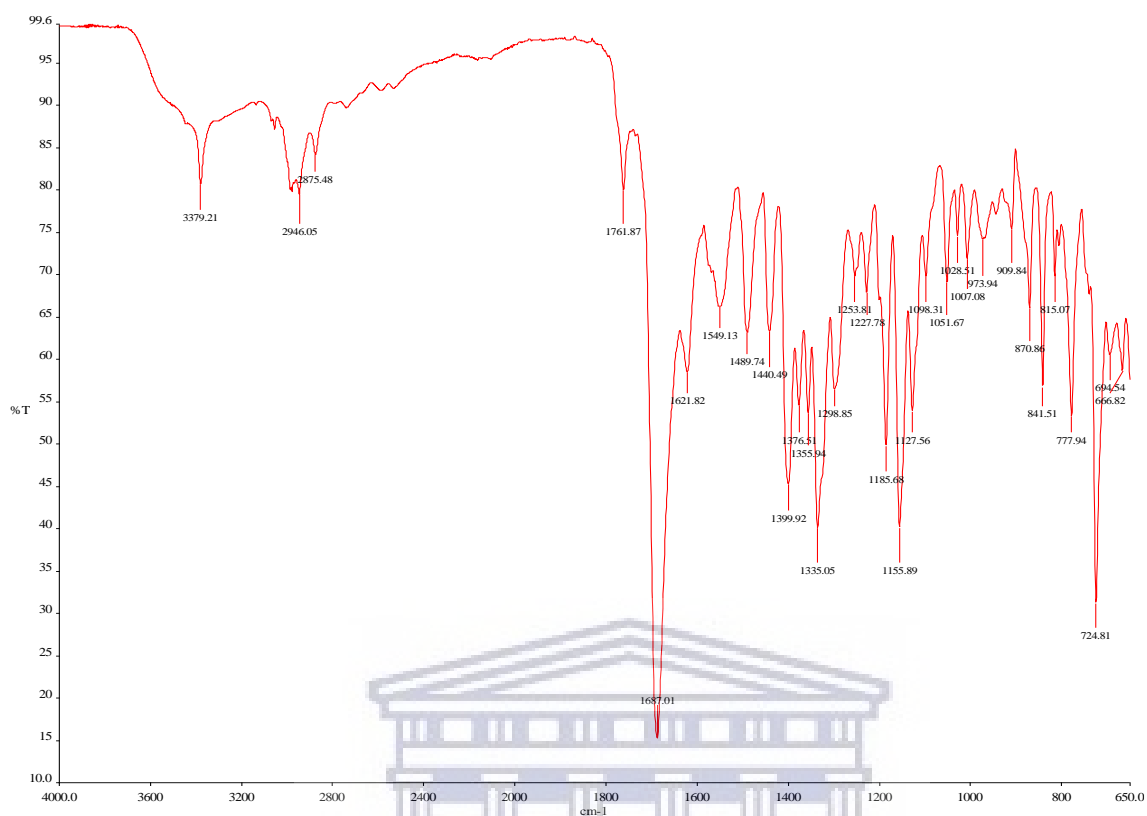
^{13}C spectrum of compound 14



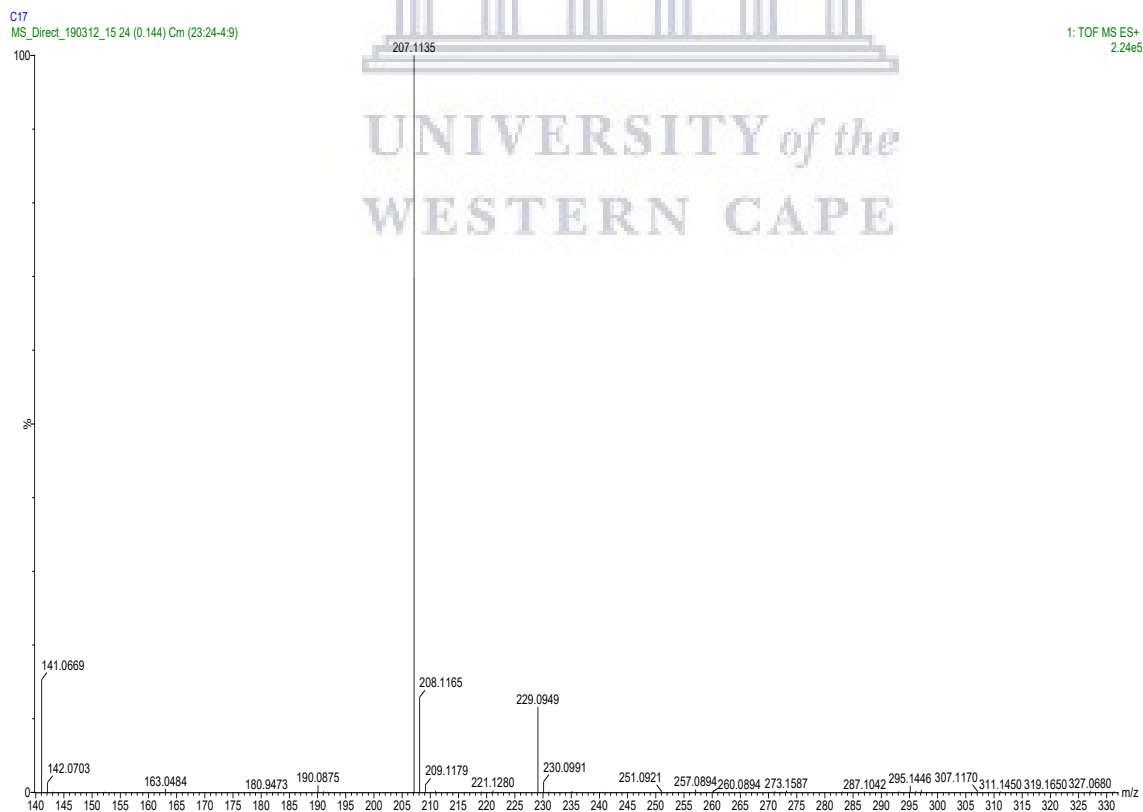
DEPT-135 spectrum of compound 14



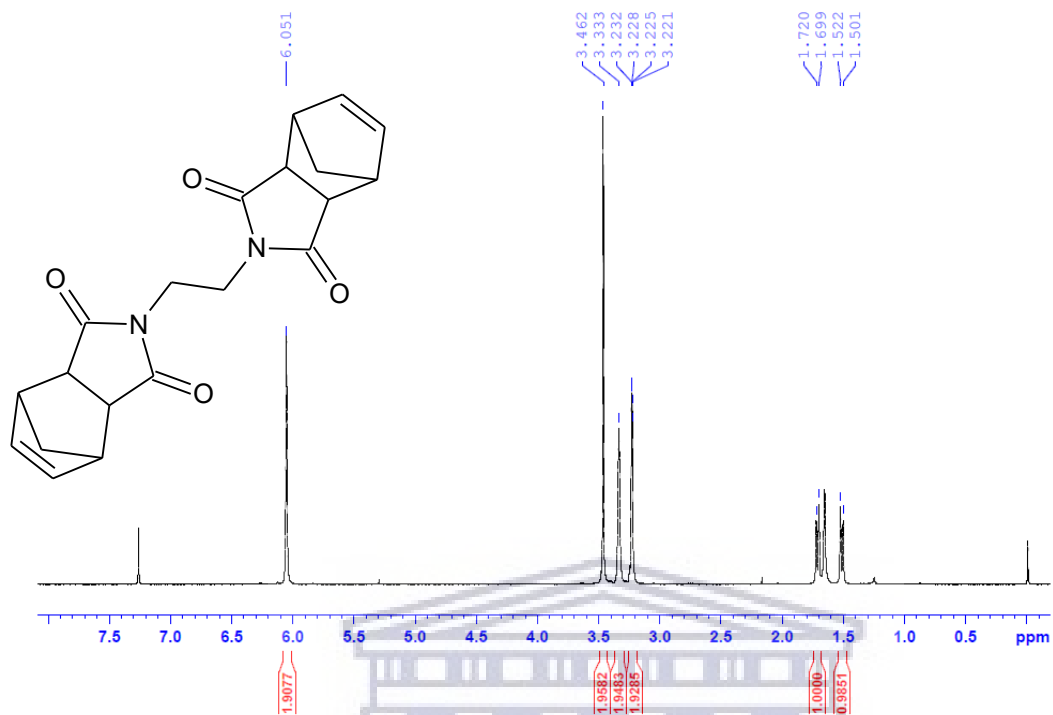
IR spectrum of compound 14



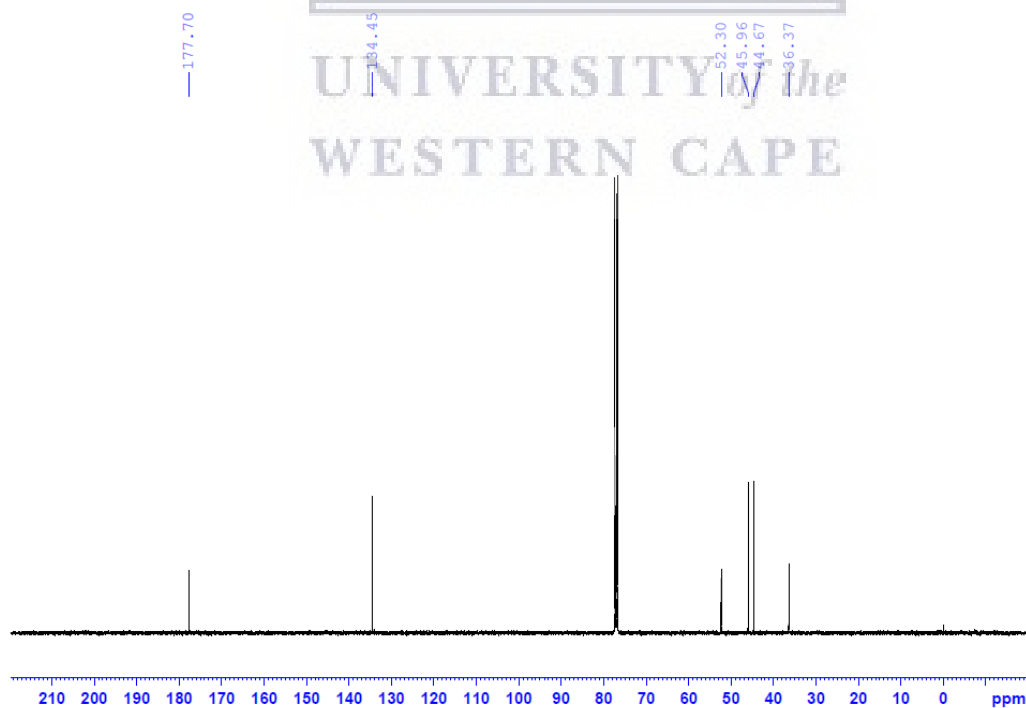
MS spectrum of compound 14



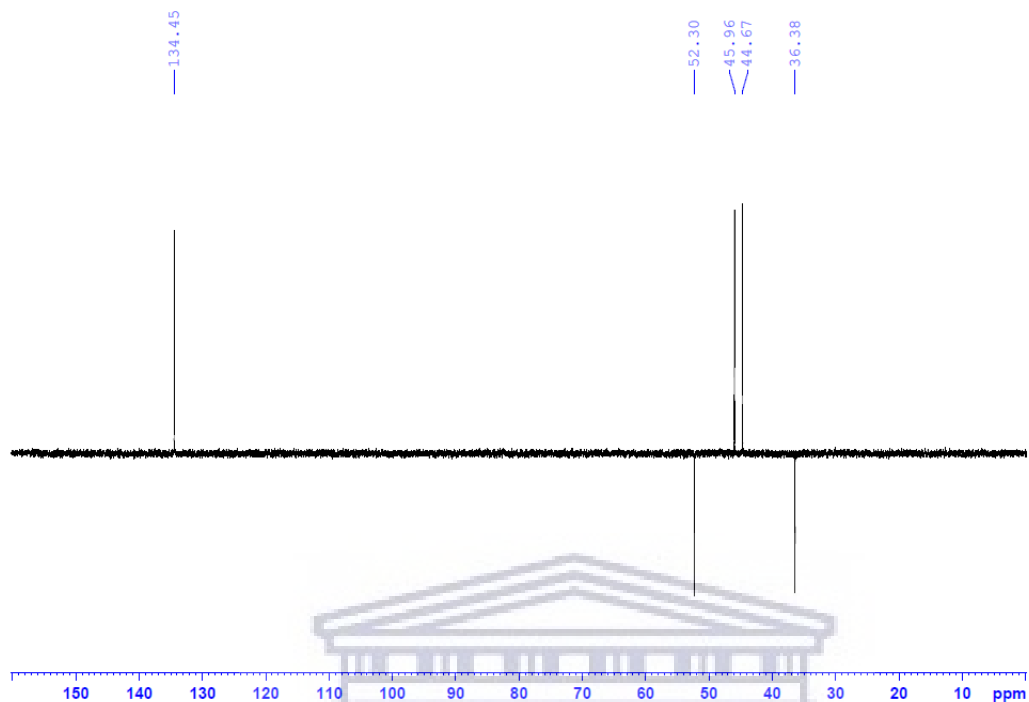
^1H spectrum of compound 15



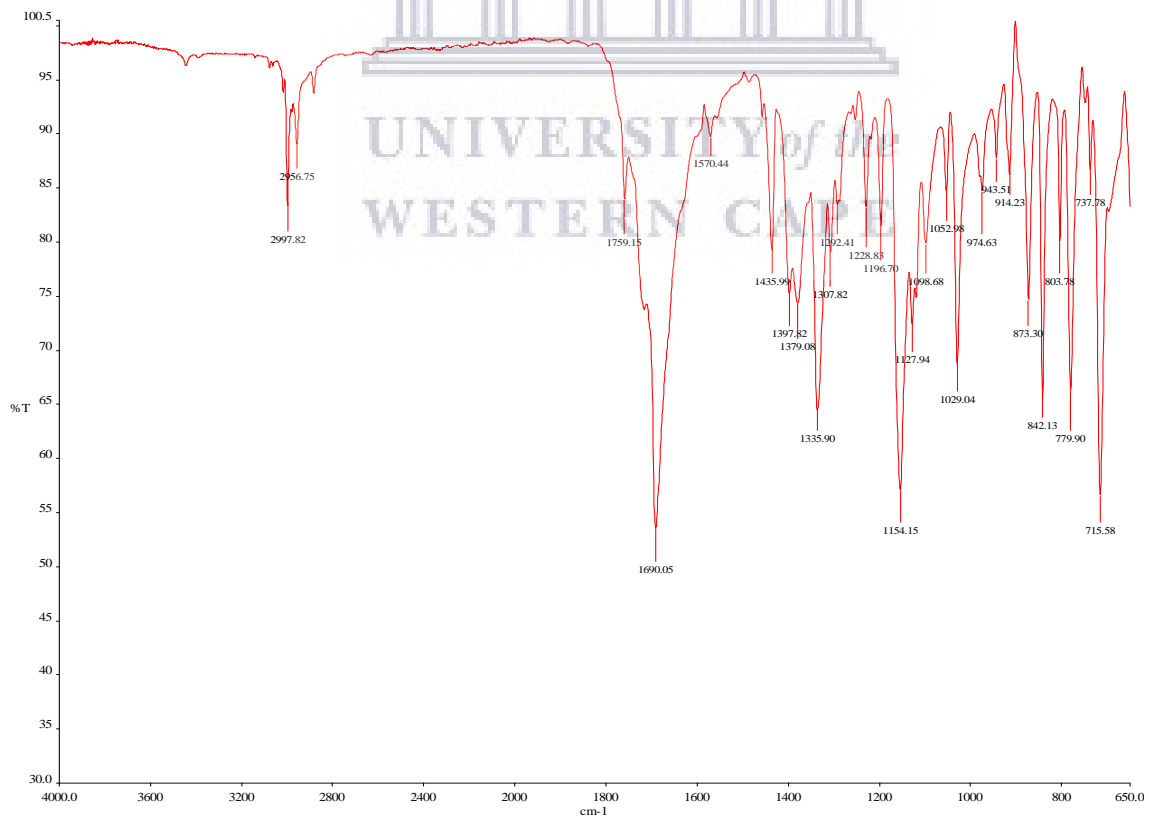
^{13}C spectrum of compound 15



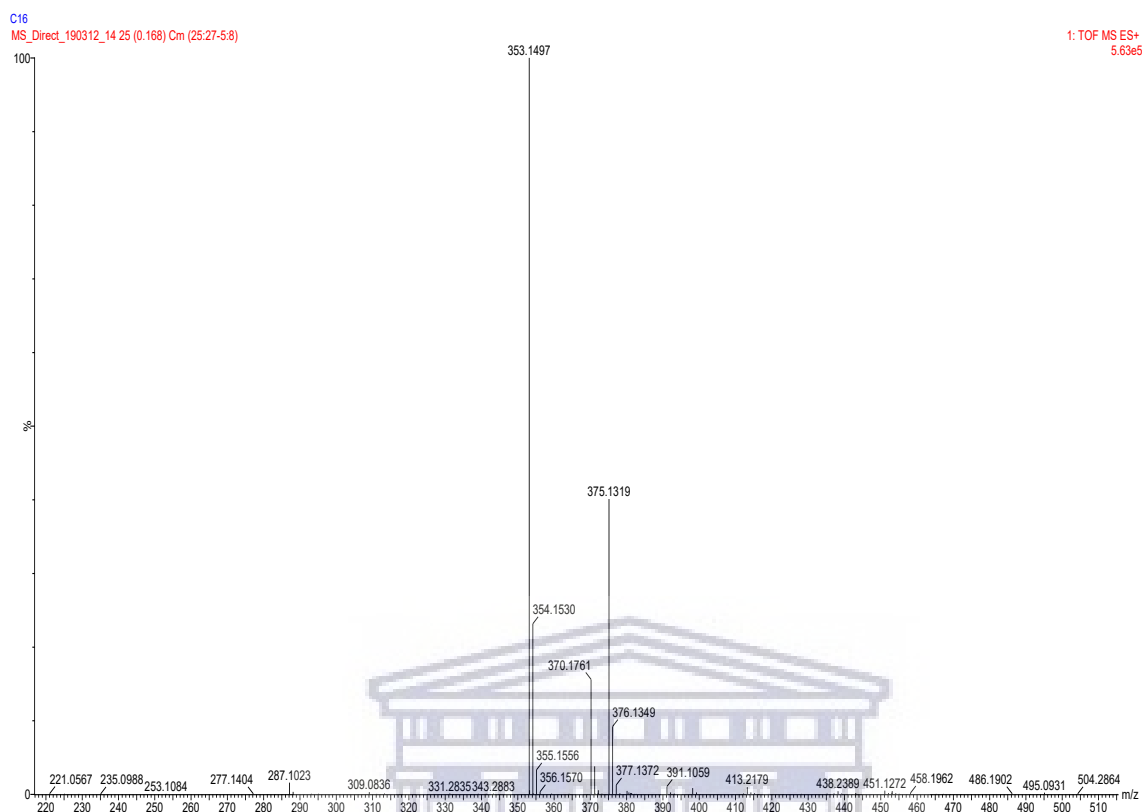
DEPT-135 spectrum of compound 15



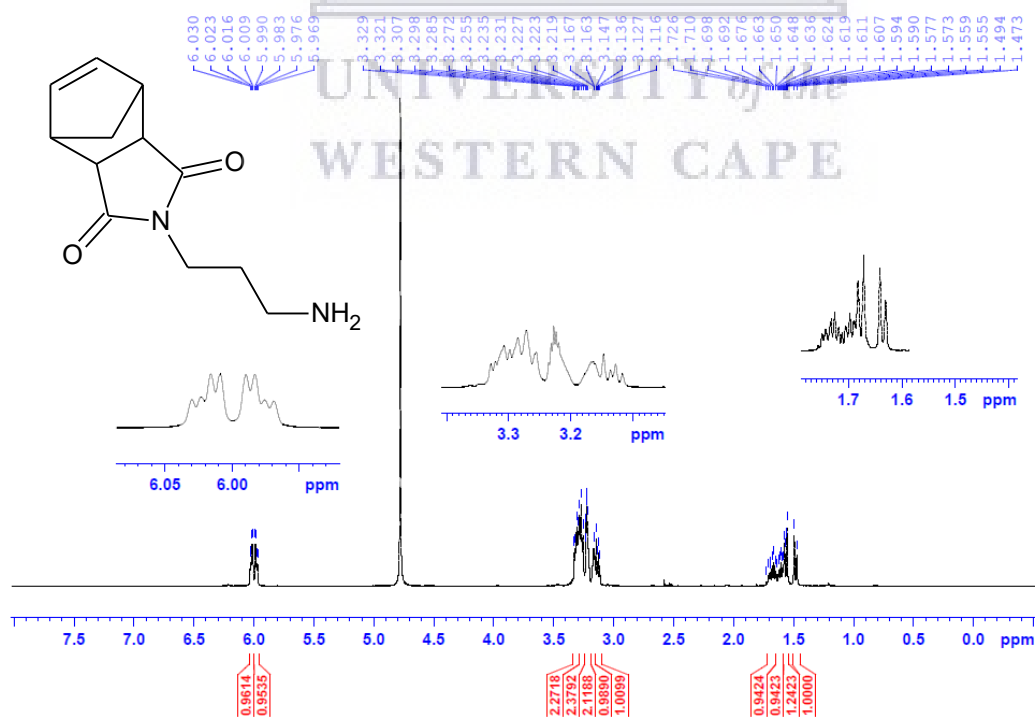
IR spectrum of compound 15



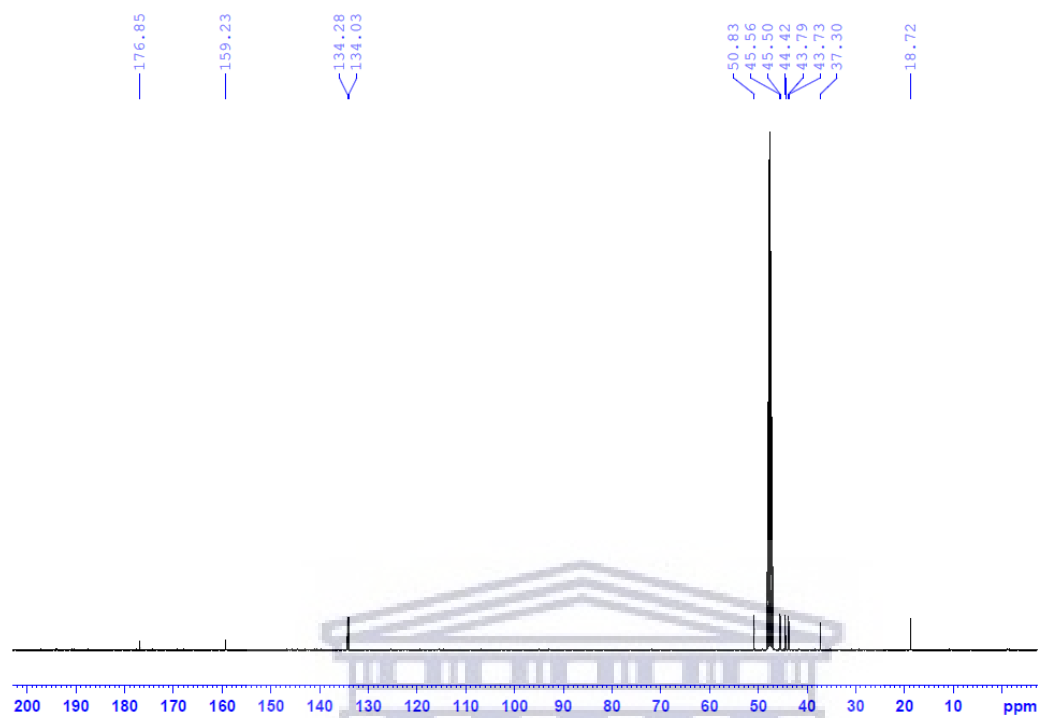
MS spectrum of compound 15



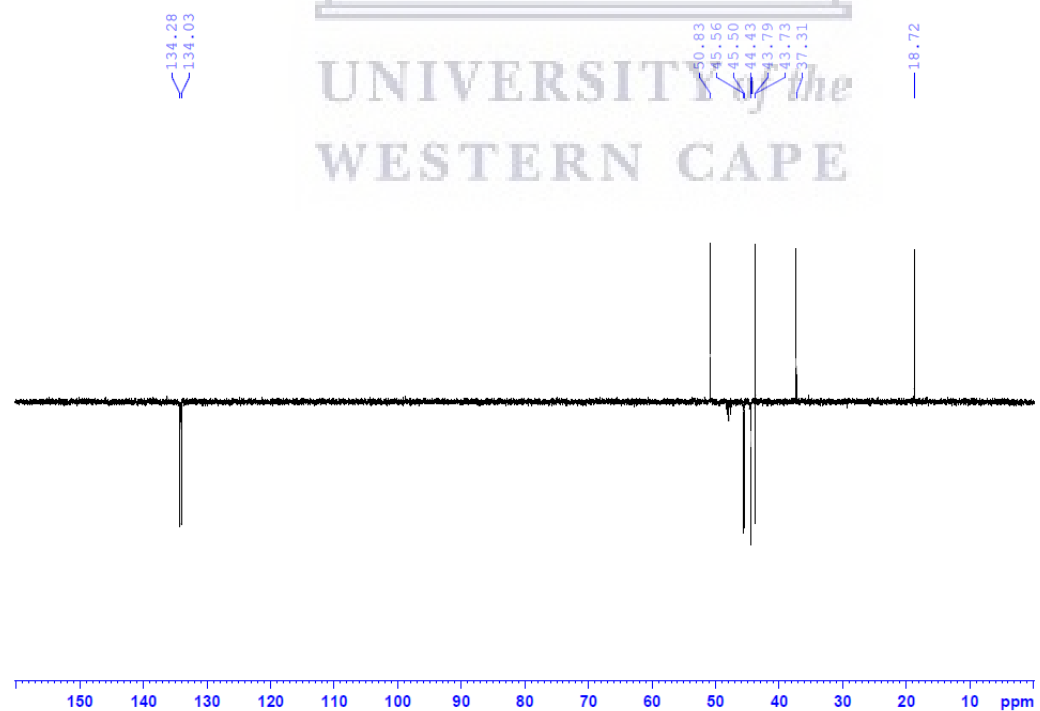
¹H spectrum of compound 16



^{13}C spectrum of compound 16



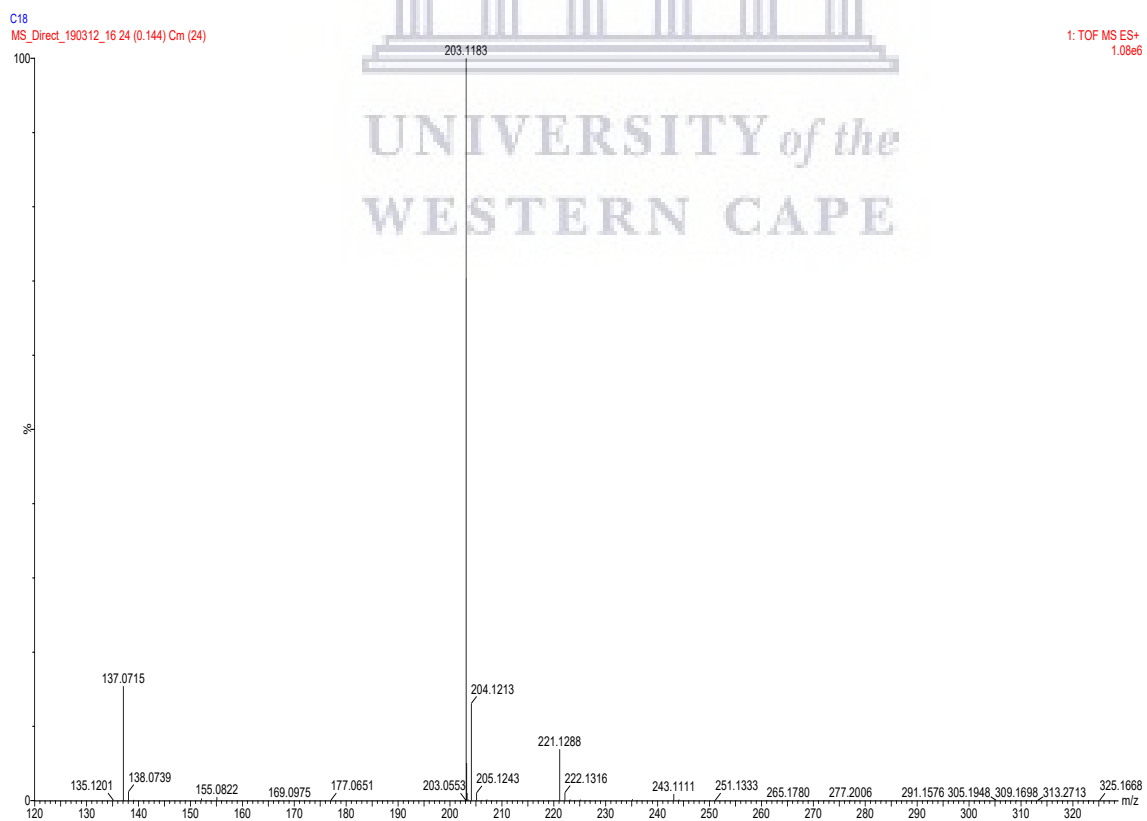
DEPT-135 spectrum of compound 16



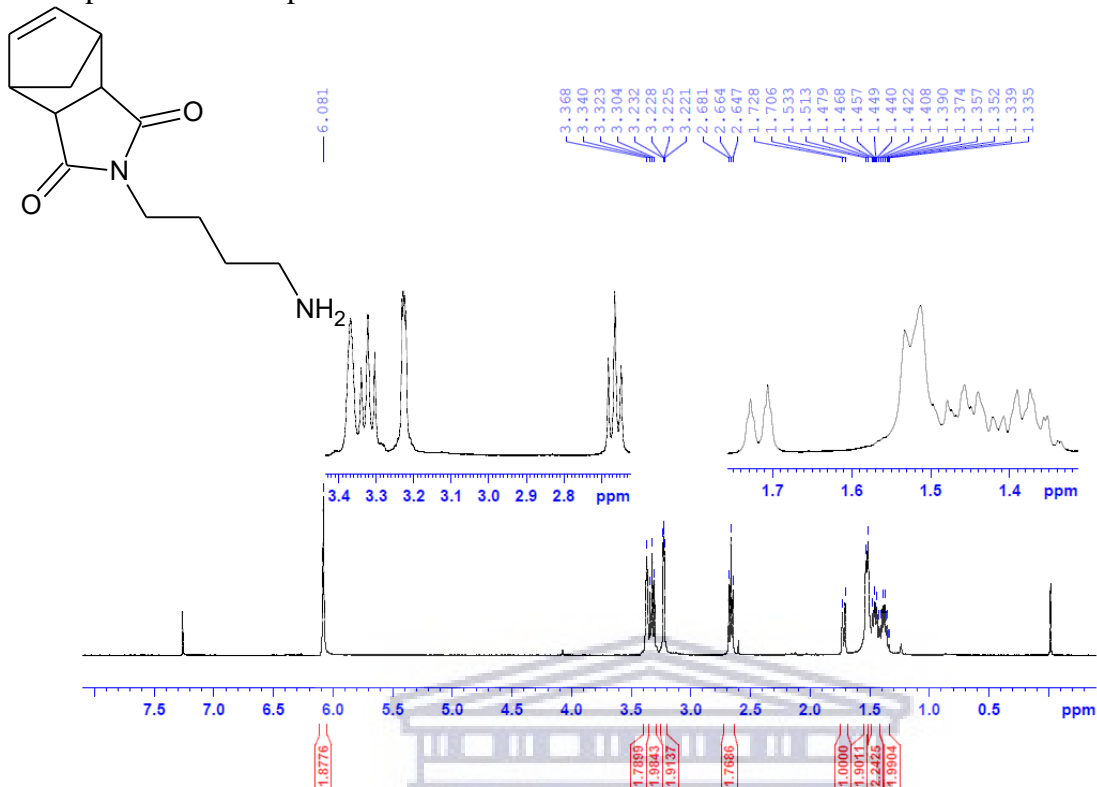
IR spectrum of compound 16



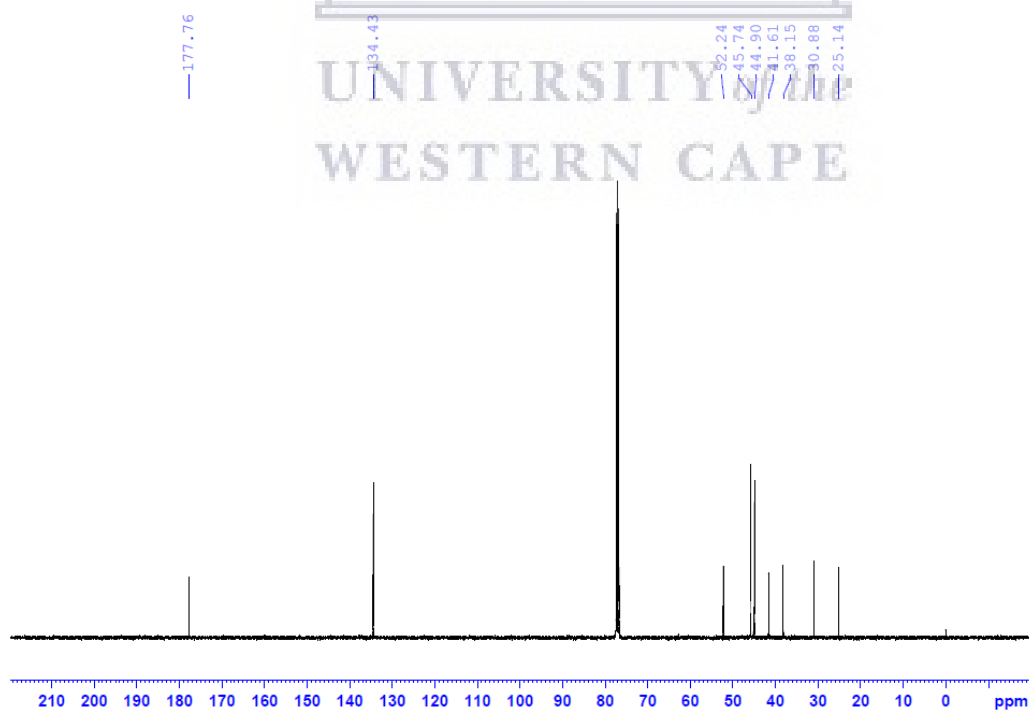
MS spectrum of compound 16



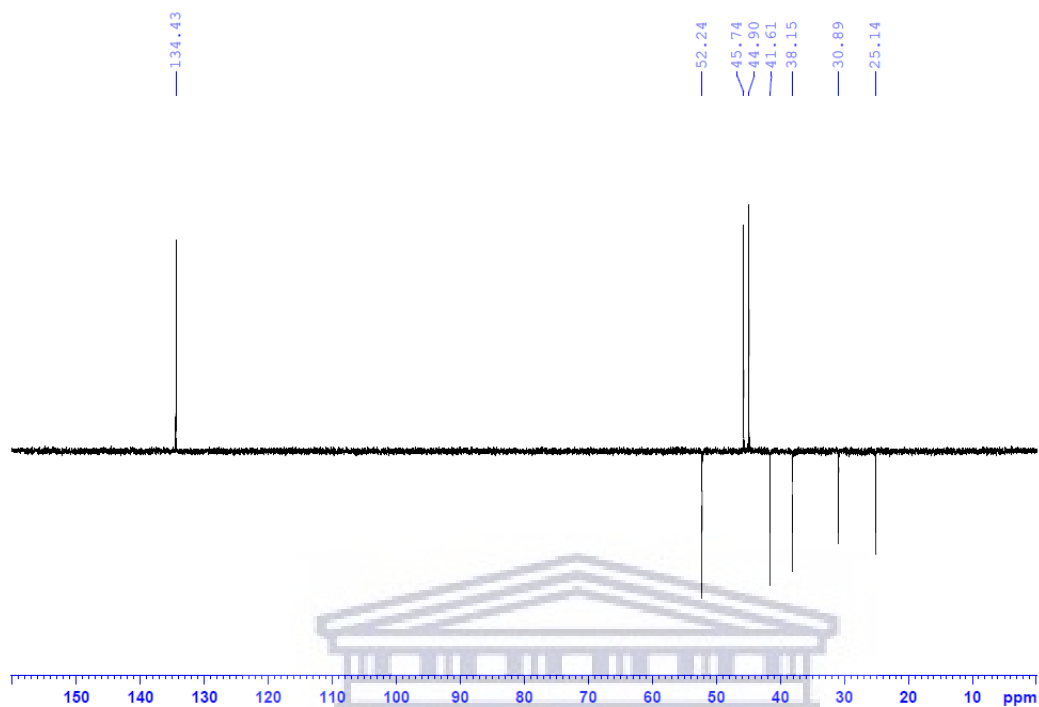
¹H spectrum of compound 17



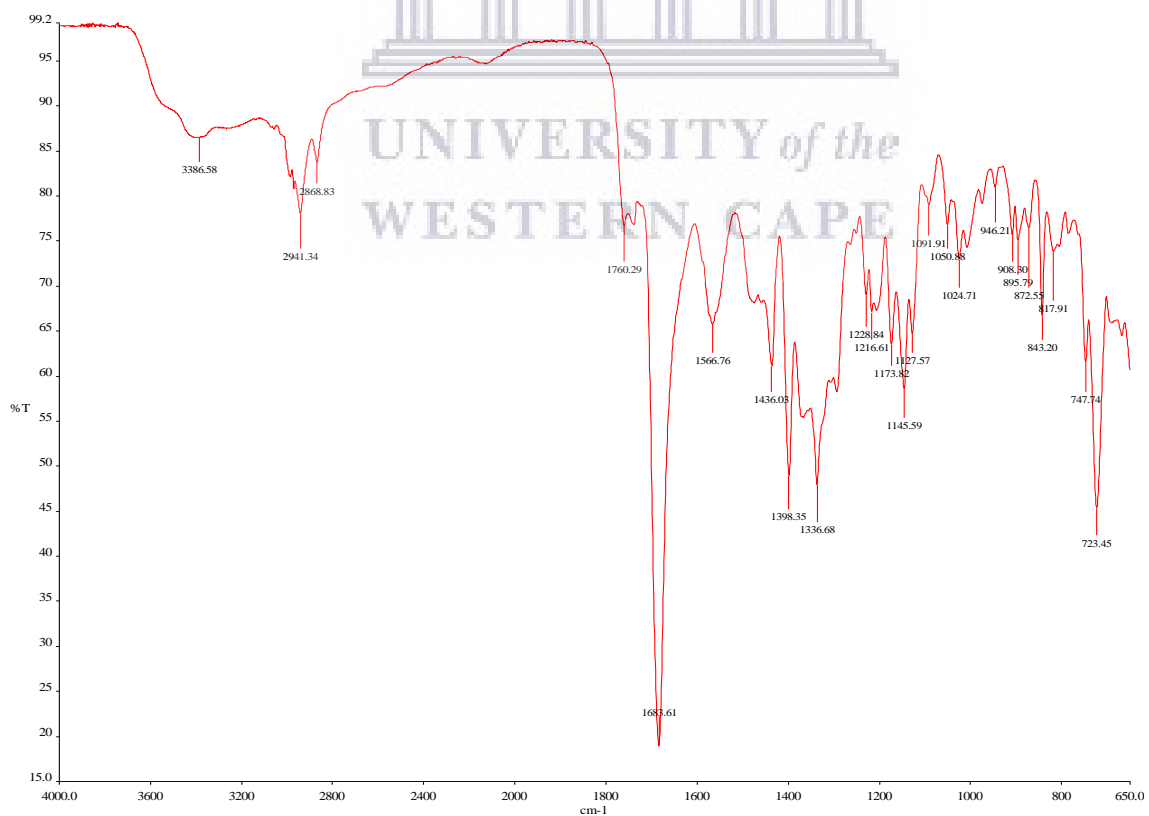
¹³C spectrum of compound 17



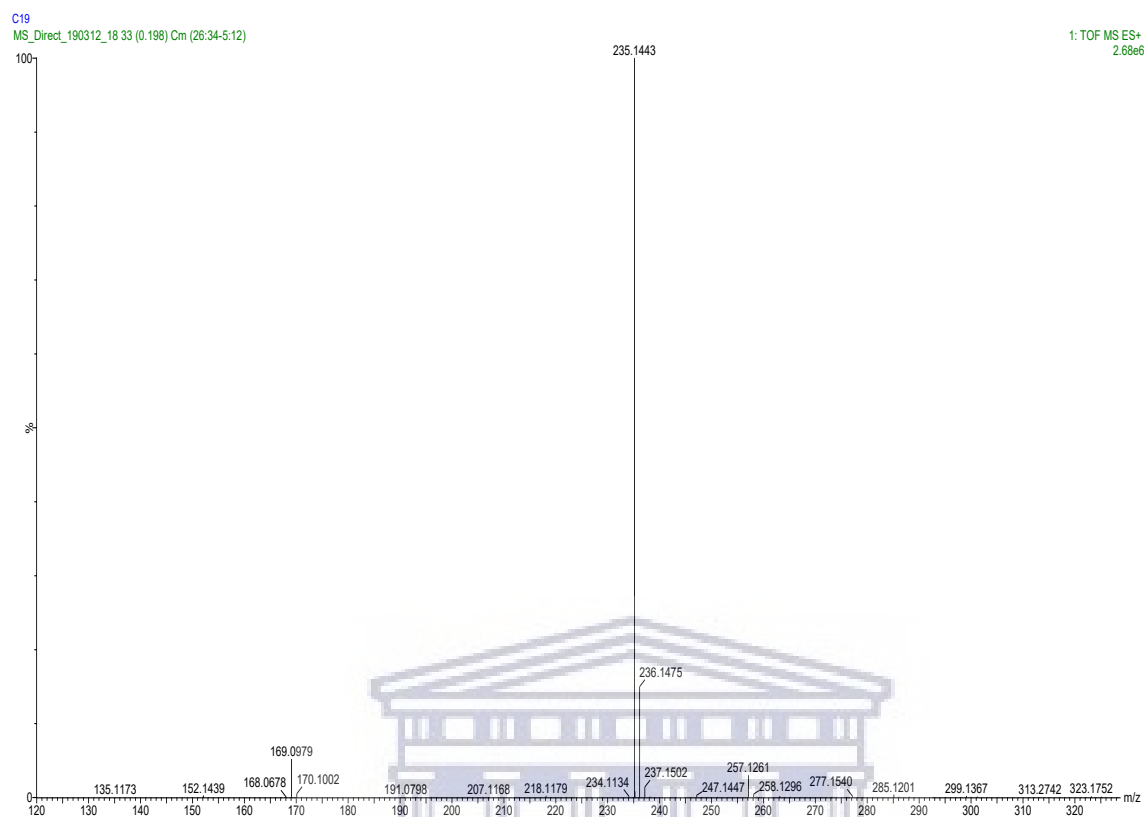
DEPT-135 spectrum of compound 17



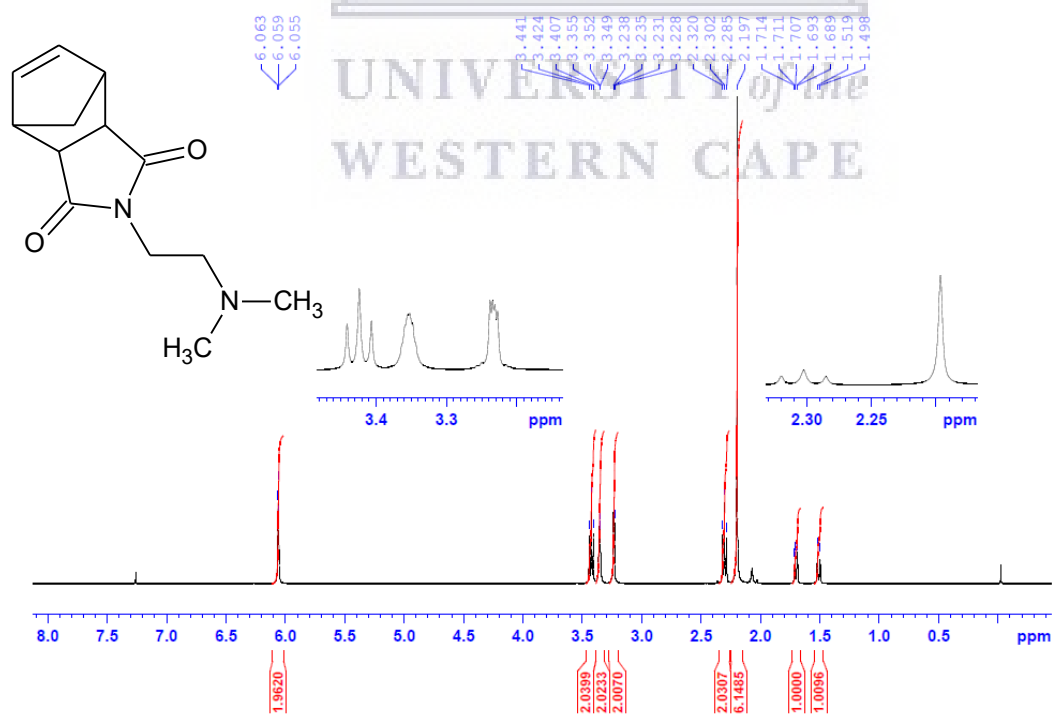
IR spectrum of compound 17



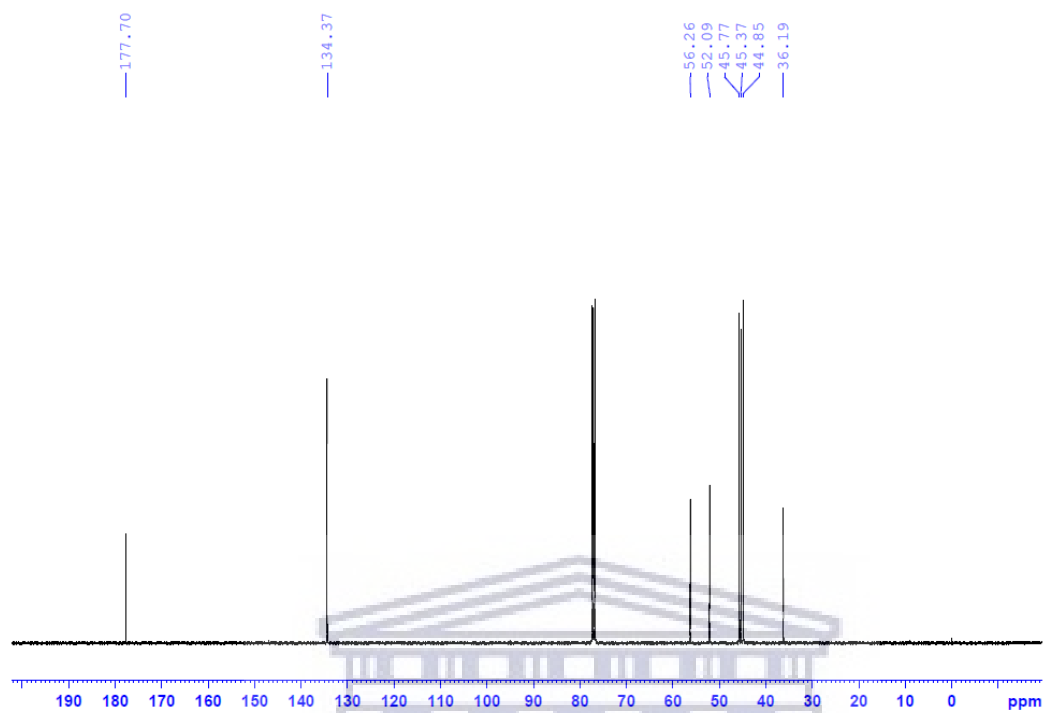
MS spectrum of compound 17



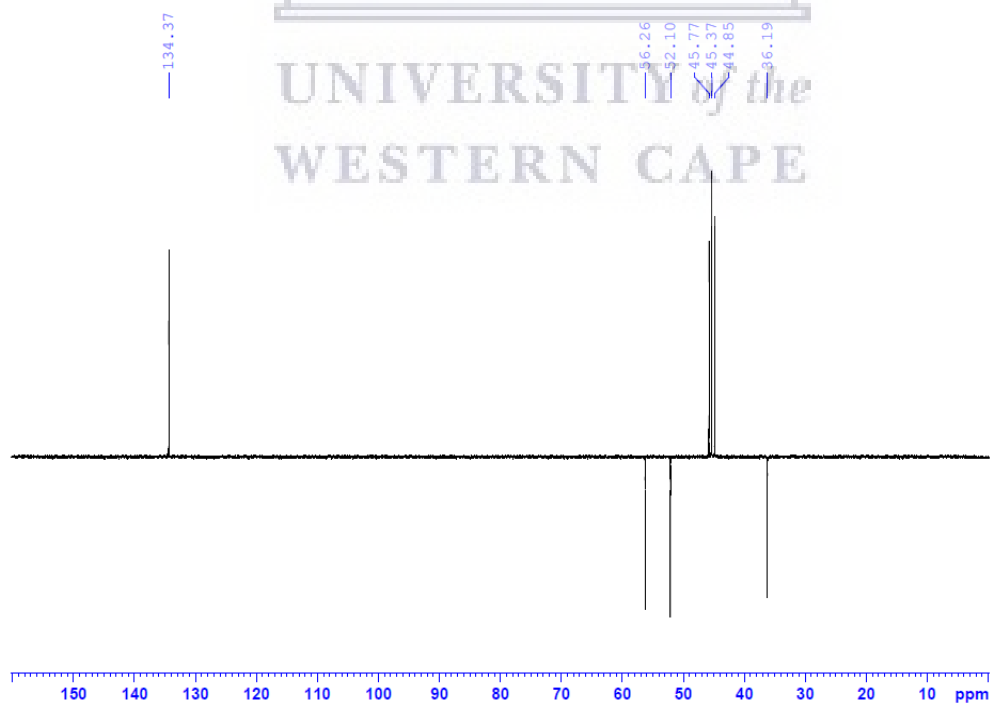
¹H spectrum of compound 18



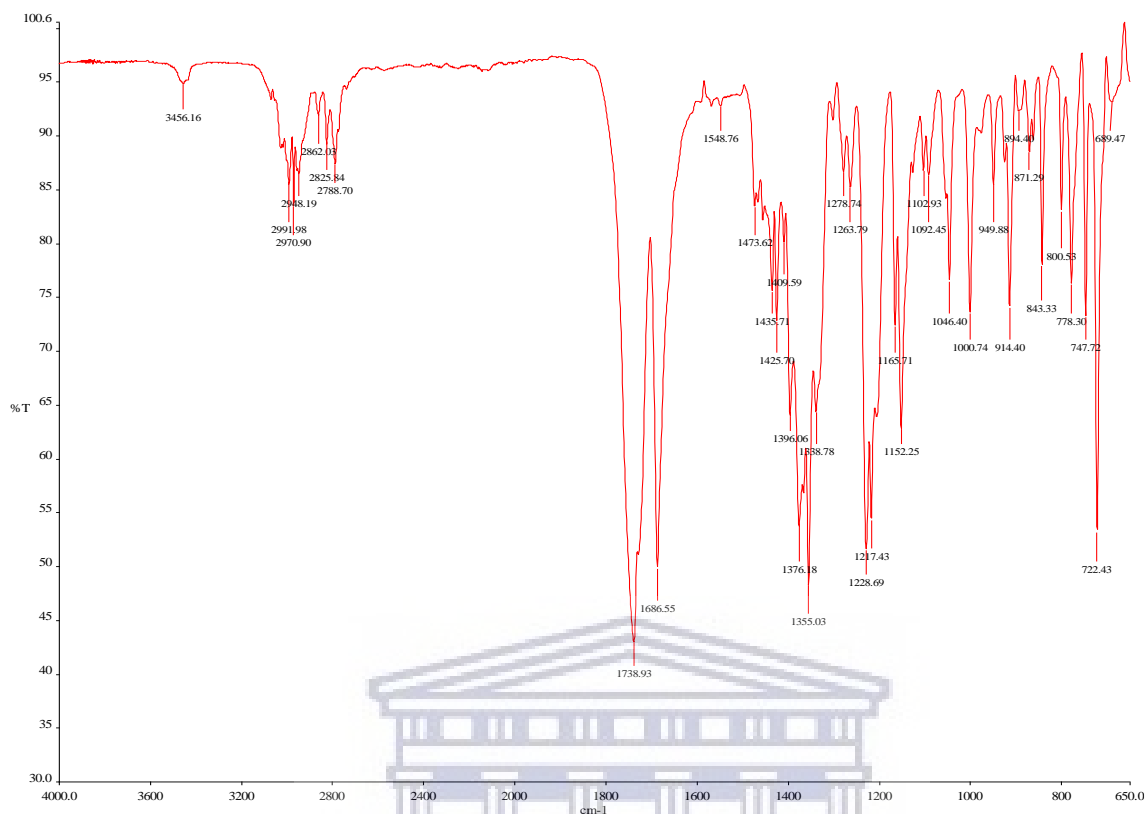
^{13}C spectrum of compound 18



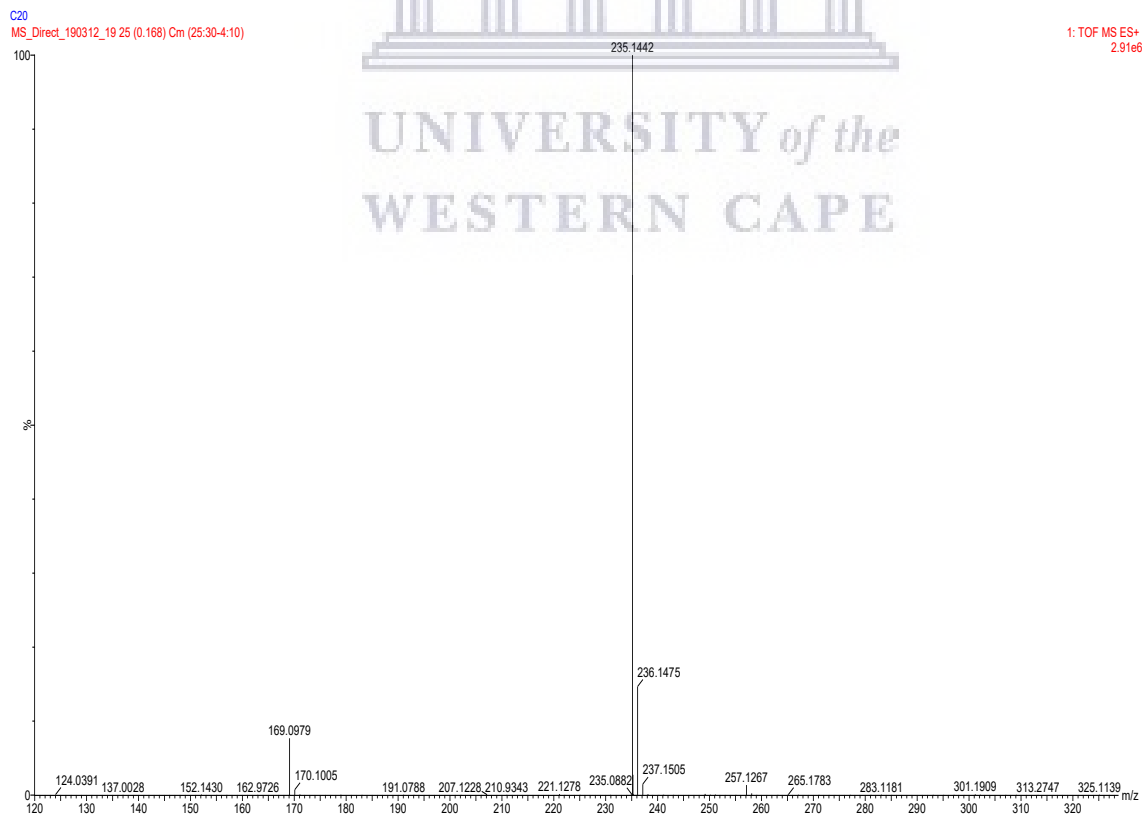
DEPT-135 spectrum of compound 18



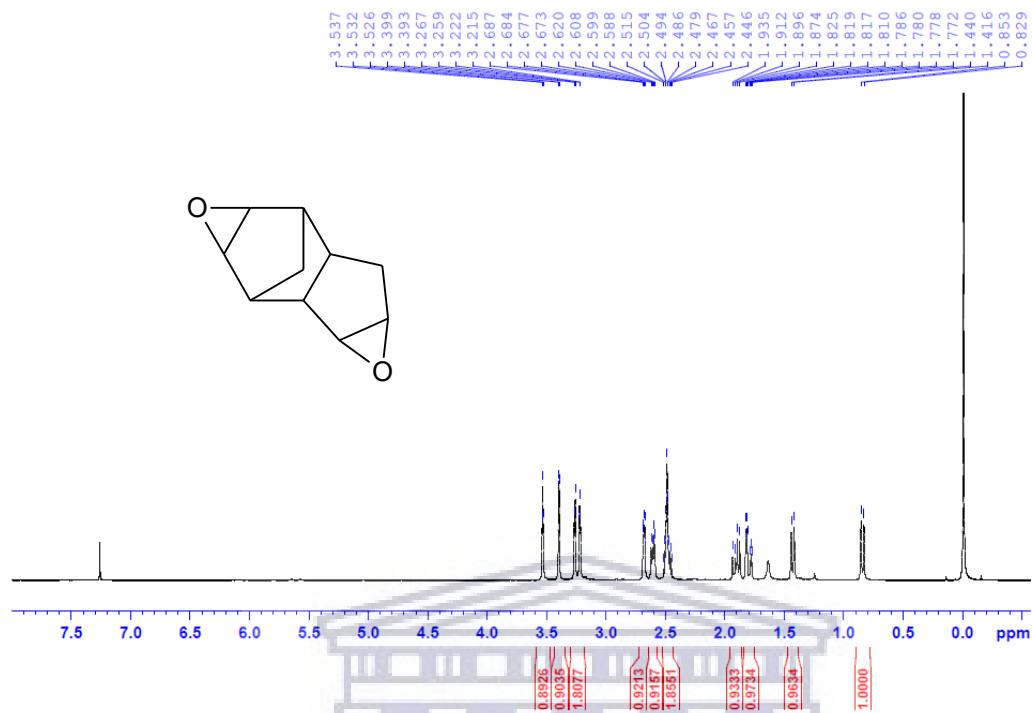
IR spectrum of compound 18



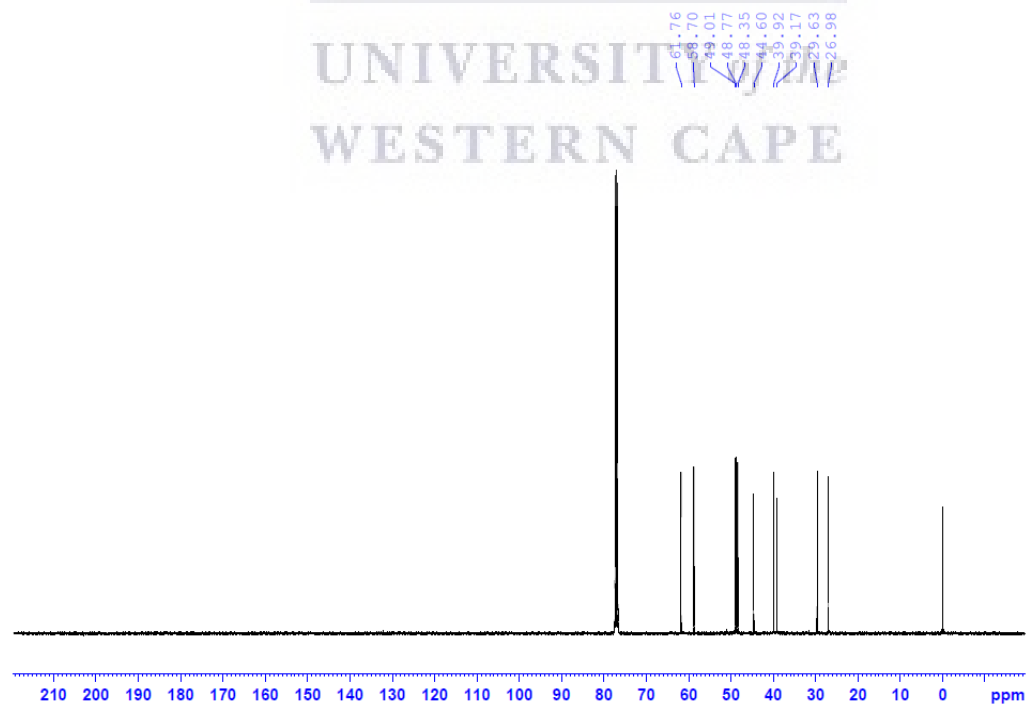
MS spectrum of compound 18



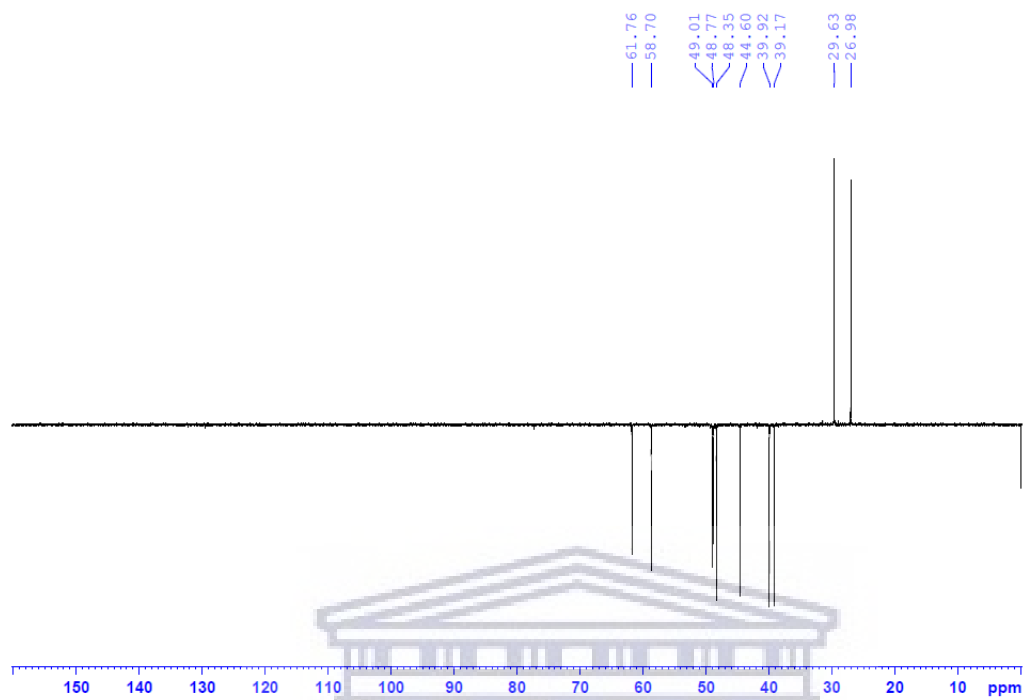
^1H spectrum of compound 19



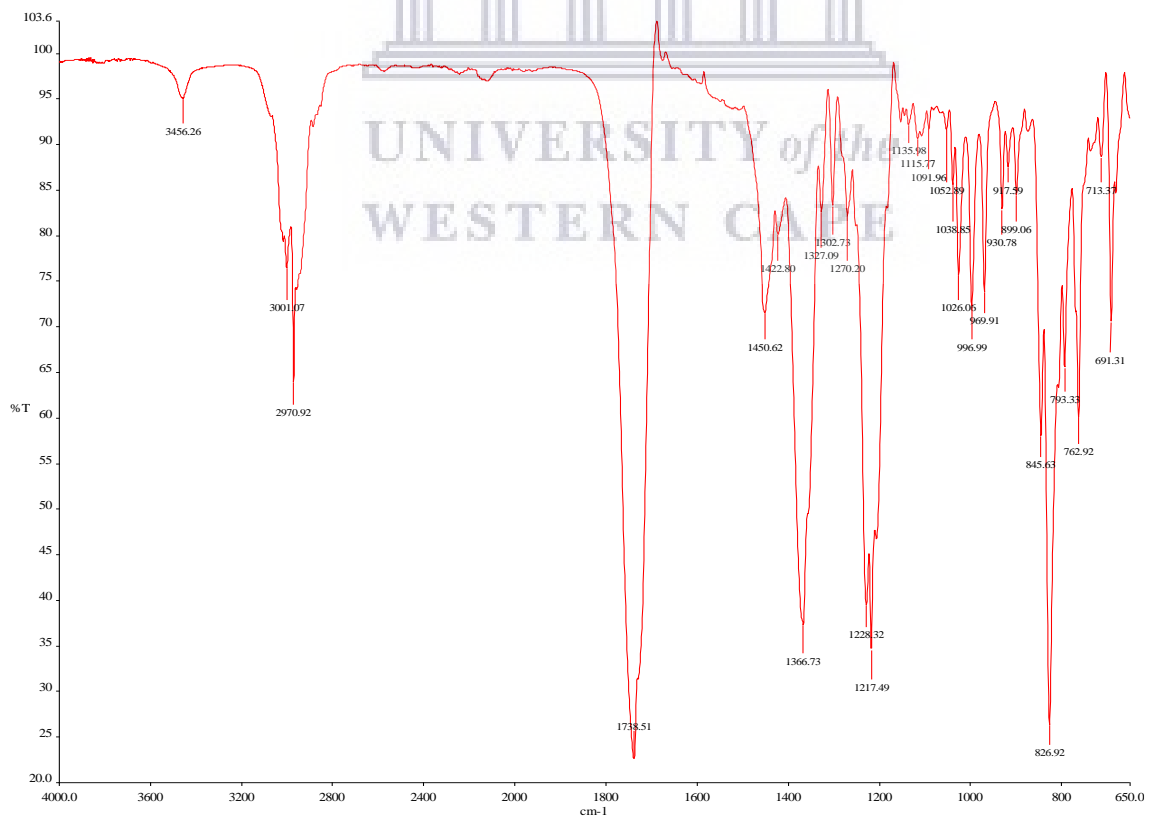
^{13}C spectrum of compound 19



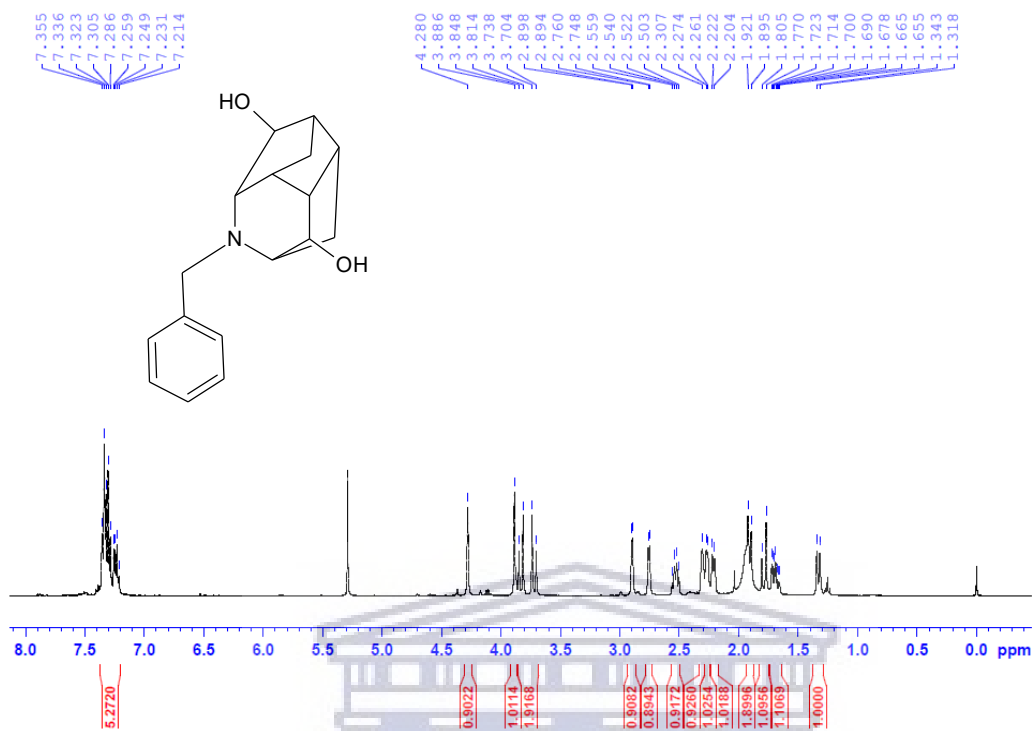
DEPT-135 spectrum of compound 19



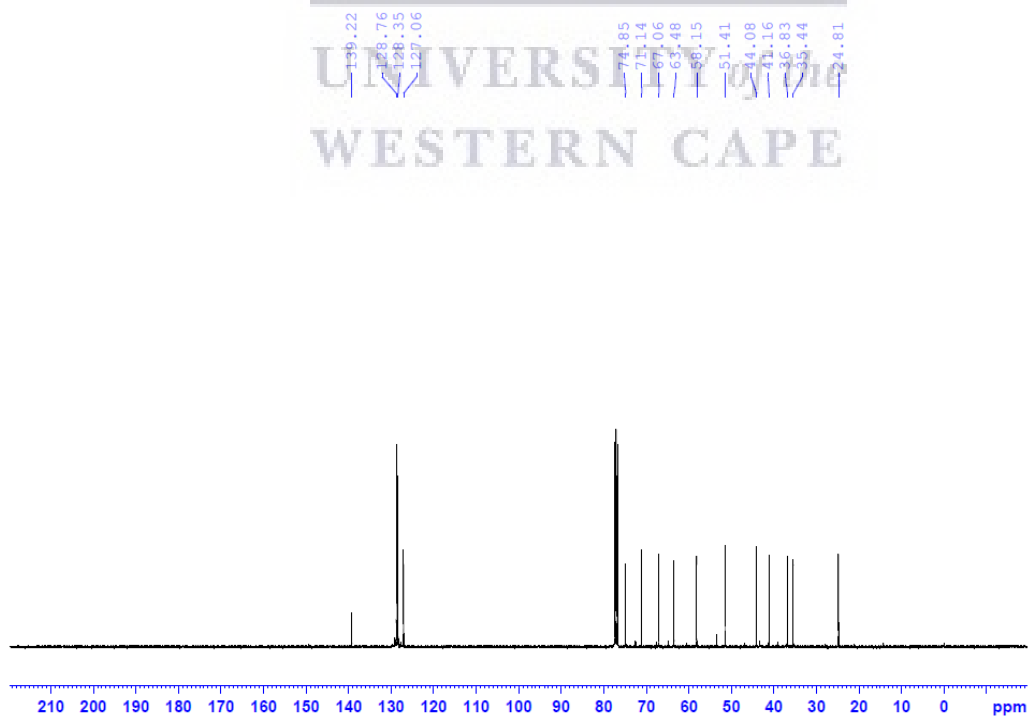
IR spectrum of compound 19



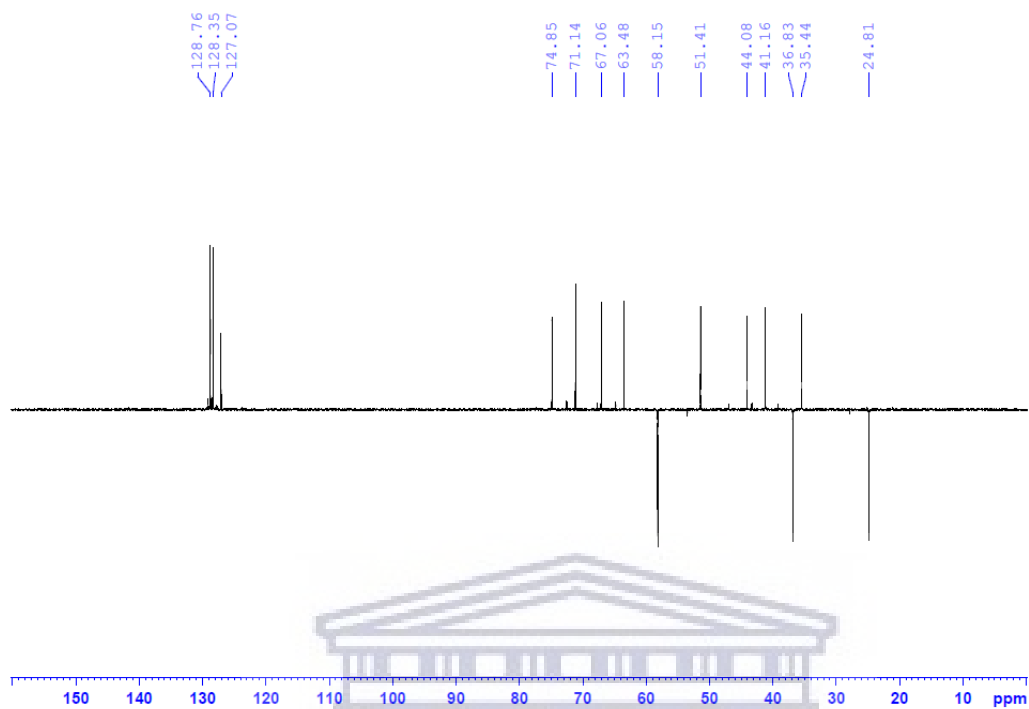
¹H spectrum of compound 20



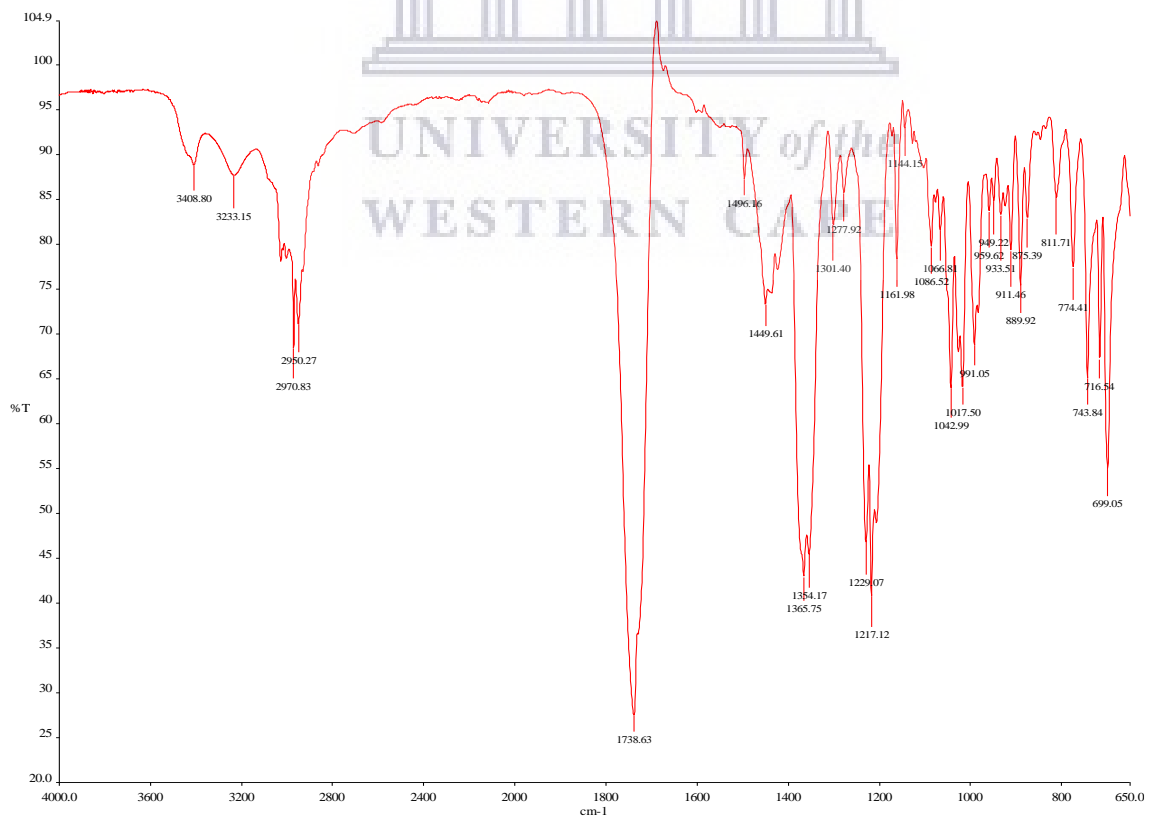
¹³C spectrum of compound 20



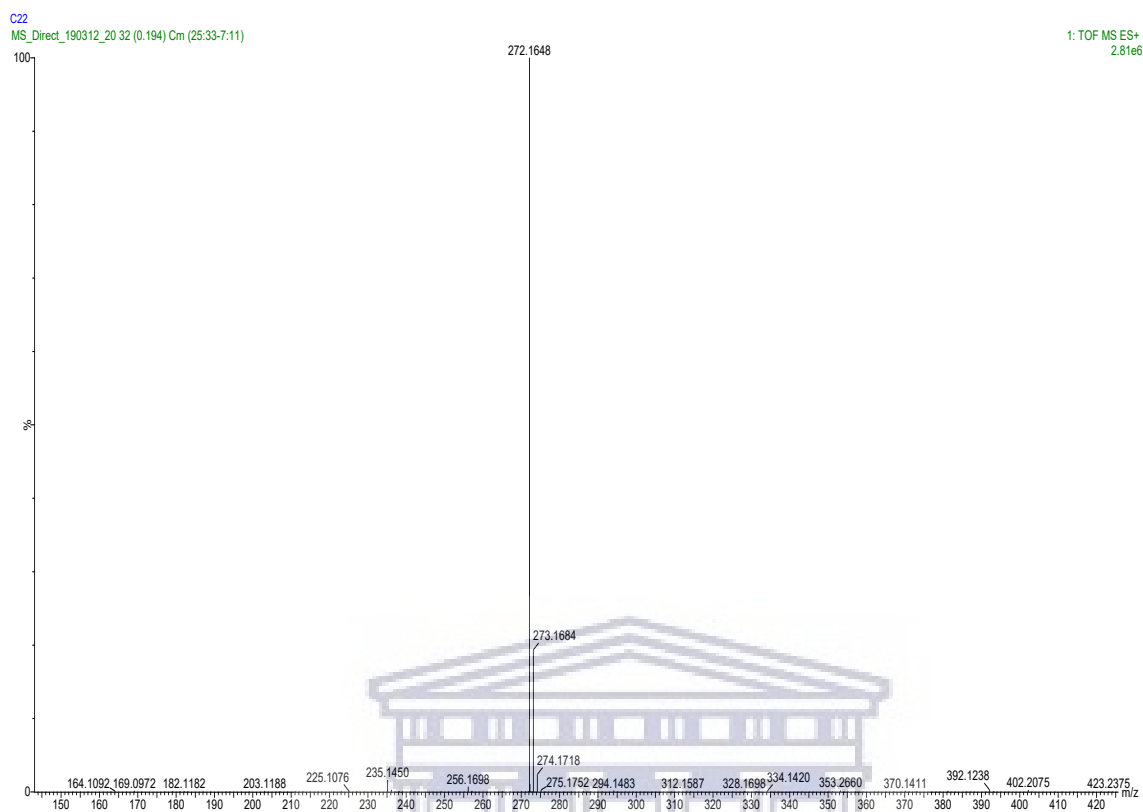
DEPT-135 spectrum of compound 20



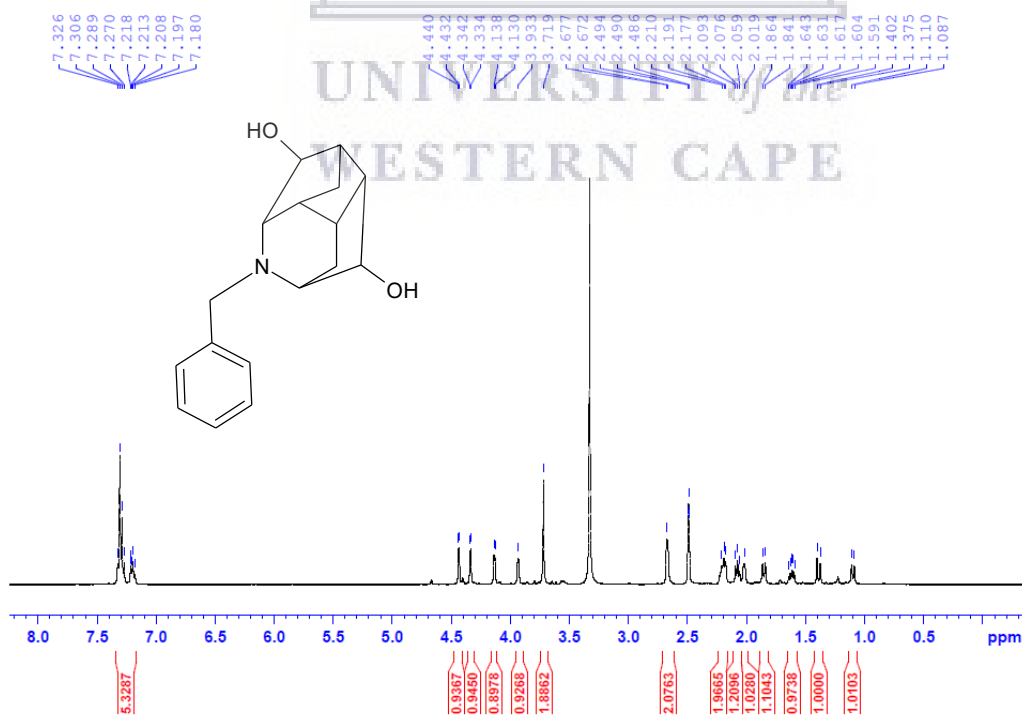
IR spectrum of compound 20



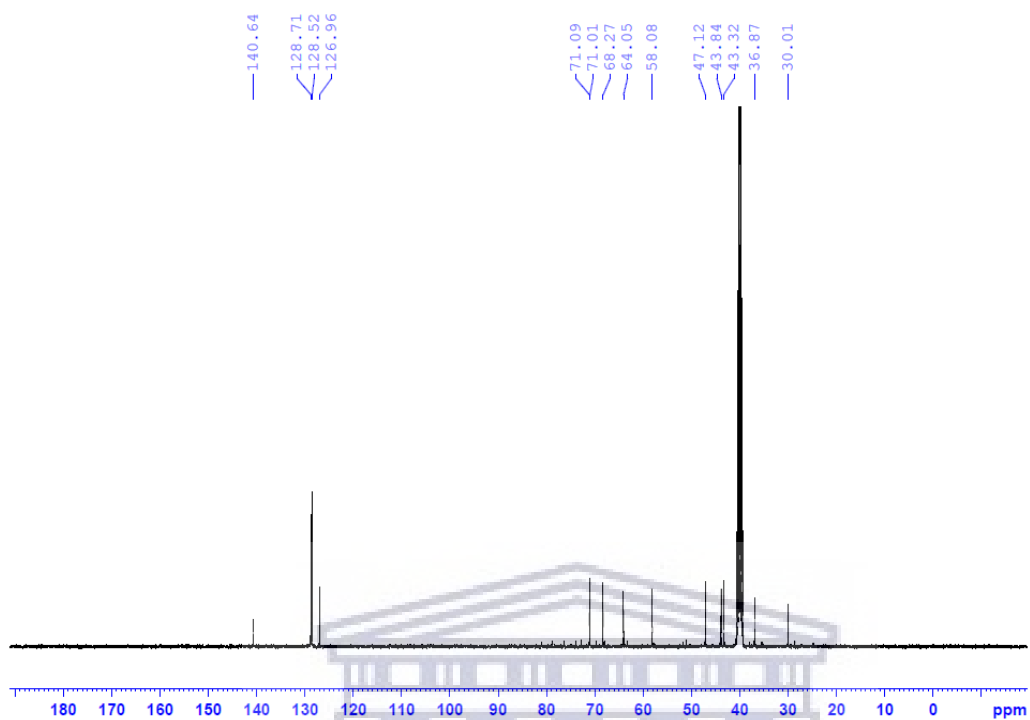
MS spectrum of compound 20



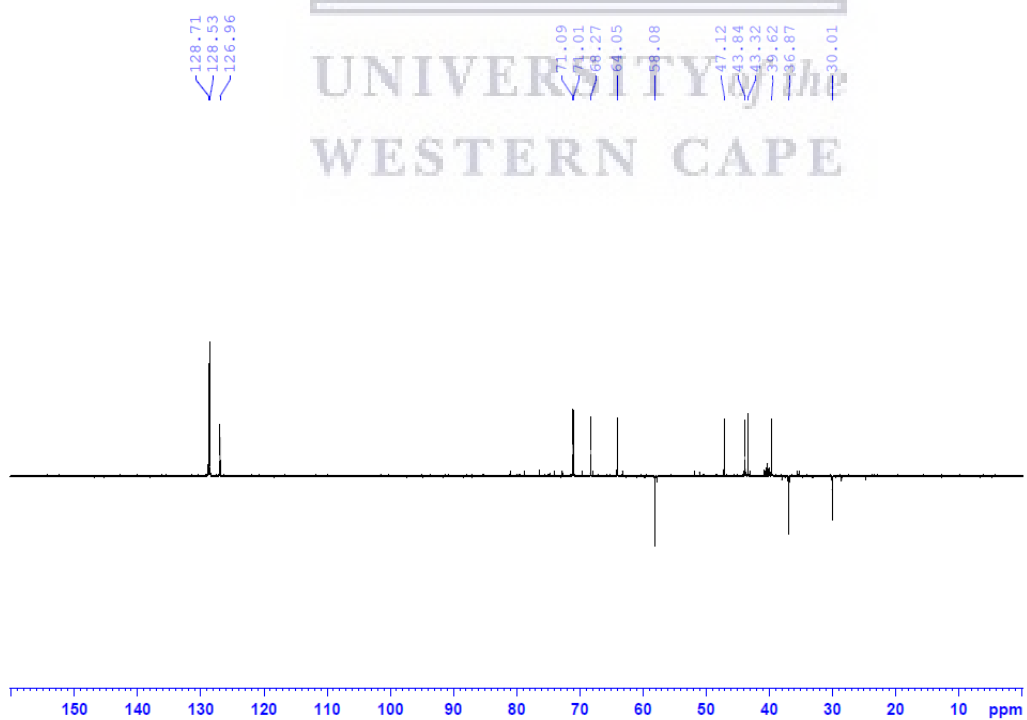
¹H spectrum of compound 21



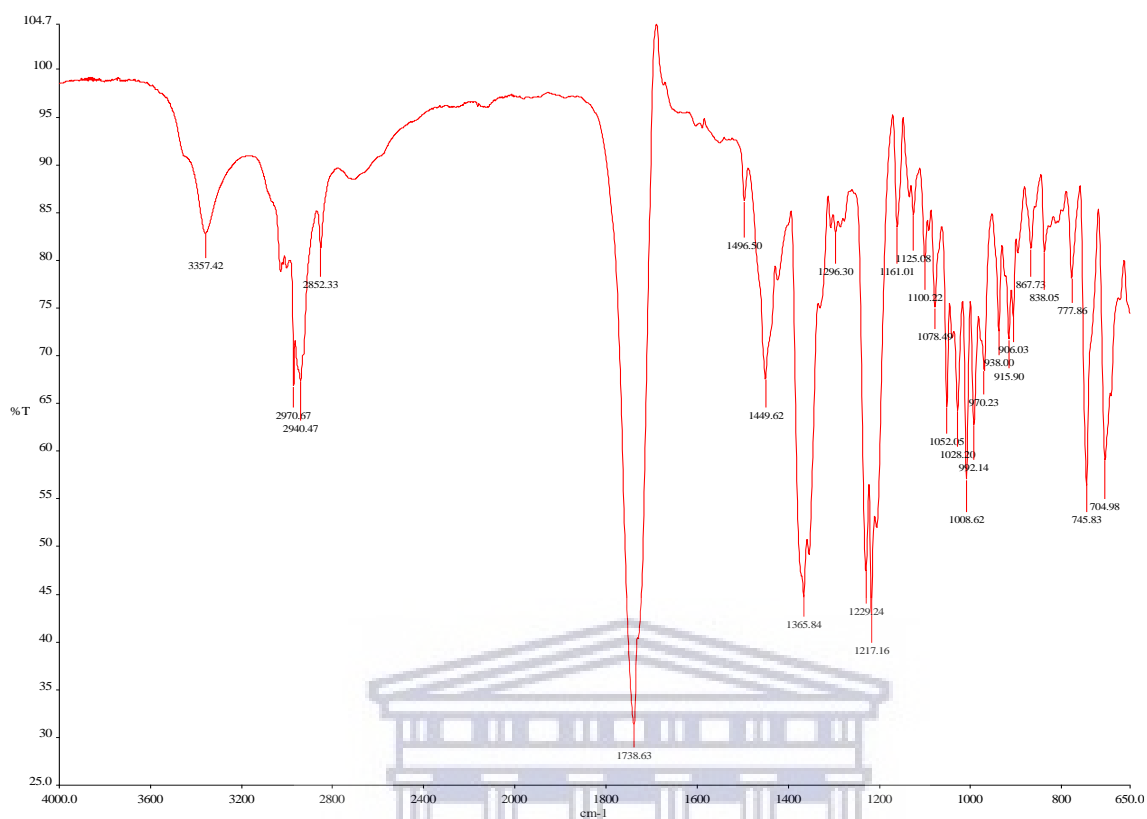
^{13}C spectrum of compound 21



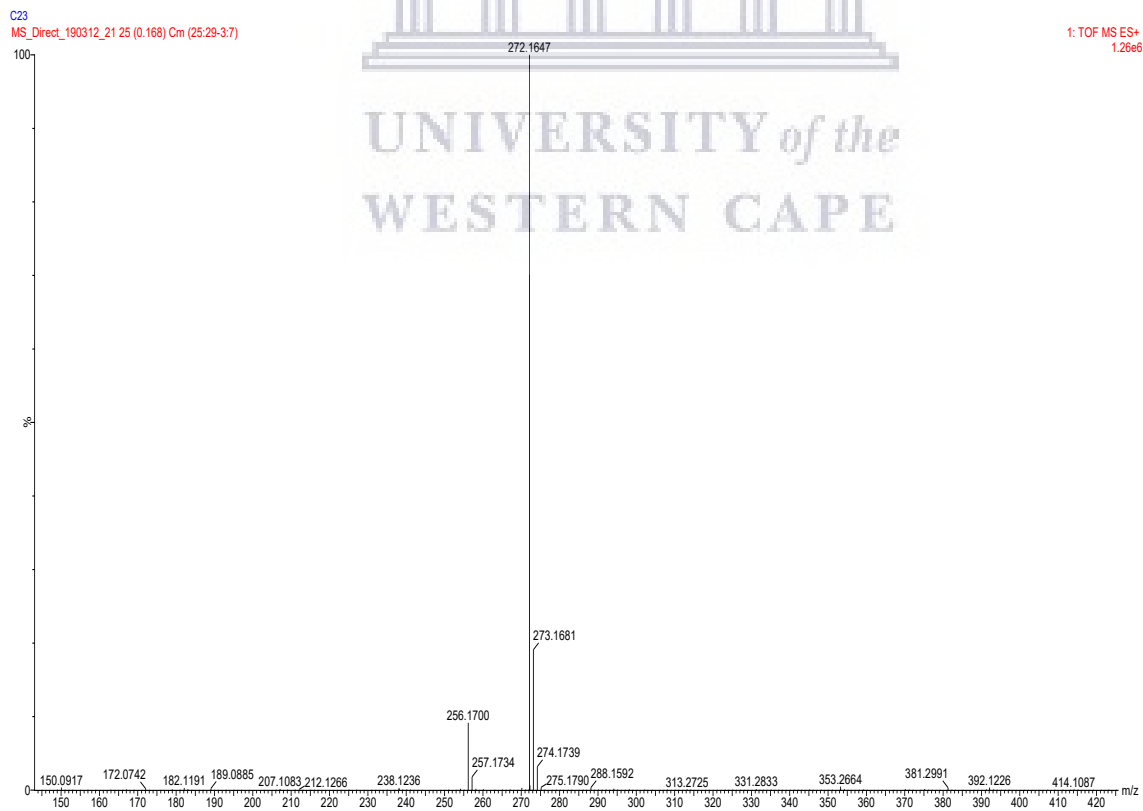
DEPT-135 spectrum of compound 21



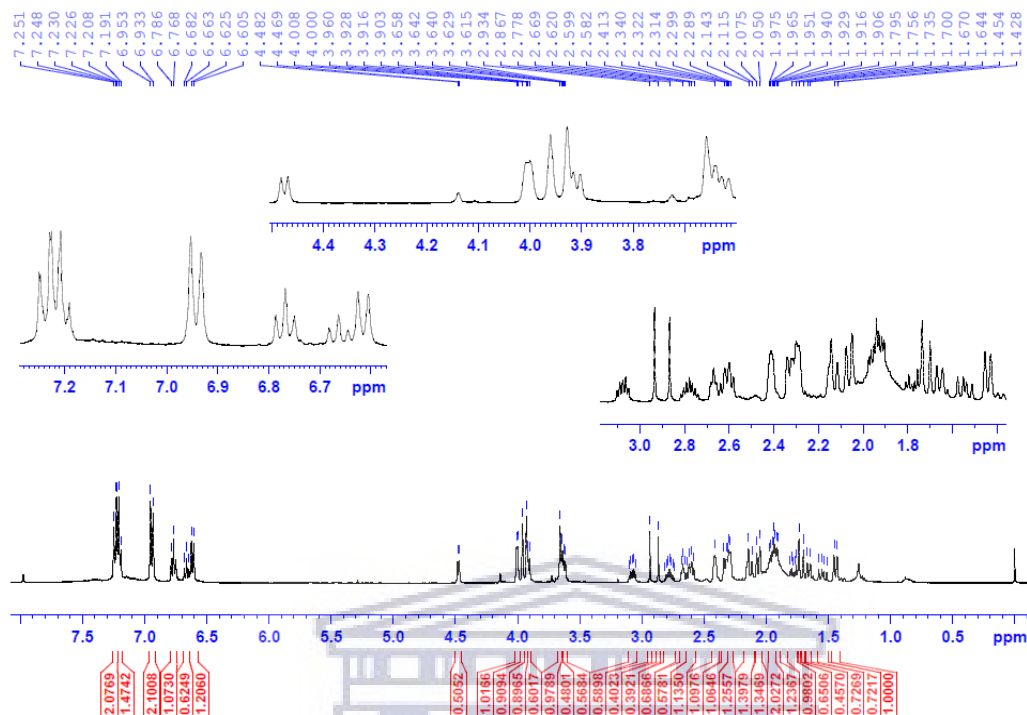
IR spectrum of compound 21



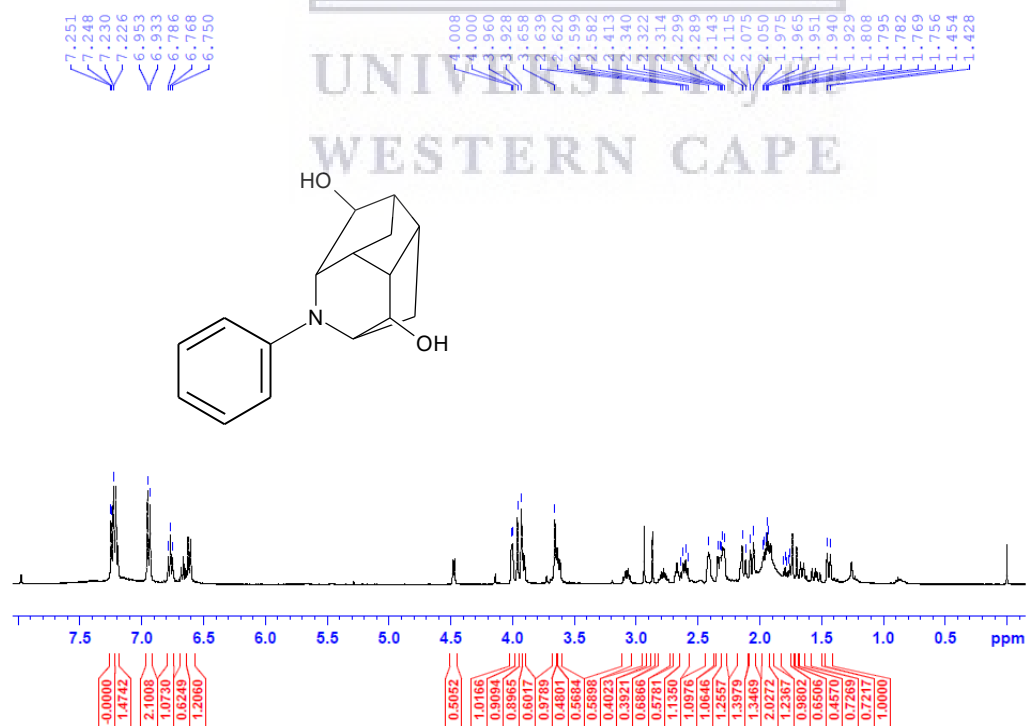
MS spectrum of compound 21



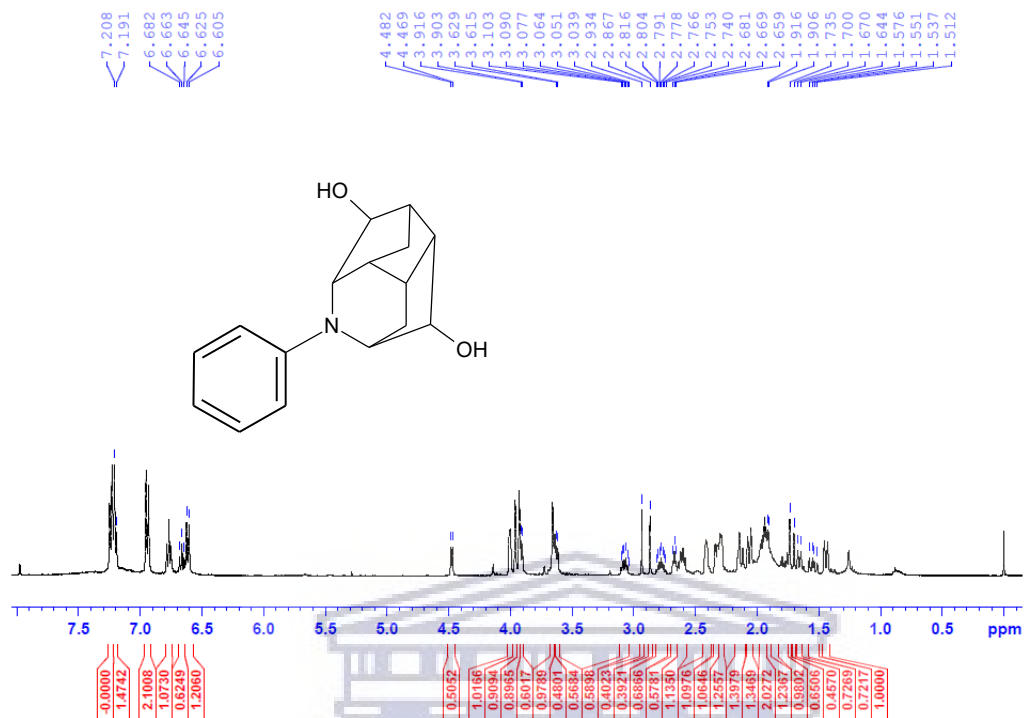
¹H spectrum of compound 22 & 23



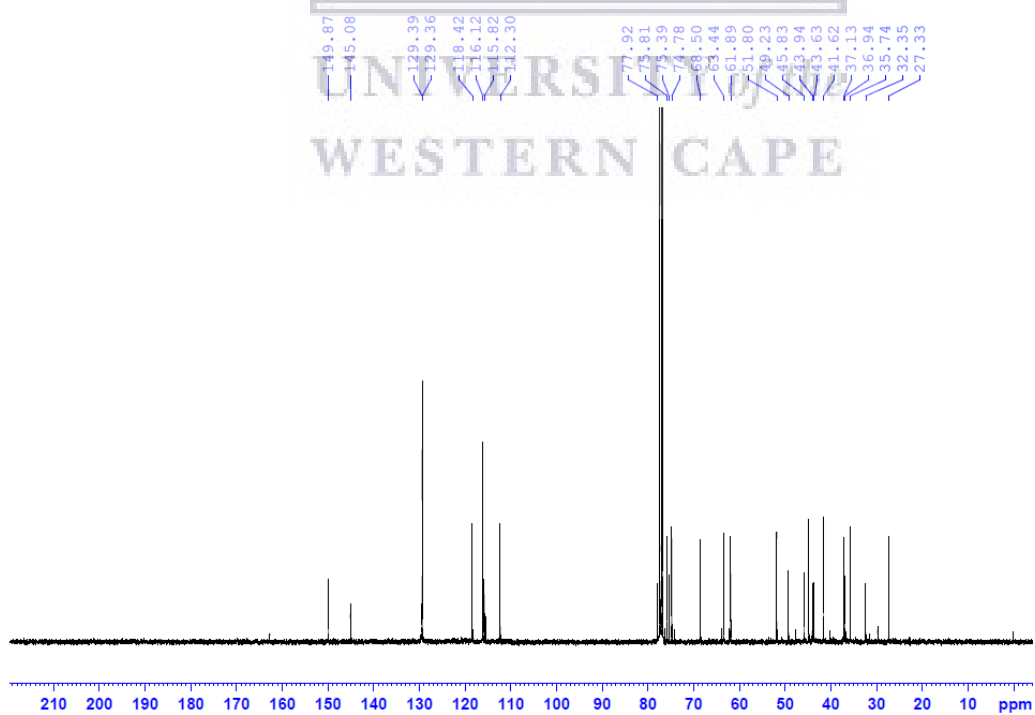
¹H spectrum of compound 22



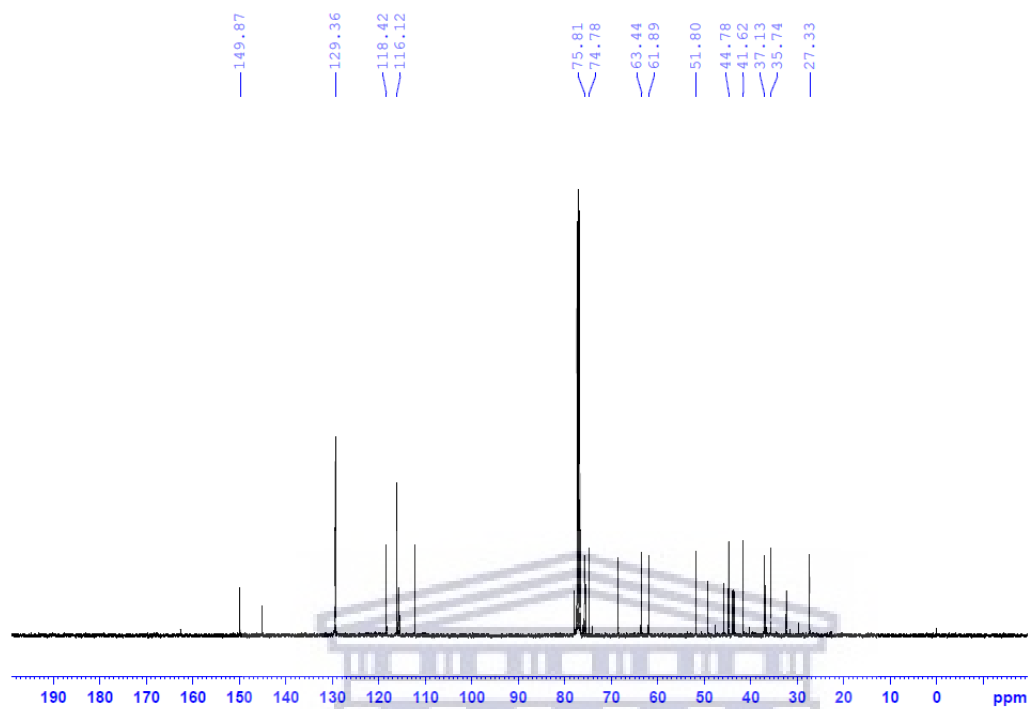
¹H spectrum of compound 23



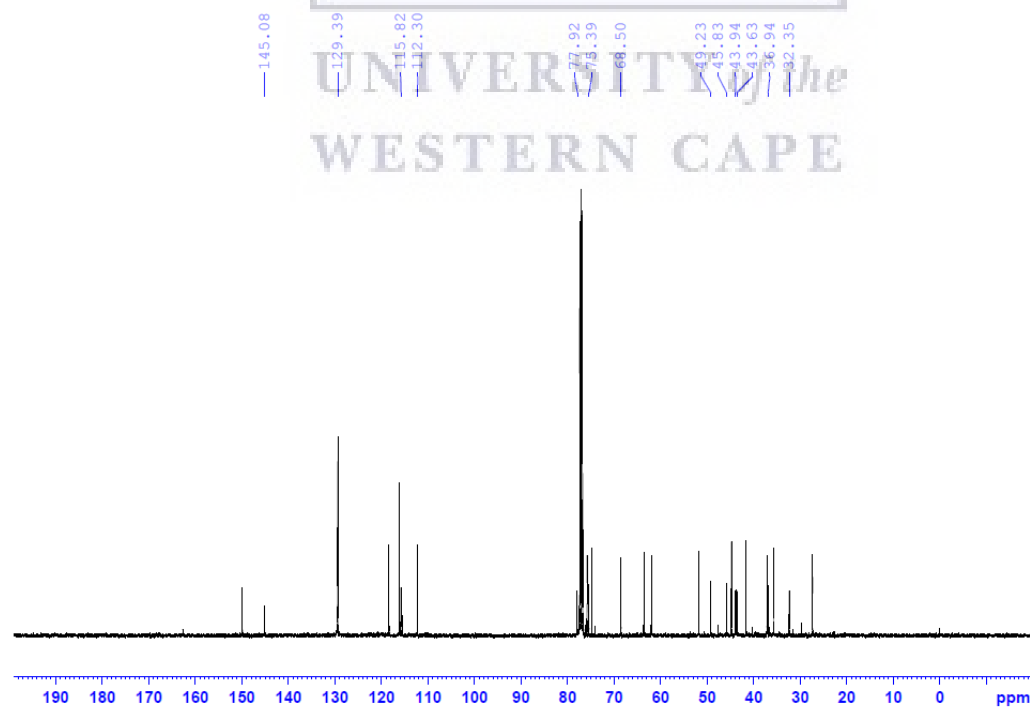
¹³C spectrum of compound 22 & 23



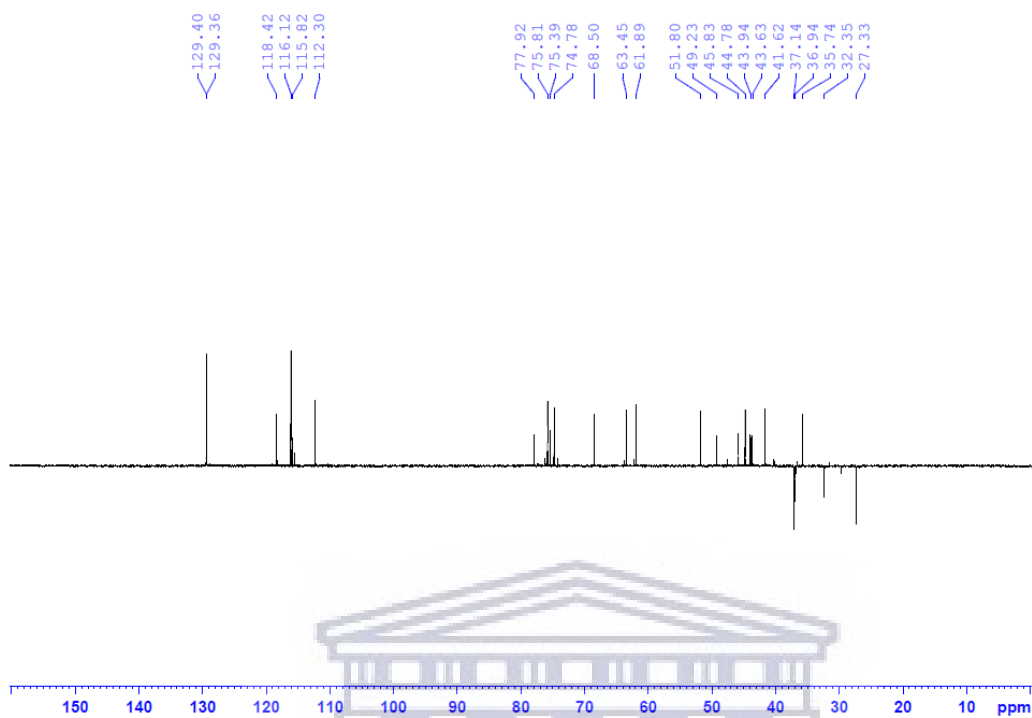
^{13}C spectrum of compound 22



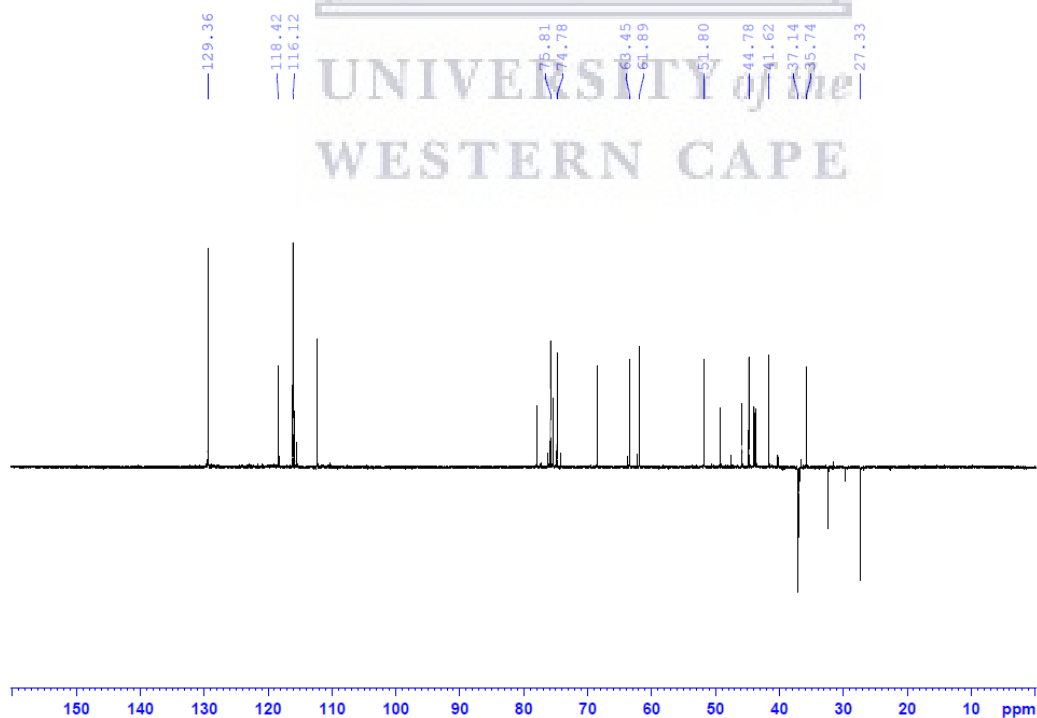
^{13}C spectrum of compound 23



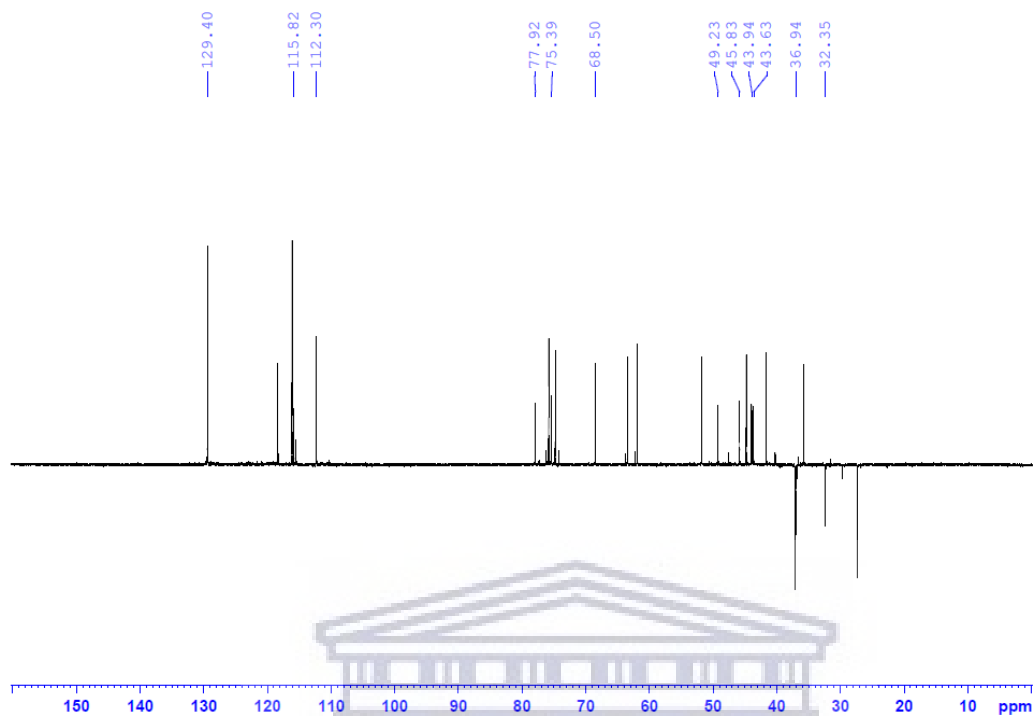
DEPT-135 spectrum of compound 22 & 23



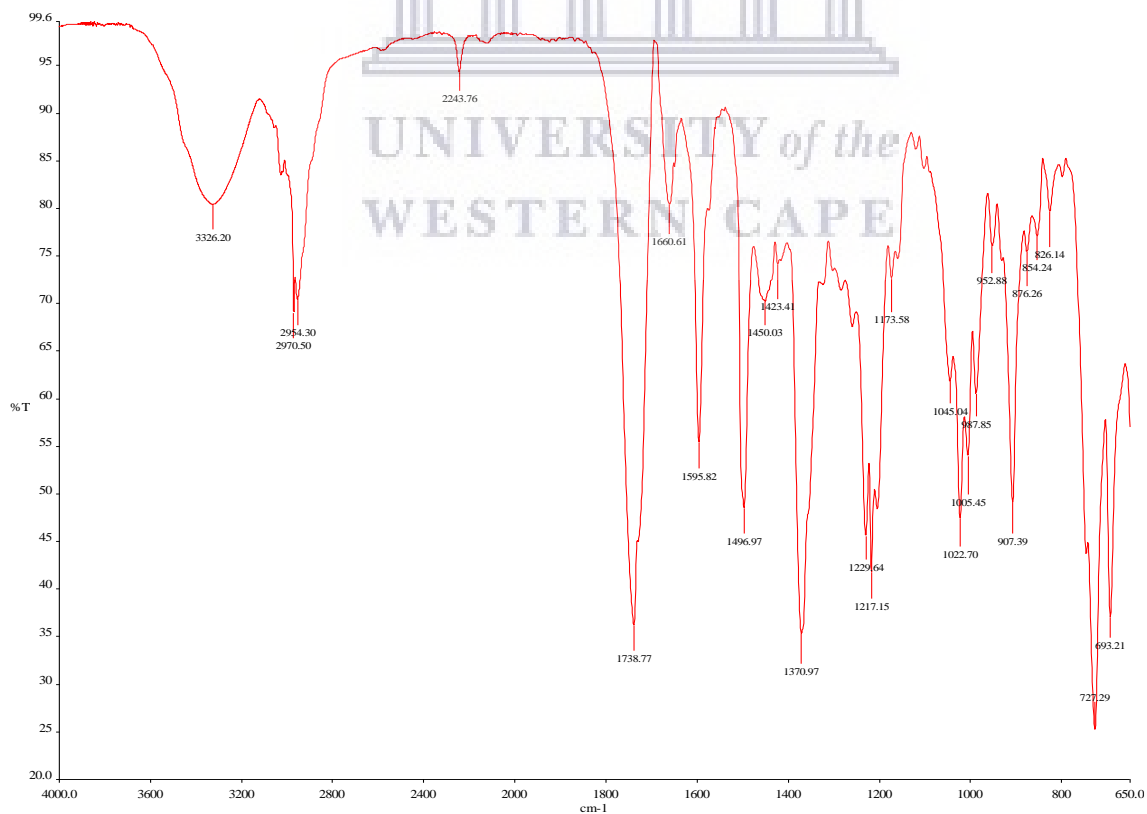
DEPT-135 spectrum of compound 22



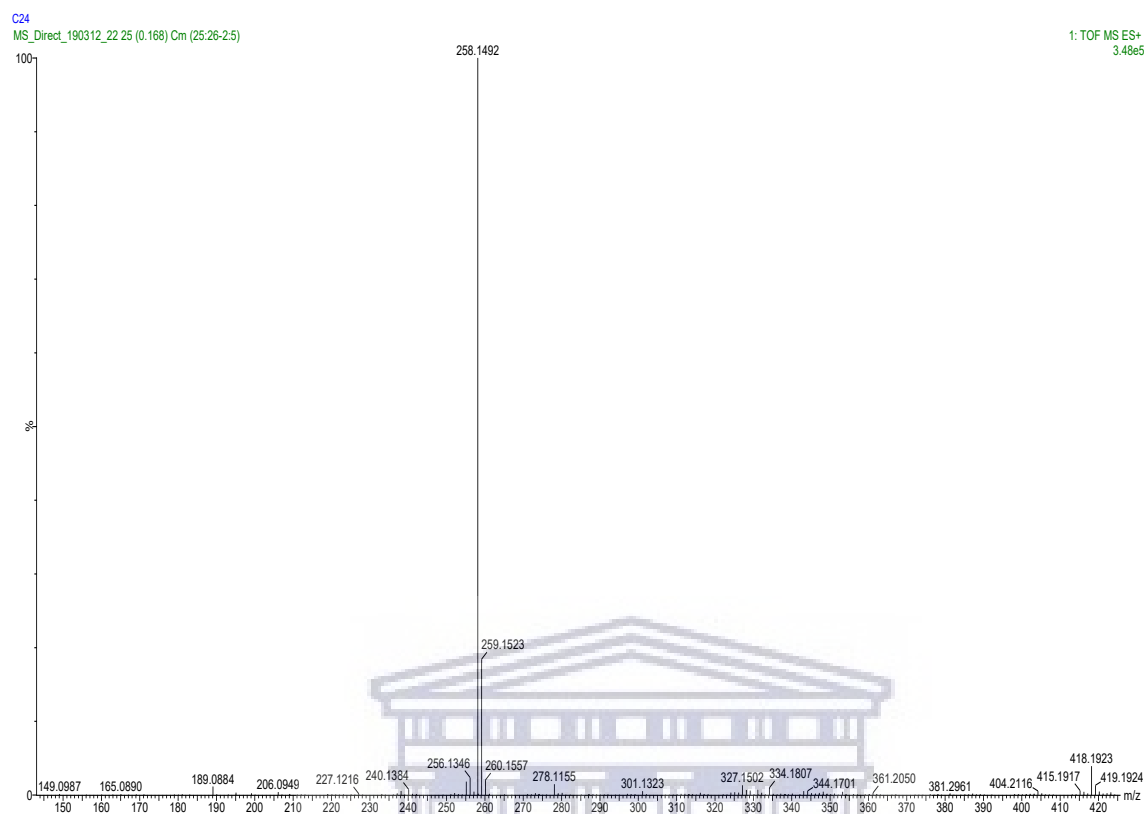
DEPT-135 spectrum of compound 23



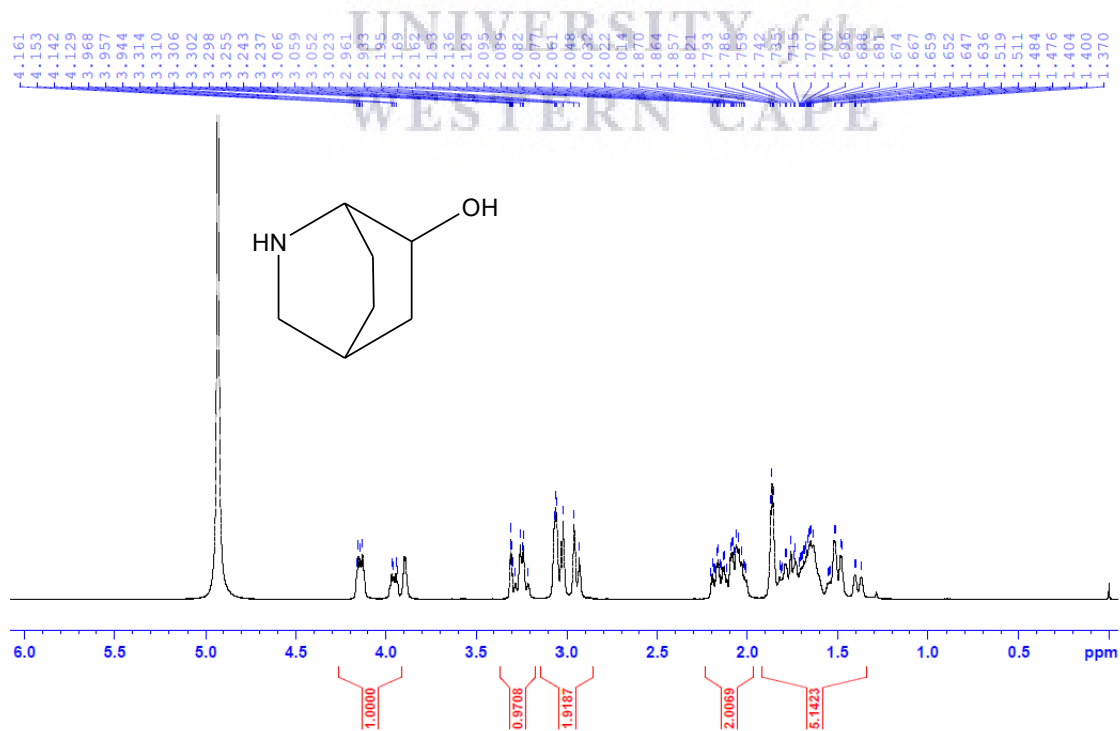
IR spectrum of compound 22 & 23



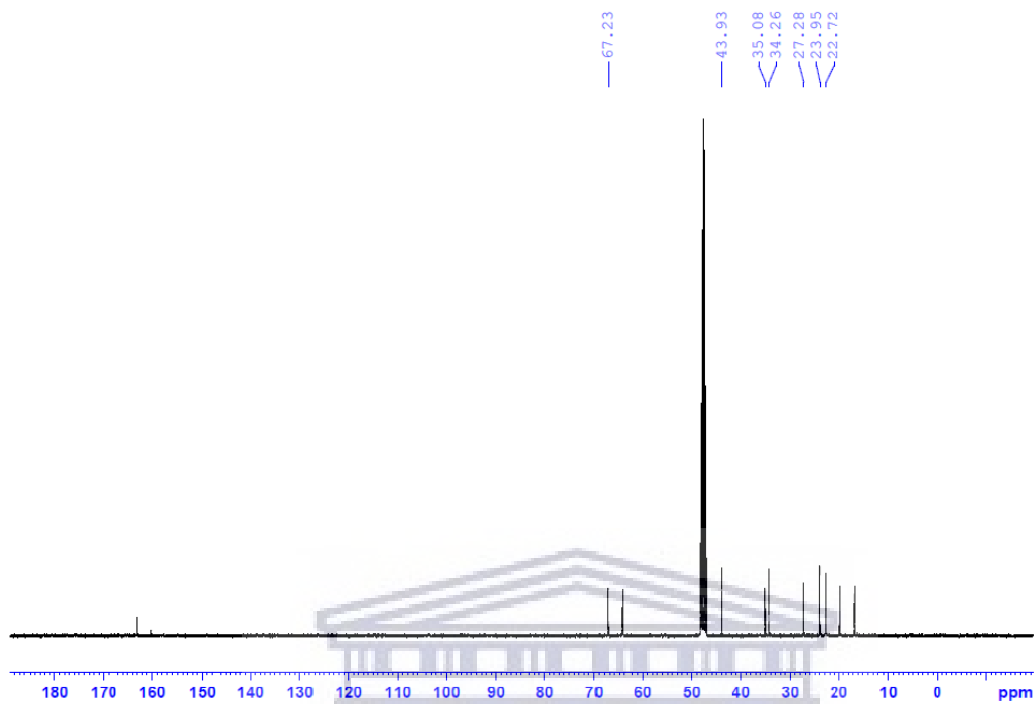
MS spectrum of compound 22 & 23



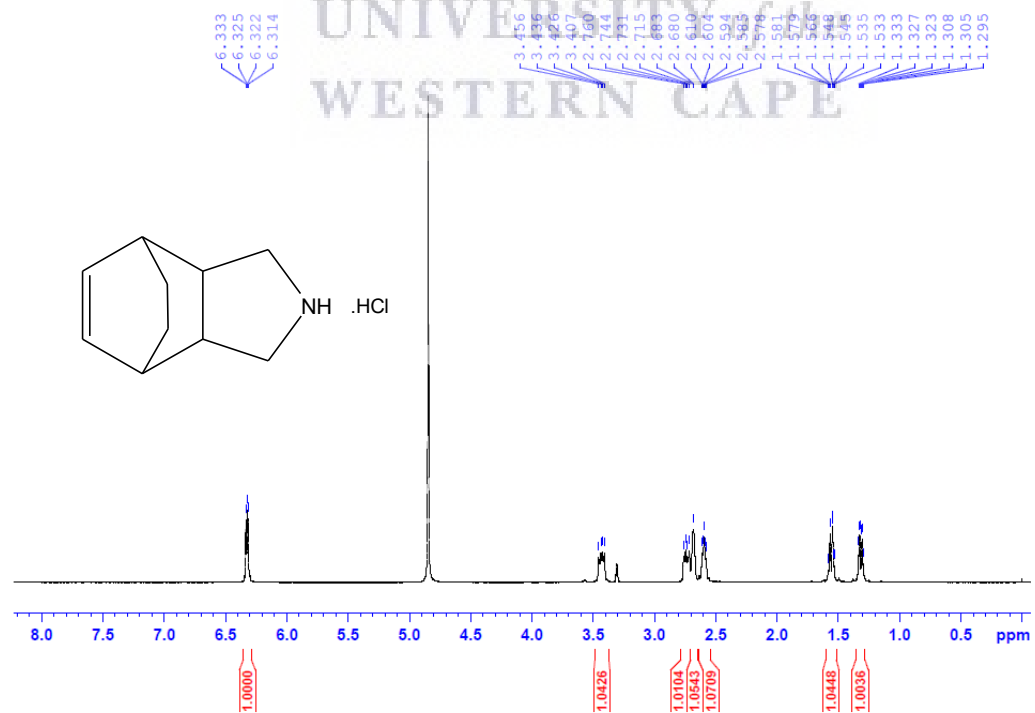
¹H spectrum of compound 24



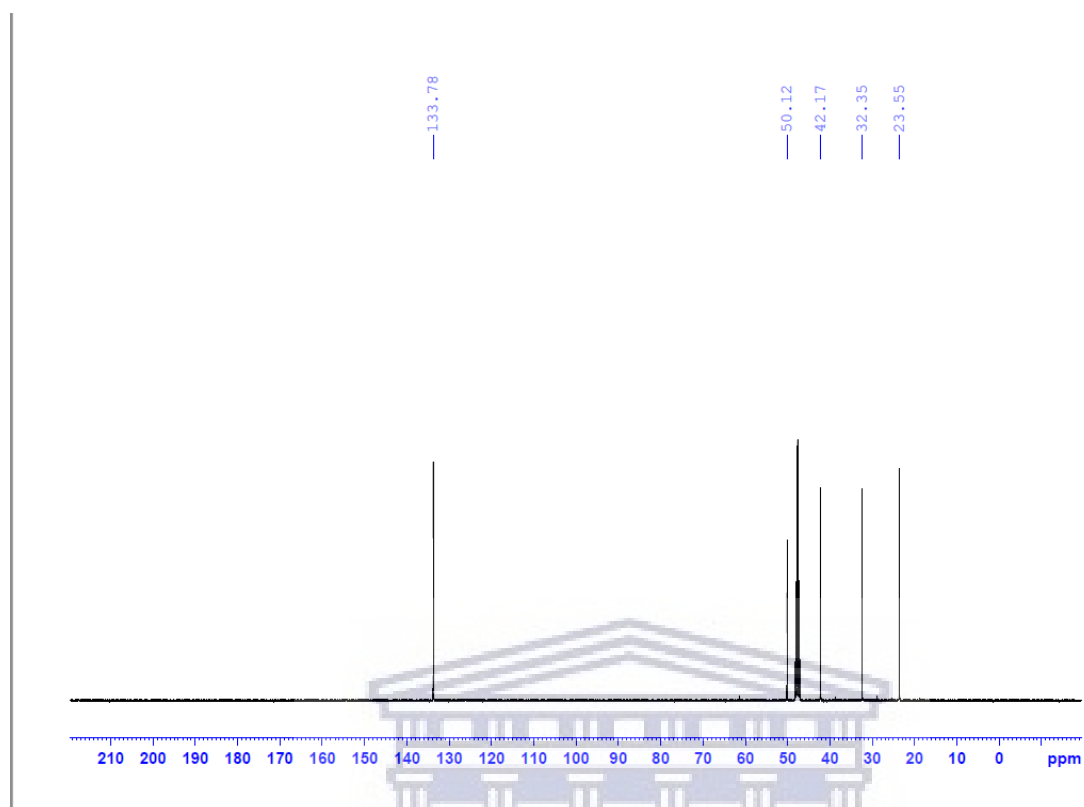
^{13}C spectrum of compound 24



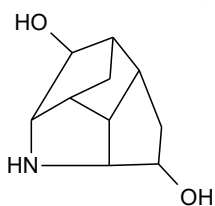
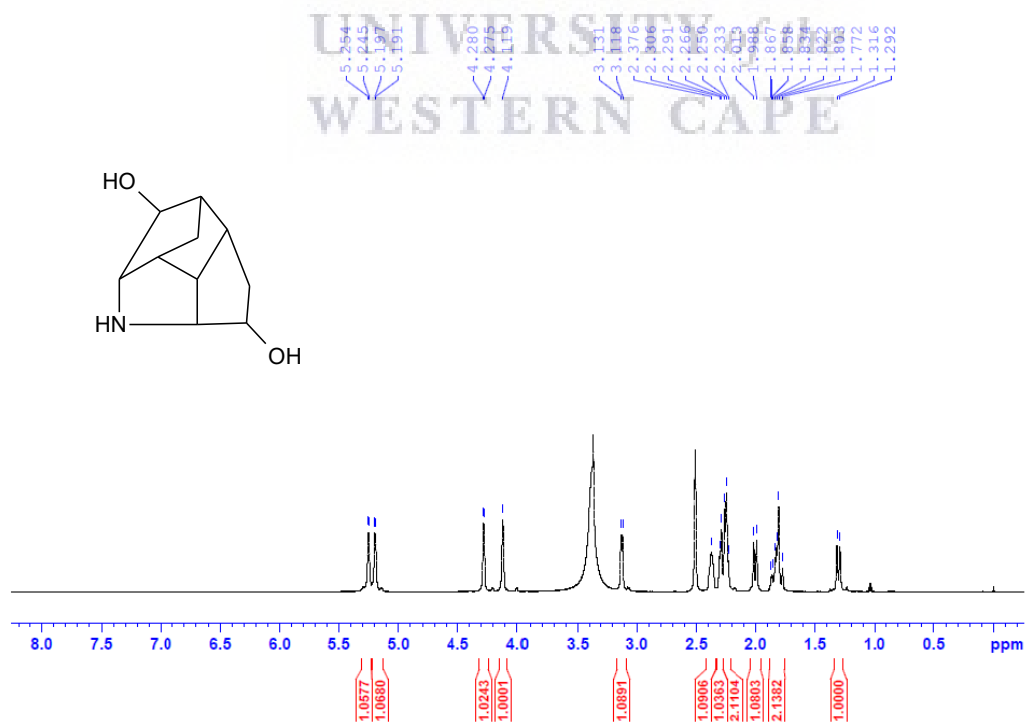
^1H spectrum of compound 25



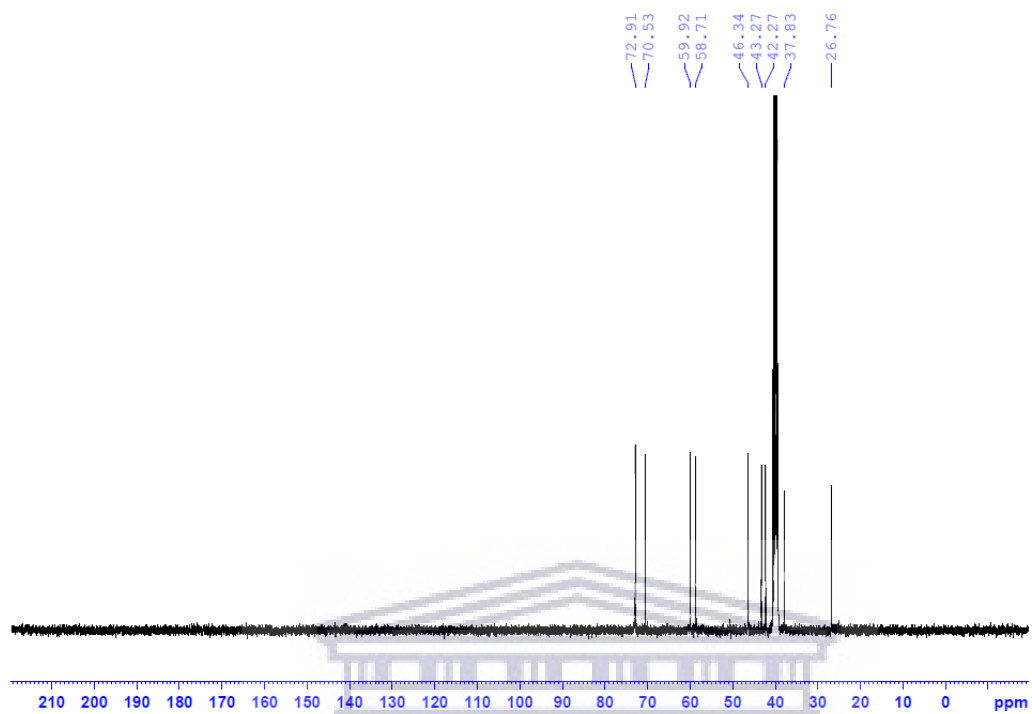
^{13}C spectrum of compound 25



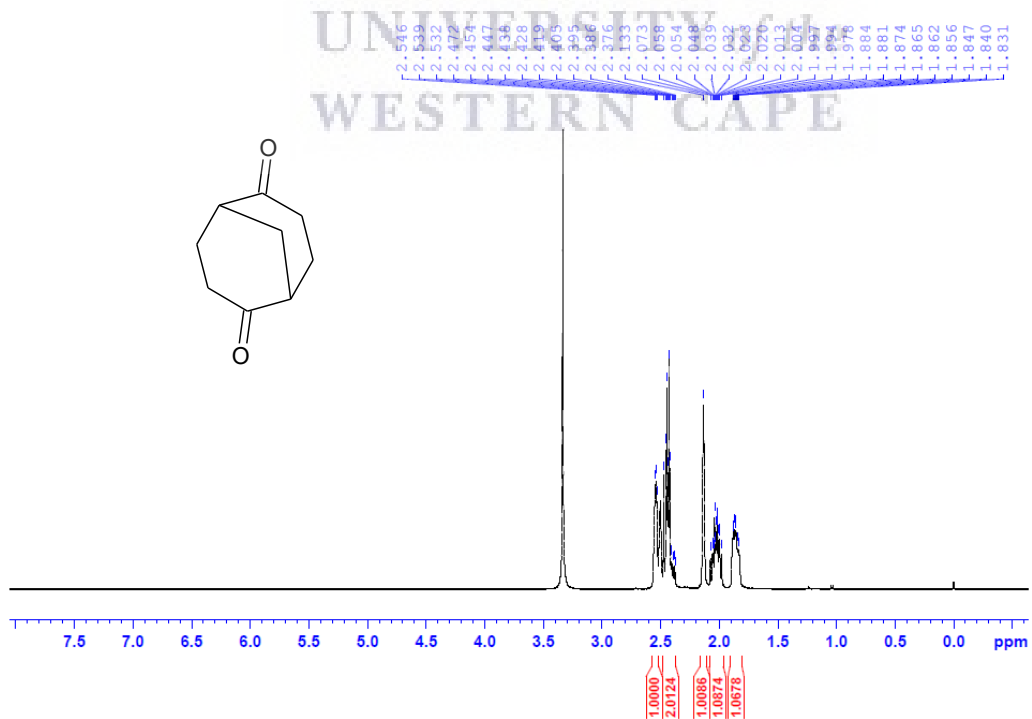
^1H spectrum of compound 26



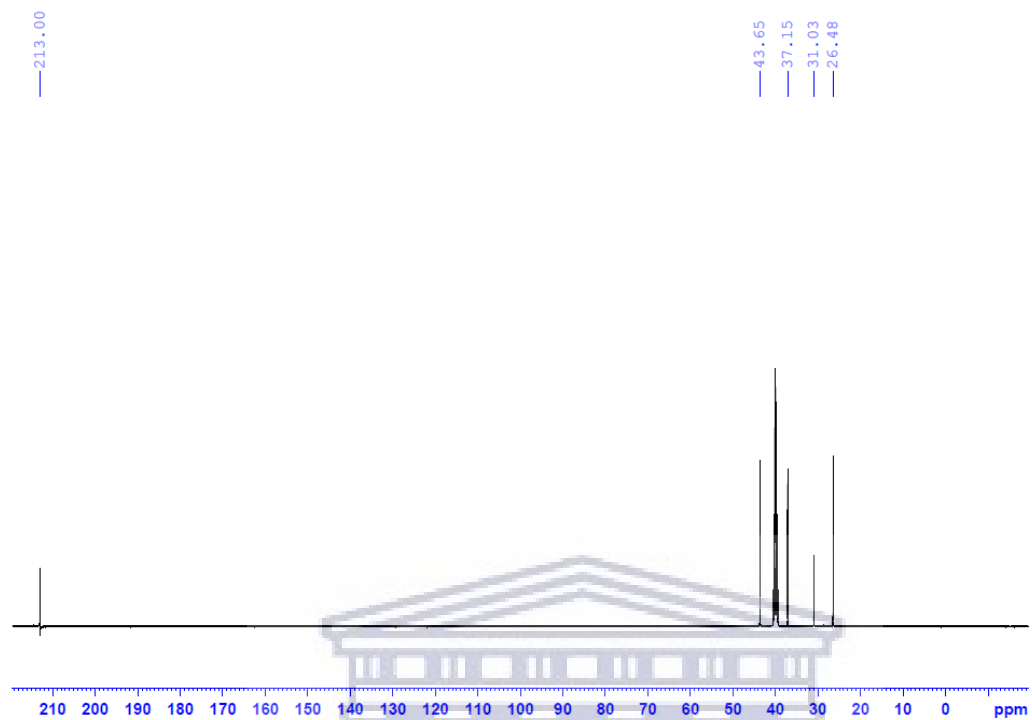
^{13}C spectrum of compound 26



^1H spectrum of compound 27



^{13}C spectrum of compound 27



UNIVERSITY of the
WESTERN CAPE